Roles of cell adhesion and adhesion regulatory proteins during collective cell migration and invasion

by

Nirupama Somappa Kotian

B.Sc., University of Mumbai, India, 2011
M.Sc., University of Mumbai, India, 2013

AN ABSTRACT OF A DISSERTATION

submitted in partial fulfillment of the requirements for the degree

DOCTOR OF PHILOSOPHY

Division of Biology
College of Arts and Sciences

KANSAS STATE UNIVERSITY
Manhattan, Kansas

2022

Abstract

Collective cell migration is the highly dynamic and coordinated movement of groups of cells. Various types of collectives are crucial for embryogenesis, neural crest migration, mammary gland development and wound healing. Collective cell movements are also found in cancer, which leads to tumor spreading and invasion to secondary sites in the body. These tumor collectives are efficient at invading deeper into tissues and enhance resistance to available therapies. Cells in collectives are tightly connected to each other through cell-cell contacts, which allows the cells to stay together during migration. The cellular and molecular mechanisms that regulate cell-cell communication and adhesion during collective cell migration and collective tumor cell invasion are not well understood. Cell adhesion and adhesion-regulatory proteins therefore are strong candidates to regulate collective cell behaviors. In this thesis, I used the *Drosophila* ovary border cell system to identify mechanisms that regulate cell-cell adhesion during collective cell migration *in vivo*. The ovary is made of repeating subunits called egg chambers. Each egg chamber is enveloped by a monolayer of follicular epithelial cells that surround the oocyte, nurse cells and a pair of polar cells on each end. During oogenesis, the anterior polar cells recruit 4-6 neighboring epithelial follicle cells to form the migratory border cell cluster. Border cells migrate through the dense nurse cell environment using guidance cues to reach their final target, the oocyte. This is an excellent, genetically tractable *in vivo* system to study conserved regulators of collective cell migration and invasion including cancer. Collective cell invasion is also observed in the primary malignant brain tumor glioblastoma. These cancer collectives are highly invasive and spread into the brain parenchyma leading to disease progression and poor patient prognosis. I performed a glioblastoma-related genetic screen to identify novel cell adhesion and adhesion regulatory proteins that contribute to collective border cell migration and brain tumor invasion. I identified

eight adhesion genes that disrupted border cell collective migration when knocked down: *α-catenin* (*α-Cat*), *Symplekin* (*Sym*), *Lachesin* (*Lac*), *roughest* (*rst*), *dreadlocks* (*dock*), *Wnt4*, *dachsous* (*ds*), and *fat* (*ft*). Bioinformatics analyses showed that subsets of the orthologous genes were enriched at the invasive edge of human glioblastoma patient tumors. Next, I demonstrated two mechanisms through which adhesion proteins are regulated during collective border cell migration. First, I showed that small GTPase Rap1 mediates E-cadherin distribution at border cell-border cell contacts during collective migration. Additionally, I found that Rap1 is spatially regulated in the border cell cluster by the conserved GTPase activating protein, Rapgap. Next, I correlated crosstalk between protein phosphatase 1 (Pp1) and the cadherin-catenin complex during collective cell migration. Further, knocking down *α-catenin* and other members of the cadherin-catenin complex in border cells caused the cluster to dissociate and fail to migrate. Through these experiments, I thus identified a role for the cadherin-catenin complex in keeping border cells attached to each other during migration. Pp1 promotes levels of cadherin-catenin complex members at cell-cell junctions and keeps the cells in the cluster connected. Overall, in my thesis I provide insights into conserved mechanisms that mediate collective cell migration and collective cancer cell invasion through cell adhesion proteins.

Roles of cell adhesion and adhesion regulatory proteins during collective cell migration and invasion

by

Nirupama Somappa Kotian

B.Sc., Kansas State University, 2011
M.Sc., University of Kansas, 2013

A DISSERTATION

submitted in partial fulfillment of the requirements for the degree

DOCTOR OF PHILOSOPHY

Division of Biology
College of Arts and Sciences

KANSAS STATE UNIVERSITY
Manhattan, Kansas

2022

Approved by:

Major Professor
Dr. Jocelyn A. McDonald

Copyright

Abstract

Collective cell migration is the highly dynamic and coordinated movement of groups of cells. Various types of collectives are crucial for embryogenesis, neural crest migration, mammary gland development and wound healing. Collective cell movements are also found in cancer, which leads to tumor spreading and invasion to secondary sites in the body. These tumor collectives are efficient at invading deeper into tissues and enhance resistance to available therapies. Cells in collectives are tightly connected to each other through cell-cell contacts, which allows the cells to stay together during migration. The cellular and molecular mechanisms that regulate cell-cell communication and adhesion during collective cell migration and collective tumor cell invasion are not well understood. Cell adhesion and adhesion-regulatory proteins therefore are strong candidates to regulate collective cell behaviors. In this thesis, I used the *Drosophila* ovary border cell system to identify mechanisms that regulate cell-cell adhesion during collective cell migration *in vivo*. The ovary is made of repeating subunits called egg chambers. Each egg chamber is enveloped by a monolayer of follicular epithelial cells that surround the oocyte, nurse cells and a pair of polar cells on each end. During oogenesis, the anterior polar cells recruit 4-6 neighboring epithelial follicle cells to form the migratory border cell cluster. Border cells migrate through the dense nurse cell environment using guidance cues to reach their final target, the oocyte. This is an excellent, genetically tractable *in vivo* system to study conserved regulators of collective cell migration and invasion including cancer. Collective cell invasion is also observed in the primary malignant brain tumor glioblastoma. These cancer collectives are highly invasive and spread into the brain parenchyma leading to disease progression and poor patient prognosis. I performed a glioblastoma-related genetic screen to identify novel cell adhesion and adhesion regulatory proteins that contribute to collective border cell migration and brain tumor invasion. I identified

eight adhesion genes that disrupted border cell collective migration when knocked down: *α-catenin* (*α-Cat*), *Symplekin* (*Sym*), *Lachesin* (*Lac*), *roughest* (*rst*), *dreadlocks* (*dock*), *Wnt4*, *dachsous* (*ds*), and *fat* (*ft*). Bioinformatics analyses showed that subsets of the orthologous genes were enriched at the invasive edge of human glioblastoma patient tumors. Next, I demonstrated two mechanisms through which adhesion proteins are regulated during collective border cell migration. First, I showed that small GTPase Rap1 mediates E-cadherin distribution at border cell-border cell contacts during collective migration. Additionally, I found that Rap1 is spatially regulated in the border cell cluster by the conserved GTPase activating protein, Rapgap. Next, I correlated crosstalk between protein phosphatase 1 (Pp1) and the cadherin-catenin complex during collective cell migration. Further, knocking down *α-catenin* and other members of the cadherin-catenin complex in border cells caused the cluster to dissociate and fail to migrate. Through these experiments, I thus identified a role for the cadherin-catenin complex in keeping border cells attached to each other during migration. Pp1 promotes levels of cadherin-catenin complex members at cell-cell junctions and keeps the cells in the cluster connected. Overall, in my thesis I provide insights into conserved mechanisms that mediate collective cell migration and collective cancer cell invasion through cell adhesion proteins.

Table of Contents

List of Figures

List of Tables

Acknowledgements

I am grateful for the career growth I had as a scientist during my PhD journey. Along with the hard work and efforts that goes behind getting a doctorate, the support and inspiration I received from many people during my journey was equally important.

First, I would like to thank my family who cheered me on through the toughest and best times of my journey from another continent in a different part of the world. As an international student and a first-generation college student, paving my career path was not straightforward. Being the first in the family to study abroad and a first to get a Ph.D., it was difficult to not have a role model or a guidance of any sort from the field. Leaving the kind of support and love from your family behind to move forward and not knowing what is coming next all while figuring things out by myself in a foreign country was scary. That being said, I am super proud of how far I have come, and I have my family to thank for that. They have been my biggest support especially my mother, **Shashikala Kotian**, my father **Somappa Kotian** and my brother **Nikhil Kotian**. Therefore, I feel grateful as I reflect back on my journey when I was a naïve undergrad navigating my interest and skills in research. It has been because of their encouragement and trust in me that I could accomplish this feat.

I would also like to extend my thanks to my mentor and major advisor, **Dr. Jocelyn McDonald** for her guidance and training throughout my graduate career. She has created a positive lab environment and allowed us space to grow as scientists. Her willingness to help us succeed and pushing graduate students to think out of the box to develop as independent scientists are qualities that I appreciate a lot. She is also very meticulous and that reflects in her approach, which trained me to be rigorous with my experiments. I am thankful to have learned skills like effective science illustration and communication which made me promote my research better. I would like

to also thank all the McDonald lab members for their support and willingness to help and for motivating me when I came across failures in experiments. I would also like to acknowledge the scientists of *Drosophila* community I had the privilege of knowing. A fun group of creative researchers who have made exceptional discoveries and continue to amaze the scientific community worldwide. I want to acknowledge the efforts of my committee members, **Drs. Erika Geisbrecht, Brad Olson, Jeroen Roelofs (former member) and Stephanie Shames** for their valuable inputs and for providing endless list of reference letters throughout my graduate training. Their inputs for my projects have been very helpful in steering my projects in the right direction. I also want to sincerely thank my first mentor from ACTREC in India, **Dr. Narendra Joshi** for training me during my Masters and research fellowship at ACTREC. I am very grateful to have started my biomedical research journey at this institute. I also want to thank the Graduate Student Council, KAWSE (K-state office for Advancement for Women in Science and Engineering) and the International Coordinating Council for all the leadership opportunities I had the honor to be a part of at K-State. Taking on different leadership roles and learning from my peers has been one of the best experiences in graduate school.

Finally, I want to thank my friends Shilpa Hebbar, Aakash Pandey, Shweta Tyagi and many more who I met in Manhattan and made this journey memorable. Thank you for constantly supporting, inspiring and cheering me on.

Dedication

In memory of my grandparents Mansa Salian, Kamala Maindan, Sanki Kotian and Raju Kotian

I dedicate this thesis to my grandparents and my parents, who I am forever grateful for. Their continuous support, unconditional love, and encouragement to pursue my ambitions was essential in my personal and career growth. A special remembrance in honor of my late grandfather, Mansa Salian, who passed away this month. Thank you Ajja for inspiring us to be better version of ourselves, we miss you. As a first-generation college student, I would also like to reflect on the sacrifices my mom and dad have made to make this accomplishment possible. Thank you for showing faith in me and giving me the confidence to navigate a career in STEM as I go on to become the first Ph.D. holder in the family.

1 Introduction

Collective cell migration is the coordinated movement of a group of cells fundamental for shaping and remodeling organs during development, wound healing, and tissue renewal (Friedl and Gilmour 2009; Scarpa and Mayor 2016). However, abnormal yet well-orchestrated movement of these cell clusters is also observed in cancers and contributes to disease progression (Weiss *et al.* 2022). Because multiple cells form the collective, each cell is regulated globally to function as a single unit by cellular and molecular mechanisms employed by the cells in the collective and the microenvironment. While there are similarities between collective and single cell migrations; there is one major difference. The group of cells remain connected to each other through stable cell contacts whereas single cells need to lose connections in order to migrate. Collective cell migration has been widely studied across invertebrate and vertebrate models using *in vivo* and *in vitro* systems to understand their role in development and disease. Collectives are also shown to promote tumor invasion and metastasis by providing a higher chance of survival to the cancer cells as compared to a single cell mode of migration (Aceto *et al.* 2014; Cheung *et al.* 2016; Haeger *et al.* 2019). However, the cellular and molecular pathways that mediate communication between cells clusters to stay connected and continue migrating are still unclear. Specifically, how adhesion mediated cell-cell communication translates to collective cell invasion in cancers is unknown. Identifying conserved mechanisms that regulate collective cell migration can further help reveal potential therapeutic targets for invasive cancers.

The *Drosophila* ovary border cell system is an excellent model to study *in vivo* collective cell migration. This is a genetically tractable and simple system that can help reveal multiple conserved pathways that govern collective cell migration. The ease of genetic manipulation and low maintenance costs along with the ability to perform high resolution live and fixed cell imaging

makes this a unique and powerful model. Importantly, about 75% of genes associated with diseases in humans have orthologs in *Drosophila* (Ugur *et al.* 2016). The fly community is ever expanding and provides access to reagents that are continuously evolving. The willingness to share these resources among community members, provides fly researchers critical opportunities to decipher and answer fundamental questions in biology. Overall, these advantages make the border cell model an ideal system to study collective cell movements *in vivo* and unravel mechanisms that drive collective cell migration and invasion.

In this dissertation, I defined a human glioblastoma-informed approach to identify cell adhesion and adhesion regulatory proteins involved in collective border cell migration and collective cancer cell invasion. Further, I also identified an additional role of cadherin-catenin complex members in maintaining the adhesion of border cells to each other. I contributed to revealing a mechanism that led to the identification of crosstalk between members of the cadherin-catenin complex, protein phosphatase 1, and a small GTPase that regulates overall collective border cell migration and cell-cell adhesion. These mechanisms further shape our understanding of conserved regulators that drive cell-cell communication during collective cell migration and collective cancer cell invasion.

1.1 Hallmarks of collective cell migration

Collective movement of cells utilizes cellular and molecular mechanisms which can be categorized into three hallmarks that ensure proper migration of collectives towards their target (Fig. 1.1). First, a collective polarizes to form a front-back axis which leads to an actin-rich protrusion at the front; second, a collective maintains cell adhesions to keep the cells of the collective together and third, a collective adheres to a extracellular substrate or other cells along its migration path. These processes must be coordinated at a supracellular level for the collective

to navigate through complex environments so that cells that were otherwise non-motile can now develop and maintain migratory abilities (Montell *et al.* 2012; Friedl and Gilmour 2009).

1.1.1 Follow the leader: leader cells and follower cell chemistry in a collective

When collectives migrate, cells at the front become the "brains" of the cluster, termed as leader cells, while those at the rear become follower cells. The leader cells sense guidance cues from the microenvironment, generate actin-rich protrusions to generate traction on the substrate and determine a path for the collective to follow (Fig 1.1). This front-rear orientation also exists in individual motile cells but in the case of the collective this must be synchronized to reflect the whole group. The front position of the leader cells plays in their favor to respond to the highest concentration of the extracellular cues while the followers maintain cell-cell contacts which can impair the formation of leading edge in these cells (Fig 1.1).

There can be multiple extracellular guidance signals in place to direct the leader cells of the cluster to drive movement of the collective including the extracellular matrix (ECM), soluble factors (chemokines, growth factors) and cells in direct contact (Scarpa and Mayor 2016; Mayor and Etienne-Manneville 2016). Generation of membrane protrusions such as filipodia and lamellipodia from the leader cells are crucial to initiate interaction with the substrate (ECM or other cells) and these protrusions are most often generated by F-actin polymerization. Protrusions are a result of ligand-receptor signaling mechanisms that activate CDC42 and/or RAC which leads to cytoskeletal remodeling and generation of actin rich protrusion at the leading edge of the migrating cluster (Friedl and Gilmour 2009; Haeger *et al.* 2015; Ilina and Friedl 2009). Forward-directed protrusions regardless of the cell type and substrate of migration allows the cluster to reach their target. Any impediment in this process, for example a short-lived protrusion in the wrong direction, or the wrong length or area of extension will cause disruption in collective

behaviors due to lack of directionality and forward traction forces (McDonald *et al.* 2008). Although an actin-rich pseudopod or lamellipodia generates traction for the follower cells in the rear to keep the cell sheets moving forward, cryptic protrusions are observed in follower cells of cultured epithelial cells (Farooqui and Fenteany 2005). These cryptic basal protrusions develop against the substrate in follower cells, towards the wound and allow cells in the rear to migrate actively on the substrate to enhance closure of wounds.

How do cells in collectives communicate with each other so that group moves forward? Leader cells gain a delicate balance between a mesenchymal- and epithelial-like state as they guide the cell cluster (Fig. 1.1). These front cells stay attached to their neighbors and maintain their epithelial- like state while generating protrusions and increased spreading like mesenchymal cells. Follower cells on the other hand primarily maintain epithelial characteristics staying connected to each other with cell-cell contacts. Communication with the follower cells is equally important to coordinate the migration of the entire group and is mediated by intercellular connections. When leaders generate traction at the front, followers need to respond to these forces and retract in the back to continue moving with the leader at the same time. This property of mechanosensing by cells is regulated by adherens junctions and focal adhesion proteins that undergo conformational changes and inducing signaling to transmit the forces from the leader cells (Mayor and Etienne-Manneville 2016; Friedl and Gilmour 2009). Leader and follower cells each display these characteristic behaviors for coordinating the dynamic process of collective migration. However, there are some cell types like border cells in the *Drosophila* ovary, the tip-stalk cells during sprouting angiogenesis and cultured MDCK cells during wound healing assays, that can swap leader cell positions with cells in the rear so that a new leader cell can take over (Montell *et al.*

2012; Jakobsson *et al.* 2010; Poujade *et al.* 2007). Whether leader cell switching occurs in other cell collectives during migration is still unknown.

1.1.2 Cell-cell adhesion and intercellular connection during collective cell migration

One of the major differences between an individual cell and collective cell migration is the maintenance of stable cohesive intercellular contacts in collectives. When single cells migrate, they attain a mesenchymal state and lose epithelial characteristics like adhesion in order to move (Friedl and Gilmour 2009). However, collectives maintain cell-cell contacts through adherens junction proteins, immunoglobulin superfamily members, tight junction proteins, integrins and connexins, and intracellular adhesion regulatory proteins (Fig. 1.2; Friedl and Wolf 2003; Theveneau and Mayor 2012; Collins and Nelson 2015; Friedl and Mayor 2017). These adhesion proteins recruit cytoskeletal proteins to directly or indirectly bind to actin and intermediate filament proteins to stabilize the attachment between cells during collective migration. Additionally, adhesion proteins also facilitate communication between leader and follower cells for transmission of physical forces during migration.

Most collectives rely on cadherin-dependent adhesions between cells (Friedl and Mayor 2017). Cadherins are crucial in regulating collective migration of cells in many developmental processes like the *Drosophila* ovary, vessel sprouting and branching morphogenesis of mammary gland (Friedl and Gilmour 2009; Scarpa and Mayor 2016). Cadherins are transmembrane glycoproteins that are intracellularly coupled to the actin cytoskeleton to maintain cohesion between cells (Fig. 1.2). Classical cadherins regulate binding through the cadherin-catenin complex which includes α-Catenin, β-Catenin and p120-Catenin and together form the adherens junction (Fig. 1.2). Cadherins are highly robust, though plastic, and have the ability to reorganize cell-cell contacts as the collective migrates through complex tissue environments through confined

spaces. Adherens junctions are also highly stable for hours to days (Ilina and Friedl 2009; Friedl and Mayor 2017). Additionally, protocadherins, a subgroup of the Cadherin superfamily regulate actin polymerization through the WAVE complex. Protocadherins have conserved cadherin repeats in their transmembrane regions but lack catenin binding sites in the cytoplasmic region (Hayashi and Takeichi 2015). The extracellular interactions between cadherins can either be homophilic or heterophilic and ensure a tight binding with the actin cytoskeleton (Takeichi 2014; Friedl and Mayor 2017).

Selective diffusion of solutes between two epithelial cells is regulated by tight junctions in vertebrates (Friedl and Mayor 2017; Friedl and Wolf 2003; Ilina and Friedl 2009; Matter and Balda 2003; Alberts *et al.* 2002). Tight junctions also have an additional role in keeping adjacent cells tightly sealed together with the help of three major transmembrane proteins–junctional adhesion molecules (JAM), occludins and claudins (Fig 1.2; Matter and Balda 2003). Tight junction proteins can activate β- integrins to promote collective migration of cancer cells *in vitro* (Mandicourt *et al.* 2007). Septate junctions in invertebrates are vertebrate tight junction equivalents, seeing as they both serve the same function of paracellular diffusion barriers (Fig. 1.2). Septate junctions can form very distinct bands between adjacent epithelial cells giving a ladder-like appearance. However, the molecular composition and structure of septate versus tight cell junctions are different between flies and vertebrates (Izumi and Furuse 2014). Some fly orthologs of vertebrate tight junction proteins in fact localize to the adherens junction and subapical complex. The subapical complex in flies is required for formation and establishing proper positioning of adherens junctions (Grawe *et al.* 1996; Tepass *et al.* 2001; Choi *et al.* 2011). Flies have two major types of septate junctions–the pleated septate junction (pSJ) and the smooth septate junction (sSJ). The pSJ

is found in ectoderm-derived epithelia, such as epidermis, salivary glands, hindgut, trachea, and imaginal discs and the sSJ in endoderm-derived epithelia (Tepass 2003).

In vertebrates, the third type of adhesion junction is the desmosome, which connects the intermediate filaments of adjacent cells by forming a meshwork of intracellular anchor proteins (Fig. 1.2; Friedl and Mayor 2017; De Pascalis and Etienne-Manneville 2017; Etienne-Manneville 2018). The anchor proteins plakoglobin and desmoplakin form a cytoplasmic plaque and connect the cytoskeleton of one cell to transmembrane adhesion proteins from the cadherin family called desmoglein and desmocollin. These junctions are found in most epithelial cells and heart muscle cells. During epidermal wound regeneration, migrating epithelial cell sheets maintain desmosomal cell-cell junctions as they crawl into the cell free space to initiate wound closure (Shaw and Martin, 2009). However, the presence of intermediate filaments in *Drosophila* remains controversial. While orthologous cytoplasmic intermediate filaments are absent in flies, a recent study identified an intermediate filament-like protein (Etienne-Manneville 2018; Cho *et al.* 2016). Future experiments will be required to confirm the functional roles of these intermediate-like filaments in flies.

Finally, other cell junctional proteins also play roles in collective cell migration. Immunoglobulin-like cell adhesion molecules (IgCAMs) are transmembrane cell adhesion molecules that possess one or more Immunoglobulin-like domains (Cavallaro and Christofori 2004; Friedl and Mayor 2017). IgCAMs are involved in regulating cell-cell and cell-matrix communication during cell migration in tissue morphogenesis and tumor metastasis (Cavallaro and Christofori 2004; van Kempen *et al.* 2000). They can form both homophilic and heterophilic interactions and contribute to a broad range of functions in nervous systems, endothelial cells and epithelial cells. Other cell junctions required during collective migration include gap junctions,

which act as intercellular hydrophilic channels and allow the size-restricted passage of molecules (Fig. 1.2; Friedl and Mayor 2017). Connexins are major gap junction proteins that mediate tight cell-cell connections and contribute to cell migration during wound healing and cancers (Friedl and Mayor 2017; Zhang *et al.* 2015). Finally, integrins are a superfamily of transmembrane cell adhesion proteins that connect the actin cytoskeleton and ECM by forming a focal adhesion complex (Friedl and Wolf 2003). Integrin dependent adhesions are required during both development like wound healing and neural crest migration and observed in collectively invading cancers (Friedl and Wolf 2003; Friedl and Mayor 2017).

1.1.3 Interaction of the collective with the extracellular substrate

As collectives migrate, they attach to the substrate and modify the connections with the substrate during migration. Collectives move through different types of substrates like basement membranes or other cells in the tissue (Fig. 1.1). Collectively migrating cells adhere to their substrates through heterodimeric (α- and a β-chain) cell-membrane receptors called integrins. Integrin dependent cell-substrate interaction promote directionality and regulate traction forces in the back of the cluster (Scarpa and Mayor 2016; Friedl and Mayor 2017). During blood vessel sprouting, a process involving generation of nascent blood vessels from existing ones, integrin dependent adhesions form between endothelial cells and the ECM. Integrins are also required during neural crest migration in Xenopus to connect with the fibronectin-rich substrate (Fig. 1.3C; Alfandari *et al.* 2003). However, *Drosophila* border cells migrate upon and between the nurse cells in the egg chamber instead of an ECM. Collective-substrate interaction in this type of migration is E-cadherin dependent (Niewiadomska *et al.* 1999; Cai *et al.* 2014). In this scenario, integrins are rather required for cell-cell cohesion than cell-ECM (Dinkins *et al.* 2008). In a similar zebrafish model, prechordal mesendoderm uses E-cadherin to migrate on epiblast (Montero *et al.* 2005).

Additionally, collectives also participate in two processes of modifying the substrate depending on the type of collective migration. They either modify the substrate by causing ECM degradation or generating a migration path by basement membrane deposition as they migrate. Degradation of local tissue ECM helps the collectives generate space and choose the path of least resistance for smooth migration (Gaggioli *et al.* 2007; Wolf *et al*. 2007; Ilina and Friedl 2009). This phenomenon is observed mainly in cancers as collectives invade through the ECM and metastasize (Wolf and Friedl 2009). ECM is also degraded by the endothelial tip (leader) cells during blood vessel sprouting using matrix metalloproteases (MMPs) (Fig. 1.3B; Yana *et al.* 2007*).* On the other hand, basement membrane deposition allows the collective to provide a migration scaffold instead. During mammary gland development, mammary ducts undergoing branching morphogenesis deposit basement membrane proteins through basal myoepithelial cells (Gudjonsson e*t al.* 2002; Ewald *et al*. 2012). This also occurs in vascular sprouting, during which endothelial cells cooperate with pericytes to deposit basement membrane proteins like laminins and Collagen IV (Brachvogel *et al.* 2007). Other than functioning as a migration track, basement membrane deposition also maintains cell polarization into apical and basolateral areas and allows polarized cell-substrate integrin-dependent adhesions (Gudjonsson *et al.* 2005; Brachvogel *et al.* 2007).

1.2 Collective cell migration in development

Diverse forms of collective cell movements occur in different types of tissues depending on the objective of the migration and the microenvironment they are migrating in (Fig. 1.3). These groups of cells either move as monolayers in the form of 2-dimensional (2D) sheets or as multicellular groups or strands through a three-dimensional (3D) epithelium. The next few

sections will cover the commonly observed variants of collective cell migration and *in vivo* collective cell model systems of *Drosophila* and zebrafish.

1.2.1 Types of collective cell migration

Epithelial cells can form a monolayer of cells to migrate through a 2D substrate. Cells are connected through adherens junctions to maintain a continuous monolayer and generate actin rich protrusions that lead the cell cluster (Fig. 1.1). This is observed after a sudden injury of any organ which initiates 2D sheet migration of epithelial or endothelial cells towards the free/ injured edge on a basement membrane to "close" the wound and trigger wound repair (Poujade *et al.* 2007; Fenteany *et al.* 2000).

Blood vessel sprouting is required during vascular regeneration during wound repair or simply for formation of new vessels during embryogenesis (Fig 1.3A). This type of collective movement involves new vessels sprouting from old existing vessels by coordinated regulation of endothelial cell proliferation and migration. Vascular sprouting also entails a front tip (leader) cell that responds to chemoattractants, protrudes multiple actin-rich filipodia and guides the movement of the follower stalk cells. Endothelial cells are tightly connected by VE-cadherin (vascular epithelial-cadherin) at cell-cell contacts during sprouting and migrate through a fibrin- and fibrinogen-rich ECM (Friedl and Gilmour 2009; Scarpa and Mayor 2016). Tight stable connections make way for formation of an open lumen to allow extension of new blood vessels. During migration the follower stalk cells also undergo proliferation to support the generation of nascent vessels. Endothelial tip cells respond to an extracellular gradient of vascular endothelial growth factor (VEGF) and upregulate expression of the Notch ligand Delta like-4 (Dll4) in the leader tip cells. This leads to downregulation of the VEGF receptor in neighboring cells. This competitive process for becoming a tip (leader) cell is called the lateral inhibition pathway. Tip endothelial

cells can switch positions with the follower cells during migration (Jakobsson *et al.* 2010). Vascular sprouting in zebrafish and mammals follow similar signaling and cell communication pathways as that found during tracheal morphogenesis in *Drosophila.* The *Drosophila* tracheal branching is an *in vivo* model to study branching of tubular organs. Fibroblast growth factor (FGF) ligand induces collective migration of tip cell and stalk cells from the primary branch of tracheal network to generate secondary branches during tracheogenesis in this model (Friedl and Gilmour 2009). This process also utilizes the Notch-Delta negative feedback that specify the tip leader cells to guide the cluster towards the extracellular ligand FGF.

After injury, the monolayer of epithelial cells lining organs become first responders, moving to heal wounds along with the combined efforts of the immune system. Epithelial cell sheets collectively migrate to the wound site and initiate wound closure by closing the cell free space caused by the wound (Fig. 1.3B). At the wound margin, epithelial cells at the cell free edge extend lamellipodial protrusions and start crawling together as cell sheets (Fenteany *et al.* 2000). Cells in all rows are tightly connected by cell-cell junction proteins like E-cadherin and desmosomes in keratinocytes, and the tight junction protein occludin in mice corneal epithelium during wound repair (Friedl and Gilmour 2009). These cell adhesions also transmit mechanical tension from the leading edge to the cell rows in the back (Fig. 1.3B; Vitorino *et al.* 2011). During skin wound healing, keratinocytes in the front rows rely on integrins to produce force on the substrate. Keratinocytes also cooperate with dermal fibroblasts to rebuild the basement membrane by depositing laminins and collagen IV as the epithelial sheets migrate (Smola *et al.* 1998; Nischt *et al.* 2007). During migration, guidance cues in the tissues involve growth factors such as FGF and Transforming growth factor beta (TGFβ) are signals secreted into the stroma to which the cell

sheets respond (Poujade *et al.* 2007). Eventually, sheets of epithelial cells migrate to ensure wound closure and conclude tissue repair.

1.2.2 Neural crest and Zebrafish lateral line

Neural crest cell migration

Neural crest (NC) cells are a transient embryonic cell population induced in vertebrates during embryogenesis (Fig. 1.3C). These cells collectively migrate as distinct streams from the interface between the neuroepithelium and ectoderm along the anterior-posterior axis of the embryo. NC cells detach from the neuroepithelium at the dorsal border of the neural plate and migrate to distant sites in the embryo. They eventually differentiate to form tissues and organs in the cephalic and trunk regions such as the craniofacial bones and cartilage, heart structures, and the enteric and peripheral nervous systems (Szabó and Mayor 2018; Theveneau and Mayor 2012). The distinct cell streams that are generated pursue a specific direction and migrate to either the cephalic or trunk regions are regulated by ligand-receptor signaling of Ephrin and Ephrin (Eph) receptors, and class 3-semaphorins with neuropilin/plexinA family of receptors. Further, a host of extracellular signaling factors like complement component factor C3a (secreted by NC cells), FGF, VEGF, Platelet-derived growth factor (PDGF) and Stromal cell-derived factor 1 (Sdf1) control NC cell migration through chemotaxis (Szabó and Mayor 2018).

NC cells undergo an epithelial to mesenchymal transition (EMT) and reduce stable cell-cell adhesions to become mesenchymal. EMT during NC cell delamination happens rather slowly and the cells are loosely attached to each other through transient cell-cell adhesions (Fig. 1.3C). The switch allows NC cells in contact to initiate a process termed Contact inhibition of Locomotion (CIL) (Abercrombie and Heaysman 1954). In this process, when a cell encounters another cell, it stops migrating in the direction of its partner (Fig. 1.3C). Instead, they move away from each other

and choose a different path for migration by either collapsing their protrusions or pausing their movement (Fig. 1.3C, right panel). In NC cells, cell adhesions and CIL work together to allow successful, guided migration (Olson and Nechiporuk 2018). Studies have confirmed that NC cells can switch from E-cadherin to N-cadherin expression to initiate CIL (Scarpa *et al.* 2015). Further, RhoA is known to break cell-substrate adhesions in the rear follower cells during collective migration, while Rac1 promotes forward actin-rich protrusion. In NC cells, Rac1 is excluded during CIL from the contact edge and inhibits protrusion in the direction of the contact. On the other hand, NC cells release C3a and attract individual cells to each other in a process called co-attraction (Theveneau and Mayor 2012). This generates a polarized collective ready to migrate, but they are at a risk of constant collisions. This is where a balance is created by CIL. CIL alone will lead to dispersion of NC cells but together with transient cell adhesion and a gradient of essential chemoattractants, the movement of collective cells in streams is maintained.

Zebrafish lateral line

The Zebrafish lateral line is a cohesive group of more than 100 cells called the posterior lateral line primordium (pLLP) that migrate anteroposteriorly along the lateral midline during embryogenesis from the anterior trunk to the tip of the tail region (Fig. 1.3D; Olson and Nechiporuk, 2018). During migration, pLLP deposits 20-30 cell clusters of proneuromasts from its trailing edge, which further differentiate into mechanosensory hair cell organs. Protoneuromasts are generated during NC cell migration by cell proliferation, and this is one example of a collective where cell proliferation and migration both need to be coordinated. Like any collective, this large cluster of cells also form a front-rear polarity with the front leader cells (2-3 tip cells) developing protrusions and the rear forming polarized rosettes of epithelial cells that are dropped off as

proneuromasts. The front tip cells sense the guidance cues from the environment and lead the cluster towards the tail region. The collective responds to the chemokine CXCL12/SDF-1, which is uniformly expressed along the fish horizontal myoseptum instead of in a gradient (Donà *et al.* 2013; Venkiteswaran *et al.* 2013; Olson and Nechiporuk 2018). Therefore, the differential expression of two chemokine receptors, Cxcr4b in the leader cells and Cxcr7b in the trailing edge cells of the collective are required for cells to detect the ligand CXCL12 and to create an internal gradient (Haas and Gilmour 2006; Dambly-Chaudière *et al.* 2007; Valentin *et al.* 2007). Cxcr4b is expressed in all the cells of the primordium; however, activation of Cxcr4b in the leading edge inhibits expression of Cxcr7b (Dambly-Chaudiere *et al*. 2007). Meanwhile in the trailing edge, Cxcr7b acts as a "CXCL12 ligand sink" by binding to the CXCL12 and internalizing CXCL12 with the receptor thereby inhibiting activation of Cxcr4 receptor in the trailing edge (Donà *et al.* 2013; Venkiteswaran *et al.* 2013; Olson and Nechiporuk 2018). This creates an internal gradient of CXCL12 within the primordium with high levels in the leading region and low levels in the trailing edge, thereby establishing directionality while maintaining front-back polarity.

Additionally, two signalling pathways, Wnt and Fgf are also required during pLLP migration (Aman and Piotrowski 2008; Lecaudey *et al.* 2008; Nechiporuk and Raible 2008). The canonical Wnt signaling pathway is active in the leading region and initiates expression of Fgf ligands which in turn activate Fgf signaling in trailing edge. Both these pathways also initiate the expression of inhibitory ligands to inhibit each other–Wnt in the trailing edge and Fgf in the leading edge. These pathways are not only required for maintaining polarity and migration but also contribute to cell proliferation and differentiation. A chemokine based internal gradient mediates front-back polarity; tightly connected cells along with these two major signaling pathways regulate the migration of pLLP in zebrafish embryos.

1.2.3 Migration of the collective border cell cluster in the *Drosophila* ovary

Another well-studied model with a hybrid EMT-like phenotype is the *Drosophila* ovary border cell system. In each ovary pair of a *Drosophila* female, strings of egg chambers that progress through different developmental stages are lined up together and resemble an "assembly line" (Fig. 1.4A). Egg chambers go through 14 developmental stages to form a mature egg (; Montell *et al.* 2012). Oogenesis starts with an anteriorly located germarium which consists of both germline and somatic cells. Progressively growing egg chambers then bud off from the germarium and develop in a stage-wise fashion (Bastock and St Johnston 2008). Each egg chamber is surrounded by a monolayer of somatic epithelial cells called the follicle cells (Fig. 1.4A and 1.4B; Montell *et al.* 2012). Follicular epithelial cells surround an oocyte and 15 support cells called nurse cells and are derived from the germline precursor in the germarium. Nurse cells nourish and support the developing oocyte by dumping the nutrients through the intercellular ring canals (Mahajan-Miklos and Cooley 1994). In the follicular epithelial monolayer, there are two pairs of cells specified on each side of the egg chamber called the polar cells starting as early as stage 1. These cells initiate the signaling mechanisms for specification of the border cell cluster. Once the cluster is specified, the collective detaches from the epithelium and migrates approximately 150µm through dense nurse cells to reach the posteriorly located oocyte (Fig 1.4 B). Towards late oogenesis, once border cells reach the oocyte, they contribute to the formation of micropyle through which sperm enters and fertilizes the oocyte. Without border cells, the micropyle is deformed and fertility is compromised (Montell *et al.* 1992).

At stage 8, anterior polar cells recruit 4-6 neighboring follicular epithelial cells to form the border cell cluster with the non-motile polar cells in the center (Fig. 1.4B,C; Montell *et al.* 2012).

Polar cells secrete a cytokine called Unpaired (Upd) which activates the Janus-Kinase- signal transducer and activator of transcription (JAK-STAT) signaling pathway in the neighboring follicle epithelial cells (Harrison *et al.* 1998; Montell *et al.* 2012). Follicle cells with the strongest STAT levels and closest to the polar cells respond to UPD and differentiate into the border cell cluster. STAT activation through UPD further activates the C/EBP transcription factor SLBO which in turn switches on a cascade of genes required for border cell migration (Montell *et al.* 1992; Borghese *et al.* 2006; Wang *et al.* 2006). STAT expression levels are also crucial in determining the number of follicle epithelial cells that will be fated to become migratory border cells Silver and Montell 2001; Xi *et al.* 2003; Van de Bor *et al.* 2011; Montell *et al.* 2012).

Once the cluster detaches from the epithelium and starts migration, there is a front-rear polarity established in the collective (Fig. 1.4C). Front leader cells develop long and stable actin-rich protrusions in response to the guidance cues from the microenvironment. The oocyte at the anterior end secretes PVF1 (platelet-derived growth factor (PDGF)- and vascular endothelial growth factor (VEGF)-related factor 1), Spitz, Gurken, and Keren (Duchek and Rørth 2001; McDonald *et al.* 2006). Border cells (and all follicle cells) express two receptor tyrosine kinases (RTKs): PVR, which binds to PVF1, and Epidermal growth factor receptor (EGFR), which binds to Spitz, Gurken and Keren (Duchek and Rørth 2001; Duchek *et al.* 2001; McDonald *et al.* 2003; 2006), to induce Rac signaling and stimulate generation of protrusion in the leader cell (Murphy and Montell 1996; Wang *et al.* 2010). Additionally, Engulfment and cell motility (Elmo) and RacGEF Myoblast city (Mbc) regulate Rac signaling during border cell migration (Geisbrecht *et al.* 2008; Bianco *et al.* 2007). Later, the RTK pathway also activates MAPK signaling and JNK signaling to inhibit active protrusion in the follower cells (Bianco *et al.* 2007; Wang *et al.* 2010). Another receptor called Tie was also identified but its ligand is still unknown (Wang *et al.* 2006).

During migration, border cells rotate in the first early phase of migration and towards the later phase undergo increased tumbling (Poukkula *et al.* 2011). PVF1 guides the first phase of the migration, and the second phase of tumbling movement is guided by EGF alone. Ectopic expression of EGFR ligands alters the direction of the border cell cluster and downregulating either of the receptors causes severe border cell migration defects (Duchek and Rørth 2001; Duchek *et al.* 2001; McDonald *et al.* 2006; 2003). Previous studies have shown that the RTKs involved in border cell migration undergo endocytosis through the recycling endosome pathway mediated by two small GTPases, Rab5 and Rab11 (Assaker *et al.* 2010; Ramel *et al.* 2013). A trafficking loop between the plasma membrane of border cells and the recycling endosomes allows for spatial localization of active receptors at the leading edge.

A developmental timing cue is also required along with guidance cues for border cells to start and finish migration at the correct time. Arriving too late or too early at the oocyte disrupts the developmental timeline during egg chamber development. The timing of border cell migration is controlled by the insect steroid hormone, ecdysone released in the ovary **(**Riddiford1993**).** Ecdysone levels are highest at stage 9 but levels rise initially during stage 8 when border cells are about to start migration. The ecdysone receptor complex consists of ecdysone receptor (EcR) and Ultraspiracle (USP) which interacts with co-activator Taiman (TAI) (Montell 2003; Bai *et al.* 2000). Activation of these receptors leads to binding of this complex to DNA and transcription of downstream target genes required for border cell migration. These three proteins together control collective border cell migration in response to ecdysone (Jang *et al.* 2009).

Generation of actin-rich protrusion from the leading edge is a characteristic hallmark of leader cells that is displayed during border cell migration (Fig 1,4 C). It is crucial to restrict the leading protrusions in the front leader cell(s) and multiple pathways come into play during this

process. Guidance cues like PVF1 and EGFR generate a strong forward-bias for protrusions in the leader cells (Poukkula *et al.* 2011; Prasad and Montell 2007). Additionally, the guidance receptor signaling pathway turns on Rac activity in the border cell cluster where it is highly enriched in the lead cell (Wang *et al.* 2010). Rac, a small GTPase from the Rho superfamily of GTPases is polarized in the border cell cluster and this asymmetric Rac activity in the lead cell generates a single protrusion and senses direction to lead the whole group. Inhibiting Rac activity in the leader cell causes the follower cells to protrude in all directions, causing the cluster to stop migrating. Therefore, Rac also limits the single protrusion to the front cell and allows protrusion retraction in cells of the rear of the cluster (Wang *et al.* 2010). Additionally, the anti-apoptotic protein, *Drosophila* inhibitor of apoptosis 1 (DIAP1) also regulates border cell migration through Rac (Geisbrecht and Montell 2004). Here, DIAP1 functions in an apoptotic-independent role to regulate Rac-dependent actin dynamics in border cells during migration.

Polarization of the border cell cluster is not limited to the leading and trailing edges. Pre-migration, apical proteins like Partitioning defective 3 or Bazooka (Par3), partitioning defective 6 (Par6) and atypical protein kinase C (aPKC) are enriched in the apical region of follicle cells and polar cells whereas the Lethal giant larvae (LGL), and Scribble polarity proteins localize to basolateral junctions (Pinheiro and Montell 2004; Montell *et al.* 2012; Campanale *et al.* 2022). During migration, the apical markers are now oriented orthogonally to the direction of migration in border cells, establishing an apical-basal polarity in the cluster (Montell *et al.* 2012). Both front-back and apico-basal polarity are required for cell-cell communication and successful migration of the border cell cluster. Additionally, apical-basal polarity in border cells is regulated by the Jun N-terminal Kinase (JNK) signaling cascade (Llense and Martín-Blanco 2008). JNK signaling pathway also maintains cluster shape and cohesion by potentially mediating Rho GTPase Cell

division cycle (Cdc42). Disrupting JNK activity in border cells causes abnormal integrin and myosin VI (MyoVI) localization to the leading edge (Llense and Martín-Blanco 2008). The JNK pathway finally activates transcription factors Jun and Jra which regulate cell cohesion. The transcription factor Hindsight (Hnt) limits JNK activity, finally giving rise to a cohesive cluster (Melani *et al.* 2008).

Continued communication between cells of a collective is crucial to keep the cells intact during migration. Border cells also rely on E-cadherin dependent cell-cell adhesion during border cell migration (Niewiadomska *et al.*1999; Cai *et al.* 2014). In addition, E-cadherin also regulates mechanotransduction mediated signaling in the border cells to control the protrusion force in the leading edge. Details about cell adhesion and adhesion regulatory proteins will be discussed further in the next section.

1.2.4 Cell-cell adhesion in collective border cell migration

Collective cell movements depend on stable cell-cell and cell-matrix adhesions. Cell adhesion and adhesion regulatory systems include adherens junctions, IgCAMs, septate junctions and focal adhesions that together regulate collective cell migration. In border cells, E-cadherin was identified to maintain adhesion and keep the cells tightly connected (Niewiadomska *et al.*1999; Cai *et al.* 2014). E-cadherin serves multiple functions during border cell migration and is required in three major cell-cell contacts in the egg chamber. First, E-cadherin levels are the highest between polar cells and is required to maintain adhesion of border cells to the cluster (Cai *et al.* 2014). Reducing E-cadherin levels between polar cells leads to cluster dissociation. Next, E-cadherin between nurse cell/border cell contacts provides traction for border cell movement (Cai *et al.* 2014). Additionally, E-cadherin works in a feedback loop with small GTPase Rac and guidance receptor signaling to generate a stable protrusion at the front in the direction of the

migration. Using a photoactivable form of Rac, Wang and others (2010) previously showed that activating Rac in any cell of the cluster causes other cells to retract protrusions and follow the cell with the highest Rac activity. Further, knocking down E-cadherin in border cells mimics the direction sensing defects seen in guidance receptor mutants. Reducing E-cadherin in border cells also alters the distribution of Rac in the cluster. Finally, between the border cell contacts, E-cadherin is required for cell-cell communication by sensing and transmitting mechanical forces between the front leader cells and cells in the rear. When an F-actin rich protrusion is generated in the cell during cell movement, it can push out the plasma membrane and build up stress on the actin cytoskeleton through E-cadherin mediated adhesions. E-cadherin is intracellularly connected to F-actin through cytoskeletal binding partners, β-catenin and α-catenin, which are also enriched between border cells and polar cells, within the border cells and within polar cells (Sarpal *et al.* 2012; Peifer 1993). The tension received during front protrusion is regulated by contractile actomyosin filaments. Using an E-cadherin tension sensor to measure the tensile forces generated in the front versus back of cluster, Cai and others, demonstrated that E-cadherin functions as a mechanotransducer in the border cells (Cai *et al.* 2014). This ensures that border cells in the rear can retract protrusions as the front develops a major protrusion and leads the cluster during migration. E-cadherin acts in a feedback loop between the actin-based cytoskeletal network, Rac and guidance receptor signaling to generate stable forward protrusion and maintain directionality of the cluster. Additionally, MyoVI, a motor protein that regulates actin filaments, is also required for stabilization of border cell E-cadherin dependent adhesion (Geisbrecht and Montell 2002).

Collectives migrate through an extracellular substrate; however, border cells migrate on a substrate of nurse cells instead of a matrix. As border cells migrate between nurse cells, border cells continue to form weak E-cadherin based adhesions with the nurse cells and these adhesions

are retracted in the rear so that the follower cells can go along with leader cells. While integrins are known to play a role in connecting collectives to the ECM, integrin-based adhesion are required to keep the cells connected to each other rather than to regulate cell-matrix contacts (Llense and Martín-Blanco 2008; Montell *et al.* 2012).

1.3 Collective cell migration in cancer

Metastasis remains one of the major hallmarks of cancer and therapeutic strategies targeting mechanisms that contribute to this phenomenon are of interest in the cancer field (Hanahan and Weinberg 2011; Hanahan 2022). Cancer cells are highly plastic and employ different modes of invasion including single cell, and collective mode of compact clusters or elongated strands (Fig. 1.5; Fig. 1.6; Friedl and Wolf 2003; Friedl *et al.* 2012). Typically, epithelial cancer cells were thought to invade and metastasize by undergoing loss of E-cadherin and acquiring mesenchymal characteristics through epithelial to mesenchymal transition (Friedl *et al.* 2012). However, cancer cells can migrate as compact clusters or elongated strands and when required can switch from a collective mode to a disseminated individual mode through EMT (Fig. 1.5; Friedl and Wolf 2003). Collectively migrating cancer cells are frequently observed in different cancer types including oral squamous cell carcinomas, squamous cell carcinomas and breast cancers (Ilina and Friedl 2009; Cheung and Ewald 2016; Christiansen and Rajasekaran 2006). The molecular and cellular mechanisms that facilitate collective cell migration during development and regeneration are comparable to those involved in collective cancer cell invasion. *In vitro* 2D and 3D models are excellent resources to provide insight into mechanisms that regulate collective cell invasion. However, the ability to assess live time-lapse imaging of collectives in *in vivo* models during development is very powerful. Specifically, analysis of collective cell dynamics as the

cluster migrates and responds to extracellular signals has led to scientific advancement in the field (Friedl *et al*. 2012; Friedl and Gilmour 2009).

1.3.1 Diversity of migration modes in cancer

Cancer cells exhibit phenotypic plasticity, in that epithelial cancer cells can migrate either as multicellular sheets or strands, single cells or collective clusters and often switch between a single and collective mode depending on extracellular stimuli (Friedl *et al*. 2012; Scheel and Weinberg 2011; Ilina *et al.* 2018). Single cell mode of invasion can occur through both an amoeboid or mesenchymal-like movement (Fig. 1.5; Fig. 1.6). This process is mediated through epithelial to mesenchymal transition (EMT) and is observed in many epithelial cancers. In this model, loss of cell-cell adhesion and increase in mesenchymal markers like vimentin and N-cadherin is required to achieve a mesenchymal "migratory" state (Fig. 1.5). Pathways like growth factor and MAPK signaling or upregulation of MMPs and integrins are responsible for downregulation of E-cadherin based adhesions. Tumor cells that undergo EMT further disseminate into secondary sites where they may undergo a mesenchymal to epithelial transition (MET) to form secondary tumors (Celià-Terrassa and Kang 2016). However, recent evidence suggests that an individual, complete EMT program is not necessarily binary but instead consists of a range of mixed cell migration behaviors (Jolly *et al.* 2015; Pastushenko *et al.* 2018; Braga and Ewald 2018; Padmanabhan *et al.* 2019; Haerinck and Berx 2021). A partial or incomplete EMT mode maintains both mesenchymal and epithelial features of tumor cells and enables collective migration of cancer cells. In this case, cell-cell contacts are weakly maintained in cancer cells giving them the benefit of a collective cluster with high plasticity to switch to a high colonization mode by gaining stem-like properties (Jolly *et al.* 2015). Mesenchymal cells can also undergo a single cell mesenchymal to secondary single cell amoeboid transition (MAT) where cells undergo cell shape change from

elongated to roundish shape and cell-matrix and cell-cell interactions are weakened (Fig. 1.5, 1.6; Friedl and Wolf 2003; Friedl and Alexander 2011; Friedl *et al*. 2012). These are commonly observed in lymphomas and small-cell lung carcinomas (Friedl *et al*. 2012; Friedl and Wolf 2003).

Cancer cells however also use collective modes of invasion, the most common invasion pattern of carcinomas (Friedl and Wolf 2003; Friedl *et al.* 2012). Advantages of invading cell collectives include having better survival capabilities due to group dynamics and drug resistance which helps bypass different bottlenecks that cancer cells face during metastasis as compared to mesenchymal-only single cell mode of invasion. Collectively invading cancer cells either migrate as strands of one-two cells in diameter or as bigger collective clusters seen in breast and prostate carcinomas (Fig. 1.5, 1.6; Christiansen and Rajasekaran 2006). Neuronal-like networks of connected cells are also observed in highly invasive cancers like glioblastoma (Friedl and Mayor 2017; Volovetz e*t al.* 2020). Multiple factors such as cell-cell contacts, cell-matrix contacts and degradation of ECM together determine the final size and shape of the collective (Fig. 1.6; Friedl *et al.* 2012). Comparable to collective migration systems during development, cancer cell collectives also possess cell adhesion-based mechanics that tightly connect invasive cell clusters with front-rear polarity and ability to modify the substrate as they migrate. However, cells can also migrate in multicellular streams as observed in the neural crest migration model. Cells in this migration mode type are connected by transient, weak cell adhesions and often guided by a chemokine gradient. Individual cells in this group interact with the matrix to generate traction force instead of relying on cell-cell contacts for communication. This allows the cells to travel faster as compared to collective clusters. Multicellular streaming has been observed in breast and melanoma tumors (Friedl *et al.* 2012).

1.3.2 Factors contributing to collective cell invasion

Collective cancer cell invasion also mimics multiple molecular and cellular mechanisms that regulate collective cell migration during development. Local matrix degradation is one of the classic hallmarks of collectives to generate a migration track as they invade from the primary tumor site. The ECM is a network of secreted macromolecules that provides physical scaffolding and biochemical signals to the cells. The ECM is composed of collagens, fibronectins, and laminins, which together form a supportive fibrous meshwork (Frantz *et al.* 2010). Fibrillar collagen is one of the most abundant proteins and forms the backbone of ECM. Cell surface matrix metalloproteases like Mt1-MMP and MMP2 are localized to the leading edge of colon adenocarcinoma cells and fibrosarcoma cells *in vitro* (Fig 1.6; Nabeshima *et al. 2000*; Wolf *et al.* 2007). These proteases start degrading the ECM by cleaving collagen fibers and initiating proteolysis (Wolf *et al.* 2007). This proteolysis provides a head start for the collective to remodel the ECM and drive dissemination of cancer cells to secondary sites. Additionally, the composition of the tumor microenvironment determines the extent of cell-matrix interactions and whether cells choose a single or collective mode of migration. *In vitro* experiments with 3D ECM showed that a denser extracellular matrix switches mesenchymal cancer cell migration mode from single to collective (Haeger *et al.* 2014). This is achieved by attaining cell-cell adhesion, front-rear polarity and transitioning to sheet-like migration called cell jamming.

Next, guidance signals or growth factors like SDF1 and FGF, which are essential in neural crest migration and endothelial sheet migration, also stimulate collective cell invasion of *in vitro* cancer cells (Grünert *et al.* 2003). During collective invasion, the leading cells will protrude in response to chemokines to generate a forward movement (Wolf *et al.* 2007). Finally, maintaining cell-cell contacts in an invading collective keeps the cells in a cluster together (Ilina and Friedl

2009). The role of cell adhesion during collective invasion of cancers is explained in detail in the next section.

1.3.3 Cell adhesion proteins during collective cell invasion

Collective cancer cell invasion relies on a myriad of cell adhesion mechanisms that keeps groups of cells connected during movement (Fig 1.6). Along with adherens junctions, cancer cells utilize Ig superfamily members, gap junctions, desmosomes and tight junctions to maintain cell adhesion (Friedl and Mayor 2017). Epithelial-derived cancers and melanomas that invade collectively in the form of sheets or multicellular strands maintain stable adhesions through cadherin superfamily members like E-cadherin, N-cadherin, VE-cadherin and cadherin-11 (Friedl and Wolf 2003). Immunoglobulin family members like activated leukocyte cell adhesion molecule (ALCAM) and L1 cell adhesion molecule (L1CAM), regulate homophilic cell-cell interactions between cells of a collective and are upregulated in highly invasive melanoma and colorectal carcinomas (Fig. 1.6; Friedl and Alexander 2011; Friedl and Wolf 2003; Cavallaro and Christoforri 2004; van Kempen *et al.* 2000; Gavert *et al.* 2008). Desmosomes, connected to the intermediate filament network are also maintained at cell junctions during collective invasion of cancers such as colorectal adenocarcinomas and melanomas (Friedl and Wolf 2003; De Pascalis and Etienne-Manneville 2018). Expression of intermediate filament protein keratin is upregulated in breast cancer cells and hepatocellular carcinomas (Cheung *et al.* 2013; Etienne-Manneville 2018; Leduc and Etienne-Manneville 2015). Integrins that connect cells to the ECM are also required for collective invasion of melanoma clusters (Hegerfeldt *et al.* 2002). Tight junction proteins are detected in invasive edges on squamous cell carcinomas and melanomas *in vitro* (Langbein *et al.* 2003). Gap junctions mediated by connexins form both homotypic and heterotypic cell

connections in squamous cell carcinomas, melanomas and prostate cancer cells (Ito *et al.* 2006; Zhang *et al.* 2015).

However, during EMT cell-cell junctions are lost between cancer cells (Kalluri and Weinberg 2009). Cell junctions including cadherins, tight junctions, gap junctions and desmosomes are reprogrammed and downregulated (Friedl and Mayor 2017). Proteolytic cleavage of E-cadherin mediated by proteases and upregulation of EMT-inducing transcription factors like Snail and Slug are some of the key reprogramming events that help epithelial cells achieve mesenchymal state (Fig. 1.6; Cavallaro and Christoforri 2004). Loss of E-cadherin also reorganizes actin cytoskeleton through Rho GTPases (Cavallaro and Christoforri 2004; Kalluri and Weinberg 2009). These reprogramming events work together to achieve single cell invasion mode by gaining mesenchymal characteristics. Though EMT is not restricted to a single cell behavior and instead displays a range of intermediate behaviors known as partial EMT in which cells are loosely connected to each other during invasion (Jolly *et al.* 2015).

1.4 Using the *Drosophila* ovary border cell system to answer cell adhesion-related open questions during collective movement of cells

With the high impact of collective cell invasion in cancers leading to disease progression and worse patient outcomes, it is crucial to explore mechanisms that target cell adhesion molecules. Primary malignant tumors like glioblastoma present with a very low survival rate and high degree of invasion to adjacent brain parenchyma that hampers treatment strategies. Current approaches to study cancer cell invasion use *in vitro* 3D ECM-based assays that utilize the ability of cancer cells to invade an artificial substrate mimicking the cancer microenvironment. *In vivo* cancer cell invasion experiments involve less genetically accessible approaches like injection of

3D spheroids into the skin tissue of mice (Alexander *et al.* 2008). Alternatively, the *Drosophila* border cell model has been a classical *in vivo* model to study conserved regulators of collective cell migration and invasion. Analysis of collective cell dynamics via live time-lapse imaging and high conserved homology with human disease-related genes makes this an ideal model to identify conserved targets of collective cell movements.

Preliminary data from the lab combining the *Drosophila* border cell model and the glioblastoma model, identified a regulator of collective cell invasion (Volovetz *et al.* 2020). Here, I applied a similar approach to answer the following questions- How do cell collectives maintain cell-cell contacts and coordinate movement of multiple cells? Are there specific conserved cell adhesions and adhesion-regulatory mechanisms required during collective migration and cancer cell invasion? Border cells maintain strong cell-cell contacts through E-cadherin mediated adherens junctions and actin regulatory proteins like Myosin VI that stabilize E-cadherin dependent adhesion (Cai *et al*. 2014; Niewiadomska *et al*. 1999; Montell *et al*. 2012; Geisbrecht and Montell 2002). Additionally, many other adhesion proteins are also expressed in border cells but their roles in collective migration and cohesion of border cell cluster have not yet been studied. Careful dissection of intercellular cell adhesion and adhesion regulatory mechanisms in border cells can identify potential therapeutic targets for invasive cancers.

Through a targeted glioblastoma-related RNAi screen in border cells, I identified eight adhesion-related genes required for border cell migration and subsets of the orthologous adhesion genes that were highly expressed in invasive glioblastoma patient tumors. Interestingly, KIRREL1 and KIRREL2, both human orthologs of Roughest were downregulated in the invasive regions. I was also able to correlate crosstalk between a small GTPase and a protein phosphatase with E-cadherin distribution in migrating border cells. This approach also confirms highly conserved

cellular mechanisms across flies and humans that can be exploited to determine pathways required for migration and development. Further experiments to reveal their direct role in collective cell invasion will further strengthen our understanding of conserved regulators that control cell adhesion during collective cell movements.

1.5 Figures

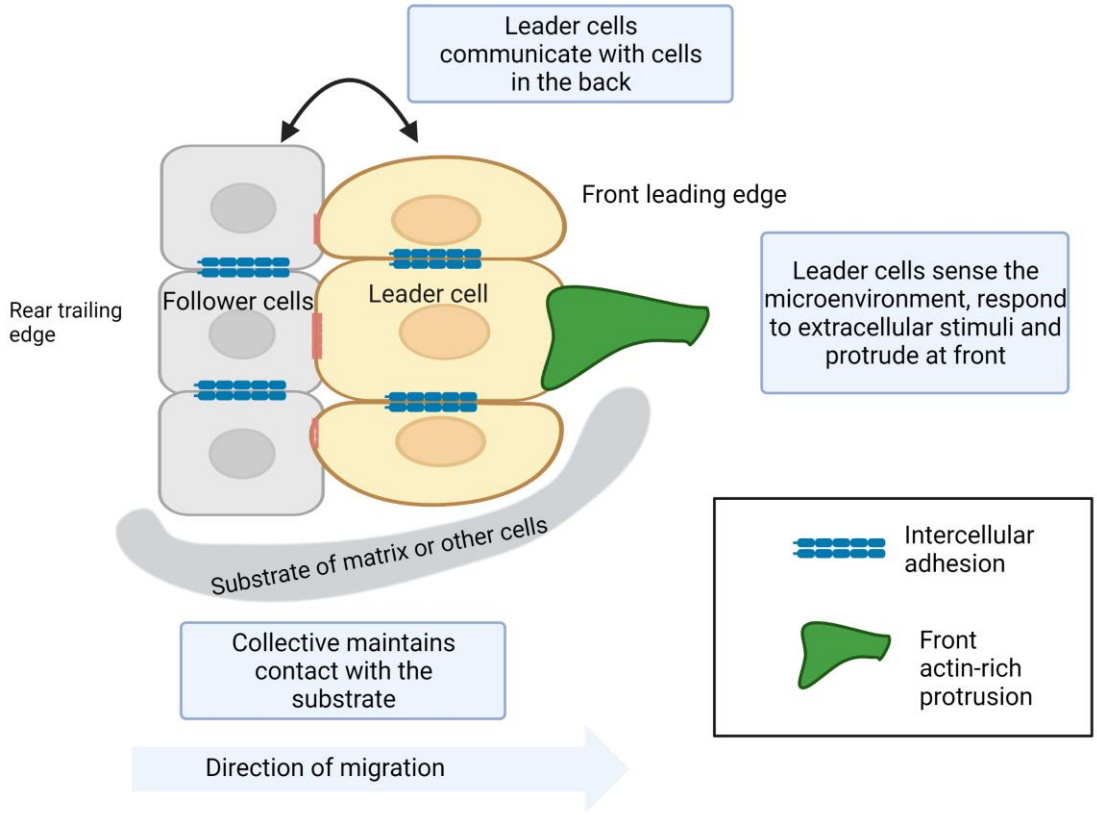

Figure 1.1 Overview of three hallmarks of collective cell migration.

A polarized collective with leader cells at the front of the cluster, protruding at front and followers in the back all connected through cell adhesions migrating on a substrate (Created with Biorender.com).

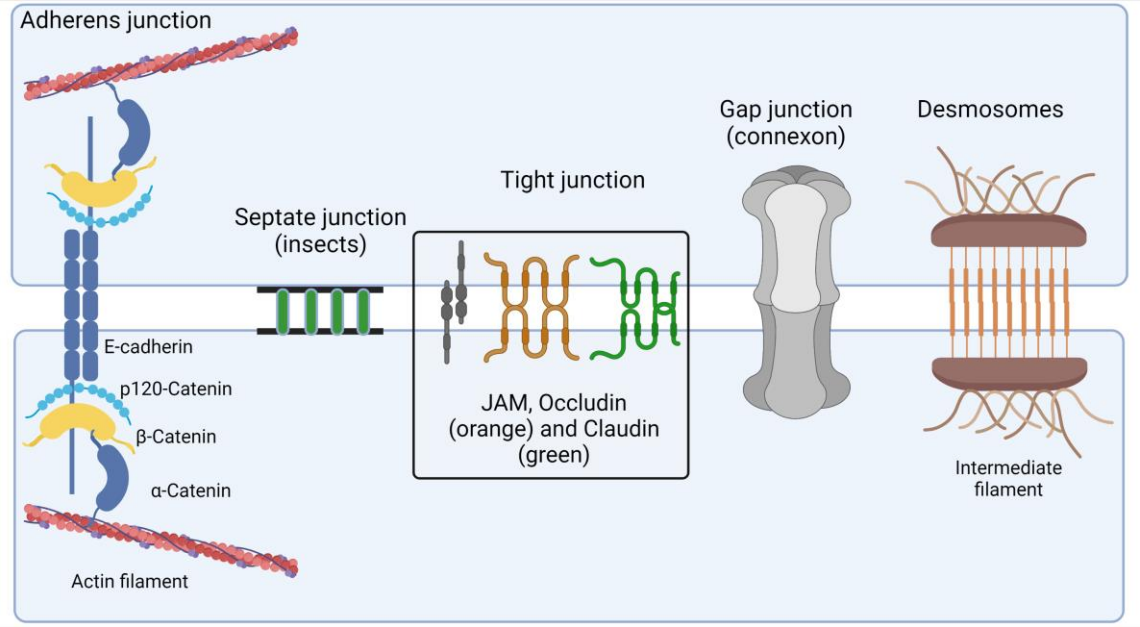

Figure 1.2 Schematic of intercellular cell adhesion proteins required during collective cell migration. E-cadherin dependent adherens junction connects to the cytoskeletal actin filaments through cadherin-catenin complex. Septate junctions, functional equivalents of tight junctions in insects are required for paracellular solute diffusion. Tight junctions are multiprotein junctional complexes in vertebrates and three major transmembrane tight junction proteins are Junctional adhesion molecules (JAM), Occludins and Claudins. Gap junctions are formed by channel forming proteins connexins that allow direct transfer of ions and small molecules between neighboring cells. Six connexins come together to form a pore called a connexon. Desmosomes consist of desmosomal cadherin proteins that connect intermediate filaments of adjacent cells and maintain adhesion (Created with Biorender.com).

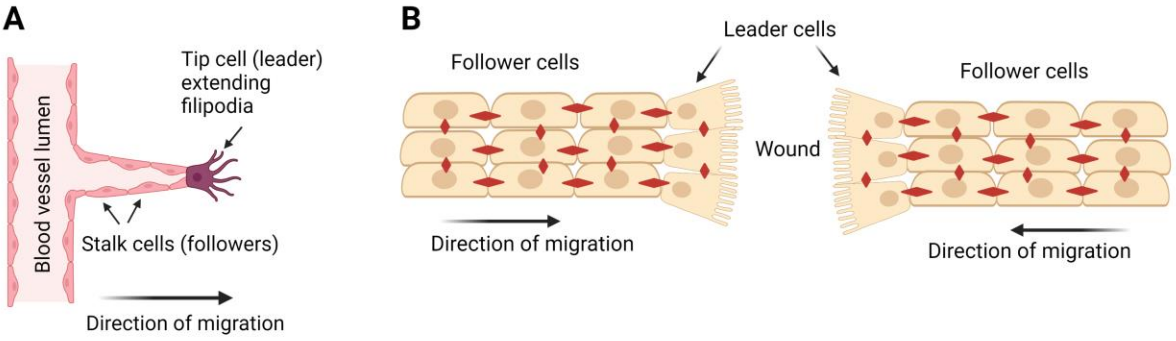

Vascular sprouting **Wound healing**

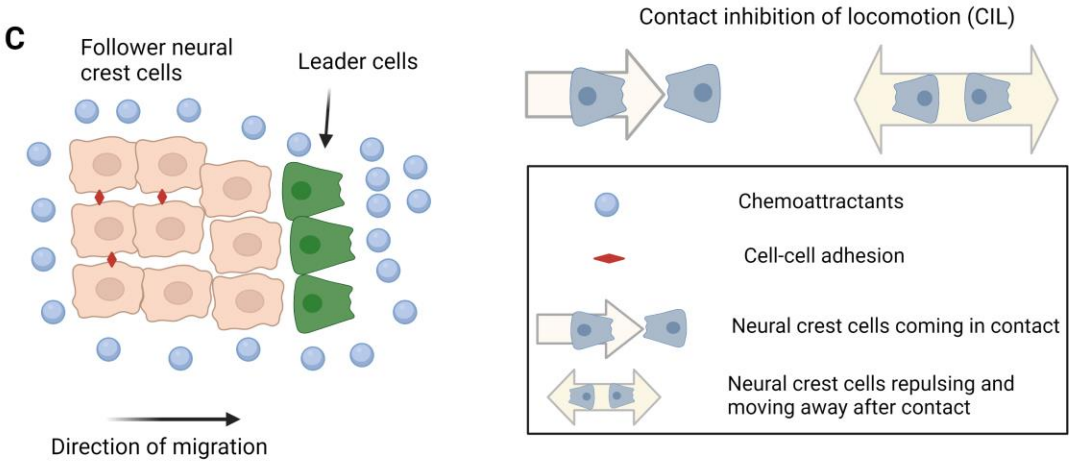

Neural crest cell migration

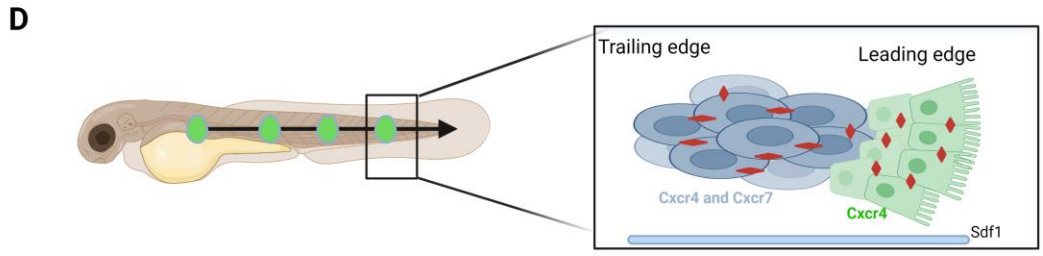

Zebrafish lateral line migration

Figure 1.3 Schematic of models of collective cell migration in development.

A) Schematic shows vascular sprouting or formation of new blood vessels led by a filipodia extending tip (leader) cell. Stalk cells in the back are interconnected by cell adhesions and follow the tip cell while undergoing cell proliferation allowing the new vessel to grow. B) Epithelial sheet migration during wound healing. To repair a wound, epithelial cells on both sides of the wound act as leader cells and migrate collectively in sheets and close the gap. Cells are tightly connected by stable cell adhesion (red) and follower cells move in sheets with the leader cells that develop protrusions and sense the microenvironment. Cell adhesions transmit force to pull the epithelial sheet closer and generate cryptic protrusions in the follower cells. These protrusions are generated below the cells in front of them (not shown). C) Loosely attached neural crest cells migrate collectively by staying connected through transient adhesions (red) during embryogenesis. These cells migrate in response to a chemoattractant, complement factor c3a. Through contact inhibition of locomotion (CIL), a repulsive response is initiated between cells that come in contact with each other. During CIL, transient adhesions ensure the protrusions in contact are quickly disassembled and a new one formed away from the point of contact allowing them to change their migration path. D) Zebrafish lateral line primordium (green) migrating from head to the trunk of the embryo (left panel). A closeup view on the right shows the primordium distinguished based on the patterning of SDF1/CXCL12 receptors. The primordium tightly connected by cell adhesions (red) collectively migrates by sensing the SDF1 chemokine; cells in the leading edge use the Cxcr4 receptor and in the trailing edge express Cxcr7 along with Cxcr4 to respond to SDF1 which differentiates them from the leading edge. Created with Biorender.com

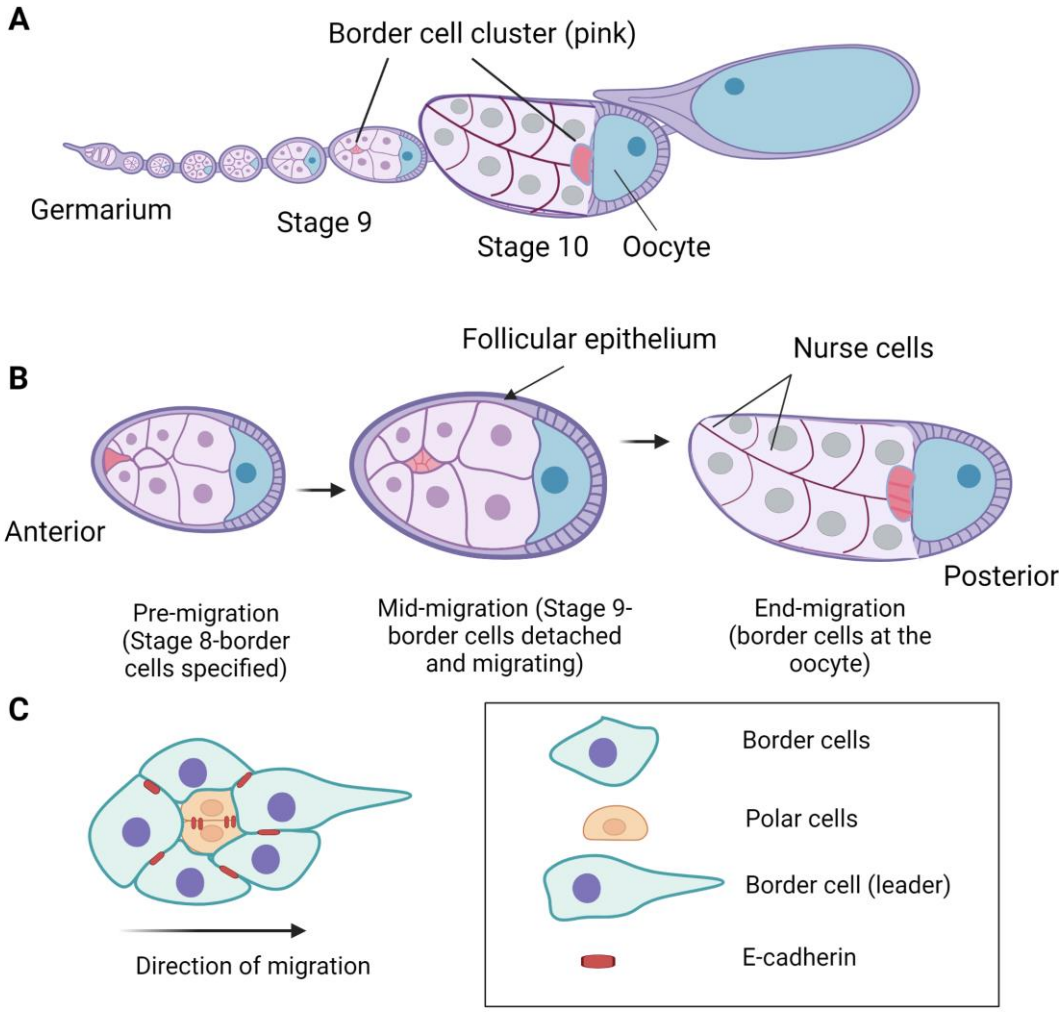

Figure 1.4 Border cells migrate collectively during *Drosophila* oogenesis.

A) Stages of *Drosophila* oogenesis in an ovariole. Egg chambers developing from the germarium undergo progressively grow to form the mature egg. Border cell cluster (pink) starts migration in stage 9 and finishes migrating to the posteriorly located oocyte in stage 10. B) Schematic of border cell migration in detail. Border cells are specified from the follicular epithelium by the anterior polar cell in stage 8. The cluster detaches from the epithelium to migrate towards the oocyte through dense nurse cells in stage 9. C) Close-up of the tightly connected border cell cluster. Non-motile polar cells in the center of the cluster migrate along with the border cells. Leader cell at the

front generates a protrusion in response to growth factors and cells in the cluster are connected by stable cell-cell adhesions (red). Created with Biorender.com

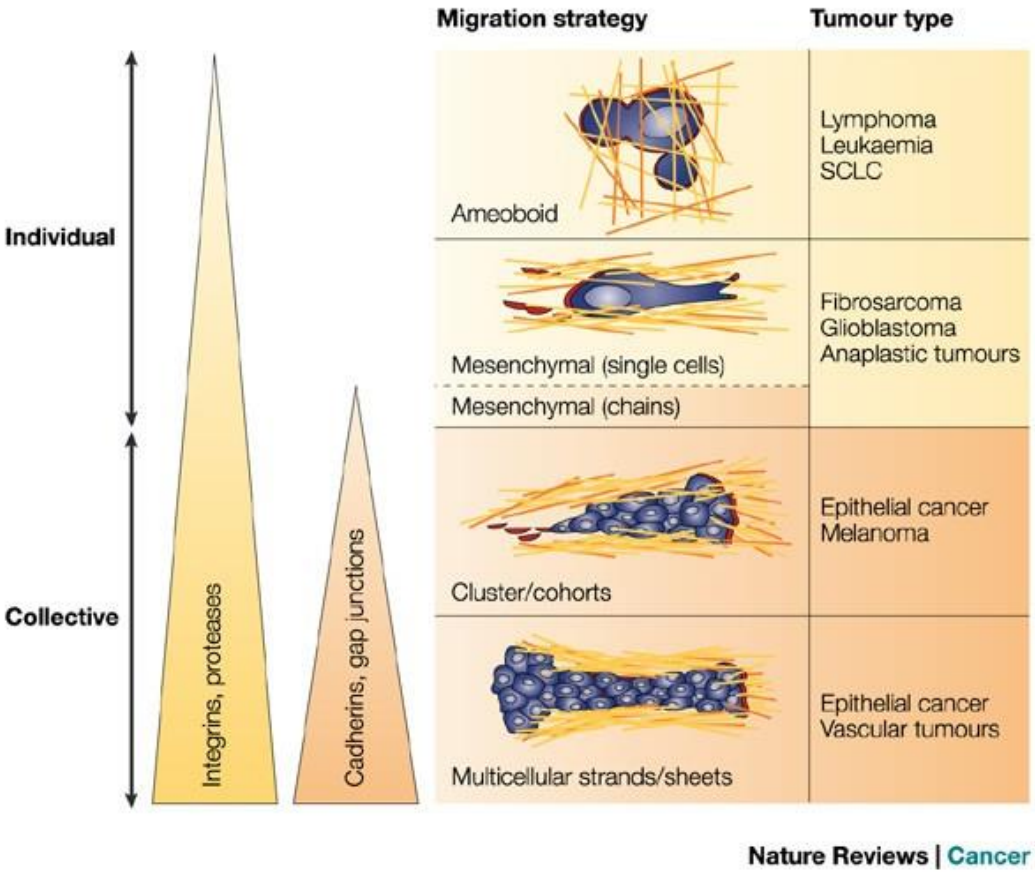

Figure 1.5 Migration modes of cancer cells including collective and single modes of invasion. From the bottom, cancers invade in collective mode either as multicellular strands or clusters and maintain high intercellular adhesion. Moving up to the top are individual modes of invasion, where cell-cell junctions are lost, and single cells begin migrating. High levels of integrins and proteases are required to start movement of single cells also known as epithelial-mesenchymal transition (EMT). Amoeboid cells can originate from a primary tumor or as a result of secondary transition of mesenchymal cells to amoeboid cells known as mesenchymal to amoeboid transition (MAC). Reused with permission from Springer Nature, Friedl and Wolf, 2003.

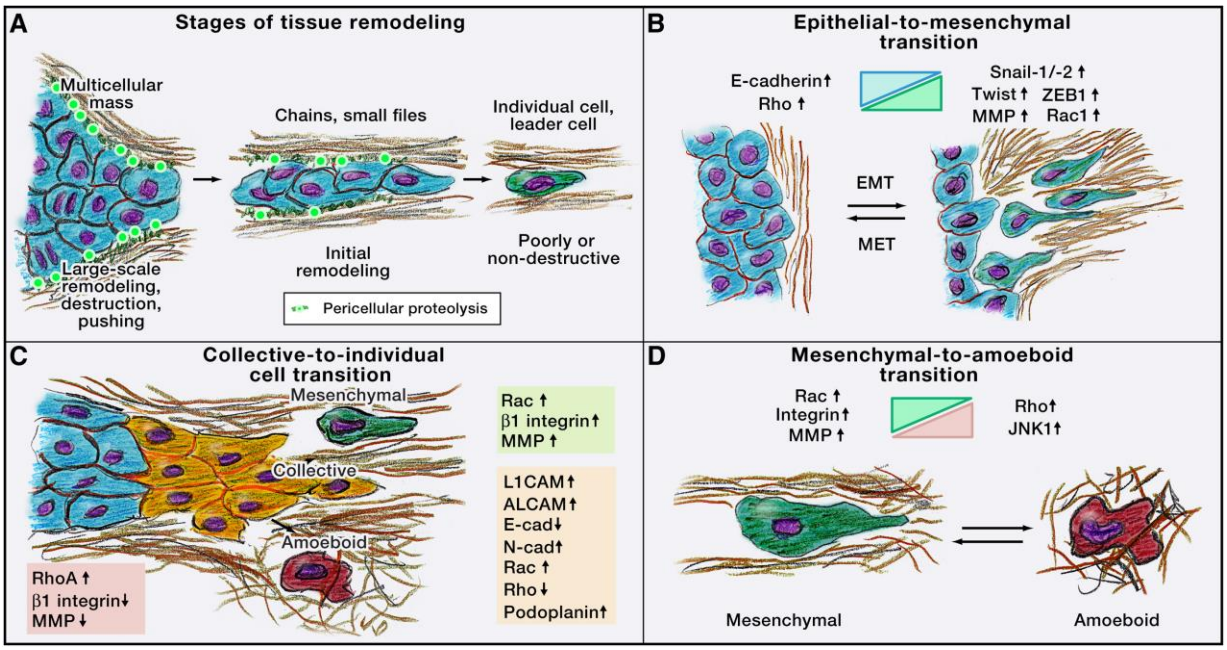

Figure 1.6 Factors contributing to different cancer variants

A) Process of tissue remodeling from a primary tumor to collective and to a single cell. B-D) Transition of cancer modes from epithelial to mesenchymal (EMT), collective to mesenchymal or amoeboid single cell mode and a mesenchymal to amoeboid mode with markers like transcription factors, cell adhesion proteins, proteolytic enzymes, small GTPAses and kinases contributing to the transition. Reused with permission from Cell, Friedl and Alexander 2011.

1.6 References

Abercrombie, M., and J. E. Heaysman, 1954 Observations on the social behaviour of cells in tissue culture. II. Monolayering of fibroblasts. Exp Cell Res 6: 293–306.

Aceto, N., A. Bardia, D. T. Miyamoto, M. C. Donaldson, B. S. Wittner *et al.*, 2014 Circulating tumor cell clusters are oligoclonal precursors of breast cancer metastasis. Cell 158: 1110–1122.

Alberts, B., A. Johnson, J. Lewis, M. Raff, K. Roberts *et al.*, 2002 Cell Junctions. Molecular Biology of the Cell. 4th edition.

Alfandari, D., H. Cousin, A. Gaultier, B. G. Hoffstrom, and D. W. DeSimone, 2003 Integrin alpha5beta1 supports the migration of Xenopus cranial neural crest on fibronectin. Dev Biol 260: 449–464.

Alexander, S., G. E. Koehl, M. Hirschberg, E. K. Geissler, and P. Friedl, 2008 Dynamic imaging of cancer growth and invasion: a modified skin-fold chamber model. Histochem Cell Biol 130: 1147–1154.

Aman, A., and T. Piotrowski, 2008 Wnt/β-Catenin and Fgf Signaling Control Collective Cell Migration by Restricting Chemokine Receptor Expression. Developmental Cell 15: 749–761.

Assaker, G., D. Ramel, S. K. Wculek, M. González-Gaitán, and G. Emery, 2010 Spatial restriction of receptor tyrosine kinase activity through a polarized endocytic cycle controls border cell migration. Proc Natl Acad Sci U S A 107: 22558–22563.

Bai, J., Y. Uehara, and D. J. Montell, 2000 Regulation of Invasive Cell Behavior by Taiman, a *Drosophila* Protein Related to AIB1, a Steroid Receptor Coactivator Amplified in Breast Cancer. Cell 103: 1047–1058.

Bastock, R., and D. S. Johnston, 2008 *Drosophila* oogenesis. Current Biology 18: R1082–R1087.

Bianco, A., M. Poukkula, A. Cliffe, J. Mathieu, C. M. Luque *et al.*, 2007 Two distinct modes of guidance signalling during collective migration of border cells. Nature 448: 362–365.

Borghese, L., G. Fletcher, J. Mathieu, A. Atzberger, W. C. Eades *et al.*, 2006 Systematic analysis of the transcriptional switch inducing migration of border cells. Dev Cell 10: 497–508.

Brachvogel, B., F. Pausch, P. Farlie, U. Gaipl, J. Etich *et al.*, 2007 Isolated Anxa5+/Sca-1+ perivascular cells from mouse meningeal vasculature retain their perivascular phenotype *in vitro* and *in vivo*. Exp Cell Res 313: 2730–2743.

Braga, V. M., and A. J. Ewald, 2018 Editorial Overview: Integration of dynamic processes in cell behaviour and tissue architecture. Curr Opin Cell Biol 54: iii–v.

Cai, D., S.-C. Chen, M. Prasad, L. He, X. Wang *et al.*, 2014 Mechanical feedback through E-cadherin promotes direction sensing during collective cell migration. Cell 157: 1146–1159.

Campanale, J. P., J. A. Mondo, and D. J. Montell, 2022 Specialized protrusions coordinate migratory border cell cluster cohesion via Scribble, Cdep, and Rac. 2022.01.04.474957.

Cavallaro, U., and G. Christofori, 2004 Cell adhesion and signalling by cadherins and Ig-CAMs in cancer. Nat Rev Cancer 4: 118–132.

Celià-Terrassa, T., and Y. Kang, 2016 Distinctive properties of metastasis-initiating cells. Genes Dev. 30: 892–908.

Cheung, K. J., E. Gabrielson, Z. Werb, and A. J. Ewald, 2013 Collective Invasion in Breast Cancer Requires a Conserved Basal Epithelial Program. Cell 155: 1639–1651.

Cheung, K. J., and A. J. Ewald, 2016 A collective route to metastasis: Seeding by tumor cell clusters. Science 352: 167–169.

Cheung, K. J., V. Padmanaban, V. Silvestri, K. Schipper, J. D. Cohen *et al.*, 2016 Polyclonal breast cancer metastases arise from collective dissemination of keratin 14-expressing tumor cell clusters. PNAS 113: E854–E863.

Cho, A., M. Kato, T. Whitwam, J. H. Kim, and D. J. Montell, 2016 An Atypical Tropomyosin in *Drosophila* with Intermediate Filament-like Properties. Cell Rep 16: 928–938.

Choi, W., K.-C. Jung, K. S. Nelson, M. A. Bhat, G. J. Beitel *et al.*, 2011 The single *Drosophila* ZO-1 protein Polychaetoid regulates embryonic morphogenesis in coordination with Canoe/afadin and Enabled. Mol Biol Cell 22: 2010–2030.

Christiansen, J. J., and A. K. Rajasekaran, 2006 Reassessing epithelial to mesenchymal transition as a prerequisite for carcinoma invasion and metastasis. Cancer Res 66: 8319–8326.

Collins, C., and W. J. Nelson, 2015 Running with neighbors: coordinating cell migration and cell-cell adhesion. Curr Opin Cell Biol 36: 62–70.

Dambly-Chaudière, C., N. Cubedo, and A. Ghysen, 2007 Control of cell migration in the development of the posterior lateral line: antagonistic interactions between the chemokine receptors CXCR4 and CXCR7/RDC1. BMC Dev Biol 7: 23.

De Pascalis, C., and S. Etienne-Manneville, 2017 Single and collective cell migration: the mechanics of adhesions. MBoC 28: 1833–1846.

Dinkins, M. B., V. M. Fratto, and E. K. Lemosy, 2008 Integrin alpha chains exhibit distinct temporal and spatial localization patterns in epithelial cells of the *Drosophila* ovary. Dev Dyn 237: 3927–3939.

Donà, E., J. D. Barry, G. Valentin, C. Quirin, A. Khmelinskii *et al.*, 2013 Directional tissue migration through a self-generated chemokine gradient. Nature 503: 285–289.

Duchek, P., and P. Rørth, 2001 Guidance of cell migration by EGF receptor signaling during *Drosophila* oogenesis. Science 291: 131–133.

Duchek, P., K. Somogyi, G. Jékely, S. Beccari, and P. Rørth, 2001 Guidance of cell migration by the *Drosophila* PDGF/VEGF receptor. Cell 107: 17–26.

Etienne-Manneville, S., 2018 Cytoplasmic Intermediate Filaments in Cell Biology. Annual Review of Cell and Developmental Biology 34: 1–28

Ewald, A. J., R. J. Huebner, H. Palsdottir, J. K. Lee, M. J. Perez *et al.*, 2012 Mammary collective cell migration involves transient loss of epithelial features and individual cell migration within the epithelium. J Cell Sci 125: 2638–2654.

Farooqui, R., and G. Fenteany, 2005 Multiple rows of cells behind an epithelial wound edge extend cryptic lamellipodia to collectively drive cell-sheet movement. Journal of Cell Science 118: 51–63.

Fenteany, G., P. A. Janmey, and T. P. Stossel, 2000 Signaling pathways and cell mechanics involved in wound closure by epithelial cell sheets. Curr Biol 10: 831–838.

Frantz, C., K. M. Stewart, and V. M. Weaver, 2010 The extracellular matrix at a glance. J Cell Sci 123: 4195–4200.

Friedl, P., and K. Wolf, 2003 Tumour-cell invasion and migration: diversity and escape mechanisms. Nat Rev Cancer 3: 362–374.

Friedl, P., and D. Gilmour, 2009 Collective cell migration in morphogenesis, regeneration and cancer. Nat Rev Mol Cell Biol 10: 445–457.

Friedl, P., and S. Alexander, 2011 Cancer invasion and the microenvironment: plasticity and reciprocity. Cell 147: 992–1009.

Friedl, P., J. Locker, E. Sahai, and J. E. Segall, 2012 Classifying collective cancer cell invasion. Nat Cell Biol 14: 777–783.

Friedl, P., and R. Mayor, 2017 Tuning Collective Cell Migration by Cell–Cell Junction Regulation. Cold Spring Harb Perspect Biol 9: a029199.

Gaggioli, C., S. Hooper, C. Hidalgo-Carcedo, R. Grosse, J. F. Marshall *et al.*, 2007 Fibroblast-led collective invasion of carcinoma cells with differing roles for RhoGTPases in leading and following cells. Nat Cell Biol 9: 1392–1400.

Gavert, N., M. Sheffer, S. Raveh, S. Spaderna, M. Shtutman *et al.*, 2007 Expression of L1-CAM and ADAM10 in human colon cancer cells induces metastasis. Cancer Res 67: 7703–7712.

Geisbrecht, E. R., and D. J. Montell, 2002 Myosin VI is required for E-cadherin-mediated border cell migration. Nat Cell Biol 4: 616–620.

Geisbrecht, E. R., and D. J. Montell, 2004 A Role for Drosophila IAP1-Mediated Caspase Inhibition in Rac-Dependent Cell Migration. Cell 118: 111–125.

Geisbrecht, E. R., S. Haralalka, S. K. Swanson, L. Florens, M. P. Washburn *et al.*, 2008 Drosophila ELMO/CED-12 interacts with Myoblast city to direct myoblast fusion and ommatidial organization. Dev Biol 314: 137–149.

Gudjonsson, T., M. C. Adriance, M. D. Sternlicht, O. W. Petersen, and M. J. Bissell, 2005 Myoepithelial cells: their origin and function in breast morphogenesis and neoplasia. J Mammary Gland Biol Neoplasia 10: 261–272.

Grawe, F., A. Wodarz, B. Lee, E. Knust, and H. Skaer, 1996 The *Drosophila* genes crumbs and stardust are involved in the biogenesis of adherens junctions. Development 122: 951–959.

Grünert, S., M. Jechlinger, and H. Beug, 2003 Diverse cellular and molecular mechanisms contribute to epithelial plasticity and metastasis. Nat Rev Mol Cell Biol 4: 657–665.

Haas, P., and D. Gilmour, 2006 Chemokine Signaling Mediates Self-Organizing Tissue Migration in the Zebrafish Lateral Line. Developmental Cell 10: 673–680.

Haeger, A., M. Krause, K. Wolf, and P. Friedl, 2014 Cell jamming: collective invasion of mesenchymal tumor cells imposed by tissue confinement. Biochim Biophys Acta 1840: 2386–2395.

Haeger, A., K. Wolf, M. M. Zegers, and P. Friedl, 2015 Collective cell migration: guidance principles and hierarchies. Trends in Cell Biology 25: 556–566.

Haerinck, J., and G. Berx, 2021 Partial EMT takes the lead in cancer metastasis. Developmental Cell 56: 3174–3176.

Hanahan, D., 2022 Hallmarks of Cancer: New Dimensions. Cancer Discovery 12: 31–46.

Hanahan, D., and R. A. Weinberg, 2011 Hallmarks of cancer: the next generation. Cell 144: 646–674.

Harrison, D. A., P. E. McCoon, R. Binari, M. Gilman, and N. Perrimon, 1998 Drosophila unpaired encodes a secreted protein that activates the JAK signaling pathway. Genes Dev 12: 3252–3263.

Hayashi, S., and M. Takeichi, 2015 Emerging roles of protocadherins: from self-avoidance to enhancement of motility. J Cell Sci 128: 1455–1464.

Hegerfeldt, Y., M. Tusch, E.-B. Bröcker, and P. Friedl, 2002 Collective cell movement in primary melanoma explants: plasticity of cell-cell interaction, beta1-integrin function, and migration strategies. Cancer Res 62: 2125–2130.

Ilina, O., and P. Friedl, 2009 Mechanisms of collective cell migration at a glance. Journal of Cell Science 122: 3203–3208.

Ilina, O., L. Campanello, P. G. Gritsenko, M. Vullings, C. Wang *et al.*, 2018 Intravital microscopy of collective invasion plasticity in breast cancer. Dis Model Mech 11: dmm034330.

Ito, A., Y.-I. Koma, K. Uchino, T. Okada, C. Ohbayashi *et al.*, 2006 Increased expression of connexin 26 in the invasive component of lung squamous cell carcinoma: significant correlation with poor prognosis. Cancer Lett 234: 239–248.

Izumi, Y., and M. Furuse, 2014 Molecular organization and function of invertebrate occluding junctions. Semin Cell Dev Biol 36: 186–193.

Jakobsson, L., C. A. Franco, K. Bentley, R. T. Collins, B. Ponsioen *et al.*, 2010 Endothelial cells dynamically compete for the tip cell position during angiogenic sprouting. Nat Cell Biol 12: 943–953.

Jang, A. C.-C., Y.-C. Chang, J. Bai, and D. Montell, 2009 Border cell migration requires integration of spatial and temporal signals by the BTB protein Abrupt. Nat Cell Biol 11: 569–579.

Jolly, M. K., M. Boareto, B. Huang, D. Jia, M. Lu *et al.*, 2015 Implications of the Hybrid Epithelial/Mesenchymal Phenotype in Metastasis. Frontiers in Oncology 5:.

Kalluri, R., and R. A. Weinberg, 2009 The basics of epithelial-mesenchymal transition. J Clin Invest 119: 1420–1428.

Langbein, L., U.-F. Pape, C. Grund, C. Kuhn, S. Praetzel *et al.*, 2003 Tight junction-related structures in the absence of a lumen: occludin, claudins and tight junction plaque proteins in densely packed cell formations of stratified epithelia and squamous cell carcinomas. Eur J Cell Biol 82: 385–400.

Lecaudey, V., G. Cakan-Akdogan, W. H. J. Norton, and D. Gilmour, 2008 Dynamic Fgf signaling couples morphogenesis and migration in the zebrafish lateral line primordium. Development 135: 2695–2705.

Leduc, C., and S. Etienne-Manneville, 2015 Intermediate filaments in cell migration and invasion: the unusual suspects. Curr Opin Cell Biol 32: 102–112.

Llense, F., and E. Martín-Blanco, 2008 JNK Signaling Controls Border Cell Cluster Integrity and Collective Cell Migration. Current Biology 18: 538–544.

Mahajan-Miklos, S., and L. Cooley, 1994 Intercellular Cytoplasm Transport during *Drosophila* Oogenesis. Developmental Biology 165: 336–351.

Mandicourt, G., S. Iden, K. Ebnet, M. Aurrand-Lions, and B. A. Imhof, 2007 JAM-C regulates tight junctions and integrin-mediated cell adhesion and migration. J Biol Chem 282: 1830–1837.

Matter, K., and M. S. Balda, 2003 Signalling to and from tight junctions. Nat Rev Mol Cell Biol 4: 225–237.

Mayor, R., and S. Etienne-Manneville, 2016 The front and rear of collective cell migration. Nat Rev Mol Cell Biol 17: 97–109.

McDonald, J. A., E. M. Pinheiro, and D. J. Montell, 2003 PVF1, a PDGF/VEGF homolog, is sufficient to guide border cells and interacts genetically with Taiman. Development 130: 3469–3478.

McDonald, J. A., E. M. Pinheiro, L. Kadlec, T. Schupbach, and D. J. Montell, 2006 Multiple EGFR ligands participate in guiding migrating border cells. Dev Biol 296: 94–103.

McDonald, J. A., A. Khodyakova, G. Aranjuez, C. Dudley, and D. J. Montell, 2008 The PAR-1 serine/threonine kinase regulates epithelial detachment and directional protrusion of migrating border cells. Curr Biol 18: 1659–1667.

Melani, M., K. J. Simpson, J. S. Brugge, and D. Montell, 2008 Regulation of cell adhesion and collective cell migration by hindsight and its human homolog RREB1. Curr Biol 18: 532–537.

Montell, D. J., P. Rorth, and A. C. Spradling, 1992 slow border cells, a locus required for a developmentally regulated cell migration during oogenesis, encodes *Drosophila* C/EBP. Cell 71: 51–62.

Montell, D. J., 2003 Border-cell migration: the race is on. Nat Rev Mol Cell Biol 4: 13–24.

Montell, D. J., W. H. Yoon, and M. Starz-Gaiano, 2012 Group choreography: mechanisms orchestrating the collective movement of border cells. Nat Rev Mol Cell Biol 13: 631–645.

Montero, J.-A., L. Carvalho, M. Wilsch-Bräuninger, B. Kilian, C. Mustafa *et al.*, 2005 Shield formation at the onset of zebrafish gastrulation. Development 132: 1187–1198.

Murphy, A. M., and D. J. Montell, 1996 Cell type-specific roles for Cdc42, Rac, and RhoL in Drosophila oogenesis. Journal of Cell Biology 133: 617–630.

Nabeshima, K., T. Inoue, Y. Shimao, Y. Okada, Y. Itoh *et al.* Front-Cell-specific Expression of Membrane-Type 1 Matrix Metalloproteinase and Gelatinase A during Cohort Migration of Colon Carcinoma Cells Induced by Hepatocyte Growth Factor/Scatter Factor. 7.

Nechiporuk, A., and D. W. Raible, 2008 FGF-Dependent Mechanosensory Organ Patterning in Zebrafish. Science 320: 1774–1777.

Niewiadomska, P., D. Godt, and U. Tepass, 1999 DE-Cadherin is required for intercellular motility during *Drosophila* oogenesis. J Cell Biol 144: 533–547.

Nischt, R., C. Schmidt, N. Mirancea, A. Baranowsky, S. Mokkapati *et al.*, 2007 Lack of Nidogen-1 and -2 Prevents Basement Membrane Assembly in Skin-Organotypic Coculture. Journal of Investigative Dermatology 127: 545–554.

Olson, H. M., and A. V. Nechiporuk, 2018 Using Zebrafish to Study Collective Cell Migration in Development and Disease. Front Cell Dev Biol 6: 83.

Padmanaban, V., I. Krol, Y. Suhail, B. M. Szczerba, N. Aceto *et al.*, 2019 E-cadherin is required for metastasis in multiple models of breast cancer. Nature 573: 439–444.

Pastushenko, I., A. Brisebarre, A. Sifrim, M. Fioramonti, T. Revenco *et al.*, 2018 Identification of the tumour transition states occurring during EMT. Nature 556: 463–468.

Peifer, M., 1993 The product of the *Drosophila* segment polarity gene armadillo is part of a multi-protein complex resembling the vertebrate adherens junction. J Cell Sci 105 (Pt 4): 993–1000.

Pinheiro, E. M., and D. J. Montell, 2004 Requirement for Par-6 and Bazooka in Drosophila border cell migration. Development 131: 5243–5251.

Prasad, M. & Montell, D. J. Cellular and molecular mechanisms of border cell migration analyzed using time-lapse live-cell imaging. *Dev. Cell* **12**, 997–1005 (2007).

Poukkula, M., A. Cliffe, R. Changede, and P. Rørth, 2011 Cell behaviors regulated by guidance cues in collective migration of border cells. Journal of Cell Biology 192: 513–524.

Poujade, M., E. Grasland-Mongrain, A. Hertzog, J. Jouanneau, P. Chavrier *et al.*, 2007 Collective migration of an epithelial monolayer in response to a model wound. Proc Natl Acad Sci U S A 104: 15988–15993.

Ramel, D., X. Wang, C. Laflamme, D. J. Montell, and G. Emery, 2013 Rab11 regulates cell–cell communication during collective cell movements. Nat Cell Biol 15: 317–324.

Riddiford, L. M. in *The Development of Drosophila Melanogaster*, Cold Spring Harbor Laboratory Press, 1993.

Sarpal, R., M. Pellikka, R. R. Patel, F. Y. W. Hui, D. Godt *et al.*, 2012 Mutational analysis supports a core role for *Drosophila* α-catenin in adherens junction function. J Cell Sci 125: 233–245.

Scarpa, E., and R. Mayor, 2016 Collective cell migration in development. J Cell Biol 212: 143–155.

Scarpa, E., A. Szabó, A. Bibonne, E. Theveneau, M. Parsons *et al.*, 2015 Cadherin Switch during EMT in Neural Crest Cells Leads to Contact Inhibition of Locomotion via Repolarization of Forces. Dev Cell 34: 421–434.

Scheel, C., and R. A. Weinberg, 2011 Phenotypic plasticity and epithelial-mesenchymal transitions in cancer and normal stem cells? Int J Cancer 129: 2310–2314.

Shaw, T. J., and P. Martin, 2009 Wound repair at a glance. J Cell Sci 122: 3209–3213.

Silver, D. L., and D. J. Montell, 2001 Paracrine Signaling through the JAK/STAT Pathway Activates Invasive Behavior of Ovarian Epithelial Cells in Drosophila. Cell 107: 831–841.

Smola, H., H. J. Stark, G. Thiekötter, N. Mirancea, T. Krieg *et al.*, 1998 Dynamics of basement membrane formation by keratinocyte-fibroblast interactions in organotypic skin culture. Exp Cell Res 239: 399–410.

Stuelten, C. H., C. A. Parent, and D. J. Montell, 2018 Cell motility in cancer invasion and metastasis: insights from simple model organisms. Nat Rev Cancer 18: 296–312.

Szabó, A., and R. Mayor, 2018 Mechanisms of Neural Crest Migration. Annu Rev Genet 52: 43–63.

Takeichi, M., 2014 Dynamic contacts: rearranging adherens junctions to drive epithelial remodelling. Nat Rev Mol Cell Biol 15: 397–410.

Tepass, U., G. Tanentzapf, R. Ward, and R. Fehon, 2001 Epithelial cell polarity and cell junctions in *Drosophila*. Annu Rev Genet 35: 747–784.

Tepass, U., 2003 Claudin complexities at the apical junctional complex. Nat Cell Biol 5: 595–597.

Theveneau, E., and R. Mayor, 2012 Neural crest delamination and migration: From epithelium-to-mesenchyme transition to collective cell migration. Developmental Biology 366: 34–54.

Ugur, B., K. Chen, and H. J. Bellen, 2016 Drosophila tools and assays for the study of human diseases. Dis Model Mech 9: 235–244.

Valentin, G., P. Haas, and D. Gilmour, 2007 The chemokine SDF1a coordinates tissue migration through the spatially restricted activation of Cxcr7 and Cxcr4b. Curr Biol 17: 1026–1031.

Van de Bor, V., G. Zimniak, D. Cérézo, S. Schaub, and S. Noselli, 2011 Asymmetric localisation of cytokine mRNA is essential for JAK/STAT activation during cell invasiveness. Development 138: 1383–1393.

van Kempen, L. C., J. J. van den Oord, G. N. van Muijen, U. H. Weidle, H. P. Bloemers *et al.*, 2000 Activated leukocyte cell adhesion molecule/CD166, a marker of tumor progression in primary malignant melanoma of the skin. Am J Pathol 156: 769–774.

Venkiteswaran, G., S. W. Lewellis, J. Wang, E. Reynolds, C. Nicholson *et al.*, 2013 Generation and dynamics of an endogenous, self-generated signaling gradient across a migrating tissue. Cell 155: 674–687.

Vitorino, P., M. Hammer, J. Kim, and T. Meyer, 2011 A Steering Model of Endothelial Sheet Migration Recapitulates Monolayer Integrity and Directed Collective Migration. Mol Cell Biol 31: 342–350.

Volovetz, J., A. D. Berezovsky, T. Alban, Y. Chen, A. Lauko *et al.*, 2020 Identifying conserved molecular targets required for cell migration of glioblastoma cancer stem cells. Cell Death Dis 11: 152.

Wang, X., J. Bo, T. Bridges, K. D. Dugan, T. Pan *et al.*, 2006 Analysis of cell migration using whole-genome expression profiling of migratory cells in the *Drosophila* ovary. Dev Cell 10: 483–495.

Wang, X., L. He, Y. I. Wu, K. M. Hahn, and D. J. Montell, 2010 Light-mediated activation reveals a key role for Rac in collective guidance of cell movement *in vivo*. Nat Cell Biol 12: 591–597.

Weiss, F., D. Lauffenburger, and P. Friedl, 2022 Towards targeting of shared mechanisms of cancer metastasis and therapy resistance. Nat Rev Cancer 22: 157–173.

Wolf, K., Y. I. Wu, Y. Liu, J. Geiger, E. Tam *et al.*, 2007 Multi-step pericellular proteolysis controls the transition from individual to collective cancer cell invasion. Nat Cell Biol 9: 893–904.

Wolf, K., and P. Friedl, 2009 Mapping proteolytic cancer cell-extracellular matrix interfaces. Clin Exp Metastasis 26: 289–298.

Xi, R., J. R. McGregor, and D. A. Harrison, 2003 A gradient of JAK pathway activity patterns the anterior-posterior axis of the follicular epithelium. Dev Cell 4: 167–177.

Yana, I., H. Sagara, S. Takaki, K. Takatsu, K. Nakamura *et al.*, 2007 Crosstalk between neovessels and mural cells directs the site-specific expression of MT1-MMP to endothelial tip cells. J Cell Sci 120: 1607–1614.

Zhang, A., M. Hitomi, N. Bar-Shain, Z. Dalimov, L. Ellis *et al.*, 2015 Connexin 43 expression is associated with increased malignancy in prostate cancer cell lines and functions to promote migration. Oncotarget 6: 11640–11651.

2 A *Drosophila* RNAi screen reveals conserved glioblastoma-related adhesion genes that regulate collective cell migration

Nirupama Kotian[1], Katie M. Troike[2], Kristen N. Curran[1], Justin D. Lathia[2] and Jocelyn A. McDonald[1, *]

[1] Division of Biology, Kansas State University, Manhattan, KS 66506, USA

[2] Lerner Research Institute, Cleveland Clinic, Cleveland, OH 44195, USA

Published in the journal *G3 Genes|Genomes|Genetics*, Volume 12, Issue 1, January 2022, jkab356. https://doi.org/10.1093/g3journal/jkab356

Author contributions

Nirupama Kotian (N.K) performed all the experiments (Fig. 2.1, 2.2, 2.3), analyzed the data using statistical tests (Table 2.1, Table 2.2, Suppl table 2.1, Suppl files 2.1 and 2.2), prepared figures and tables and wrote the manuscript.

Katie Troike (K.M.T) performed glioblastoma database analyses, statistics and prepared materials for Fig. 2.4, Suppl fig. 2.1, Suppl Fig. 2.2, Suppl Fig. 2.3 and Suppl table 2.2.

Kristen Curran (K.N.C) performed preliminary RNAi screen experiments.

Jocelyn McDonald (J.A.M) and Justin Lathia (J.D.L.) used fly and cancer databases for identification of candidate genes and prepared the manuscript.

2.1 Abstract

Migrating cell collectives are key to embryonic development but also contribute to invasion and metastasis of a variety of cancers. Cell collectives can invade deep into tissues, leading to tumor progression and resistance to therapies. Collective cell invasion is also observed in the lethal brain tumor glioblastoma, which infiltrates the surrounding brain parenchyma leading to tumor growth and poor patient outcomes. *Drosophila* border cells, which migrate as a small cell cluster in the developing ovary, are a well-studied and genetically accessible model used to identify general mechanisms that control collective cell migration within native tissue environments. Most cell collectives remain cohesive through a variety of cell-cell adhesion proteins during their migration through tissues and organs. In this study, we first identified cell adhesion, cell matrix, cell junction, and associated regulatory genes that are expressed in human brain tumors. We performed RNAi knockdown of the *Drosophila* orthologs in border cells to evaluate if migration and/or cohesion of the cluster was impaired. From this screen, we identified eight adhesion-related genes that disrupted border cell collective migration upon RNAi knockdown. Bioinformatics analyses further demonstrated that subsets of the orthologous genes were elevated in the margin and invasive edge of human glioblastoma patient tumors. These data together show that conserved cell adhesion and adhesion regulatory proteins with potential roles in tumor invasion also modulate collective cell migration. This dual screening approach for adhesion genes linked to glioblastoma and border cell migration thus may reveal conserved mechanisms that drive collective tumor cell invasion.

2.2 Introduction

While migrating cells contribute to many processes during embryonic development and adult wound healing, abnormal cell migration drives tumor cell invasion and metastasis. During development and in cancer, cells either migrate as single cells or as interconnected small to large groups of cells called collectives (Friedl and Gilmour 2009; Friedl *et al*. 2012; Scarpa and Mayor 2016; Te Boekhorst *et al*. 2016b). Especially in cancer, cells can interconvert their modes of movement, transitioning from collective to single cell movement and back (Te Boekhorst and Friedl 2016a). A wide variety of cancer cells, including breast, colorectal, and thyroid carcinomas, are now known to migrate and invade as collectives both *in vitro* and *in vivo* (Cheung and Ewald 2016a; Wang *et al*. 2016; Kim *et al*. 2017; Ilina *et al*. 2018; Libanje *et al*. 2019; Padmanaban *et al*. 2019). Recent work has shown that tumor cell collectives promote tumor invasion and metastasis and may provide a mechanism for resistance to radiation (Aceto *et al*. 2014; Cheung *et al*. 2016b; Haeger *et al*. 2019).

The *Drosophila* border cells, which migrate collectively during late oogenesis, are a simple and genetically tractable model to identify genes required for collective cell migration (Montell *et al*. 2012; Saadin and Starz-Gaiano 2016). The border cell cluster consists of 4-8 epithelial-derived follicle cells that surround a central pair of polar cells (Figure 2.1, A-C, and F). Individual border cells stay adhered together and their movement is coordinated as an entire unit during the 3- to 4-hour journey to the oocyte (Figure 2.1, A-C). Multiple studies have used border cells to identify conserved genes that contribute to the migration of a variety of cancer cells, including those that invade as collectives (Yoshida *et al*. 2004; Madsen *et al*. 2015; Stuelten *et al*. 2018; Volovetz *et al*. 2020).

Glioblastoma (GBM) is the most common primary malignant brain tumor (Ostrom *et al*. 2014) and is refractory to many therapies including radiation and chemotherapy (Bao *et al*. 2006, Chen *et al*. 2012,). Given the dismal prognosis of GBM, identifying the underlying mechanisms that drive progression, including cell invasion, remains an immediate priority. While many genes are known to be dysregulated in glioma patients, it is difficult to know which ones are most relevant to disease progression, including tumor invasion. We and others recently showed that glioma cells and GBM cancer stem cells (CSCs), which can drive tumor growth, migrate collectively in some contexts (Gritsenko *et al*. 2017; Gritsenko and Friedl 2018; Volovetz *et al*. 2020). Using several patient derived GBM CSC tumor models, we found that a gene required in border cells, the small GTPase Rap1, also contributes to GBM collective cell invasion (Chang *et al*. 2018; Sawant *et al*. 2018; Volovetz *et al*. 2020). Due to their cellular conservation and large degree of genetic homology with humans, *Drosophila* brain tumor models have been established and used to provide critical molecular insight into gliomas (Chen and Read 2019, Chen *et al*. 2018. Agnihotri *et al*. 2016, Gangwani *et al*. 2020, Chi *et al*. 2019). Because patient derived GBM CSC tumor models are less genetically accessible for screening approaches, and *Drosophila* glioma models entail multiple mutations, we turned to border cells as an initial simpler approach to identify conserved genes that may drive GBM collective tumor invasion but that may also have a more general role in collective cell migration.

Cell-cell and cell-matrix adhesions are critical for cells to stay together and move collectively *in vivo* (Friedl and Mayor 2017; Janiszewska *et al*. 2020). Thus, genes that regulate cell adhesion are strong candidates to promote collective cell cohesion, migration, and invasion. Here we used the border cell system to screen a subset of adhesion and adhesion-related genes that have the potential to regulate GBM tumor migration and invasion. We selected conserved adhesion

genes, genes associated with cell junctions, and genes that regulate cell-cell and cell-matrix adhesion. We further focused on those adhesion-related genes whose expression correlated with glioma patient survival but at the time of the screen did not have known functions in brain cancer. We performed an RNAi screen targeting 23 of these adhesion genes in border cells. Here, we report the identification of eight genes, *α-catenin* (*α-Cat*), *Symplekin* (*Sym*), *Lachesin* (*Lac*), *roughest* (*rst*), *dreadlocks* (*dock*), *Wnt4*, *dachsous* (*ds*), and *fat* (*ft*), whose knockdown disrupted border cell migration and/or cluster cohesion to differing degrees. We then identified three human orthologs of target genes that were enriched in the leading edge and invasive portion of GBM tumors, the α-Cat ortholog CTNNA2, the Lac ortholog NEGR1, and the Rst ortholog KIRREL3. While further work needs to be done to test these genes in GBM tumors, this study supports the use of *Drosophila* genetic approaches to provide insights into human diseases such as GBM.

2.3 Methods & materials

Identification of candidate genes

FlyBase FB2014_5 version (released September 9, 2014) was queried for adhesion genes using the following Gene Ontology (GO) controlled vocabulary (CV) terms: ‘apical junction complex’, ‘focal adhesion’, ‘cell adhesion molecule binding’, ‘cell junction maintenance’, ‘cell junction assembly’, and ‘cell-cell adherens junction’. A total of 133 *Drosophila* genes were identified. Human orthologs were identified by *Drosophila* RNAi Screening Center Integrative Ortholog Prediction Tool (DIOPT) scores (Hu *et al*. 2011; Table 2.1). A PubMed search was performed for these genes along with ‘glioma’, ‘glioblastoma’, or ‘brain cancer’ to eliminate genes with a known function in or association with these cancers. This step narrowed the list to 44 genes. The NCBI REMBRANDT database was next used to identify genes that are associated with brain cancer

patient survival; these results were then confirmed using The Cancer Genome Atlas (TCGA). Genes associated with better ("positive"), or worse ("negative") patient survival were selected. These analyses resulted in 23 conserved fly genes (34 human genes) that were the final candidate genes tested in the *in vivo* border cell RNAi screen.

Bioinformatics analyses of human genes in tumor databases

Regional gene expression data from GBM tumor tissue was obtained from the Ivy Glioblastoma Atlas Project (Ivy GAP) database (https://glioblastoma.alleninstitute.org/static/home, accessed June 20, 2021), which contains gene expression data from several anatomical features of GBM tumors in a 41 patient dataset. Analysis of gene expression based on glioma grade (grades II, III, and IV) was performed using The Cancer Genome Atlas (TCGA) data downloaded from the Gliovis data portal (http://gliovis.bioinfo.cnio.es/, accessed May 5, 2021). The GEPIA (Gene Expression Profiling Interactive Analysis; http://gepia.cancer-pku.cn/, accessed March 30, 2021) database (Tang *et al*. 2017) was used to compare differential expression of gene orthologs in GBM tumor tissue (n=163) and non-tumor brain tissue (n=207). Thresholds were set at a log2 fold change > 1 and a p value < 0.01.

***Drosophila* RNAi Screen and Genetics**

All genetic crosses were set up at 25°C. The tub-GAL80ts ('tsGAL80') transgene (McGuire *et al*., 2004) was included to prevent early GAL4-UAS expression and potential lethality at larval or pupal stages of development. *c306*-GAL4, tsGal80*;* Sco/CyO was used to drive UAS-RNAi line expression in border cells. UAS-mCherry RNAi crossed to c306-GAL4 tsGal80*;* Sco/CyO was used as a control. The expression pattern of *c306*-GAL4 was confirmed by crossing *c306*-GAL4, tsGal80*;* Sco/CyO to UAS-nls.GFP (BDSC 4776). Multiple RNAi lines for the 23 cell adhesion candidate genes and UAS-mCherry RNAi were obtained from the Vienna *Drosophila* RNAi

Center (VDRC) or the Harvard Transgenic RNAi Project (TRiP) collection from the Bloomington *Drosophila* Stock Center (BDSC). All lines with stock numbers and construct IDs are listed in Table 2. Males from each UAS-RNAi line were crossed to virgin c*306*-GAL4, tsGal80 females. Three-to-five-day old F1 progeny females (*c306*-GAL4, tsGAL80/+; +/UAS-RNAi) from these crosses were fattened on wet yeast paste for ≥14 hours at 29°C prior to dissection. This allowed maximum GAL4-UAS expression and full inactivation of tsGAL80. Each RNAi line was tested one time in the primary screen, with a subset of lines tested at least three times in the secondary screen unless otherwise noted (Table 2.2).

Immunostaining and Imaging

Ovaries were dissected in Schneider's *Drosophila* Medium (Thermo Fisher Scientific, Waltham, MA, USA). After dissection, ovaries were fixed in 4% formaldehyde (Polysciences, Inc., Warrington, PA, USA) in 0.1 M potassium phosphate buffer, pH 7.4 for 10 minutes. NP40 block (50 mM Tris-HCl, pH 7.4, 150 mM NaCl, 0.5% NP40, 5 mg/ml bovine serum albumin [BSA]) was used for intermediate washes and antibody dilutions. Primary antibodies were obtained from Developmental Studies Hybridoma Bank (DSHB, University of Iowa, Iowa City, IA, USA) and used at the following dilutions: rat monoclonal anti-E-Cadherin 1:10 (DCAD2), mouse monoclonal anti-Armadillo 1:100 (N27A1), and mouse monoclonal anti-Singed 1:25 (Sn7C). Anti-rat or isotype-specific anti-mouse secondary antibodies conjugated to Alexa Fluor-488 or -568 (Thermo Fisher Scientific) were used at 1:400 dilution. 4',6-Diamidino-2-phenylindole (DAPI, Millipore Sigma) was used at 2.5µg/ml to label nuclei. Aqua-Poly/Mount (Polysciences, Inc.) was used to mount egg chambers on slides, a coverslip was added, and the mounting media allowed to harden for three days prior to microscope imaging. The stained egg chambers were imaged either using an upright Zeiss AxioImager Z1 microscope with Apotome.2 optical

sectioning or on a Zeiss LSM 880 confocal microscope (KSU College of Veterinary Medicine Confocal Core), using a 20x 0.75 numerical aperture (NA) objective. Images were processed in Zeiss ZEN 2 or FIJI software. Figures were prepared in Adobe Photoshop 2021 and line drawings were made in Adobe Illustrator 2021 or Affinity Design.

Graphs and statistics

Graphs were prepared in GraphPad Prism 8 and GraphPad Prism 9 (GraphPad Software, San Diego, CA, USA). For the secondary screen and subsequent analyses, three trials were performed for each RNAi line ($n \geq 30$ egg chambers scored in each trial). The cutoff value for a migration defect was calculated based on the background mean migration defect (3% ± 0.02) in control egg chambers (*c306*-GAL4 tsGAL80/+; +/UAS-mCherry RNAi). To determine genuine "hits" from the screen, RNAi lines with ≥10% migration defects were scored as positive hits in the primary and secondary screens. P-values were calculated using an unpaired two-tailed t test in Microsoft Excel. For GBM regional and grade-dependent gene expression analyses, differences between groups were determined using a one-way ANOVA. N's and p-values for each trial are included in the figure legends and tables.

2.4 Results and discussion

Identification of conserved brain tumor-associated adhesion genes

Cell-cell adhesion is essential for cells to stay connected during cohesive collective migration (Friedl and Mayor 2017). Reduction (or loss) of adhesion genes, such as E-cadherin (*Drosophila shotgun* [*shg*]), disrupts the integrity of the cluster and blocks the migration of the border cell cluster to the oocyte (Figure 2.1, D and E) (Niewiadomska *et al*. 1999; Sarpal *et al*. 2012; Desai *et al*. 2013; Cai *et al*. 2014; Chen *et al*. 2020, Raza *et al*. 2019). Many adhesion genes are conserved from flies to humans and could contribute to both border cell migration and GBM invasion (Figure

2.1F). To identify these conserved adhesion genes, we first performed a search of the *Drosophila* genome (FB2014_05), using Gene Ontology (GO) controlled vocabulary (CV) terms associated with cell adhesion (see Methods & Materials for details; Figure 2.1G). It is important to note that while these 'adhesion-related' candidate genes were originally chosen due to their known or predicted roles in cell adhesion, many of these genes have additional cellular roles, including cell-ECM interactions, cell signaling, cell polarity, as well as other functions. From the 133 fly genes associated with one or more of these terms, we identified likely human orthologs by analyzing their DIOPT scores (Table 2.1; Hu *et al.*, 2011). Using these human orthologs, we performed a PubMed search for those genes to determine if there was an already-known association with either glioma or GBM. This allowed us to focus on genes that may have a novel association with brain tumors. The remaining 44 genes were then analyzed in the Repository of Molecular Brain Neoplasia Data (REMBRANDT), a database for transcript expression levels that are associated with brain tumor patient survival (Gusev *et al.*, 2018). Ten genes were not found in REMBRANDT. Of the remaining 34 human genes, expression of 18 genes (13 fly genes) were associated with better ("positive") patient survival while expression of 16 genes (13 fly genes) were associated with worse ("negative") patient survival (Table 2.1). Many fly genes have multiple human orthologs. A few of these, for example *α-cat*, *G protein alpha i subunit*, and *G protein alpha o subunit*, have multiple human orthologs each of whose expression is associated with different predicted glioma patient outcomes (Table 2.1). For comparison, we have included any current known roles for these genes in cell migration or glioma (Table 2.1; Supplementary File 2.1). The 23 unique fly genes were chosen for further follow-up to determine their role, if any, in border cell collective migration.

RNAi screen in border cells identifies eight genes associated with GBM

For the primary screen, multiple RNAi lines were used to specifically target and knock down each of the 23 conserved fly adhesion and adhesion-related genes in border cells (Table 2.2). These lines include independent targeted sequences, overlapping targeted sequences, and independent insertions of the same RNAi construct (*see* Table 2.2). Some RNAi lines used in this screen were validated in different *Drosophila* systems, whereas others have not yet been reported in published studies (FlyBase; Supplementary Table 2.1; Supplementary File 2.2). We drove expression of the respective UAS-RNAi lines using *c306*-GAL4 tsGAL80, a follicle cell driver highly enriched in border cells prior to and during their migration; tsGAL80 was used to bypass potential early lethality (Figure 2.1, A-C). All border cell clusters from control (*c306*-GAL4 tsGAL80/+; +/UAS-mCherry RNAi) egg chambers completed their migration by stage 10 (Figure 2.2, A and B; Table 2.2). Twenty-one of these genes displayed a migration defect above the minimum cutoff of ≥10% with at least one RNAi line (*see* Methods & Materials).

To further determine which of these genes were genuine hits, we retested the RNAi lines in a secondary screen. Each RNAi line was crossed to *c306*-GAL4 tsGAL80 three times and scored for the ability of border cells to complete their migration to the oocyte. For three genes (*ds, Lac, rst*), additional RNAi lines were obtained from stock centers and tested. We specifically analyzed if RNAi border cells failed to initiate migration ("no migration"), stopped along the migration pathway but did not reach the oocyte ("partial migration"), reached the oocyte ("complete migration"), or if clusters had defective cohesion and split into multiple parts ("% splitting"). Control border cells completed their migration to the oocyte by stage 10 (Figure 2.2, A and B; Figure 2.3, A and B; Table 2.2). We found that knockdown of eight genes, *α-Cat*, *Sym*, *Lac*, *rst*, *dock*, *Wnt4*, *ds*, and *ft*, consistently disrupted border cell migration with at least two RNAi lines,

providing more confidence that these genes are required for collective cell migration (Figures 2.2 and 2.3; Table 2.2). Border cell migration defects upon knockdown of these genes ranged from 10 to 76% depending on the gene and the RNAi line; some RNAi lines for these genes had less than 10% migration defects. Below we report and discuss the results for these eight genes in more detail.

Adherens junction genes: α-Cat (human CTNNA1, CTNNA2, CTNNA3) is a critical component of the cadherin-catenin complex that regulates adherens junctions by linking E-cadherin and β-catenin to the F-actin cytoskeleton (Maiden and Hardin 2011). E-cadherin is required for adhesion of border cells to the nurse cell substrate, which provides traction for border cells to keep moving forward and thus facilitates forward movement while maintaining tension-based directional motility (Niewiadomska *et al*. 1999; Cai *et al*. 2014). α-Cat was the strongest candidate from our primary screen (Table 2.2), and we recently described the phenotypes for *α-Cat* knockdown in detail (Chen *et al*. 2020). *α-Cat* was knocked down using two independent RNAi lines, which reduced α-Cat protein levels in border cells (Chen *et al*. 2020). *α-Cat* RNAi strongly disrupted migration, with 66-76% border cells failing to complete their migration (Figure 2.2, C, D and M; Table 2.2). Border cell clusters deficient for *α-Cat* also had significant cohesion defects, with the cluster splitting into two or more parts in 35% of egg chambers (Figure 2.2, C and D). Thus, *Drosophila α-Cat* is required for both successful border cell migration and for proper cohesion of cells within the cluster (this study; Sarpal *et al*. 2012; Desai *et al*. 2013; Chen *et al*. 2020). The role for α-Cat in cluster cohesion and migration closely resembles that of β-Cat (*Drosophila* Armadillo) and E-cadherin, thus it is likely that α-Cat functions in the classical cadherin-catenin complex in border cells (Niewiadomska *et al*. 1999; Sarpal *et al*. 2012; Desai *et al*. 2013; Cai *et al*. 2014; Chen *et al*. 2020).

Other junctional genes: Four genes, *Sym*, *Lac*, *rst*, and *dock*, encode proteins that localize to various types of cell junctions and/or are known to regulate cell adhesions. Sym (human SYMPK) is a scaffolding protein, which along with other polyadenylation factors, forms a complex that mediates processing of polyadenylated and histone mRNAs but also functions at tight junctions (Keon *et al*. 1996; McCrea *et al*. 2009; Sullivan *et al*. 2009). During *Drosophila* oogenesis, Sym is required for histone pre-mRNA processing in the histone locus body during endoreplication of the follicular epithelium (Tatomer *et al*. 2014). Later in oogenesis, Sym protein localizes to the tricellular junctions of follicle cells. Here, Sym may facilitate cytoplasmic mRNA polyadenylation and thus translation of mRNAs required to regulate and/or maintain adhesion at cell junctions (Tatomer *et al*, 2014). Border cells expressing *Sym* RNAi had significant migration defects along with splitting of the cluster (Figure 2.2, E and F, N; Table 2.2). The two strongest *Sym* RNAi lines (VDRC 33469 and 33470), which target the same region of the *Sym* gene, caused significant migration defects, with 5-10% of border cells failing to start migration and an additional 18-22% failing to reach the oocyte. *Sym* RNAi border cell clusters had cohesion defects, with 11% of clusters visibly splitting apart. A third independent RNAi line (BL 39041) did not impair migration (Figure 2.2N). Based on our observed phenotypes and the known roles for Sym, we speculate that *Sym* may maintain cell-cell contacts between border cells during collective migration, possibly through regulation of as-yet-unknown targets by mRNA polyadenylation at cell-cell junctions.

Lac (human LSAMP and NEGR1) is a membrane-localized protein with three extracellular immunoglobulin-like (Ig-like) domains that can mediate cell-cell adhesion (Finegan and Bergstralh 2020). Lac localizes to both immature and mature basolateral septate junctions and is required for tracheal morphogenesis in *Drosophila* (Llimargas *et al*. 2004). Knockdown of *Lac* by four RNAi lines, which together target two non-overlapping regions of the *Lac* gene, mildly

disrupted migration and cohesion of the cluster (Figure 2.2, G and H, O; Table 2.2). Two *Lac* RNAi lines (VDRC 35524 and BL 28940) disrupted migration in 11% of egg chambers, whereas two RNAi lines (VDRC 107450 and BL 38536) had fewer migration defects and were not significantly different from control (Figure 2.2O; Table 2.2). While the phenotypes caused by *Lac* RNAi knockdown are mild, recent work by Alhadyian *et al*. found that four additional septate junction proteins, Macroglobulin complement-related (Mcr), Contactin, Neurexin-IV and Coracle, localize to border cells and are required for both border cell cluster migration and cohesion (Alhadyian *et al*. 2021). Because border cells do not have mature septate junctions (which form the tight occluding junctions), septate junction proteins may instead regulate cluster polarity and/or adhesion during migration (Alhadyian *et al*. 2021). Thus, Lac is likely to have a specific role in border cell migration along with other septate junction proteins. Further work will be needed to determine if the mild phenotypes observed with *Lac* RNAi are due to partial knockdown or to redundancy with other septate junction genes.

Rst (human KIRREL1, KIRREL2, KIRREL3) is a member of the Irre Cell Recognition Module (IRM) family of transmembrane proteins. In particular, Rst encodes an immunoglobulin superfamily cell adhesion molecule (IgCAM) with five Ig-like domains (Finegan and Bergstralh 2020). IRM proteins, including Rst, control the adhesion and patterning of various tissues including the developing ommatidia in the *Drosophila* eye (Bao and Cagan 2005; Johnson *et al*. 2011; Finegan and Bergstralh 2020). Border cells expressing *rst* RNAi showed consistent though mild migration defects with three RNAi lines (VDRC 27223, VDRC 27225, and BL 28672), which in total target two non-overlapping regions of the *rst* gene. Migration defects ranged from 10-16% (Figure 2.2, I and J, P; Table 2.2). Cluster cohesion was mildly affected (6% of clusters split apart; Figure 2.2I). A fourth RNAi line did not disrupt migration or cohesion compared to control (Figure

2.2P; VDRC 951). Interestingly, Rst is required for progression through *Drosophila* adult oogenesis, including development of the germline (Valer *et al*. 2018; Ben-Zvi and Volk 2019). Rst is also expressed in follicle cells prior to the stages that border cells develop from the follicle cell epithelium (Valer *et al*. 2018), further supporting a later role in border cell migration.

Dock (human NCK1) is an SH2/SH3 domain-containing adaptor protein involved in receptor tyrosine kinase signaling, actin regulation, cell adhesion, and other processes (Buday *et al*. 2002; Chaki and Rivera 2013). In *Drosophila*, Dock regulates axon guidance, myoblast fusion during embryonic development, and ring canal morphogenesis in the ovarian germline-derived nurse cells (Garrity *et al*. 1996; Rao and Zipursky 1998; Kaipa *et al*. 2013; Stark *et al*. 2021). Knockdown of *dock* in border cells, using two independent RNAi lines that target non-overlapping regions of the *dock* gene (VDRC 37524 and BL 27228), resulted in migration defects but did not disrupt cohesion of border cells (Figure 2.2, K, L, and Q; Table 2.2). Specifically, *dock* RNAi disrupted migration in 13-19% of stage 10 egg chambers (Figure 2.2Q; Table 2.2). One RNAi line (VDRC 107064) did not impair border cell migration but showed mild splitting (6%), whereas another line (VDRC 37525) from the primary screen was no longer available so could not be confirmed in the secondary screen (Figure 2.2Q; Table 2.2). Dock is required for myoblast fusion during muscle formation by regulating cell adhesion and F-actin (Kaipa *et al*. 2013). In this context, Dock colocalizes with and/or binds to several cell adhesion proteins from the IgCAM superfamily including Rst, one of the genes identified in this screen (see above). Additionally, Dock genetically and biochemically interacts with the Ste20-like serine-threonine kinase Misshapen (Msn) to control motility of photoreceptor growth cones in the developing eye (Ruan *et al*. 1999). Notably, Msn is required for border cell migration, where it is required for the formation of polarized protrusions and

coordinated actomyosin contractility of the cluster (Plutoni *et al*. 2019). Thus, it will be of interest in the future to determine if Dock, Rst, and Msn interact to control border cell migration.

Atypical cadherins and planar cell polarity genes: Three genes, *Wnt4*, *ds*, and *ft* encode proteins with annotated roles in both planar cell polarity and cell-cell adhesion (FlyBase; Figure 2.3; Table 2.2). Wnt4 (human WNT9A) is a conserved secreted protein of the Wnt family, which regulates cell adhesion through recruitment of focal adhesion complexes during the migration of epithelial cells in the pupal ovary (Cohen *et al*. 2002). We tested four RNAi lines for *Wnt4*, which in total target two independent regions of the gene. Migration defects for the four tested *Wnt4* RNAi lines ranged from 9 to 23% (Figure 2.3, C, D, I; Table 2.2). These data suggest a role for Wnt4 in regulating border cell movement. Previous studies suggested that Wnt4 participates in establishing planar polarity within the developing eye and wing (Lim *et al*. 2005; Wu *et al*. 2013). Indeed, several core planar cell polarity genes including *frizzled* and *dishevelled* regulate border cell migration (Bastock and Strutt 2007). However, recent studies that used multiple gene knockouts now indicate that the Wnt family of proteins, including Wnt4, are not required for *Drosophila* planar cell polarity (Ewen-Campen *et al*. 2020; Yu *et al*. 2020). Thus, we favor a role for Wnt4 in the movement and adhesion of border cells, similar to what was found during earlier stages of *Drosophila* ovarian development (Cohen *et al*. 2002).

Ds (human DCHS1) and Ft (human FAT4) encode large protocadherin proteins, each of which has multiple extracellular cadherin repeats (27 for Ds and 34 for Ft) (Fulford and McNeill 2020). Heterophilic binding between Ds and Ft via their extracellular domains is essential for cell-cell communication, particularly in the regulation of tissue growth through Hippo signaling and planar polarization of various tissues (Matakatsu and Blair 2004; Bosveld *et al*. 2016; Blair and McNeill 2018; Fulford and McNeill 2020). Knockdown of *ds* with any of three independent RNAi lines

(VDRC 36219, VDRC 4313, and BL 32964) mildly disrupted migration, ranging from 12-14% of border cells failing to reach the oocyte (Figure 2.3, E, F, J; Table 2.2). *ds* RNAi border cell clusters only displayed mild cohesion defects, with 5% of clusters splitting apart (Figure 2.3E). Two independent RNAi lines that target *ft* (VDRC 108863 and VDRC 9396) also showed consistent though mild migration defects (11-13%), with only a few clusters (3%) splitting apart (Figure 2.3, G, H, K; Table 2.2). Interestingly, *ds* is required for the collective directional migration of *Drosophila* larval epidermal cells (LECs) during morphogenesis of the pupal abdominal epithelium (Bischoff 2012; Arata *et al*. 2017). An imbalance in Ds protein levels between LECs during collective migration is detected by Ft at cell junctions leading to the formation of lamellipodia at the posterior side of the LECs (Arata *et al*. 2017). Further experiments will be needed to determine if Ft and Ds similarly coordinate protrusions in border cells or regulate some other aspect of border cell collective migration.

The RNAi screen approach used in this study allows rapid functional testing of genes but comes with technical limitations (Booker *et al*. 2011, Perrimon *et al*. 2010). Possible caveats of RNAi-mediated knockdown include potential off-target effects ('false positives'), RNAi constructs that fail to knock down a given gene's function ('false negatives'), genomic-insertion effects that reduce expression of an RNAi transgene and thus knockdown efficiency, transient or partial functional knockdown in cells and tissues by a given RNAi transgene, and/or compensation by related genes. We attempted to address some of these potential RNAi issues. To control for general activation of the RNAi machinery, we performed RNAi knockdown to monomeric Cherry (mCherry), a fluorescent protein not normally found in *Drosophila* (e.g., Figure 2.2, A, B, M; Table 2.2). Whenever possible, to provide better confidence of RNAi-mediated knockdown results, we tested multiple RNAi lines for each gene, which include RNAi transgenes that target

independent gene regions and independent insertions that target overlapping gene sequences (Table 2.2). Many of these RNAi lines have been used in other *Drosophila* screens and other functional studies, with various phenotypes observed such as pupal lethality, bristle defects, and others (FlyBase; Supplementary Table 2.1; Supplementary File 2.2).

Partial functional knockdown could also be due to expression levels of the GAL4-UAS system itself. We included tsGAL80 in our genetic crosses to prevent early GAL4-UAS-RNAi expression and potential lethality prior to the stages of oogenesis when border cells migrate. Under the experimental conditions of the screen (see Methods & Materials), it is possible that leaky tsGAL80 could further dampen expression of GAL4-UAS-RNAi in border cells. However, we have previously used the same GAL4 line, *c306*-GAL4, in combination with tsGAL80 under similar experimental conditions to drive RNAi-mediated knockdown in border cells; RNAi for at least two genes reduced levels of the respective proteins within border cells (Aranjuez *et al*. 2012, Aranjuez *et al*. 2016). As with all RNAi screens, further follow up experiments with loss-of-function mutant alleles or cell-specific CRISPR-Cas9 are needed to confirm the specificity of the phenotypes (Mohr *et al*. 2014). Future experiments include performing live cell imaging and other cellular assays to determine when each of these genes is required and how the genes precisely regulate collective border cell migration.

Analysis of regional expression of border cell screen hits in GBM tumors

Based on the results of the functional *Drosophila* screen, we next sought to link individual genes to invasion in human GBM patient tumors. We first assessed the Ivy GAP database that provides regional RNA expression across anatomically defined regions of tumors ranging from the tumor core to the infiltrating edge (see Methods & Materials). Using this database, we found that NEGR1

and KIRREL3 were specifically enriched in anatomical regions with elevated invasion potential, namely the leading edge (LE) and infiltrating tumor (IT), compared to all other assessed anatomical regions (Figure 2.4A; Supplementary Table 2.2). These regions included cellular tumor (CT), perinecrotic zone (PNZ), pseudopalisading cells around necrosis (PAN), hyperplastic blood vessels (HBV), and microvascular proliferation (MP). Additionally, CTNNA2 had significant expression in the LE and IT regions though was also expressed in other regions of the tumor (Supplementary Figure 2.1; Supplementary Table 2.2). However, we also observed some *Drosophila* screen hits that did not demonstrate regional heterogeneity in terms of expression, such as SYMPK and CTNNA1 (Figure 2.4B; Supplementary Table 2.2). Other genes had a mixture of expression profiles across human GBM anatomical regions (CTNNA3, DCHS1, FAT4, KIRREL1, KIRREL2, NCK1; Supplementary Figure 2.1; Supplementary Table 2.2). WNT9A was not found in the Ivy GAP database. It is worth noting that this initial validation approach takes advantage of regional differences within the same GBM tumor. Therefore, such GBM anatomical expression surveys may be a better surrogate of cellular invasion than expression in GBM compared to lower-grade or non-neoplastic neural tissue; these latter analyses rely on gene expression in tissue obtained mainly from the core of the tumor and may miss areas of the tumor that undergo active invasion (Supplementary Figures 2.2 and 2.3). Nonetheless, we observed a variety of human adhesion ortholog gene-dependent increases or decreases in GBM tumors compared to lower-grade or non-neoplastic neural tissue (Supplementary Figures 2.2 and 2.3). Together, these assessments provide a first step in validating novel, conserved molecular mechanisms of GBM invasion for future therapeutic development. Invasive GBM is thought to be driven by CSCs, which can migrate and invade as single cells, finger-like collectives, or as a mixture of migration modes (Cheng *et al*. 2011; Volovetz *et al*., 2020). Human Rap1a, originally identified in a

Drosophila screen of collective border cell migration, influences CSC-mediated GBM cell invasion (Aranjuez *et al*., 2012; Volovetz *et al*. 2020). Interestingly, knocking down *Sym* and *α-Cat* in the border cells caused the most severe migration and cluster cohesion defects. While the respective human orthologs SYMPK, CTNNA1, and CTNNA2 did not show regional tumor heterogeneity, they are each expressed in GBM tumors and/or are generally elevated in different grades of glioma including GBM (Grade IV; Supplementary Figure 2.2).

A limitation of this study involves the use of GBM expression and survival data from TCGA. The samples used to curate this database are primarily taken from core biopsies of resected GBM tumors, which restricts the availability of invasive cells and therefore the use of these data for assessing invasive potential. Similarly, direct associations between expression and survival may be impacted by variable gene expression across different regions of the tumor. To counteract this, we used the Ivy GAP database to provide additional information about expression in each tumor region. Conversely, a large proportion of cells in the leading edge and infiltrating tumor of the Ivy atlas are non-tumoral, which may confound interpretation of regional expression. It should also be noted, however, that expression alone is not necessarily indicative of function and that these studies are being used as a foundation upon which to build future studies.

2.5 Conclusion

GBM, the most common primary malignant brain tumor in adults, is also one of the most lethal (Ostrom *et al*. 2014; Ostrom *et al*. 2018). These tumors are highly invasive and possess a self-renewing CSC population. CSCs are highly invasive and can migrate either individually or collectively (Cheng *et al*. 2011, Volovetz *et al*. 2020). Here we used a human GBM-informed approach to identify conserved regulators of adhesion during collective cell migration and invasion, particularly focused on testing genes in the border cell model. We identified eight

adhesion-related *Drosophila* genes (orthologs of 13 human genes) associated with glioma patient survival. Of the eight adhesion-related *Drosophila* genes found to be essential for collective cell migration, two human orthologs, NEGR1 and KIRREL3 showed significant regional enrichment in the leading edge and infiltrating tumor of human GBM tumors, areas associated with enhanced cell invasion. CTNNA2 was expressed in these invasive regions, though was also expressed at high levels in other regions of the tumor. Knockdown of these eight genes disrupted border cell migration to varying degrees, with two genes *α-cat* and *Sym* significantly disrupting both cohesion of the cluster and successful cell migration. Although the objective of this study was broadly directed towards understanding the adhesion-associated roles of genes in collective cell migration and invasion, many of these genes may have additional functions apart from cell adhesion. These eight *Drosophila* genes thus represent a starting point to further investigate the specific mechanisms by which these genes regulate normal collective cell migration. Future experiments using loss-of-function alleles and live imaging approaches are required to confirm the adhesion-related, or other, functions of these genes in the border cell system. Additionally, whether the human orthologs function through an adhesion-dependent or -independent manner in GBM tumors needs to be determined with follow up experiments, using both mammalian and non-mammalian models of GBM, including *Drosophila* glioma models (Shahzad *et al*. 2021, Chen and Read 2019, Chen *et al*. 2018, Agnihotri *et al*. 2016, Gangwani *et al*. 2020, Chi *et al*. 2019). Overall, the strategy used in this study has the potential to identify new genes and conserved mechanisms that drive collective cell migration of normal cells and those in invasive cancers such as GBM.

2.6 Figures and tables

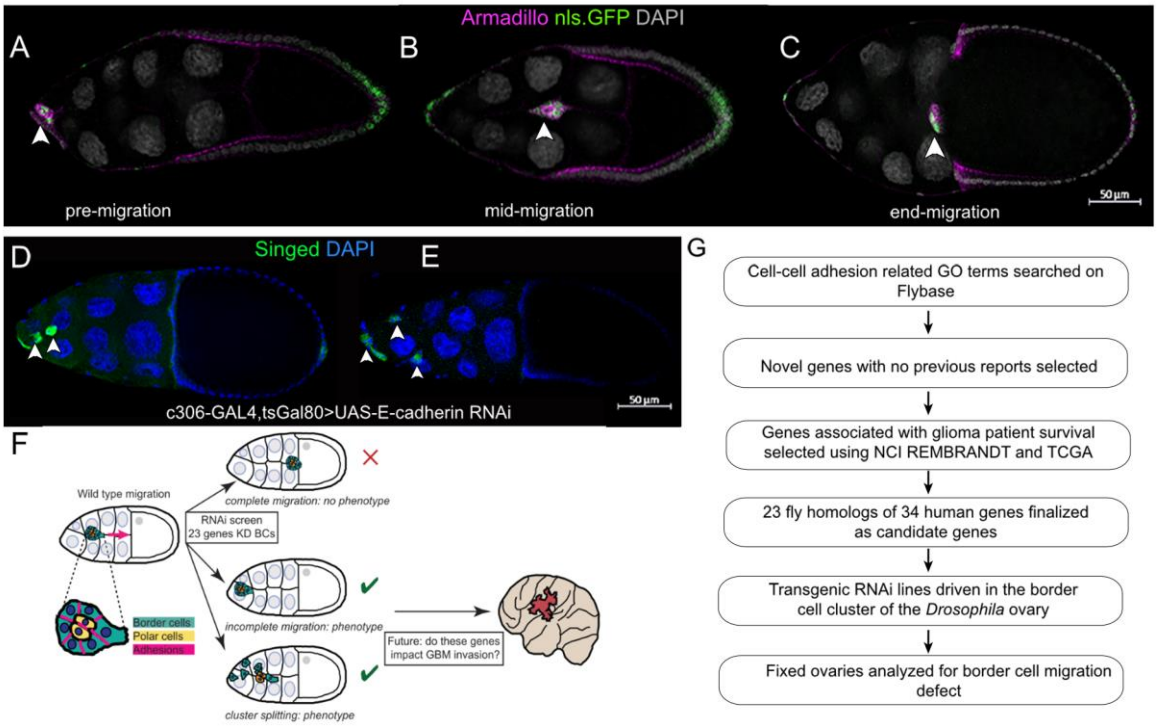

Figure 2.1 Screen to identify conserved GBM-associated adhesion genes in collective cell migration.

(A-C) Migration of wild type border cells in stage 9 and 10 egg chambers. *C306*-GAL4 drives nuclear GFP (UAS-nls.GFP, green) in egg chambers labelled with Armadillo (magenta) to show cell membranes, and DAPI to show nuclei (grey). Arrowheads indicate the position of the border cell cluster within the egg chamber during migration stages: pre-migration (A), mid-migration (B), and end-migration (C). (D-E) Knockdown of *E-cadherin* by RNAi (*c306*-GAL4 tsGAL80/+; +/UAS-E-cadherin RNAi line v103962) in border cells disrupts migration and cluster cohesion at stage 10. Arrowheads indicate border cell clusters and split clusters. (F) Schematic overview of the RNAi screening approach in border cells. (G) Experimental flow chart used to identify novel GBM-associated adhesion genes through *Drosophila* and human glioma databases.

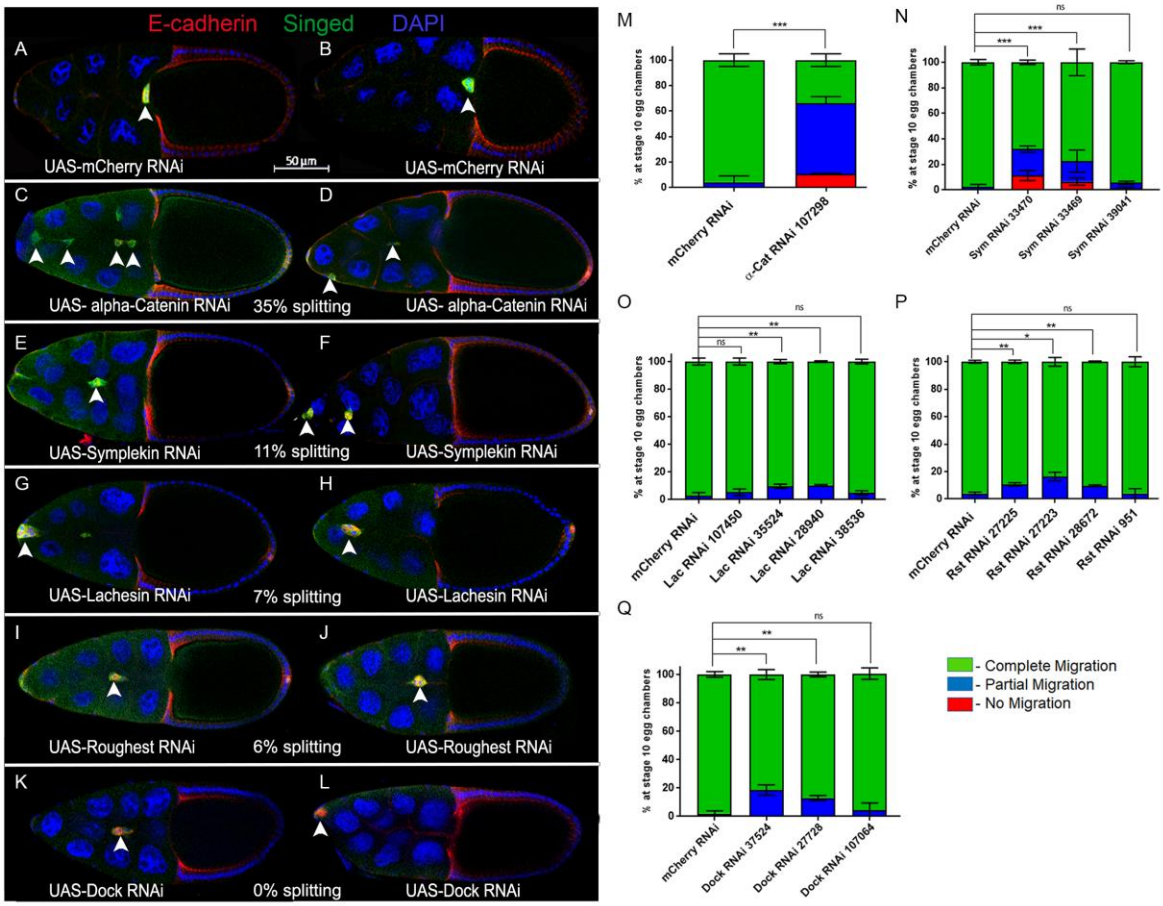

Figure 2.2 Cell adhesion and cell junction-associated genes whose RNAi knockdown impairs border cell migration.

(A-L) Stage 10 egg chambers expressing RNAi for the indicated genes (or control) in border cells labeled for E-cadherin (red), a cell membrane and adhesion marker, Singed (green), which is highly expressed in and marks border cells, and DAPI to label all cell nuclei (blue). Two images are shown to indicate the general extent of phenotypes with RNAi knockdown for each gene. White arrowheads show the position of border cell clusters; the scale bar (A, B) indicates the image magnification for all images in the figure. Anterior is to the left. (A and B) Border cells expressing the control, *mCherry* RNAi, reach the oocyte at stage 10. (C-L) RNAi knockdown of *α-Catenin/α-Cat* (C and D, line v107298), *Symplekin/Sym* (E, line v33470; F, line v33469), *Lachesin/Lac* (G

and H, line BL28940), *Roughest/Rst* (I and J, line v27223) and *Dock* (K, line v37524; L, line BL27728) driven by *c306*-GAL4 tsGAL80 disrupts the collective migration of border cells. The average percentage of egg chambers with border cell cluster splitting defects (% splitting) from the RNAi line with the strongest migration defect is indicated. (M-Q) Quantification of the extent of border cell migration (no migration, red; partial migration, blue; complete migration, green) in stage 10 egg chambers expressing the indicated RNAi lines for *α-Cat* (M), *Sym* (N), *Lac* (O), *Rst* (P) and *Dock* (Q) along with the matched control *mCherry* RNAi. Error bars represent SEM for three trials, $n \geq 30$ egg chambers in each trial. *$p<0.05$; **$p<0.005$; ***$p<0.001$, unpaired two-tailed t test.

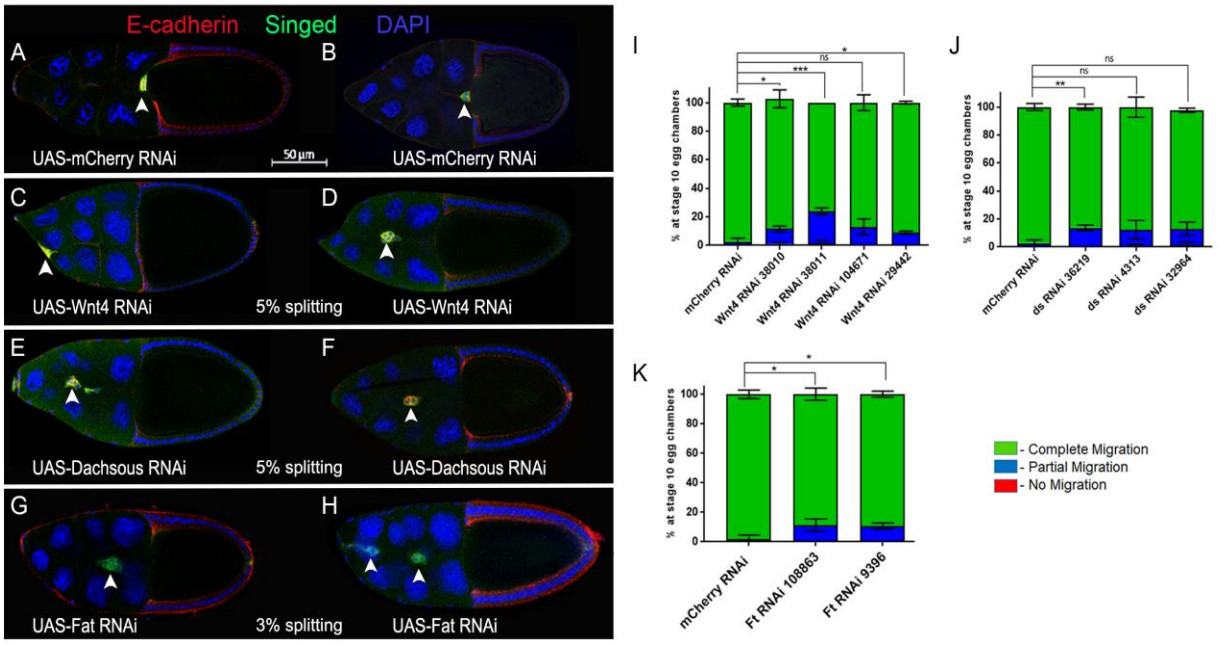

Figure 2.3 Atypical cadherins and planar cell polarity genes whose RNAi knockdown impairs border cell migration.

(A-H) Stage 10 egg chambers expressing RNAi for the indicated genes (or control) in border cells labeled for E-cadherin (red), a cell membrane and adhesion marker, Singed (green), which is highly expressed in border cells, and DAPI to label all cell nuclei (blue). Two images are shown to indicate the general extent of phenotypes with RNAi knockdown for each gene. White arrowheads show the position of border cell clusters; the scale bar (A, B) indicates the image magnification for all images in the figure. Anterior is to the left. (A and B) Border cells expressing the control, *mCherry* RNAi, reach the oocyte at stage 10. (C-H) RNAi knockdown of *Wnt4* (C and D, line v38011), *Dachsous/ds* (E, line 32964; F, line v4313) and *Fat/ft* (G and H, line BL28940) driven by *c306*-GAL4 tsGAL80 disrupts the collective migration of border cells. The average percentage of egg chambers with border cell cluster splitting defects from the RNAi line with the strongest migration defect is indicated. (I-K) Quantification of border cell migration (no migration, red; partial migration, blue; complete migration, green) in stage 10 egg chambers expressing the

indicated RNAi lines for *Wnt4* (I), *ds* (J), and *ft* (K) along with the matched control *mCherry* RNAi. Error bars represent SEM for three trials, n ≥30 egg chambers in each trial. *p<0.05; **p<0.005; ***p<0.001, unpaired two-tailed t test.

Figure 4

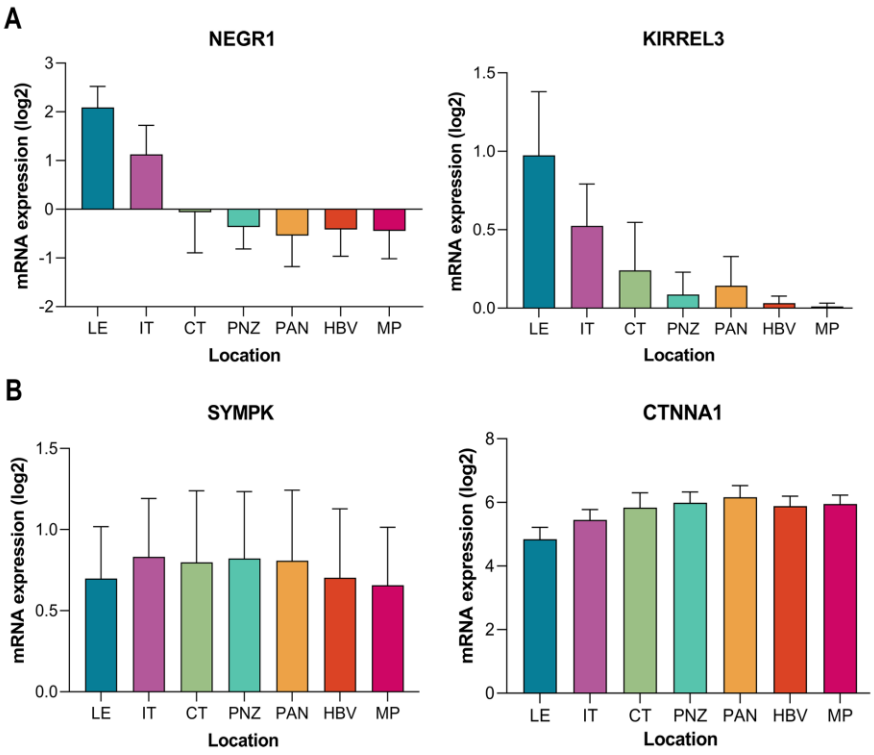

Figure 2.4 Regional expression of representative human ortholog adhesion-related genes in GBM patient tumors.

(A) Expression of human orthologs of neuronal growth regulator 1 (NEGR1) and kirre like nephrin family adhesion molecule 3 (KIRREL3) is significantly enriched in the leading edge (LE) and infiltrating tumor (IT) compared to other tumor regions, including the cellular tumor (CT), perinecrotic zone (PNZ), pseudopalisading cells around necrosis (PAN), hyperplastic blood vessels (HBV), and microvascular proliferation (MP). (B) In contrast, expression of human orthologs symplekin (SYMPK) and catenin alpha 1 (CTNNA1) demonstrated little to no significant change when comparing different regions of tumor. Data from the Ivy GAP are shown as mean expression +/- SD across GBM tumor regions. Statistics are shown in Supplementary Table 2: *p<0.05; **p<0.01; ***p<0.001, one way ANOVA with Tukey HSD.

Table 2.1 *Drosophila* and human brain tumor-associated adhesion genes

Gene name (*Drosophila*)	Human ortholog	DIOPT score out of 15	Best score	Best reverse score	Role in migration	Glioma patient survival	Role in glioma
alpha-Catenin	CTNNA1	12	No	Yes	Cytosolic αE-catenin pool sequestered to mitochondria of MDCK cells increases epithelial cell sheet migration but does not alter overall cadherin based adhesion[1]; loss leads to human keratinocyte cell migration[2]; anisotropically activated in epithelial sheet collective migration[3;] collective cell migration in MDCK cells[4]; αE-catenin relocates to lamellipodia during migration of neural crest and glioma cells[5]; mouse angiogenic and glial cells[6,8]; homodimerize to PIP3 vesicles in lamellopodia[7]; prostate cancer cells[9]; wound healing in keratinocytes[10]; migration of dorsal ridge primordia[11];	Negative	GBM cell migration, invasion, and proliferation *in vitro*[13,14]
	CTNNA2	13	Yes	Yes		ND	NA
	CTNNA3	7	No	Yes		Positive	NA

Gene name (*Drosophila*)	Human ortholog	DIOPT score out of 15	Best score	Best reverse score	Role in migration	Glioma patient survival	Role in glioma
					epithelial invagination of *Drosophila* embryonic dorsal fold[12]		
CAP	SORBS1	5	No	Yes	Links focal adhesion sites to nuclei during collective cardiac cell migration in flies[15,16]; ECM stiffness dependent mechanotransduction in mouse fibroblasts[17]	Positive	NA
Caskin	CASKIN1	4	Yes	Yes	NA	Positive	NA
	CASKIN2	4	Yes	Yes		Positive	NA
CG3770	LHFPL2	12	Yes	Yes	NA	Negative	NA
CG45049	PERP	10	No	Yes	NA	Negative	NA
Dachsous	DCHS1	11	Yes	Yes	Collective migration of larval epidermal cells[18,22]; glial migration during eye development[19,22];	Negative	NA

Gene name (*Drosophila*)	Human ortholog	DIOPT score out of 15	Best score	Best reverse score	Role in migration	Glioma patient survival	Role in glioma
					collective tangential migration of murine facial motor neurons[20]; uniform axial orientation of *Drosophila* abdominal epithelial cells[21]		
Dock	NCK1	14	Yes	Yes	Dorsal appendage morphogenesis[23]; interacts with Misshapen during dorsal closure[24]; NCK1 promotes podosome biogenesis during tumor invasion[25]; endothelial front-rear polarity and migration[26]; formation of dorsal ruffles in mice embryonic fibroblasts[27]	Negative	Expression levels of NCK1 in gliomas[29]
Fat	FAT4	13	Yes	Yes	Collective tangential migration of murine facial motor neurons[19]; mutations in FAT4 causes defects in	Positive	NA

Gene name (*Drosophila*)	Human ortholog	DIOPT score out of 15	Best score	Best reverse score	Role in migration	Glioma patient survival	Role in glioma
					neuronal migration of cerebral organoids[28]		
G protein alpha i	GNAI2	11	No	Yes	Dorsal appendage morphogenesis[30]; modulates migration-proliferation dichotomy in breast and colon cancer cells[31]	Negative	Part of a signaling axis that enhances proliferation of GBM cells[32]
	GNAZ	5	No	Yes		Positive	NA
G protein alpha o	GNAI3	3	No	No	Promotes protrusion membrane dynamics[33]	Negative	NA
	GNAT3	3	No	No		Positive	NA
Gliotactin	NLGN2	5	Yes	No	Expressed in tricellular septate junctions in stage 10B egg chambers and border cells throughout migration[34]; Overexpression in the wing disc driven by apterous-GAL4 leads to migration of cells from dorsal to ventral compartment[35,36]	Positive	NA

Gene name (*Drosophila*)	Human ortholog	DIOPT score out of 15	Best score	Best reverse score	Role in migration	Glioma patient survival	Role in glioma
Lachesin	LSAMP	5	No	No	Tracheal morphogenesis[37,38]	Positive	Expression of LSAMP negatively correlates with glioma survival in patients with EGFR mutation or amplification[39]
	NEGR1	9	Yes	Yes		Positive	NEGR1 variants and expression in pediatric gliomas[40]
Liprin-alpha	PPFIA1	11	No	Yes	Tumorigenesis and metastasis in fly eye tumor model [41;] metastasis of breast cancer cells in mice[42;] regulates actin cytoskeleton through Rho-mDia pathway[43]; forms scaffold network that promote protrusion and FA turnover in motile and cancer cells[44,45]	Negative	PPFIA1 activation by PTPRD promotes glioma progression[46]

Gene name (*Drosophila*)	Human ortholog	DIOPT score out of 15	Best score	Best reverse score	Role in migration	Glioma patient survival	Role in glioma
Lowfat	LIX1L	13	Yes	Yes	LIX1L is a driver of tumor growth and metastasis in hepatocellular carcinoma in mice[47]	Positive	NA
	LIX1	7	No	Yes		Positive	NA
Mesh	SUSD2	13	Yes	Yes	Promotes ovarian cancer metastasis[48]	Negative	SUSD2 is part of a signaling axis that contributes to glioma progression[49]
Parvin	PARVA	14	Yes	Yes	Invasion in human colorectal cancer cells, PARVB inhibits *in vitro* invasion of breast cancer cells[50,51]	Positive	NA
	PARVB	13	No	Yes		Positive	NA
Roughest	KIRREL1	13	Yes	Yes	KIRREL3 participates in myoblast directed migration[52]	Negative	NA
	KIRREL3	12	No	Yes		Negative	NA
	KIRREL2	11	No	Yes		Negative	NA

Gene name (*Drosophila*)	Human ortholog	DIOPT score out of 15	Best score	Best reverse score	Role in migration	Glioma patient survival	Role in glioma
schizo	IQSEC2	12	No	Yes	Cell movements during eye patterning[53]	Positive	NA
Shroom	SHROOM1	2	No	Yes	Regulates epithelial cell shape in the wing disc A-P boundary and required for tissue morphogenesis[54]; germband extension[55]; apical constriction during neural tube closure[56]; epithelial morphogenesis during axis elongation through actomyosin contractility[57]	Negative	NA
	SHROOM3	8	Yes	Yes		Negative	NA
							NA
Symplekin	SYMPK	14	Yes	Yes	Elevated Symplekin mRNA expression in human colorectal cancers including metastatic tumors[58]	Negative	NA
Vulcan	DLGAP1	7	Yes	Yes	Leg disc morphogenesis[59]	Positive	LncRNA upregulated in glioma correlates

Gene name (*Drosophila*)	Human ortholog	DIOPT score out of 15	Best score	Best reverse score	Role in migration	Glioma patient survival	Role in glioma
							with poor prognosis[60,61]
	DLGAP2	6	No	Yes		Positive	NA
Wnt4	WNT9A	4	No	Yes	*Drosophila* salivary gland migration[63]; focal adhesion kinase regulation and cell migration during ovarian morphogenesis[63,64]; chick lung branching and development[65]	Positive	NA
Wunen	PLPP2	9	No	No	Caudal visceral mesoderm cell migration[66,67]; heart cell movement in flies[68]	Negative	NA

Key: ND, not determined; NA, not available.

References are in Supplementary File 2.1.

Table 2.2 Results of the border cell RNAi screen.

Gene	RNAi	Stock center	Construct ID	Construct target sequence	Migration defect (Primary screen)	Migration defect (Secondary screen): Mean ± [SD]
alpha-catenin (α-cat)	**20123[#]**	**VDRC**	**GD8808**	**Same construct[*]**	**89%**	**76% ± 0.07[#]**
	40882	**VDRC**	**GD8808**	**Same construct[*]**	**73%**	ND
	107298	**VDRC**	**KK107916**	**Independent construct**	**86%**	**66% ± 0.05**
CAP	106309	VDRC	KK107936	Independent construct	0.80%	2% ± 0.01
	19054	VDRC	GD8545	Independent construct	7%	4% ± 0.01
	30506	BL	HMS05250	Independent construct	11%	4% ± 0.03
	36663	BL	HMS01551	Independent construct	6.30%	5% ± 0.01
Caskin	24526	VDRC	GD7723	Same construct[*]	11%	9% ± 0.02
	25222	VDRC	GD7723	Same construct[*]	10%	9% ± 0.00
CG3770	4064	VDRC	GD2223	Overlap with KK101078 and HMJ2304[¥]	8%	9% ± 0.01[§]
	103556	VDRC	KK101078	Overlap with GD2223 and HMJ2304 [¥]	26%	2% ± 0.01

Gene	RNAi	Stock center	Construct ID	Construct target sequence	Migration defect (Primary screen)	Migration defect (Secondary screen): Mean ± [SD]
	61262	BL	HMJ2304	Overlap with KK101078 and GD2223[¥]	9%	8% ± 0.01
CG45049	102985	VDRC	KK112983	Independent construct	13%	4% ± 0.01
	102025	VDRC	KK110412	Overlap with GD3956 and GD8606[¥]	8%	8% ± 0.01
	32403	VDRC	GD8606	Overlap with GD3956 and KK112983[¥]	20%	12% ± 0.02
	9673	VDRC	GD3956	Overlap with GD8606 and KK112983[¥]	8%	8%[§]
Dachsous (ds)	**36219**	**VDRC**	**GD14350**	**Independent construct**	**5%**	**14 ± 0.02**
	4313	**VDRC**	**GD2646**	**Independent construct**	**11%**	**12% ± 0.07**
	32964	**BL**	**HMS00759**	**Independent construct**	**ND**	**13% ± 0.05**
	37524	**VDRC**	**GD4034**	**Independent construct**	**9%**	**19% ± 0.03**

Gene	RNAi	Stock center	Construct ID	Construct target sequence	Migration defect (Primary screen)	Migration defect (Secondary screen): Mean ± [SD]
Dreadlocks (dock)	**37525**	**VDRC**	**GD4035**	**Unknown**[†]	**11%**	**NA**[§]
	107064	**VDRC**	**KK102500**	**Independent construct**	**5%**	**4% ± 0.04**
	27728	**BL**	**JF02810**	**Independent construct**	**8%**	**13% ± 0.02**
Fat	**108863**	**VDRC**	**KK101190**	**Independent construct**	**11%**	**11% ± 0.04**
	9396	**VDRC**	**GD881**	**Independent construct**	**8%**	**11% ± 0.02**
G protein alpha i subunit	40890	BL	HMS02138	Overlap with JF0168[¥] and HMS1273[¥]	20%	2% ± 0.02
	31133	BL	JF01608	Overlap with HMS02138[¥] and HMS1273 [¥]	12%	3% ± 0.02
	28150	VDRC	GD12576	Overlap with JF0168[¥]	5%	5% ± 0.01
	34924	BL	HMS01273	Overlap with JF0168 [¥] and HMS02138[¥]	16%	2% ± 0.01
	34653	BL	HMS01129	Independent construct	4%	3% ± 0.04

Gene	RNAi	Stock center	Construct ID	Construct target sequence	Migration defect (Primary screen)	Migration defect (Secondary screen): Mean ± [SD]
G protein alpha o subunit	110552	VDRC	KK109018	Overlap with GD8640¥	21%	3% ± 0.01
	19124	VDRC	GD8640	Overlap with KK109018¥	6%	15% ± 0.06
Gliotactin	37115	VDRC	GD1735	Same construct*	9%	10% ± 0.01
	37116	VDRC	GD1735	Same construct*	12%	6% ± 0.02
	107258	VDRC	KK105971	Independent construct	8%	2% ± 0.03
	38284	BL	HMS01737	Overlap with GD1735 ¥	10%	1% ± 0.01
	58115	BL	HMJ22052	Independent construct	10%	3% ± 0.04
Lachesin (Lac)	**35524**	**VDRC**	**GD12649**	**Overlap with KK107469 and HM05151¥**	**15%**	**10% ± 0.02**
	107450	**VDRC**	**KK107469**	**Overlap with GD12649 and HM05151¥**	**17%**	**5% ± 0.03**
	38536	**BL**	**HMS01756**	**Independent construct**	**23%**	**5% ± 0.02**

Gene	RNAi	Stock center	Construct ID	Construct target sequence	Migration defect (Primary screen)	Migration defect (Secondary screen): Mean ± [SD]
	28940	**BL**	**HM05151**	**Overlap with KK107469 and GD12649¥**	**ND**	**10% ± 0.01**
Liprin-alpha	106588	VDRC	KK100116	Independent construct	6%	5% ± 0.05
	51707	VDRC	GD7232	Independent construct	14%	7% ± 0.01
	53868	BL	HMC03183	Independent construct	19%	5% ± 0.06
Lowfat	32145	VDRC	GD7934	Overlap with KK102118 and JF03183 ¥	5%	ND
	32146	VDRC	GD7934	Overlap with KK102118 and JF03183 ¥	3%	ND
	107630	VDRC	KK102118	Overlap with GD7934 and JF03183 ¥	9.4%	ND
	28755	BL	JF03183	Overlap with KK102118 and GD7934¥	3.5%	ND
Mesh	40940	VDRC	GD3139	Independent construct	16%	3% ± 0.04
	6867	VDRC	GD3140	Unknown†	6%	NA

Gene	RNAi	Stock center	Construct ID	Construct target sequence	Migration defect (Primary screen)	Migration defect (Secondary screen): Mean ± [SD]
Parvin	11670	VDRC	GD3687	Overlap with KK102567¥	7.40%	8% ± 0.01
	105356	VDRC	KK102567	Overlap with GD3687¥	5%	2% ± 0.04
	42831	BL	HMS02523	Independent construct	19%	3% ± 0.02
Roughest (rst)	**27223**	**VDRC**	**GD14475**	**Same construct***	**22%**	**16% ± 0.03**
	27225	**VDRC**	**GD14475**	**Same construct***	**9.6%**	**11% ± 0.01**
	951	**VDRC**	**GD86**	**Overlap with GD14475¥**	**5%**	**4% ± 0.04**
	28672	**BL**	**JF03087**	**Independent construct**	**ND**	**10% ± 0.01**
Schizo	36625	VDRC	GD14895	Same construct*	7%	13% ± 0.03
	36627	VDRC	GD14895	Same construct*	1.50%	NA
	106168	VDRC	KK103616	Independent construct	14%	4% ± 0.03
	39060	BL	HMS01980	Overlap with GD14895¥	5%	3% ± 0.01
	47147	VDRC	GD16363	Independent construct	6%	5% ± 0.005
	100672	VDRC	KK106863	Independent construct	34%	7% ± 0.04

Gene	RNAi	Stock center	Construct ID	Construct target sequence	Migration defect (Primary screen)	Migration defect (Secondary screen): Mean ± [SD]
Shroom	107966	VDRC	KK108450	Overlap with HMS02190[¥]	9.7%	7% ± 0.02
	40942	BL	HMS02190	Overlap with KK108450[¥]	9.7%	7% ± 0.02
Symplekin (Sym)	**33469**	**VDRC**	**GD9722**	Same construct[*]	**14%**	**23% ± 0.1**
	33470	**VDRC**	**GD9722**	Same construct[*]	**23%**	**32% ± 0.02**
	39041	**BL**	**HMS01961**	Independent construct	**8%**	**6% ± 0.01**
Vulcan	46229	VDRC	GD16319	Same construct[*]	14%	3% ± 0.05
	46230	VDRC	GD16319	Same construct[*]	10%	6% ± 0.01
	40925	BL	HMS02173	Independent construct	4%	10% ± 0.03
Wnt4	**38011**	**VDRC**	**GD5347**	Same construct[*]	**23%**	**24%**
	38010	**VDRC**	**GD5347**	Same construct[*]	**7%**	**12% ± 0.02**
	104671	**VDRC**	**KK102348**	Independent construct	**11%**	**13% ± 0.06**

Gene	RNAi	Stock center	Construct ID	Construct target sequence	Migration defect (Primary screen)	Migration defect (Secondary screen): Mean ± [SD]
	29442	**BL**	**JF03378**	Overlap with GD5347¥	**10%**	**9% ± 0.01**
Wunen	51090	VDRC	GD15706	Same construct*	5.1%	ND
	51091	VDRC	GD15706	Same construct*	7%	ND
	6446	VDRC	GD1640	Overlap with GD15706¥	7.6%	ND
mCherry	35785	BL	VALIUM20-mCherry		2-11%	3% ± 0.02

Key: ND, not determined; NA, stock not available to retest; SD, standard deviation; ¥, Overlapping target sequences either partial or identical; *, Same construct but independent insertions; §, RNAi line tested in two trials (stock dead or no longer available at the stock center); #, data from Chen et al., 2020; †, Stock no longer available and the targeted sequence is unknown.

2.7 References

Aceto, N., A. Bardia, D. T. Miyamoto, M. C. Donaldson, B. S. Wittner *et al*., 2014 Circulating tumor cell clusters are oligoclonal precursors of breast cancer metastasis. Cell 158: 1110–1122.

Agnihotri, S., B. Golbourn, X. Huang, M. Remke, S. Younger *et al*., 2016 PINK1 Is a Negative Regulator of Growth and the Warburg Effect in Glioblastoma. Cancer Res 76: 4708–4719.

Alhadyian, H., D. Shoaib, and R. E. Ward, 2021 Septate junction proteins are required for egg elongation and border cell migration during oogenesis in *Drosophila*. G3 (Bethesda).

Aranjuez, G., E. Kudlaty, M. S. Longworth, and J. A. McDonald, 2012 On the Role of PDZ Domain-Encoding Genes in *Drosophila* Border Cell Migration. G3: Genes, Genomes, Genetics 2: 1379–1391.

Aranjuez, G., A. Burtscher, K. Sawant, P. Majumder, and J. A. McDonald, 2016 Dynamic myosin activation promotes collective morphology and migration by locally balancing oppositional forces from surrounding tissue. Mol Biol Cell 27: 1898–1910.

Arata, M., K. Sugimura, and T. Uemura, 2017 Difference in Dachsous Levels between Migrating Cells Coordinates the Direction of Collective Cell Migration. Developmental Cell 42: 479-497.e10.

Bao, S., and R. Cagan, 2005 Preferential adhesion mediated by Hibris and Roughest regulates morphogenesis and patterning in the *Drosophila* eye. Dev Cell 8: 925–935.

Bao, S., Q. Wu, R. E. McLendon, Y. Hao, Q. Shi *et al*., 2006 Glioma stem cells promote radioresistance by preferential activation of the DNA damage response. Nature 444: 756–760.

Bastock, R., and D. Strutt, 2007 The planar polarity pathway promotes coordinated cell migration during *Drosophila* oogenesis. Development 134: 3055–3064.

Ben-Zvi, D. S., and T. Volk, 2019 Escort cell encapsulation of *Drosophila* germline cells is maintained by irre cell recognition module proteins. Biol Open 8.

Bischoff, M., 2012 Lamellipodia-based migrations of larval epithelial cells are required for normal closure of the adult epidermis of *Drosophila*. Dev Biol 363: 179–190.

Blair, S., and H. McNeill, 2018 Big roles for Fat cadherins. Curr Opin Cell Biol 51: 73–80.

Booker, M., A. A. Samsonova, Y. Kwon, I. Flockhart, S. E. Mohr *et al*., 2011 False negative rates in *Drosophila* cell-based RNAi screens: a case study. BMC Genomics 12: 50.

Bosveld, F., B. Guirao, Z. Wang, M. Rivière, I. Bonnet *et al*., 2016 Modulation of junction tension by tumor suppressors and proto-oncogenes regulates cell-cell contacts. Development 143: 623–634.

Buday, L., L. Wunderlich, and P. Tamás, 2002 The Nck family of adapter proteins: regulators of actin cytoskeleton. Cell Signal 14: 723–731.

Cai, D., S.-C. Chen, M. Prasad, L. He, X. Wang *et al*., 2014 Mechanical feedback through E-cadherin promotes direction sensing during collective cell migration. Cell 157: 1146–1159.

Chaki, S. P., and G. M. Rivera, 2013 Integration of signaling and cytoskeletal remodeling by Nck in directional cell migration. Bioarchitecture 3: 57–63.

Chang, Y.-C., J.-W. Wu, Y.-C. Hsieh, T.-H. Huang, Z.-M. Liao *et al*., 2018 Rap1 Negatively Regulates the Hippo Pathway to Polarize Directional Protrusions in Collective Cell Migration. Cell Rep 22: 2160–2175.

Chen, J., Y. Li, T.-S. Yu, R. M. McKay, D. K. Burns *et al*., 2012 A restricted cell population propagates glioblastoma growth after chemotherapy. Nature 488: 522–526.

Chen, X., S. Wanggou, A. Bodalia, M. Zhu, W. Dong *et al*., 2018 A Feedforward Mechanism Mediated by Mechanosensitive Ion Channel PIEZO1 and Tissue Mechanics Promotes Glioma Aggression. Neuron 100: 799-815.e7.

Chen, A. S., and R. D. Read, 2019 *Drosophila* melanogaster as a Model System for Human Glioblastomas. Adv Exp Med Biol 1167: 207–224.

Chen, Y., N. Kotian, G. Aranjuez, L. Chen, C. L. Messer *et al*., 2020 Protein phosphatase 1 activity controls a balance between collective and single cell modes of migration. eLife 9: e52979.

Cheng, L., Q. Wu, O. A. Guryanova, Z. Huang, Q. Huang *et al*., 2011 Elevated invasive potential of glioblastoma stem cells. Biochem Biophys Res Commun 406: 643–648.

Cheung KJ, Ewald AJ. 2016a. A collective route to metastasis: Seeding by tumor cell clusters. Science. 352(6282):167–169.

Cheung, K. J., V. Padmanaban, V. Silvestri, K. Schipper, J. D. Cohen *et al*., 2016b. Polyclonal breast cancer metastases arise from collective dissemination of keratin 14-expressing tumor cell clusters. PNAS 113: E854–E863.

Chi, K.-C., W.-C. Tsai, C.-L. Wu, T.-Y. Lin, and D.-Y. Hueng, 2019 An Adult *Drosophila* Glioma Model for Studying Pathometabolic Pathways of Gliomagenesis. Mol Neurobiol 56: 4589–4599.

Cohen, E. D., M.-C. Mariol, R. M. H. Wallace, J. Weyers, Y. G. Kamberov *et al*., 2002 DWnt4 regulates cell movement and focal adhesion kinase during *Drosophila* ovarian morphogenesis. Dev Cell 2: 437–448.

Desai, R., R. Sarpal, N. Ishiyama, M. Pellikka, M. Ikura *et al*., 2013 Monomeric α-catenin links cadherin to the actin cytoskeleton. Nat Cell Biol 15: 261–273.

Ewen-Campen, B., T. Comyn, E. Vogt, and N. Perrimon, 2020 No Evidence that Wnt Ligands Are Required for Planar Cell Polarity in *Drosophila*. Cell Rep 32: 108121.

Finegan, T. M., and D. T. Bergstralh, 2020 Neuronal immunoglobulin superfamily cell adhesion molecules in epithelial morphogenesis: insights from *Drosophila*. Philos Trans R Soc Lond B Biol Sci 375: 20190553.

Friedl, P., and D. Gilmour, 2009 Collective cell migration in morphogenesis, regeneration and cancer. Nat Rev Mol Cell Biol 10: 445–457.

Friedl, P., J. Locker, E. Sahai, and J. E. Segall, 2012 Classifying collective cancer cell invasion. Nat Cell Biol 14: 777–783.

Friedl, P., and R. Mayor, 2017 Tuning Collective Cell Migration by Cell–Cell Junction Regulation. Cold Spring Harb Perspect Biol 9: a029199.

Fulford, A. D., and H. McNeill, 2020 Fat/Dachsous family cadherins in cell and tissue organisation. Curr Opin Cell Biol 62: 96–103.

Gangwani, K., K. Snigdha, and M. Kango-Singh, 2020 Tep1 Regulates Yki Activity in Neural Stem Cells in *Drosophila* Glioma Model. Front Cell Dev Biol 8: 306.

Garrity, P. A., Y. Rao, I. Salecker, J. McGlade, T. Pawson *et al.*, 1996 *Drosophila* photoreceptor axon guidance and targeting requires the dreadlocks SH2/SH3 adapter protein. Cell 85: 639–650.

Gritsenko, P., W. Leenders, and P. Friedl, 2017 Recapitulating *in vivo*-like plasticity of glioma cell invasion along blood vessels and in astrocyte-rich stroma. Histochem Cell Biol 148: 395–406.

Gritsenko, P. G., and P. Friedl, 2018 Adaptive adhesion systems mediate glioma cell invasion in complex environments. J Cell Sci 131.

Haeger, A., S. Alexander, M. Vullings, F. M. P. Kaiser, C. Veelken *et al*., 2019 Collective cancer invasion forms an integrin-dependent radioresistant niche. Journal of Experimental Medicine 217.

Hu, Y., I. Flockhart, A. Vinayagam, C. Bergwitz, B. Berger *et al*., 2011 An integrative approach to ortholog prediction for disease-focused and other functional studies. BMC Bioinformatics 12: 357.

Ilina, O., L. Campanello, P. G. Gritsenko, M. Vullings, C. Wang *et al*., 2018 Intravital microscopy of collective invasion plasticity in breast cancer. Dis Model Mech 11.

Janiszewska, M., M. C. Primi, and T. Izard, 2020 Cell adhesion in cancer: Beyond the migration of single cells. J Biol Chem 295: 2495–2505.

Johnson, R. I., A. Sedgwick, C. D'Souza-Schorey, and R. L. Cagan, 2011 Role for a Cindr-Arf6 axis in patterning emerging epithelia. Mol Biol Cell 22: 4513–4526.

Kaipa, B. R., H. Shao, G. Schäfer, T. Trinkewitz, V. Groth *et al*., 2013 Dock mediates Scar- and WASp-dependent actin polymerization through interaction with cell adhesion molecules in founder cells and fusion-competent myoblasts. J Cell Sci 126: 360–372.

Keon, B. H., S. Schäfer, C. Kuhn, C. Grund, and W. W. Franke, 1996 Symplekin, a novel type of tight junction plaque protein. J Cell Biol 134: 1003–1018.

Kim, Y. H., Y. W. Choi, J. Lee, E. Y. Soh, J.-H. Kim *et al*., 2017 Senescent tumor cells lead the collective invasion in thyroid cancer. Nat Commun 8: 15208.

Libanje, F., J. Raingeaud, R. Luan, Z. Thomas, O. Zajac *et al*., 2019 ROCK2 inhibition triggers the collective invasion of colorectal adenocarcinomas. EMBO J 38: e99299.

Lim, J., K. K. Norga, Z. Chen, and K.-W. Choi, 2005 Control of planar cell polarity by interaction of DWnt4 and four-jointed. genesis 42: 150–161.

Llimargas, M., M. Strigini, M. Katidou, D. Karagogeos, and J. Casanova, 2004 Lachesin is a component of a septate junction-based mechanism that controls tube size and epithelial integrity in the *Drosophila* tracheal system. Development 131: 181–190.

Madsen, C. D., S. Hooper, M. Tozluoglu, A. Bruckbauer, G. Fletcher *et al*., 2015 STRIPAK components determine mode of cancer cell migration and metastasis. Nat Cell Biol 17: 68–80.

Maiden, S. L., and J. Hardin, 2011 The secret life of α-catenin: moonlighting in morphogenesis. J Cell Biol 195: 543–552.

Marcinkevicius, E., and J. A. Zallen, 2013 Regulation of cytoskeletal organization and junctional remodeling by the atypical cadherin Fat. Development 140: 433–443.

Matakatsu, H., and S. S. Blair, 2004 Interactions between Fat and Dachsous and the regulation of planar cell polarity in the *Drosophila* wing. Development 131: 3785–3794.

McCrea, P. D., D. Gu, and M. S. Balda, 2009 Junctional Music that the Nucleus Hears: Cell–Cell Contact Signaling and the Modulation of Gene Activity. Cold Spring Harb Perspect Biol 1.

McGuire, S. E., Z. Mao, and R. L. Davis, 2004 Spatiotemporal Gene Expression Targeting with the TARGET and Gene-Switch Systems in *Drosophila*. Sci. STKE 2004: pl6.

Mohr, S. E., J. A. Smith, C. E. Shamu, R. A. Neumüller, and N. Perrimon, 2014 RNAi screening comes of age: improved techniques and complementary approaches. Nat Rev Mol Cell Biol 15: 591–600.

Montell, D. J., W. H. Yoon, and M. Starz-Gaiano, 2012 Group choreography: mechanisms orchestrating the collective movement of border cells. Nat Rev Mol Cell Biol 13: 631–645.

Niewiadomska, P., D. Godt, and U. Tepass, 1999 DE-Cadherin is required for intercellular motility during *Drosophila* oogenesis. J Cell Biol 144: 533–547.

Ostrom, Q. T., L. Bauchet, F. G. Davis, I. Deltour, J. L. Fisher *et al*., 2014 The epidemiology of glioma in adults: a "state of the science" review. Neuro Oncol 16: 896–913.

Ostrom, Q. T., D. J. Cote, M. Ascha, C. Kruchko, and J. S. Barnholtz-Sloan, 2018 Adult Glioma Incidence and Survival by Race or Ethnicity in the United States From 2000 to 2014. JAMA Oncol 4: 1254–1262.

Padmanaban, V., I. Krol, Y. Suhail, B. M. Szczerba, N. Aceto *et al*., 2019 E-cadherin is required for metastasis in multiple models of breast cancer. Nature 573: 439–444.

Perrimon, N., J.-Q. Ni, and L. Perkins, 2010 *In vivo* RNAi: today and tomorrow. Cold Spring Harb Perspect Biol 2: a003640.

Plutoni, C., S. Keil, C. Zeledon, L. E. A. Delsin, B. Decelle *et al*., 2019 Misshapen coordinates protrusion restriction and actomyosin contractility during collective cell migration. Nat Commun 10: 3940.

Rao, Y., and S. L. Zipursky, 1998 Domain requirements for the Dock adapter protein in growth-cone signaling. PNAS 95: 2077–2082.

Raza, Q., J. Y. Choi, Y. Li, R. M. O'Dowd, S. C. Watkins *et al*., 2019 Evolutionary rate covariation analysis of E-cadherin identifies Raskol as a regulator of cell adhesion and actin dynamics in *Drosophila*. PLOS Genetics 15: e1007720.

Ruan, W., P. Pang, and Y. Rao, 1999 The SH2/SH3 adaptor protein dock interacts with the Ste20-like kinase misshapen in controlling growth cone motility. Neuron 24: 595–605.

Saadin, A., and M. Starz-Gaiano, 2016 Circuitous Genetic Regulation Governs a Straightforward Cell Migration. Trends Genet 32: 660–673.

Sarpal, R., M. Pellikka, R. R. Patel, F. Y. W. Hui, D. Godt *et al*., 2012 Mutational analysis supports a core role for *Drosophila* α-catenin in adherens junction function. J Cell Sci 125: 233–245.

Sawant, K., Y. Chen, N. Kotian, K. M. Preuss, and J. A. McDonald, 2018 Rap1 GTPase promotes coordinated collective cell migration *in vivo*. MBoC 29: 2656–2673.

Scarpa, E., and R. Mayor, 2016 Collective cell migration in development. J Cell Biol 212: 143–155.

Shahzad, U., M. S. Taccone, S. A. Kumar, H. Okura, S. Krumholtz *et al*., 2021 Modeling human brain tumors in flies, worms, and zebrafish: From proof of principle to novel therapeutic targets. Neuro Oncol 23: 718–731.

Stark, K., O. Crowe, and L. Lewellyn, 2021 Precise levels of the *Drosophila* adaptor protein Dreadlocks maintain the size and stability of germline ring canals. J Cell Sci 134.

Stuelten, C. H., C. A. Parent, and D. J. Montell, 2018 Cell motility in cancer invasion and metastasis: insights from simple model organisms. Nat Rev Cancer 18: 296–312.

Sullivan, K. D., M. Steiniger, and W. F. Marzluff, 2009 A core complex of CPSF73, CPSF100, and Symplekin may form two different cleavage factors for processing of poly(A) and histone mRNAs. Mol Cell 34: 322–332.

Tang, Z., C. Li, B. Kang, G. Gao, C. Li *et al*., 2017 GEPIA: a web server for cancer and normal gene expression profiling and interactive analyses. Nucleic Acids Res 45: W98–W102.

Tatomer, D. C., L. F. Rizzardi, K. P. Curry, A. M. Witkowski, W. F. Marzluff *et al*., 2014 *Drosophila* Symplekin localizes dynamically to the histone locus body and tricellular junctions. Nucleus 5: 613–625.

Te Boekhorst, V., and P. Friedl, 2016a Plasticity of Cancer Cell Invasion-Mechanisms and Implications for Therapy. Adv Cancer Res 132: 209–264.

Te Boekhorst, V., L. Preziosi, and P. Friedl, 2016b Plasticity of Cell Migration *In vivo* and In Silico. Annu Rev Cell Dev Biol 32: 491–526.

Valer, F. B., M. C. R. Machado, R. M. P. Silva-Junior, and R. G. P. Ramos, 2018 Expression of Hbs, Kirre, and Rst during *Drosophila* ovarian development. Genesis 56: e23242.

Volovetz, J., A. D. Berezovsky, T. Alban, Y. Chen, A. Lauko *et al*., 2020 Identifying conserved molecular targets required for cell migration of glioblastoma cancer stem cells. Cell Death Dis 11: 152.

Wang, X., A. Enomoto, N. Asai, T. Kato, and M. Takahashi, 2016 Collective invasion of cancer: Perspectives from pathology and development. Pathol Int 66: 183–192.

Wu, J., A.-C. Roman, J. M. Carvajal-Gonzalez, and M. Mlodzik, 2013 Wg and Wnt4 provide long-range directional input to planar cell polarity orientation in *Drosophila*. Nat Cell Biol 15: 1045–1055.

Yoshida, H., W. Cheng, J. Hung, D. Montell, E. Geisbrecht *et al*., 2004 Lessons from border cell migration in the *Drosophila* ovary: A role for myosin VI in dissemination of human ovarian cancer. PNAS 101: 8144–8149.

Yu, J. J. S., A. Maugarny-Calès, S. Pelletier, C. Alexandre, Y. Bellaiche *et al*., 2020 Frizzled-Dependent Planar Cell Polarity without Secreted Wnt Ligands. Developmental Cell 54: 583-592.e5.

3 Protein phosphatase 1 activity controls a balance between collective and single cell modes of migration

Yujun Chen[1], Nirupama Kotian[1], George Aranjuez[2,†], Lin Chen[3], C. Luke Messer[1], Ashley Burtscher[2], Ketki Sawant[1], Damien Ramel[3, §], Xiaobo Wang[3], and Jocelyn A. McDonald[1*]

[1]Division of Biology, Kansas State University, Manhattan, KS, USA

[2]Lerner Research Institute, Cleveland Clinic, Cleveland, OH, USA

[3]LBCMCP, Centre de Biologie Intégrative (CBI), Université de Toulouse, CNRS, UPS, Toulouse, France

Author contributions

Nirupama Kotian performed experiments and compiled data for for Figure 3.4, Supplementary figure 3.4-1, live time-lapse videos of control and α-catenin RNAi for analysis of protrusion dynamics (Yujun Chen) in Supplementary figure 3.5-1, Video 6, Video 11 and prepared the manuscript with Jocelyn McDonald and Yujun Chen.

3.1 Abstract

Collective cell migration is central to many developmental and pathological processes. However, the mechanisms that keep cell collectives together and coordinate movement of multiple cells are poorly understood. Using the *Drosophila* border cell migration model, we find that Protein phosphatase 1 (Pp1) activity controls collective cell cohesion and migration. Inhibition of Pp1 causes border cells to round up, dissociate, and move as single cells with altered motility. We present evidence that Pp1 promotes proper levels of cadherin-catenin complex proteins at cell-cell junctions within the cluster to keep border cells together. Pp1 further restricts actomyosin contractility to the cluster periphery rather than at individual internal border cell contacts. We show that the myosin phosphatase Pp1 complex, which inhibits non-muscle myosin-II (Myo-II) activity, coordinates border cell shape and cluster cohesion. Given the high conservation of Pp1 complexes, this study identifies Pp1 as a major regulator of collective versus single cell migration.

3.2 Introduction

Cells that migrate as collectives help establish and organize many tissues and organs in the embryo, yet also promote tumor invasion, dissemination and metastasis[1-5]. A wide variety of cells undergo collective cell migration during development, ranging from neural crest cells in *Xenopus*, the zebrafish lateral line primordium, and branching mammary glands[2,5-7], among many other examples. Despite the apparent diversity in collectively migrating cell types, there is remarkable conservation of the cellular and molecular mechanisms that underlie group cell movements. In particular, migrating collectives require fine-tuned organization and cell coordination to move effectively as a unified group. Similar to individually migrating cells, collectively migrating cells display a front-rear polarity, but this polarity is often organized at the group level[8]. Leader cells at the front extend characteristic protrusions that help collectives navigate tissues. Mechanical cell coupling and biochemical signals then reinforce collective polarity by actively repressing protrusions from follower cells and by maintaining lead cell protrusions that pull the group forward[8,9]. Importantly, cell-cell adhesions keep collectives together by maintaining strong but flexible connections between cells. Moreover, many cell collectives exhibit a "supracellular" organization of the cytoskeleton at the outer perimeter of the entire cell group that serves to further coordinate multicellular movement[7,10-12]. Despite progress in understanding how single cells become polarized and motile, less is known about the mechanisms that control the global organization, cohesion, and coordination of cells in migrating collectives.

Drosophila border cells are a genetically tractable and relatively simple model well-suited to investigate how cell collectives undergo polarized and cooperative migration within a developing tissue[13,14]. The *Drosophila* ovary is composed of strings of ovarioles made up of developing egg chambers, the functional unit of the *Drosophila* ovary. During late oogenesis, four

to eight follicle cells are specified at the anterior end of the egg chamber to become migratory border cells. The border cells then surround a specialized pair of follicle cells, the polar cells, and delaminate as a multicellular cluster from the follicular epithelium. Subsequently, the border cell cluster undergoes a stereotyped collective migration, moving between 15 large germline-derived nurse cells to eventually reach the oocyte at the posterior end of the egg chamber (Figure 3.1A-F). Throughout migration, individual border cells maintain contacts with each other and with the central polar cells so that all cells move as a single cohesive unit[15,16]. A leader cell at the front extends a migratory protrusion whereas protrusions are suppressed in trailing follower cells[17-19]. As with other collectives, polarization of the border cell cluster is critical for the ability to move together and in the correct direction, in this case towards the oocyte (Figure 3.1A-F)[17,18].

Polarization of the border cell cluster begins when two receptor tyrosine kinases (RTKs) expressed by border cells, PDGF- and VEGF-receptor related (PVR) and Epidermal Growth Factor Receptor (EGFR), respond to multiple growth factors secreted from the oocyte[20,21]. Signaling through PVR/EGFR increases activation of the small GTPase Rac, triggering F-actin polymerization and formation of a major protrusion in the lead border cell[17,19,20,22]. E-Cadherin-based adhesion to the nurse cell substrate stabilizes this lead cell protrusion via a feedback loop with Rac[16]. Furthermore, the endocytic protein Rab11 and the actin-binding protein Moesin mediate communication between border cells to restrict Rac activation to the lead cell[23]. Mechanical coupling of border cells through E-Cadherin suppresses protrusions in follower cells, both at cluster exterior surfaces but also between border cells and at contacts with polar cells[13,16]. E-Cadherin also maintains border cell attachment to the central polar cells. F-actin and non-muscle myosin II (Myo-II) are enriched at the outer edges of the border cell cluster[24-26]. Such “inside-outside” polarity contributes to the overall cluster shape, cell-cell organization, and coordinated

motility of all border cells[13]. While progress has been made in understanding the establishment of front-rear polarity, much less is known about how individual border cell behaviors are fine-tuned and adjusted to produce coordinated and cooperative movement of the cluster as an entire unit.

In the current study we made the unexpected discovery that Protein phosphatase 1 (Pp1) activity coordinates the collective behavior of individual border cells. Dynamic cycles of protein phosphorylation and dephosphorylation precisely control many signaling, adhesion and cytoskeletal pathways required for cell migration[27]. Serine-threonine kinases, such as Par-1, Jun kinase (JNK), and the p21-activated kinase Pak3, as well as phosphorylated substrate proteins such as the Myo-II regulatory light chain (MRLC; *Drosophila* Spaghetti squash, Sqh) and Moesin regulate different aspects of border cell migration[15,23,28,29]. In contrast, the serine-threonine phosphatases that counteract these and other kinases and phosphorylation events have not been extensively studied, either in border cells or in other cell collectives. Pp1 is a highly conserved and ubiquitous serine-threonine phosphatase found in all eukaryotic cells[30,31]. Pp1 can directly dephosphorylate substrates *in vitro*, but specificity for phosphorylated substrates *in vivo* is generally conferred by a large number of regulatory subunits (also called Pp1-interacting proteins [PIPs]). These regulatory subunits form functional Pp1 complexes through binding to the Pp1 catalytic (Pp1c) subunits and mediate the recruitment of, or increase the affinity for, particular substrates[31,32]. Thus, despite the potential for pleiotropy, Pp1 complexes have specific and precise cellular functions *in vivo*, that range from regulation of protein synthesis, cell division and apoptosis to individual cell migration[33,34].

We now show that Pp1 activity controls multiple collective behaviors of border cells, including timely delamination from the epithelium, collective polarization, cohesion, cell-cell coordination, and migration. Remarkably, Pp1-inhibited border cells round up, break off from the

main group, and move as single cells or small groups but are generally unable to complete their migration. We determine that Pp1 controls the levels of E-Cadherin and β-Catenin, which are needed to retain border cells within a cohesive cluster. Additionally, Pp1 activity restricts F-actin and Myo-II enrichment to the outer edges of the cluster, maintaining a supracellular cytoskeletal ultrastructure and supporting polarized collective movement. Furthermore, a major Pp1 specific complex for Myo-II activity, myosin phosphatase, coordinates border cell shape and adherence of cells to the cluster. Our work thus identifies Pp1 activity, mediated through distinctive phosphatase complexes such as myosin phosphatase, as a critical molecular regulator of collective cell versus single cell behaviors in a developmentally migrating collective.

3.3 Results

NiPp1 blocks border cell collective movement and cohesion *in vivo*

To address the role of phosphatases in border cell migration, we carried out a small-scale genetic screen to inhibit selected serine-threonine phosphatases that are expressed during oogenesis using RNAi as well as a protein inhibitor that targets Pp1 catalytic subunits (Table 3.1)[35,36]. We drove expression of RNAi and the inhibitor using *c306*-GAL4, an early anterior follicle cell driver expressed at high levels in border cells and polar cells (Figure 3.1 – figure supplement 1A). Inhibition of *Pp4-19C* (one RNAi line) and Pp1c, through overexpression of Nuclear inhibitor of Protein phosphatase 1 (NiPp1), significantly disrupted border cell migration (Table 3.1). NiPp1 is an endogenous protein that when overexpressed, effectively and specifically blocks Pp1 catalytic subunit activity *in vivo*[36-39]. Pp1 and associated complexes are important phosphatase regulators of many cellular processes. Moreover, females expressing NiPp1 driven by *c306*-GAL4 did not produce adult progeny when crossed to wild-type males, consistent with infertility and suggesting

a role for Pp1 in normal oogenesis (Figure 3.1 – figure supplement 2A). Here we focused on further elucidating the function of Pp1 in border cells.

We used two GAL4 drivers to assess phenotypes, *c306*-GAL4 to determine early broad function of Pp1 in border cells and polar cells and *slbo*-GAL4 for later more restricted function in just border cells (Figure 3.1 – figure supplement 1). Expression of NiPp1 strongly disrupted both the ability of border cells to organize into a cohesive cluster and to migrate successfully (Figure 3.1G-J). Unlike control border cells, most NiPp1-expressing border cells failed to reach the oocyte by stage 10 (98%; Figure 3.1I). Importantly, NiPp1-expressing border cells were no longer found in one cohesive cluster. Instead, individual cells and smaller groups split off from the main cluster (Figure 3.1H). Whereas control border cells migrated as a single cohesive unit ("1 part"), NiPp1-expressing border cells split into two to three (50%), or more (40%), parts (Figure 3.1H,J). Migration and cluster cohesion defects were observed when NiPp1 was expressed early in both border cells and the central polar cells (*c306*-GAL4; Figure 3.1I, J; Figure 3.1 – figure supplement 2B) or later in just border cells (*slbo*-GAL4; Figure 3.1 – figure supplement 2C-G). Polar cells, through JAK/STAT signaling, recruit border cells to form a migratory cluster, and anchor border cells to the cluster[16,40,41]. Therefore, we tested the function of Pp1 in polar cells. We observed no defects in cohesion or migration when NiPp1 was expressed only in polar cells (*upd*-GAL4; Figure 3.1 – figure supplement 2C,H-K). Fragmentation of clusters, however, was stronger when NiPp1 was driven by *c306*-GAL4 rather than *slbo*-GAL4 (compare Figure 3.1J to Figure 3.1 – figure supplement 2G), possibly due to earlier and higher expression of c306-GAL4 (Figure 3.1 – figure supplement 1)[41]. Although polar cells are normally located at the center of the border cell cluster and maintain overall cluster organization[16,42], individual NiPp1-expressing border cells could completely separate from polar cells as well as the other border cells (Figure 3.1 – figure

supplement 2L-N). Finally, NiPp1 border cells appeared rounder than normal, indicating that individual cell shapes were altered (see below). Together, these results demonstrate that NiPp1 expression in border cells, but not polar cells alone, disrupts collective migration, cluster organization and adhesion.

Because very few border cells reached the oocyte, we investigated whether NiPp1-expressing border cells were correctly specified and functional. We first examined the expression of the transcription factor Slbo, the fly C/EBP homolog, which is required for border cell specification in response to JAK/STAT signaling[41,43]. NiPp1-expressing border cells generally expressed Slbo, similarly to control cells (Figure 3.1 – figure supplement 3A-B'; 30/33 border cells expressed Slbo, n = 6 egg chambers). Proper specification through JAK/STAT signaling restricts the number of follicle cells that become migrating border cells[41,44]. When NiPp1 expression was driven by *c306*-GAL4, the total number of cells in the cluster (border cells and polar cells) was slightly increased to a mean of seven NiPp1 cells compared to six control cells per cluster (Figure 3.1 – figure supplement 3C; n = 27 egg chambers for each genotype). This modest increase in cells per cluster is far fewer than what is observed upon ectopic activation of JAK/STAT[41,44], suggesting that NiPp1 does not greatly impact the specification or recruitment of border cells. Thus, NiPp1 prevents properly specified border cells from staying together and completing migration.

Live NiPp1 border cell clusters fall apart and move slowly

To determine where and when NiPp1-expressing border cells stopped migrating and dissociated from the cluster, we examined border cell clusters using live time-lapse imaging[17,45]. Both control and NiPp1 border cells delaminated from the surrounding epithelium and began their migration as a group (Figure 3.1K-L''; Videos 1-4). NiPp1 border cells separated into multiple sub-clusters or

single cells at various points during migration, particularly after moving between the nurse cells (Videos 2-4). NiPp1 border cells typically migrated as small groups but also could arrange themselves into co-linear chains (Video 3). A few NiPp1 border cells reached the oocyte, although considerably later than control border cells. Indeed, NiPp1-expressing border cells migrated more slowly overall compared to control border cell clusters (~0.35 μm/min NiPp1 versus ~0.65 μm/min control; Figure 3.1M). Individual NiPp1 border cells also moved at variable speeds, with lagging border cells sometimes pushing ahead of the nominal leading cell (Video 2). Labeling with a cortical cell membrane marker, PLCδ-PH-EGFP (*slbo*-GAL4>UAS-PLCδ-PH-EGFP), allowed us to determine that some NiPp1 border cells completely disrupted their cell-cell contacts, whereas other border cells remained in contact (Video 5). Finally, single border cells that broke off from the cluster were frequently left behind and stopped moving forward, appearing to get "stuck" between nurse cells (Videos 2-4). Taken together, these data show that NiPp1 disrupts the ability of border cells to maintain a collective mode of migration, and leads to border cells now moving as single cells or small groups with slower speed that typically fail to reach the oocyte.

NiPp1 inhibits the function of Pp1 catalytic subunits in border cells

NiPp1 is a specific inhibitor of Pp1c activity *in vitro* as well as *in vivo*[37-39]. *Drosophila* has four Pp1c subunit genes[46,47], whereas humans have three genes[30]. Pp1α-96A, Flapwing (Flw), and Pp1-87B transcripts are each expressed at moderate-to-high levels in the adult ovary, whereas Pp1-13C RNA is mainly detected in adult males (http://flybase.org/)[48]. We examined the localization of Pp1α-96A using a genomic fosmid transgene in which the open reading frame of Pp1α-96A is driven by its endogenous genomic regulatory regions and C-terminally tagged with GFP ("Pp1α-96A-GFP")[49]. Pp1α-96A-GFP was detected in the cytoplasm, with higher levels at the cortical membranes of border cells, follicle cells, the oocyte, and nurse cells (Figure 3.2A-C). Endogenous

Flw, as visualized using a functional in-frame YFP protein trap[50] ("Flw-YFP"), was also expressed ubiquitously during the stages in which border cells migrate (Figure 3.2D-F). Specifically, Flw-YFP was enriched at the cell cortex and cytoplasm of all cells, including border cells. Due to a lack of specific reagents, we were unable to determine whether Pp1-87B or Pp1-13C proteins are present in border cells. Therefore, at least two Pp1c subunit proteins are expressed in border cells throughout their migration.

We next determined whether NiPp1 specifically inhibited Pp1c activity in border cells. Overexpression of each of the four *Drosophila* Pp1c subunits individually did not impair border cell migration (Figure 3.2 – figure supplement 3.1A-D). When co-expressed with NiPp1, two of the catalytic subunits, Pp1α-96A and Pp1-87B, strongly suppressed the migration defects caused by NiPp1, with 90% (NiPp1 + Pp1α-96A) and 75% (NiPp1 + Pp1-87B) of border cells now reaching the oocyte compared to 40% with NiPp1 alone (NiPp1 + RFP; Figure 3.2G; Figure 3.2 – figure supplement 1F-H). Co-expression of Pp1α-96A and Pp1-87B partially suppressed the NiPp1-induced cluster fragmentation, leading to 55% (NiPp1 + Pp1α-96A) and 65% (NiPp1 + Pp1-87B) of border cell clusters now found intact compared to ~10% with NiPP1 alone (NiPp1 + RFP; Figure 3.2H; Figure 3.2 – figure supplement 1F-H). Flw and Pp1-13C only mildly suppressed the NiPp1-induced cluster splitting and migration defects (Figure 3.2G,H; Figure 3.2 – figure supplement 1I,J). The observed phenotypic suppressions were likely due to titration of NiPp1 inhibitory activity by excess Pp1c protein, in agreement with previous studies in *Drosophila*[36,38]. Partial suppression could be due to levels of overexpressed Pp1c or effectiveness of the respective Pp1c to titrate NiPp1 in border cells. Co-expression of a human Pp1c homolog ("hPPP1CC") fully suppressed the NiPp1-induced phenotypes and did not disrupt migration when expressed on its own (Figure 3.2G,H; Figure 3.2 – figure supplement 1E,K). hPPP1CC has high homology to Pp1-

87B (93% identical, 96% similar), Pp1α-96A (89% identical, 94% similar), and Pp1-13C (91% identical, 95% similar), with lower homology to Flw (84% identical, 91% similar), although further analysis through the DIOPT (*Drosophila* RNAi Screening Center Integrative Ortholog Prediction Tool) database suggests higher homology to Pp1-87B and Pp1α-96A (http://flybase.org/)[51]. The suppression by multiple Pp1 proteins and full suppression by hPPP1CC suggests that Pp1 catalytic subunit genes have overlapping functions in border cells.

To better understand how NiPp1 inhibits Pp1 activity in border cells, we next analyzed the subcellular localization of Flw-YFP and Pp1α-96A-GFP when NiPp1 was co-expressed. Expression of HA-tagged NiPp1 alone was itself predominantly nuclear, with low expression in the cytoplasm (Figure 3.2 – figure supplement 3.2A-A''). Pp1α -96A-GFP and Flw-YFP normally localize to the cortical membrane and cytoplasm of border cells (Figure 3.2A-F). Upon co-expression with NiPp1, however, Flw-YFP and Pp1α -96A-GFP were now primarily localized to border cell nuclei along with NiPp1 (HA-tagged NiPp1; Figure 3.2 – figure supplement 3.2B-C"). These results suggest that ectopic NiPp1, in addition to directly inhibiting Pp1c activity also sequesters PP1 catalytic subunits in the nucleus[37,38,52].

Pp1c genes are required for border cell cluster migration and cohesion

To determine whether Pp1 catalytic activity itself is required for border cell migration, we next downregulated the *Pp1c* genes by driving the respective UAS-RNAi lines with *c306*-GAL4 (Figure 3A-D). RNAi lines that target 3 of the 4 catalytic subunits (*Pp1α-96A*, *Pp1-87B*, and *Pp1-13C*) strongly disrupted border cell migration (Figure 3.3B-E). The majority of *Pp1c* RNAi border cells either did not migrate ("no migration") or stopped along the migration pathway ("incomplete migration"; Figure 3.3E). *Pp1α-96A*-RNAi in particular, caused a significant fraction of border cells to fail to migrate at all, likely due to a failure to delaminate from the epithelium (~15%;

Figure 3.3E). Knockdown of *Pp1c* genes also caused ≥ 50% of border cell clusters to dissociate into multiple sub-clusters and single cells (Figure 3.3B-D,F). Using live time-lapse imaging, we confirmed that decreased levels of Pp1α-96A, Pp1-87B, and Pp1-13C by RNAi altered border cell migration and caused cells to split from the main cluster (Figure 3.3G; Videos 6-10). Some *Pp1α-96A*-RNAi border cells did not delaminate from the epithelium during the course of imaging (Figure 3.3 – figure supplement 1A; Video 8). Multiple *flw* RNAi lines (see Materials and Methods) did not impair migration or cluster cohesion when expressed in border cell clusters. However, RNAi does not always fully knock down gene function in cells[53]. As complete loss of *flw* is homozygous lethal, we generated border cells that were mosaic mutant for the strong loss of function allele flw^{FP41} [ref 54]. Mosaic flw^{FP41} border cell clusters were typically composed of a mixture of wild-type and mutant cells that frequently fell apart, with ~90% splitting into two or more parts (Figure 3.3H-I; Figure 3.3- figure supplement 1B-B"). In egg chambers with *flw* mutant border cells, 40% of border cell sub-clusters did not delaminate or migrate at all ("no migration") whereas 20% partially migrated but did not reach the oocyte (Figure 3.3H-H",J; Figure 3.3- figure supplement 1B-B"). NiPp1 expression results in more severe phenotypes than RNAi knockdown, or loss, of individual *Pp1c* genes, at least with respect to migration and cluster cohesion, suggesting that Pp1c subunits have both distinct and overlapping functions. In particular, Pp1α-96A and Flw appear to function in border cell delamination, whereas all four subunits likely promote migration and cluster cohesion.

Pp1 promotes cadherin-catenin complex levels and adhesion of border cells

One of the strongest effects of decreased Pp1c activity was the dissociation of border cells from the cluster. In many cell collectives, cadherins critically mediate the attachment of individual cells to each other during migration, although other cell-cell adhesion proteins can also contribute[9,55].

The cadherin-catenin complex members E-Cadherin (*Drosophila* Shotgun; Shg), β-Catenin (*Drosophila* Armadillo; Arm) and α-Catenin are all required for border cell migration[16,42,56,57]. E-Cadherin, in particular, is required for traction of border cells upon the nurse cell substrate, for producing overall front-rear polarity within the cluster, and for attachment of border cells to the central polar cells[16,42]. Complete loss of cadherin-catenin complex members in border cells prevents any movement between nurse cells[42,56,57]. This has precluded a definitive analysis of whether all, or some, complex members promote adherence of border cells to the polar cells and/or to other border cells.

To determine whether adhesion of border cells to the cluster requires a functional cadherin-catenin complex, we used *c306*-GAL4 to drive RNAi for each gene in all cells of the cluster (Figure 3.1 – figure supplement 3.2B). Multiple non-overlapping RNAi lines for *E-Cadherin*, *β-Catenin*, and *α-Catenin* each reduced the respective endogenous protein levels and disrupted border cell migration, in agreement with previous results that used mutant alleles (Figure 3.4A-E,G,I; Figure 3.4 – figure supplement 1A-H'; Video 11)[42,56,58]. Importantly, RNAi knockdown for each of the cadherin-catenin complex genes, driven by *c306*-GAL4, resulted in significant fragmentation of the border cell cluster compared to controls. *E-Cadherin* (40-50%) and *β-Catenin* (55-80%) RNAi lines exhibiting stronger, while *α-Catenin* RNAi lines exhibited milder (~20-30%), cluster fragmentation (Figure 3.4A-D,F,H,J; Video 11). Dissociated RNAi border cells could localize to the side of the egg chamber (Figure 3.4B,D), although others remained on the normal central migration pathway (Figure 3.4C,D). While *α-Catenin* RNAi knockdown in polar cells alone (*upd*-GAL4) caused border cell cluster splitting and migration defects, this effect was significantly milder than the effects of *α-Catenin* knockdown in both polar cells and border cells using *c306*-GAL4 (compare Figure 3.4I,J to Figure 3.4 – figure supplement 1I,J). These results indicate that

the cadherin-catenin complex keeps border cells attached to each other and to the polar cells, which in turn maintains a cohesive cluster.

We next wanted to determine whether Pp1 regulated these adhesion proteins in border cells. We analyzed the levels and localization of E-Cadherin and β-Catenin at cell-cell contacts in NiPp1-expressing border cell clusters that were still intact or loosely connected (Figure 3.4 K-P). In wild-type clusters, E-Cadherin and β-Catenin are highly enriched at cell contacts between border cells (BC-BC) and between border cells and polar cells (BC-PC; Figure 3.4 K-K",M-M"). NiPp1-expressing border cell clusters exhibited reduced levels of E-Cadherin and β-Catenin at most BC-BC contacts (Figure 3.4 L-L",N-N"). Pp1-inhibited polar cells generally retained E-Cadherin and β-Catenin, which was higher compared to border cells (Figure 3.4 L-L",N-N"). We quantified the relative levels of E-Cadherin (Figure 3.4O) and β-Catenin (Figure 3.4 P) at BC-BC contacts in control versus NiPp1 clusters, normalized to the levels of those proteins at nurse cell-nurse cell junctions. Both E-Cadherin and β-Catenin were reduced by almost half compared to matched controls. These data together suggest that Pp1 activity regulates cadherin-catenin proteins at cell-cell contacts, which contributes to adhesion of border cells within the cluster.

Pp1 activity promotes protrusion dynamics but is dispensable for directional migration

Border cells with impaired Pp1 activity migrated significantly slower than control clusters (Figures 3.1M, 3.3G), suggesting that border cell motility was altered. Migrating cells form actin-rich protrusions at the front, or leading edge, which help anchor cells to the migratory substrate and provide traction for forward movement[59,60]. In collectives, protrusive leader cells also help sense the environment to facilitate directional migration[8]. Border cells typically form one or two major protrusions at the cluster front[17,19,22] (Figure 3.5A-A"",C; Figure 3.5 – figure supplement 1A; Video 6). Pp1-inhibited border cells (Pp1c RNAi) still extended forward-directed protrusions

(Figure 3.5A-C; Videos 7-10). Additionally, the numbers, lifetimes, lengths and areas of side- and back-directed protrusions were not generally increased in Pp1-inhibited border cell clusters compared to control (Figure 3.5C-F; Figure 3.5 – figure supplement 1B,C). However, the number of protrusions produced at the front of the cluster was reduced in Pp1 RNAi border cells (range of 0.5-0.85 mean protrusions per frame, all genotypes) compared to control (1.0 mean protrusions per frame; Figure 3.5C). Additionally, the lifetimes of Pp1 RNAi forward-directed protrusions were reduced (Figure 3.5D). Control protrusions at the cluster front had a lifetime of ~18 min, whereas Pp1-inhibited front protrusions persisted for 5-10 min. These short-lived Pp1 RNAi protrusions were also reduced in length, from a third to half the size of control front-directed protrusions (Figure 3.5E; Figure 3.5 – figure supplement 1B). Further, Pp1-inhibited front protrusions were smaller, with a mean area of ~10-20μm^2 compared to the control mean of ~40μm^2 (Figure 3.5F; Figure 3.5F – figure supplement 1C). Thus, Pp1 activity promotes normal protrusion dynamics, including the number, lifetime and size of front-directed protrusions.

The majority of NiPp1 and Pp1c RNAi border cells followed the normal migratory pathway down the center of the egg chamber between nurse cells, even when cells broke off from the main cluster (Figures 3.1H, L-L" and 3.3B-D; Videos 2-5, 7-10). Moreover, in Pp1 RNAi border cells, front-directed protrusions still formed though with altered dynamics. These observations together suggest that Pp1 activity is not required for directional chemotactic migration. To further test this idea, we made use of a Förster Resonance Energy Transfer (FRET) activity reporter for the small GTPase Rac. Normally, high Rac-FRET activity occurs at the cluster front during early migration in response to guidance signals from the oocyte, and correlates with protrusion extension (Figure 3.5 – figure supplement 1D)[22]. Under conditions of PP1-inhibition, the most severely affected clusters fall apart, sometimes on different focal planes, making it difficult to interpret Rac-FRET

signal. We therefore measured global Rac-FRET only in those NiPp1-expressing border cell clusters that remained intact. We detected elevated Rac-FRET activity in NiPp1 border cells similar to control, indicating that Rac activity was largely preserved although with slightly elevated levels (Figure 3.5 – figure supplement 1D,E). In sum, these data indicate that Pp1 activity influences protrusion dynamics and cell motility, but does not appear to be critical for directional orientation of the cluster to the oocyte.

Pp1 promotes border cell shape through collectively polarized F-actin and Myo-II

Migrating cells, including cell collectives, change shape to facilitate their movement through complex tissue environments[61]. Some cells maintain a single morphology, such as an elongated mesenchymal or rounded amoeboid shape, throughout migration, whereas other cells interconvert from one shape to another as they migrate. The border cell cluster overall is rounded, although individual border cells within the group appear slightly elongated (Figure 3.6A,A'; Videos 1 and 6)[24]. However, NiPp1 border cells, whether present in small groups or as single cells, were visibly rounder than control border cells (Figure 3.1 H, L-L"; Videos 1-4). We observed similar cell rounding when the *Pp1c* genes were knocked down by RNAi, although some border cells appeared more noticeably round than others (Figures 3.3B-D, 5B-B""; Videos 7-10). To quantify these altered cell shapes, we expressed the membrane marker PLCδ-PH-EGFP to visualize individual cells within the cluster and measured "circularity", which indicates how well a shape approaches that of a perfect circle (1.0; Figure 3.6A-C). Control border cells overall were slightly elongated with a mean of ~0.7, although the circularity of individual cells varied substantially (range of ~0.4 to 0.95), suggesting that border cells undergo dynamic shape changes during migration (Figure 3.6C). In contrast, NiPp1 border cells were rounder, with a mean of ~0.9, and exhibited less variation than control (range of ~0.7 to 1.0; Figure 3.6C).

The rounder cell shapes suggested that Pp1 inhibition alters the cortical cytoskeleton of the border cells. Wild-type border cells exhibit a marked enrichment of F-actin at the cluster periphery, whereas lower levels are detected inside the cluster at contacts between border cells (Figure 3.6D,D',F; Video 12)[25,62]. Upon Pp1 inhibition, F-actin now accumulated around each individual border cell, especially at BC-BC membrane contacts, rather than just being enriched at outer cluster surfaces (Figure 3.6E,E',G; Video 13). Similarly, Myo-II as visualized by GFP-tagged Spaghetti Squash (Sqh-GFP), the *Drosophila* homolog of the myosin regulatory light chain (MRLC), is highly dynamic and normally concentrates in enriched foci at the outer periphery of live border cell clusters both during early (Figure 3.6 – figure supplement 1A-A''''; Video 14) and later stages of migration (Figure 3.6H-H''''; Video 16)[24,26,28]. In NiPp1 border cells, however, Sqh-GFP was now present at cortical cell membranes in dynamic foci surrounding each border cell (or sub-cluster) rather than at the entire cluster periphery, both during early migration (Figure 3.6 – figure supplement 1B-B''''; Video 15) and at mid-migration stages (Figure 3.6I-I''''; Video 17). Thus, inhibition of Pp1 converts collectively polarized F-actin and Myo-II to that characteristic of single migrating cells. As a result, individual border cells now have enriched and dynamic actomyosin localization consistent with elevated cortical contractility in single cells rather than at the collective level.

Pp1 promotes actomyosin contractility in border cells through myosin phosphatase

Rok and other kinases phosphorylate the Myo-II regulatory light chain Sqh[63]. This leads to fully activated Myo-II, which then forms bipolar filaments, binds to F-actin, and promotes cell contractility. Given the altered distribution of Sqh-GFP when Pp1 was inhibited, we next analyzed the levels and distribution of active Myo-II. We used an antibody that recognizes phosphorylated Sqh at the conserved Ser-21 (mammalian MRLC Ser-19; "p-Sqh")[28]. Control border cells

exhibited p-Sqh signal primarily at the cluster periphery ("BC-NC" contacts; Figure 3.7A-A''). This pattern of p-Sqh closely resembles the pattern of Sqh-GFP in live wild-type border cells (Figure 3.6H-H'''')[24,28,64,65]. NiPp1 border cells, however, had high levels of p-Sqh distributed throughout the cluster including at internal BC-BC contacts (Figure 3.7B-B''), similar to Sqh-GFP in live NiPp1 border cells (Figure 3.6I-I''''). We measured the relative ratio of p-Sqh fluorescence intensity at BC-NC contacts versus BC-BC contacts in control and NiPp1 border cell clusters (Figure 3.7C). Control border cells had a higher p-Sqh ratio than NiPp1, indicating less p-Sqh signal at BC-BC contacts. These data support the idea that Pp1 inhibition elevates Myo-II activation within single border cells and at BC-BC contacts.

Myo-II undergoes cycles of activation and inactivation via phosphorylation and dephosphorylation, respectively, to generate dynamic cellular contraction *in vivo*[63]. We previously showed that waves of dynamic Myo-II maintain the collective morphology of border cells to facilitate movement through the egg chamber[24]. The myosin phosphatase complex consists of a Pp1c subunit and a specific regulatory subunit, the myosin binding subunit (Mbs; also called myosin phosphatase-targeting subunit [MYPT]), which together dephosphorylate Sqh and inactivate Myo-II[66]. Previously, we found that Mbs was required for border cell cluster delamination from the epithelium and cell shape[24,28], although cluster cohesion had not been explicitly assessed. We therefore wanted to determine whether myosin phosphatase contributed to the above-described Pp1 functions in cell shape, cluster cohesion and migration. First, we confirmed that Mbs transcript and protein were expressed in border cells throughout migration (Figure 3.7 – figure supplement 1A-F). Mbs protein colocalized with Pp1c subunits near border cell membranes and in the cytoplasm (Figure 3.7 – figure supplement 1G-J). In general, Mbs

colocalized more extensively with Flw-YFP than with Pp1α-96A-GFP (Figure 3.7 – figure supplement 1G-J).

Next, we analyzed the functions of Mbs in border cells. Border cells deficient for Mbs (*Mbs*-RNAi) were rounder than control border cells, exhibited incomplete migration (~30%), and dissociated from the cluster (60%) along the migration pathway (Figure 3.7D-H). The phenotypes observed with *Mbs*-RNAi were generally milder than those observed with Pp1-inhibition (either NiPp1 or *Pp1c*-RNAi; compare to Figures 3.1I,J and 3.3E,F). This could be due to incomplete knockdown by *Mbs*-RNAi, although we observed significant decreases in the levels of endogenous Mbs (Figure 3.7 – figure supplement 1K-L"). Alternatively, myosin phosphatase, through a complex of Mbs/Pp1c, could be one of multiple Pp1 complexes required for border cell cluster migration and cohesion (*see* Discussion). Nonetheless, these findings indicate that myosin phosphatase, a specific Pp1 complex, helps promote the normal cell morphology and collective cohesion of border cells, in addition to facilitating the successful migration of the border cells.

RhoA activates Rho-associated kinase (Rok), thus leading to activation of Myo-II[63]. We and others previously found that expression of constitutively-activated RhoA (*Drosophila* Rho1) causes markedly rounder border cells and alters the distribution of F-actin and Myo-II at cell-cell contacts between border cells[24,26]. We therefore investigated whether Pp1 regulated RhoA activity in migrating border cells. We used a FRET construct that was recently shown to specifically report RhoA activity in ovarian follicle cells[67]. Inhibition of Pp1 by NiPp1 moderately increased the overall levels of Rho-FRET in intact border cell clusters compared to control border cells (Figure 3.7 – figure supplement 2A-C). These data suggest a general upregulation of the RhoA pathway upon Pp1 inhibition.

Interplay between cadherin-catenin adhesion and actomyosin dynamics

During cellular morphogenesis, the cadherin-catenin complex and actomyosin contractility can interact to influence cell-cell junction stability[68-72]. Given the effects of Pp1 inhibition on the cadherin-catenin complex, F-actin, and Myo-II, we asked whether the observed Pp1-dependent phenotypes were secondarily due to decreased adhesion and/or altered actomyosin contractility. Knockdown of *E-cadherin* or *β-catenin* by RNAi decreased the enrichment of F-actin and p-Sqh at the cluster periphery compared to controls (Figure 3.6 – figure supplement 2A-C', E-G, I-K). This is in agreement with a recent study that observed decreased cortical Myo-II in live *E-cadherin*-RNAi border cells[73]. Despite this decrease in F-actin, migrating live *α-Catenin* RNAi border cells, while slower than control, extended protrusions with normal dynamics (Figure 3.5 – figure supplement 1F-J). Interestingly, F-actin was also no longer enriched at the cluster periphery of *Sqh*-RNAi border cells (Figure 3.6 – figure supplement 2D,D',H). Thus, F-actin enrichment at the cluster periphery requires both cadherin-catenin and Myo-II. Moreover, the cadherin-catenin complex promotes enriched activated Myo-II at the outer cluster.

Next, we asked if Myo-II was required for cadherin-catenin enrichment at border cell-border cell junctions. *Sqh*-RNAi border cells had normal levels of E-cadherin (Figure 3.6 – figure supplement 3A-B'', E) and normal to slightly higher levels of β-catenin (Figure 3.6 – figure supplement 3C-D'', F). Knockdown of *Sqh* did not disrupt distribution of E-cadherin or β-catenin at border cell-border cell contacts (Figure 3.6 – figure supplement 3A-D''). These data suggest that Myo-II is not a major regulator of the cadherin-catenin complex in border cells. The phenotypes observed with RNAi-mediated knockdown of the cadherin-catenin complex and Sqh are in contrast to those observed with Pp1 inhibition (e.g. Figures 3.5-3.7). These results are

consistent with a more direct role for Pp1 activity in controlling collective versus single cell dynamics of actomyosin and cadherin-catenin in border cells.

3.4 Discussion

To migrate collectively, cells need to coordinate and cooperate at the multicellular level. Individual cells within a group must remain together, maintain optimal cell shapes, organize motility of neighboring cells, and polarize. The mechanisms that globally orchestrate single cell behaviors within migrating cell collectives are still unclear. Here we report that Pp1 activity is a critical regulator of key intra- and intercellular mechanisms that together produce collective border cell migration. Loss of Pp1 activity, through overexpression of NiPp1 or Pp1c RNAi, switches border cells from migrating as a cohesive cluster to moving as single cells or in small groups (Figure 3.8A). A critical aspect of this switch is the redistribution of enriched F-actin and Myo-II to cell contacts between individual border cells, rather than at the cluster periphery, and a concomitant loss of adhesion between cells. We identified one key Pp1 phosphatase complex, myosin phosphatase, that controls collective-level myosin contraction (Figure 3.8B). Additional phosphatase complexes, through as-yet-unknown regulatory subunits, likely function in border cells to generate collective F-actin organization, maintain cell-cell adhesions, and potentially to restrain overall RhoA activity levels. Our results support a model in which balanced Pp1 activity promotes collective border cell cluster migration, and timely delamination from the epithelium, by coordinating single border cell motility and keeping the cells together (Figure 3.8A).

Many collectively migrating cells require a supracellular enrichment of actomyosin at the group perimeter to help organize their movement[7,10-12]. Active Myo-II is required for border cell collective detachment from the epithelium, cluster shape, rotational movement of the cluster, and normal protrusion dynamics[24,26,28,73,74]. We show here that Pp1 organizes collective-level Myo-II-

contractility during border cell migration. Inhibition of Pp1 shifts the balance of dynamic activated Myo-II from the cluster-level to individual border cells, resulting in rounded, hyper-contractile border cells that dissociate from the cluster. The myosin-specific Pp1 complex, myosin phosphatase, directly dephosphorylates Sqh and inhibits Myo-II activation[66]. Depletion of Mbs, the myosin-binding regulatory subunit of myosin phosphatase, causes rounder border cells and fragmentation of the cluster. We previously found that Mbs-deficient border cells have significantly higher levels of phosphorylated Sqh (p-Myo-II)[28]. Thus, myosin phosphatase inhibits Myo-II activation to promote coordinated collective contractility of border cells. Myosin phosphatase is a downstream target of Rok, which phosphorylates and inhibits the Mbs subunit[75]. Consistent with loss of myosin phosphatase activity, Pp1-inhibition increases phosphorylated active Sqh in individual border cells within the cluster. Thus, myosin phosphatase, downstream of Rok, promotes elevated active Myo-II (p-Sqh/p-Myo-II) and cortical contraction of the entire collective (Figure 3.8B). Interestingly, expression of constitutively activated RhoA also induces cellular hypercontractility, resulting in amoeboid-like round border cells[24,26,73]. RhoA activates Rok, which directly phosphorylates and activates the Myo-II regulatory subunit Sqh[76,77]. We observe somewhat elevated RhoA activity in the absence of Pp1 activity. Thus, Pp1 may also restrain the overall levels of RhoA activity in border cells through an unknown Pp1 complex, which would further promote the collective actomyosin contraction of border cells (Figure 3.8B).

Myo-II is activated preferentially at the cluster periphery and not between internal border cell contacts. Mbs and at least one catalytic subunit, Flw, localize uniformly in border cells, both on the cluster perimeter and between cells. Such uniform phosphatase distribution would be expected to dephosphorylate and inactivate Myo-II everywhere, yet phosphorylated Sqh is only absent from internal cluster border cell contacts. Rok phosphorylates and inactivates Mbs in

addition to directly activating Myo-II[75]. Our previous results indicate that Rok localizes to the cluster perimeter similar to p-Sqh, but there appeared to be overall less Rok between border cells[24]. Thus, spatially localized Rok could inhibit myosin phosphatase and activate Myo-II preferentially at the outer edges of the cluster (Figure 3.8A). Other mechanisms likely contribute to collective polarization of Myo-II. For example, during border cell detachment from the epithelium the polarity kinase Par-1 phosphorylates and inactivates Mbs at the cluster rear resulting in increased active Myo-II, whereas the Hippo pathway prevents accumulation of phosphorylated Myo-II between border cells[25,28].

Our data also support a role for Pp1 in controlling F-actin stability, dynamics, and spatial organization. Similar to the pattern of activated Myo-II, cortical F-actin is normally high at the cluster periphery, although low levels are found between border cells[23,25,62]. Reduced Pp1 activity causes high levels of F-actin to redistribute from the cluster perimeter to surround entire cell cortices of individual border cells. In migrating cells, networks of F-actin produce forces essential for protrusion extension and retraction dynamics that generate forward movement[59,60]. Further supporting a role for Pp1 in regulating F-actin, Pp1-inhibited border cells extend fewer protrusions with shorter lifetimes, resulting in altered motility patterns. How Pp1 promotes F-actin organization and dynamics is unknown. One possibility comes from the known function for Rok in regulating F-actin through the downstream effector LIM Kinase (LIMK)[78]. LIMK phosphorylates and inhibits cofilin, an actin severing and depolymerizing factor[79]. In border cells, cofilin restrains F-actin levels throughout the cluster and increases actin dynamics, resulting in normal cluster morphology and major protrusion formation[80]. Although cofilin dephosphorylation, and thus activation, is typically mediated by the dual-specificity phosphatase Slingshot[79], Pp1-containing complexes have been shown to dephosphorylate cofilin in a variety of cell types[81-84].

Additionally, RhoA activates formin proteins such as Diaphanous, which nucleate actin to form long filaments[85]. There are at least seven formin-related proteins in *Drosophila*, several of which have domains associated with activation by Rho GTPases. However, which formin, if any, promotes border cell migration and F-actin distribution is unknown. Further work will be needed to determine whether any of these potential targets, or other actin regulatory proteins, control collective level F-actin enrichment via Pp1.

A major consequence of decreased Pp1 activity is fragmentation of the border cell cluster into single border cells and small groups. This raises the question of how Pp1 activity maintains cluster cohesion, which is critical for collective cell movement *in vivo*. Like many cell collectives, high levels of cadherin-catenin complex proteins are detected between all border cells[42]. The cadherin-catenin complex is required for border cells to adhere to the central polar cells as well as to provide migratory traction of the entire cluster upon the nurse cells[16,42]. We found that Pp1 maintains E-Cadherin and β-Catenin levels between border cells. Indeed, other mutants that disrupt the levels and localization of adhesion proteins in border cells often also disrupt cluster shape and cohesion. For example, loss of JNK signaling causes border cell clusters to dramatically elongate, with downregulation of adhesion resulting in incomplete separation of border cells[15,86]. Raskol, a putative Ras guanine nucleotide activating protein (GAP), maintains E-cadherin at BC-BC contacts and cohesion of the cluster[87]. However, while loss of *Raskol* causes a significant number of border cells to fully dissociate from the cluster (~35%)[87], similar to what we observe with knockdown of the cadherin-catenin complex, this is less than what we observe upon inhibition of Pp1 activity (~90%). Thus, while cluster fragmentation caused by Pp1 inhibition is at least partly due to deficient cadherin-catenin adhesion, other targets likely contribute.

Our results indicate that E-Cadherin, β-Catenin, and α-Catenin maintain adhesion of border cells to each other in addition to known roles in keeping border cells attached to the polar cells[16]. Knockdown of the cadherin-catenin complex members in both border cells and polar cells causes border cells to significantly dissociate from the cluster. The requirement in border cells for cadherin-catenin in cluster cohesion may have been masked in prior studies due to the inability of strong loss-of-function cadherin-catenin mutant border cells to move at all[16,42,56,57]. While RNAi for E-Cadherin, β-Catenin, and α-Catenin each strongly knock down the respective protein levels, it may be that a small amount of each protein is still present. Such remaining cadherin-catenin proteins may provide just enough traction for border cells to partially migrate upon the nurse cells. We speculate that movement of cadherin-catenin-deficient border cells within the confining tissue would provide mechanical stresses that break the cluster apart at weakened border cell-border cell contacts. Indeed, a mutant α-Catenin protein that lacks part of the C-terminal F-actin-binding domain was shown to partially rescue the migration defects caused by loss of *α-Catenin*; however, these rescued border cell clusters split into several parts along the migration path[57]. Further supporting this idea, Pp1-inhibited border cells fall apart during their effort to migrate between the nurse cells.

How do Pp1 phosphatase complexes molecularly promote cluster cohesion? Given the effects of Pp1 on E-Cadherin and β-Catenin at internal border cell contacts, and the requirement for cadherin-catenin complex proteins in maintaining cluster integrity, Pp1 could directly regulate cadherin-catenin protein stability and/or adhesive strength. In mammalian and *Drosophila* cells, phosphorylation of a conserved stretch of serine residues in the E-Cadherin C-terminal tail region regulates E-Cadherin protein stability, binding of E-Cadherin to β-Catenin, and cell-cell junction formation and turnover[88-90]. Serine-phosphorylation of α-Catenin is also required for adhesion

between epithelial cells and possibly for efficient border cell migration[91]. More work will be needed to determine whether a to-be-identified Pp1-containing phosphatase complex directly dephosphorylates E-Cadherin and/or α-Catenin, as the roles for phosphatases in cadherin-catenin junctional stability are still poorly understood.

Alternatively, or in addition, Pp1-dependent restriction of collective actomyosin contraction to the cluster periphery could allow internal cluster cell-cell junctions to be maintained. Pp1-inhibition greatly alters actomyosin distribution, causing individual border cells to contract and round up. The forces transmitted by high cell contractility alone could weaken adherens junctions, causing the border cells to break apart during migration (Figure 3.8A). Myosin phosphatase-depleted border cells, which have elevated phosphorylated Sqh[28], and thus active Myo-II, are round, highly contractile, and fall off the cluster. In support of this idea, overexpression of a phosphorylation mutant form of Sqh (Sqh^{E20E21}), which mimics activated Myo-II, causes border cells to have a similarly round shape and separate from the cluster[73]. Thus, collective-level active actomyosin contraction contributes to keeping border cells adhered to the cluster. Myo-II and cadherin-catenin complexes have dynamic and quite complex interactions that influence stability of cell-cell junctions, and which may depend on cellular context[68,69]. In border cells, the cadherin-catenin complex promotes enrichment of actomyosin to the cluster periphery, whereas Myo-II does not greatly influence cadherin-catenin levels within the cluster (this study)[73]. However, Pp1 is required for the proper distribution (or stability) of cadherin-catenin at cell contacts between border cells and prevents the enrichment of actomyosin in individual border cells. Moreover, NiPp1 expression disrupts cluster cohesion to a greater extent than knockdown of either myosin phosphatase or cadherin-catenin complex members alone. This suggests that cadherin-catenin stability and optimal collective-wide actomyosin activity both contribute to

cluster cohesion through distinct Pp1 phosphatase complexes, although this possibility remains to be formally tested (Figure 3.8B).

Our study implicates Pp1 as a major regulator of collective cohesion and migration in border cells. Pp1 catalytic subunits and their regulatory subunits are conserved across eukaryotes[30-32,34]. The roles of specific Pp1 complexes in collective cell migration during development and in cancer have not been well studied. Intriguingly, Mypt1 (Mbs homolog) promotes polarized mesodermal migration during zebrafish gastrulation[92]. Similar to what we observe in Mbs-depleted border cells, inhibition of zebrafish Mypt1 switched cells from an elongated mesenchymal mode of migration to a hyper-contractile amoeboid mode of migration. Another Pp1 phosphatase complex containing the Phactr4 (phosphatase and actin regulator 4) regulatory subunit promotes the chain-like collective migration of enteric neural crest cells, which colonize the gut and form the enteric nervous system during development[83]. Phactr4, through Pp1, specifically controls the directed migration and shape of enteric neural crest cells through integrin, Rok, and cofilin. Given the conservation of these and other phosphatase complexes, our study highlights the importance of balanced Pp1 phosphatase activity in the organization and coordination of migrating cell collectives.

3.5 Materials and Methods

Key Resources Table

Reagent type (species) or resource	Designation	Source or reference	Identifiers	Additional information
Genetic reagent (*Drosophila melanogaster*)	*c306*-GAL4 tsGAL80	Aranjuez et al., 2016		Laboratory of Jocelyn McDonald
Genetic reagent (*D. melanogaster*)	*slbo*-GAL4	other	FBal0089668	from D. Montell
Genetic reagent (*D. melanogaster*)	*upd*-GAL4	other	FBal0047063	from D. Montell
Genetic reagent (*D. melanogaster*)	*c306*-GAL4	Bloomington *Drosophila* Stock Center	BDSC Cat# 3743; RRID:BDSC_3743	
Genetic reagent (*D. melanogaster*)	*UAS*-NiPp1.HA	Bloomington *Drosophila* Stock Center	BDSC Cat# 23711; RRID:BDSC_23711	
Genetic reagent (*D. melanogaster*)	*UAS*-Pp1-87B.HA	Bloomington *Drosophila* Stock Center	BDSC Cat# 24098; RRID:BDSC_24098	
Genetic reagent (*D. melanogaster*)	*UAS*-Pp1-13C.HA	Bloomington *Drosophila* Stock Center	BDSC Cat# 23701; RRID:BDSC_23701	

Genetic reagent (*D. melanogaster*)	*UAS*-Pp1alpha-96A.HA	Bloomington *Drosophila* Stock Center	BDSC Cat# 23700; RRID:BDSC_23700	
Genetic reagent (*D. melanogaster*)	*UAS*-hPPP1CC	Bloomington *Drosophila* Stock Center	BDSC Cat# 64394; RRID:BDSC_64394	
Genetic reagent (*D. melanogaster*)	*UAS-mCherry RNAi*	Bloomington *Drosophila* Stock Center	BDSC Cat# 35785; RRID:BDSC_35785	VALIUM20-mCherry
Genetic reagent (*D. melanogaster*)	*UAS*-mCD8.ChRFP	Bloomington *Drosophila* Stock Center	BDSC Cat# 27392; RRID:BDSC_27392	
Genetic reagent (*D. melanogaster*)	*flw*^{FP41} FRT 19A	Bloomington *Drosophila* Stock Center	BDSC Cat# 51338; RRID:BDSC_51338	
Genetic reagent (*D. melanogaster*)	*Ubi*-mRFP.nls, hsFLP, FRT19A	Bloomington *Drosophila* Stock Center	BDSC Cat# 31418; RRID:BDSC_31418	
Genetic reagent (*D. melanogaster*)	*UAS*-PLCδ-PH-GFP	Bloomington *Drosophila* Stock Center	BDSC Cat# 39693; RRID:BDSC_39693	
Genetic reagent (*D. melanogaster*)	*UAS-Pp1α-96A RNAi*	Vienna *Drosophila* Resource Center	VDRC:27673	GD-11970

Genetic reagent (*D. melanogaster*)	*UAS-Pp1-87B RNAi*	Vienna *Drosophila* Resource Center	VDRC:35024	GD-11720
Genetic reagent (*D. melanogaster*)	*UAS-Pp1-13C RNAi*	Vienna *Drosophila* Resource Center	VDRC:29057	GD-14139
Genetic reagent (*D. melanogaster*)	*UAS-Mbs RNAi*	Vienna *Drosophila* Resource Center	VDRC:105762	KK-109231
Genetic reagent (*D. melanogaster*)	*UAS-E-cad RNAi*	Vienna *Drosophila* Resource Center	VDRC:103962	KK-103334
Genetic reagent (*D. melanogaster*)	*UAS-E-cad RNAi*	Vienna *Drosophila* Resource Center	VDRC:27082	GD-14421
Genetic reagent (*D. melanogaster*)	*UAS-β-cat RNAi*	Vienna *Drosophila* Resource Center	VDRC:107344	KK-102545
Genetic reagent (*D. melanogaster*)	*UAS-β-cat RNAi*	Vienna *Drosophila* Resource Center	BDSC:31305	TRiP.JF01252
Genetic reagent (*D. melanogaster*)	*UAS-α-cat RNAi*	Vienna *Drosophila* Resource Center	VDRC:107298	KK-107916
Genetic reagent (*D. melanogaster*)	*UAS-α-cat RNAi*	Vienna *Drosophila* Resource Center	VDRC:20123	GD-8808
Genetic reagent (*D. melanogaster*)	*fTRG sqh*	Vienna *Drosophila* Resource Center	VDRC:318484	fTRG 10075

Genetic reagent (*D. melanogaster*)	*fTRG Pp1α -96A*	Vienna *Drosophila* Resource Center	VDRC:318084	fTRG 290
Genetic reagent (*D. melanogaster*)	flwCPTI002264	Kyoto *Drosophila* Genomics and Genetic Resources	line 115284	FBti0143758
Genetic reagent (*D. melanogaster*)	*UAS*-Flw.HA	The Zurich ORFeome Project,FlyORF	line F001200	
Antibody	rat monoclonal anti-E-cadherin	Developmental Studies Hybridoma Bank	DCAD2; RRID:AB_528120	1:10
Antibody	mouse monoclonal anti-Fasciclin III	Developmental Studies Hybridoma Bank	7G10; RRID:AB_528238	1:10
Antibody	mouse monoclonal anti-Arm	Developmental Studies Hybridoma Bank	N2-7A1; RRID:AB_528089	1:75
Antibody	mouse monoclonal anti-Fascin (Singed)	Developmental Studies Hybridoma Bank	sn 7C; RRID:AB_528239	1:25
Antibody	rabbit polyclonal anti-Phospho-Myosin Light Chain 2 (Ser19)	Cell Signaling Technology, Inc.	#3671; RRID:AB_330248	1:10

Antibody	rat monoclonal anti-HA (3F10)	Millipore Sigma	11867423001; RRID:AB_2314622	1:1000
Antibody	rabbit polyclonal anti-Mbs	Ong et al., 2010		1:200 from Change Tan
Antibody	rabbit polyclonal anti-GFP	Thermo Fisher Scientific	A11122; RRID:AB_221569	1:1000–1:2000
Antibody	chicken polyclonal anti-GFP	Abcam	ab13970; RRID:AB_300798	1:1000
Antibody	rabbit polyclonal anti-PPP1R8 (NiPP1)	Millipore Sigma	HPA027452; RRID:AB_1854490	1:100
Antibody	Alexa Fluor 488, 568, or 647	Thermo Fisher Scientific		1:400
Chemical compound, drug	Alexa Fluor 488 or 568 Phalloidin	Thermo Fisher Scientific	A12379 or A12380	1:400
Chemical compound, drug	Phalloidin-Atto 647N	Millipore Sigma	65906	1:400
Chemical compound, drug	4’,6-Diamidino-2-phenylindole (DAPI)	Millipore Sigma	D9542	0.05 µg/ml

Software, algorithm	FIJI	PMID: 22743772		
Software, algorithm	Graphpad Prism 7, Prism 8	https://www.graphpad.com/		
Software, algorithm	Adobe Photoshop CC	https://www.adobe.com/		
Software, algorithm	Adobe Illustrator CC 2018	https://www.adobe.com/		
Software, algorithm	Affinity Designer 1.7.1	https://affinity.serif.com/		
Software, algorithm	Zeiss AxioVision 4.8	Zeiss		
Software, algorithm	Zeiss ZEN 3.0	Zeiss		
Software, algorithm	Final Cut Pro X 10.4.8	Apple		

Drosophila **genetics and strains**

Crosses were generally set up at 25°C unless otherwise indicated. The *tub*-GAL80^{ts} ("tsGAL80") transgene[93] was included in many crosses to suppress GAL4-UAS expression during earlier stages of development; these crosses were set up at 18˚-22˚C to turn on tsGAL80. For *c306*-GAL4, *c306*-GAL4-tsGal80, *slbo*-GAL4, or *upd*-GAL4 tsGAL80 crosses, flies were incubated at 29°C for ≥ 14 h prior to dissection to produce optimal GAL4-UAS transgene expression. *c306*-GAL4 is expressed early and more broadly in border cells, polar cells, and terminal (anterior and posterior)

follicle cells (Figure 3.1 – figure supplement 1A; Figure 3.1 – figure supplement 2B)[41]. During oogenesis, *slbo*-GAL4 turns on later than *c306*-GAL4, and is expressed in border cells but not polar cells, as well as a few anterior and posterior follicle cells at stage 9 (Figure 3.1 – figure supplement 1B; Figure 3.1 – figure supplement 2C,D)[41,94]. *upd*-GAL4 is restricted to polar cells at all stages of oogenesis (Figure 3.1 – figure supplement 2C,H)[16]. Mosaic mutant clones of *flw* were generated using the FLP-FRT system[95]. The flw^{FP41} FRT 19A line was crossed to *ubi*-mRFP.nls *hs*FLP FRT19A; the resulting progeny were heat shocked for 1 h at 37°C, two times a day for 3 d, followed by 3 d at 25°C prior to fattening and dissection. Mutant clones were identified by loss of nuclear RFP signal from *ubi*-mRFP.nls.

The following *Drosophila* strains (with indicated stock numbers) were obtained from the Bloomington *Drosophila* Stock Center (BDSC, Bloomington, IN, USA): *c306*-GAL4 (3743), UAS-NiPp1.HA (23711), UAS-Pp1-87B.HA (24098), UAS-Pp1-13C.HA (23701), UAS-Pp1α-96A.HA (23700), UAS-hPPP1CC (64394), UAS-mCD8-ChRFP (27392), UAS-mCherry RNAi (35785), UAS-Pp2B-14D RNAi (25929, 40872), UAS-mts RNAi (27723, 38337, 57034, 60342), UAS-Pp4-19C RNAi (27726, 38372, 57823), UAS-CanA-14F RNAi (38966), UAS-PpD3 RNAi (57307), UAS-PpV RNAi (57765), UAS-CanA1 RNAi (25850), UAS-CG11597 RNAi (57047, 61988), UAS-rgdC RNAi (60076), UAS-Flw RNAi (38336), UAS-β-Catenin RNAi JF01252 (31305), flw^{FP41} FRT 19A (51338), ubi-mRFP.nls hsFLP FRT19A (31418), UAS-PLCδ-PH-EGFP ("membrane GFP"; 39693), UAS-GFP.nls (4776).

The following *Drosophila* strains (with indicated stock numbers) were obtained from the Vienna *Drosophila* Resource Center (VDRC, Vienna, Austria): UAS-Pp1α-96A RNAi (v27673), UAS-Pp1-87B RNAi (v35024), UAS-Pp1-13C RNAi (v29058), UAS-Flw RNAi (v29622, v104677), UAS-Mbs RNAi (v105762), UAS-Pp2B-14D RNAi (v46873), UAS-Pp4-19c RNAi

(25317), UAS-E-Cadherin RNAi (v27082, v103962), UAS-β-Catenin RNAi (v107344), UAS-α-Catenin RNAi (v20123, v107298), UAS-Sqh RNAi (v7916), fTRG Pp1α -96A (v318084), fTRG Sqh (v318484).

Other *Drosophila* strains used in this study were: *slbo*-GAL4, *slbo*-GAL4 UAS-mCD8-GFP, *upd*-GAL4;; tsGAL80, and *slbo*-LifeAct-GFP line 2M (from D. Montell, University of California, Santa Barbara, Santa Barbara, CA, USA), $flw^{CPTI002264}$ protein trap (line 115284, Kyoto Stock Center, Kyoto, Japan), UAS-mCherry-Jupiter (from C. Doe, University of Oregon, Eugene, OR, USA), UAS-Rac FRET[22], UAS-Rho FRET/CyO; UAS-Rho FRET/TM6B[67], and UAS-Flw.HA (FlyORF)[96]. The *c306*-GAL4 tsGAL80[24] and *c306*-GAL4 tsGAL80/FM6; UAS-NiPp1.HA/TM3 Ser stocks were created in our lab.

Female fertility test

Fertility was determined according to established methods[97]. Briefly, four *c306*-GAL4 tsGAL80/FM6; Sco/CyO (control) or *c306*-GAL4 tsGAL80/FM6; UAS-NiPP1/TM3 Ser (experimental) females were outcrossed to four w^{1118} males. The flies were allowed to mate for 2 days followed by a 24 h egg lay at 30˚C on fresh food medium supplemented with yeast. Adults were then removed and the progeny allowed to develop in the vial at 25˚C; the food was periodically monitored to avoid drying out. Scoring of eclosed adult progeny from each vial was performed 16-20 d after egg laying and reported as the average progeny per female.

Immunostaining

Fly ovaries from 3- to 5-d-old females were dissected in Schneider's *Drosophila* Medium (Thermo Fisher Scientific, Waltham, MA, USA) supplemented with 10% fetal bovine serum (Seradigm FBS; VWR, Radnor, PA, USA). Ovaries were kept whole or dissected into individual egg chambers, followed by fixation for 10 min using 4% methanol-free formaldehyde (Polysciences,

Warrington, PA, USA) in 0.1 M potassium phosphate buffer, pH 7.4, or in 1X Phosphate Buffered Saline (PBS). Washes and antibody incubations were performed in "NP40 block" (50 mM Tris-HCl, pH 7.4, 150 mM NaCl, 0.5% NP40, 5 mg/ml bovine serum albumin [BSA]). For α-Catenin immunostaining, dissected egg chambers were fixed for 20 min in 4% paraformaldehyde (Electron Microscopy Sciences, Hatfield, PA, USA) in potassium phosphate buffer, pH 7.4, followed by a separate blocking step for 30 min (2% BSA in 1x PBS) prior to each antibody incubation. For p-Sqh antibody staining, ovaries were fixed for 5 min in 8% methanol-free formaldehyde. For the F-actin staining in Figure 3.6, the entire dissection procedure was performed in less than 10 min to preserve F-actin structures, followed by fixation in the presence of Phalloidin at 1:400 dilution; after washing off the fix, the egg chambers were incubated in Phalloidin at 1:400 for 2 h[98].

The following primary antibodies from the Developmental Studies Hybridoma Bank (DSHB, University of Iowa, Iowa City, IA, USA) were used at the indicated concentrations: rat anti-E-Cadherin 1:10 (DCAD2), mouse anti-Fasciclin III 1:10 (FasIII; 7G10), mouse anti-Arm (β-Catenin) 1:75 (N2-7A1), concentrated rat anti-α-Catenin 1:1000 (DCAT1), mouse anti-Eyes Absent 1:100 (eya10H6), mouse anti-Lamin Dm0 1:10 (ADL67.10), and mouse anti-Singed 1:25 (Sn7C). Additional primary antibodies used were: rabbit anti-Phospho-Myosin Light Chain 2 (Ser19) 1:10 (#3671, Cell Science Technology, Danvers, MA, USA), rat anti-HA 1:1000 (11867423001, Millipore Sigma, Burlington, MA, USA), rabbit anti-Mbs 1:200 (from C. Tan, University of Missouri, Columbia, MO, USA); rabbit anti-GFP polyclonal 1:1000-1:2000 (A-11122, Thermo Fisher Scientific), chicken anti-GFP polyclonal 1:1000 (ab13970, Abcam, Cambridge, MA, USA), rabbit anti-PPP1R8 (NiPP1) polyclonal 1:100 (HPA027452, Millipore Sigma), rat anti-Slbo 1:2000 (from P. Rørth, Institute of Molecular and Cell Biology, Singapore). Alexa Fluor 488, 568, or 647 secondary antibodies (Thermo Fisher Scientific) were used at 1:400

dilution. Alexa Fluor Phalloidin (488 or 568; Thermo Fisher Scientific) and Phalloidin–Atto 647N (Millipore Sigma) were used at 1:400 dilution. 4',6-Diamidino-2-phenylindole (DAPI, Millipore Sigma) was used at 0.05 µg/ml. Egg chambers were mounted on slides with Aqua-Poly/Mount (Polysciences) or FluorSave Reagent (Millipore Sigma) for imaging.

Microscopy, live time-lapse imaging, and FRET

Images of fixed egg chambers were acquired with an upright Zeiss AxioImager Z1 microscope and Apotome.2 optical sectioning, or on a Zeiss LSM 880 confocal microscope with or without Airyscan (KSU College of Veterinary Medicine Confocal Core), using either a 20× 0.75 numerical aperture (NA) or 40× 1.3 NA oil-immersion objective.

Live time-lapse imaging was performed as described[17,45]. Briefly, ovarioles were dissected in room-temperature sterile live imaging media (Schneider's *Drosophila* Medium, pH 6.95, with 15–20% FBS). Fresh live imaging media, supplemented with 0.2 µg/ml bovine insulin (Cell Applications, San Diego, CA, USA), was added to the sample prior to mounting on a lumox® dish 50 (94.6077.410; Sarstedt, Newton, NC, USA). Time-lapse videos were generally acquired at intervals of 2–3 min for 3-6 h using a 20× Plan-Apochromat 0.75 NA objective, a Zeiss Colibri LED light source, and a Zeiss Axiocam 503 mono camera. The LED light intensity was experimentally adjusted to maximize fluorescence signal and to minimize phototoxicity of the live sample. Live time-lapse Sqh-GFP imaging was performed on a Zeiss LSM 880 confocal, as described[45], with a 40× 1.2 NA water-immersion objective using an interval of 1 min for up to 20 min total time and a laser setting of 1.5%. Imaging gain and other acquisition parameters were the same, except that the range of *z*-stacks varied slightly depending on the sample. In some cases, multiple *z*-stacks were acquired and merged in Zeiss AxioVision, Zeiss ZEN 2, or FIJI[99] to produce a single, in-focus time-lapse video.

FRET images (Rac FRET, Rho FRET) of live cultured egg chambers were acquired with a Zeiss LSM710 microscope essentially as described[22]. A 40× 1.3 NA oil inverted objective was used to capture single high-resolution stationary images. A 458 nm laser was used to excite the sample. CFP and YFP emission signals were collected through channel I (470–510 nm) and channel II (525–600 nm), respectively. The CFP and YFP channels were acquired simultaneously for most experiments. Sequential acquisition of CFP and YFP channels was tested but produced the same result as simultaneous acquisition.

Image processing and data analysis

Image measurements and editing were performed using Zeiss ZEN 2 or FIJI[99]. Analyses of live border cell migration time-lapse videos was performed using Zeiss ZEN 2 software. The migration speed was calculated from the duration of border cell movement. Protrusion quantification was performed as described[100]. Briefly, a circle was drawn around the cell cluster, and extensions greater than 1.5 µm outside the circle were defined as protrusions (Supplemental Figure 3.6A). Protrusions were classified as directed to the front (0°-45° and 0°-315°), side (45°-135°and 225°-315°), or back (135°-225°), based on their positions within the cluster. The first 1 h of each video was used for protrusion quantification.

To determine the number of cells per cluster, egg chambers were stained for the nuclear envelope marker Lamin, the DNA stain DAPI, and the cell membrane marker E-Cadherin. Only clusters that had delaminated, moved forward, and had any detectable E-Cadherin were imaged. This allowed confidence that the scored cells were border cells. Acquisition of *z*-stacks that encompassed the entire cluster (border cells and polar cells) were defined by nuclear Lamin signal. This was followed by manual counting of the nuclei from the resulting images.

The circularity of border cells was measured in FIJI. Individual border cells were outlined manually based on the PLCδ-PH-GFP signal using the "Freehand Selections" tool. Within the "Set Measurements" analysis tool, "shape descriptors" was selected, followed by the "Measure" function, which provided a measurement of circularity. A value of 1.0 indicates a perfect circle, whereas 0.0 represents an extremely elongated shape.

Measurements of E-Cadherin and β-Catenin intensity at cell–cell junctions were performed on egg chambers that were stained using identical conditions. Samples were imaged with a 40× 1.3 NA oil objective. Identical confocal laser settings were used for each channel and a full *z*-stack of the cluster was produced. Images were then subjected to 3D reconstruction through the "3D Project" function in FIJI. Border cell-border cell (BC-BC) contacts and nurse cell-nurse cell (NC-NC) contacts were manually identified, a line (width set as 6) drawn, and mean fluorescence intensity across the line was obtained using the "measure" tool. A ratio of BC-BC intensity versus NC-NC intensity was calculated to normalize protein levels.

To measure colocalization between Mbs and Flw, or Mbs and Pp1α-96A, the "RGB Profiler" FIJI plugin was used. After converting the image to RGB, a line was drawn across the whole border cell cluster to generate the image intensity plot. The localization patterns of F-actin and Mbs with Pp1α-96A-GFP and Flw-YFP were measured through the "Analyze>Plot Profile" function in FIJI. A line was drawn across the border cells and polar cells and the pixel intensity value was obtained across the line. The values for each channel were normalized to the highest pixel value, and a scatter plot showing F-actin and DAPI was generated in Microsoft Excel.

For Rho-FRET and Rac-FRET, the CFP and YFP images were first processed in ImageJ. A background region of interest was subtracted from the original image. The YFP images were registered to CFP images using the TurboReg plugin. The Gaussian smooth filter was then applied

to both channels. The YFP image was thresholded and converted to a binary mask with the background set to zero. The final ratio image was generated in MATLAB, during which only the unmasked pixels were calculated as described[22].

Figures, graphs, and statistics

Figures were assembled in Adobe Photoshop CC. Illustrations were created in Affinity Designer (Serif, Nottingham, United Kingdom). Videos were assembled in Zeiss AxioVision 4.8, Zeiss ZEN 2, or FIJI. Graphs and statistical tests were performed using GraphPad Prism 7 or Prism 8 (GraphPad Software, San Diego, CA, USA). The statistical tests and *p* values are listed in the figure legends.

3.6 Figures and tables

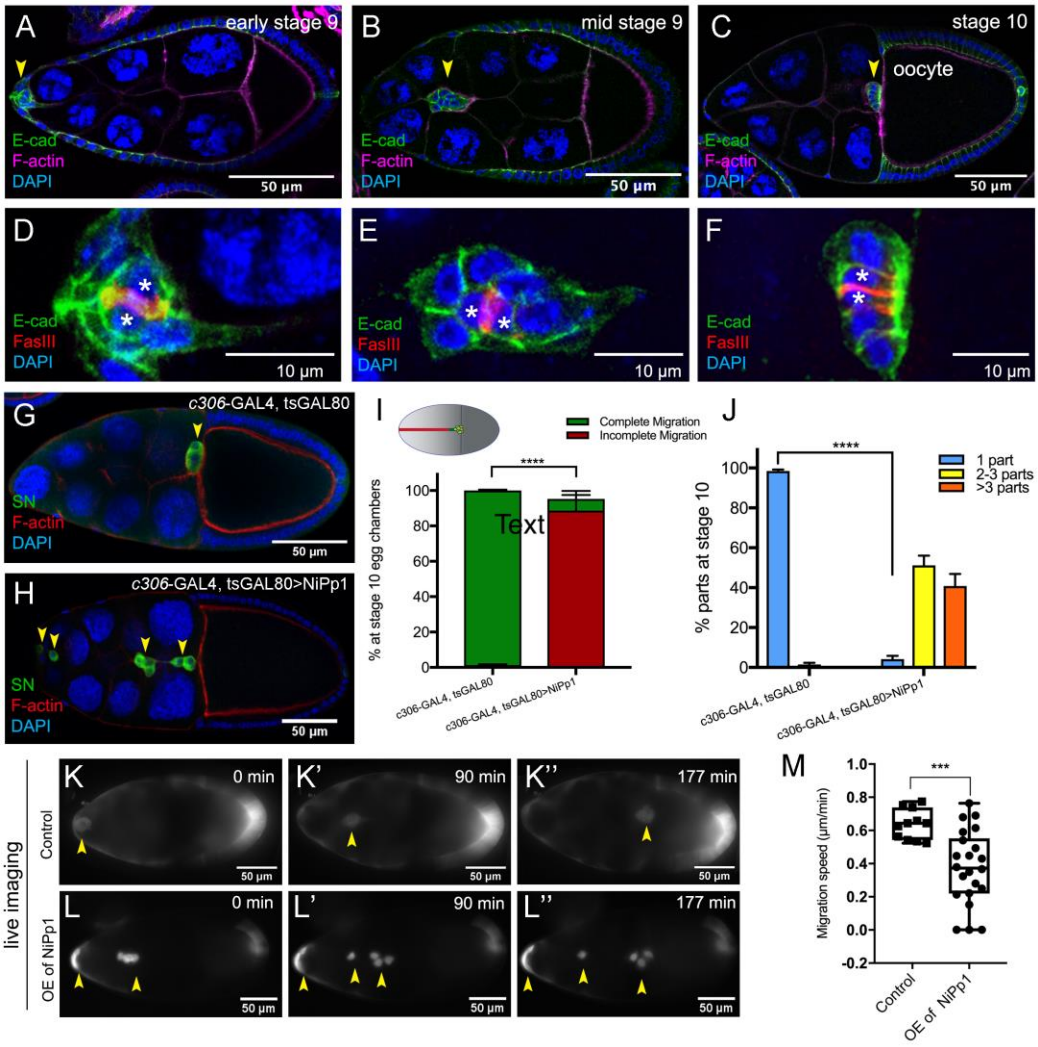

Figure 3.1 NiPp1 expression causes the border cell cluster to fall apart and disrupts migration.

(**A-F**) Wild-type border cell migration during oogenesis stages 9 and 10. (**A-C**) Egg chambers at the indicated stages labeled with E-Cadherin (E-Cad; green), F-actin (magenta) and DAPI (blue). Arrowheads indicate the border cell cluster. (**D-F**) Magnified views of the same border cell cluster from (A-C), showing FasIII (red) in the polar cells, E-Cad and DAPI. The border cell cluster is composed of two polar cells (marked by asterisks) in the center and four to eight outer border cells that are tightly connected with each other as indicated by E-Cad staining. (**G, H**) Egg chambers

labeled with Singed (SN; green) to detect border cells (arrowheads), phalloidin to detect F-actin (red), and DAPI to detect nuclei (blue). Control border cells (G) reach the oocyte as a single cluster, whereas NiPp1-expressing border cells (H) dissociate from the cluster into small groups, with only a few reaching the oocyte. (**I**) Quantification of border cell cluster migration for matched control and NiPp1 overexpression, shown as the percentage that did not complete (red), or completed (green) their migration to the oocyte, as indicated in the egg chamber schematic. (**J**) Quantification of cluster cohesion, shown as the percentage of border cells found as a single unit (1 part) or split into multiple parts (2-3 parts or >3 parts) in control versus NiPp1-expressing egg chambers. (**I, J**) Error bars represent SEM in 3 experiments, each trial assayed $n \geq 69$ egg chambers (total $n \geq 221$ egg chambers per genotype). ***$p < 0.001$, ****$p < 0.0001$, unpaired two-tailed *t* test. (**K-L’’**) Frames from a control (Video 1; K-K”) and an NiPp1 overexpression (OE; Video 2; L-L”) time-lapse video showing movement of the border cell cluster over the course of 3 h (time in minutes). Border cells (arrowheads) express UAS-mCherry-Jupiter, which labels cytoplasmic microtubules. (**M**) Measurement of border cell migration speed from control (n = 11 videos) and NiPp1 overexpression (n = 11 videos; 22 tracked border cell ‘parts’) videos, shown as a box-and-whiskers plot. The whiskers represent the minimum and maximum; the box extends from the 25th to the 75th percentiles and the line indicates the median. ****$p < 0.0001$, unpaired two-tailed *t* test. In this and all subsequent figures, anterior is to the left and the scale bars indicate the image magnification. All genotypes are listed in Table 3.2.

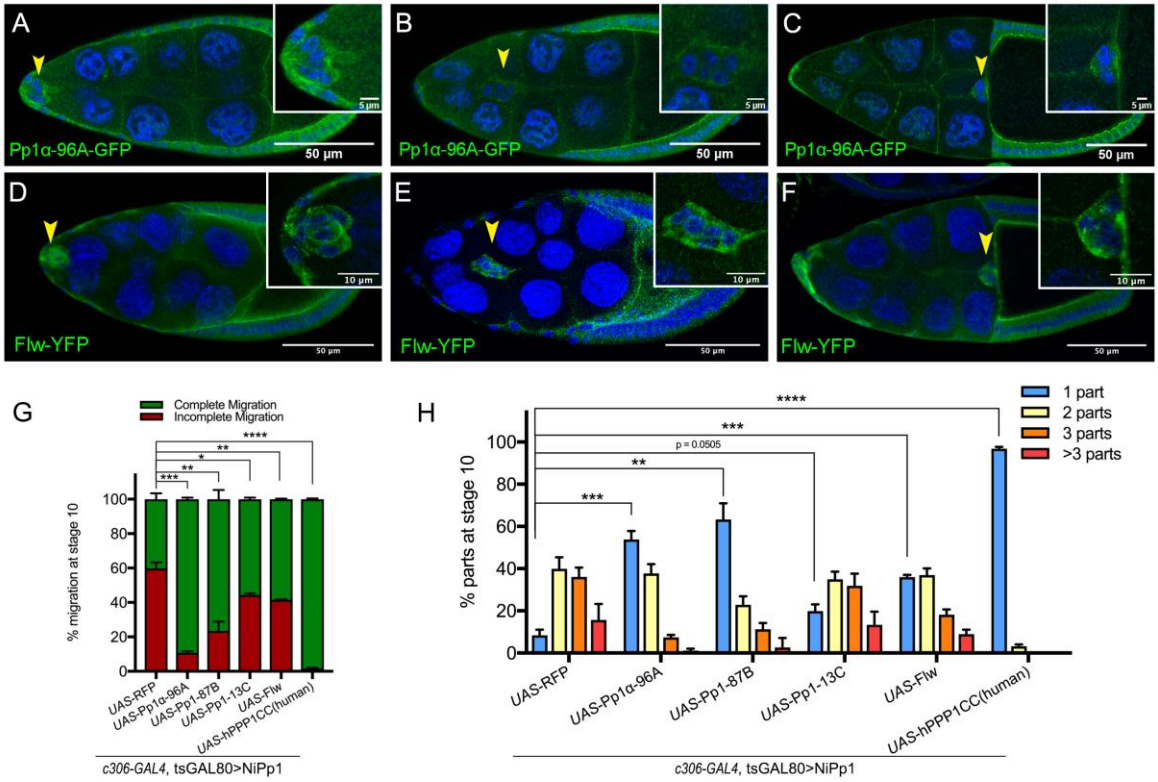

Figure 3.2 Pp1c expression in border cells and specificity of NiPp1 inhibition of Pp1c activity.

(**A-F**) Stage 9 and 10 egg chambers showing the endogenous patterns of Pp1c subunits (green) in border cells (arrowheads), follicle cells, and the germline nurse cells and oocyte. DAPI (blue) labels nuclei. Insets, zoomed-in detail of border cells from the same egg chambers. (**A-C**) Pp1α-96A (green) expression, visualized by a GFP-tagged fly-TransgeneOme (fTRG) line. (**D-F**) Flw expression (green), visualized by a YFP-protein trap in the endogenous *flw* genetic locus. (**G, H**) Overexpression of *Pp1c* genes rescues the migration (G) and cluster cohesion (H) defects of NiPp1-expressing border cells. (**G**) Quantification of the migration distance at stage 10 for border cells in NiPp1-expressing egg chambers versus rescue by overexpression of the indicated *Pp1c* genes, shown as complete (green) and incomplete (red) border cell migration (see Figure 3.1I for egg chamber schematic). (**H**) Quantification of cluster cohesion at stage 10, shown as the percentage of border cells found as a single unit (1 part) or split into multiple parts (2 parts, 3 parts,

>3 parts) in NiPp1-expressing egg chambers versus rescue by overexpression of the indicated *Pp1c* genes. (**G, H**) Error bars represent SEM in 3 experiments, each trial assayed $n \geq 44$ egg chambers (total $n \geq 148$ per genotype). *$p < 0.05$, **$p < 0.01$; ***$p < 0.001$; ****$p < 0.0001$, unpaired two-tailed *t* test. All genotypes are listed in Table 3.2.

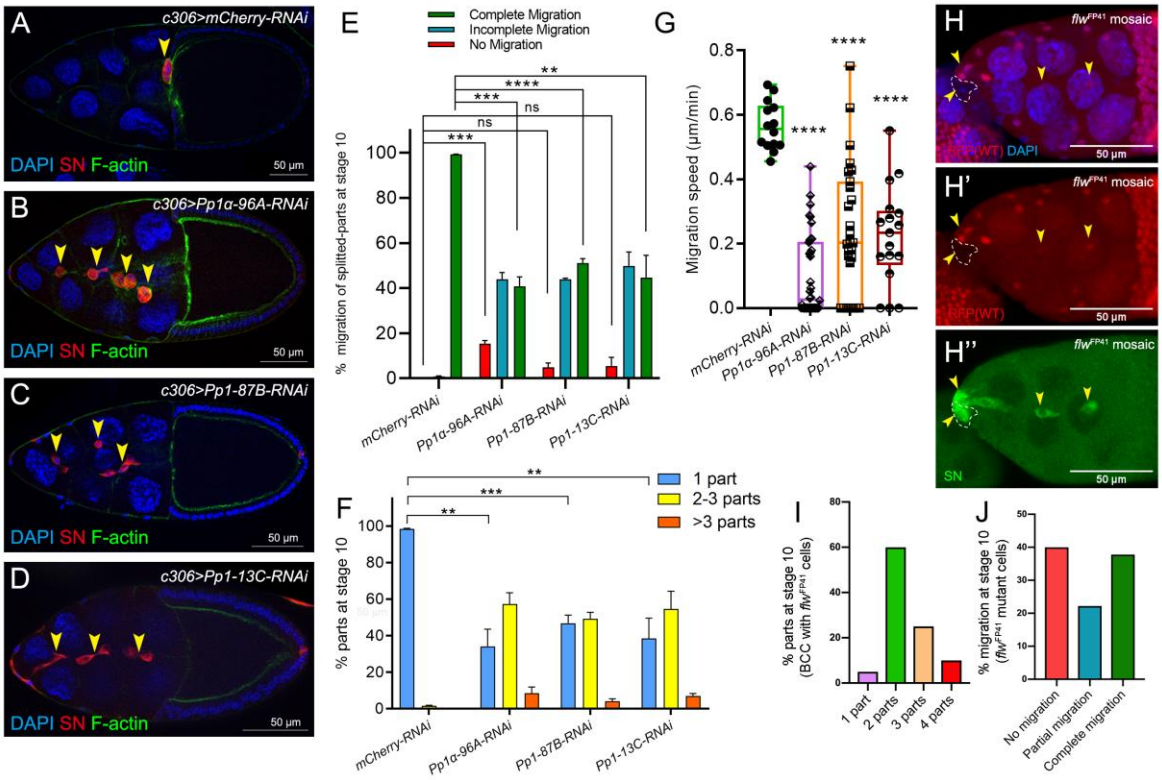

Figure 3.3 Pp1c genes are required for normal border cell migration and cluster cohesion.

Pp1c genes are required for normal border cell migration and cluster cohesion. (**A-F**) Knockdown of *Pp1c* genes by RNAi disrupts border cell cluster migration and cohesion. (**A-D**) Stage 10 egg chambers expressing RNAi against the indicated genes were stained for SN (red) to label border cells (arrowheads), phalloidin to label F-actin (green) and DAPI to label nuclei (blue). (**E**) Quantification of border cell cluster migration for matched control and RNAi knockdown of the indicated *Pp1c* genes, shown as the percentage of egg chambers with complete (green), partial (blue), or no (red) border cell migration. (**F**) Quantification of cluster cohesion, shown as the percentage of border cells found as a single unit (1 part) or split into multiple parts (2-3 parts or >3 parts) in control versus *Pp1c* RNAi egg chambers. (**E, F**) Error bars represent SEM in 3 experiments, each trial assayed n ≥ 58 (total n ≥ 229 per genotype). (**G**) Measurement of border cell migration speed in the indicated genotypes from individual videos of *Pp1c* RNAi border cells;

n = 14 videos for control, n = 11 videos for *Pp1-87B-RNAi* (27 split parts were tracked), n = 12 videos for *Pp1-13C-RNAi* (17 split parts were tracked), n = 16 videos for *Pp1alpha-96A-RNAi* (38 split parts were tracked), box-and-whiskers plot (see Figure 3.1 legend for details of plot). (**E-G**) *p < 0.05, **p < 0.01, ***p < 0.001, ****p < 0.0001, unpaired two-tailed *t* test. (**H-J**) *flw* mutant border cells split from the cluster and often fail to migrate. (**H-H''**) Representative image of a stage 10 egg chamber with flw^{FP41} mutant clones, marked by the loss of nuclear mRFP (dotted outline in H, H') and stained for SN (green in H") to mark border cells (arrowheads) and DAPI (blue in H) to mark nuclei. (**I, J**) Quantification of flw^{FP41} mutant cluster cohesion (I) and migration (J) at stage 10; n=20 egg chambers with flw^{FP41} clones were examined. (**I**) Quantification of cluster cohesion at stage 10, shown as the percentage of flw^{FP41} mosaic border cells found as a single unit (1 part) or split into multiple parts (2, 3, or 4 parts). (**J**) Quantification of the migration distance at stage 10 for flw^{FP41} mosaic mutant border cells, shown as complete (green), partial (blue), or incomplete (red) border cell migration. All genotypes are listed in Table 3.2.

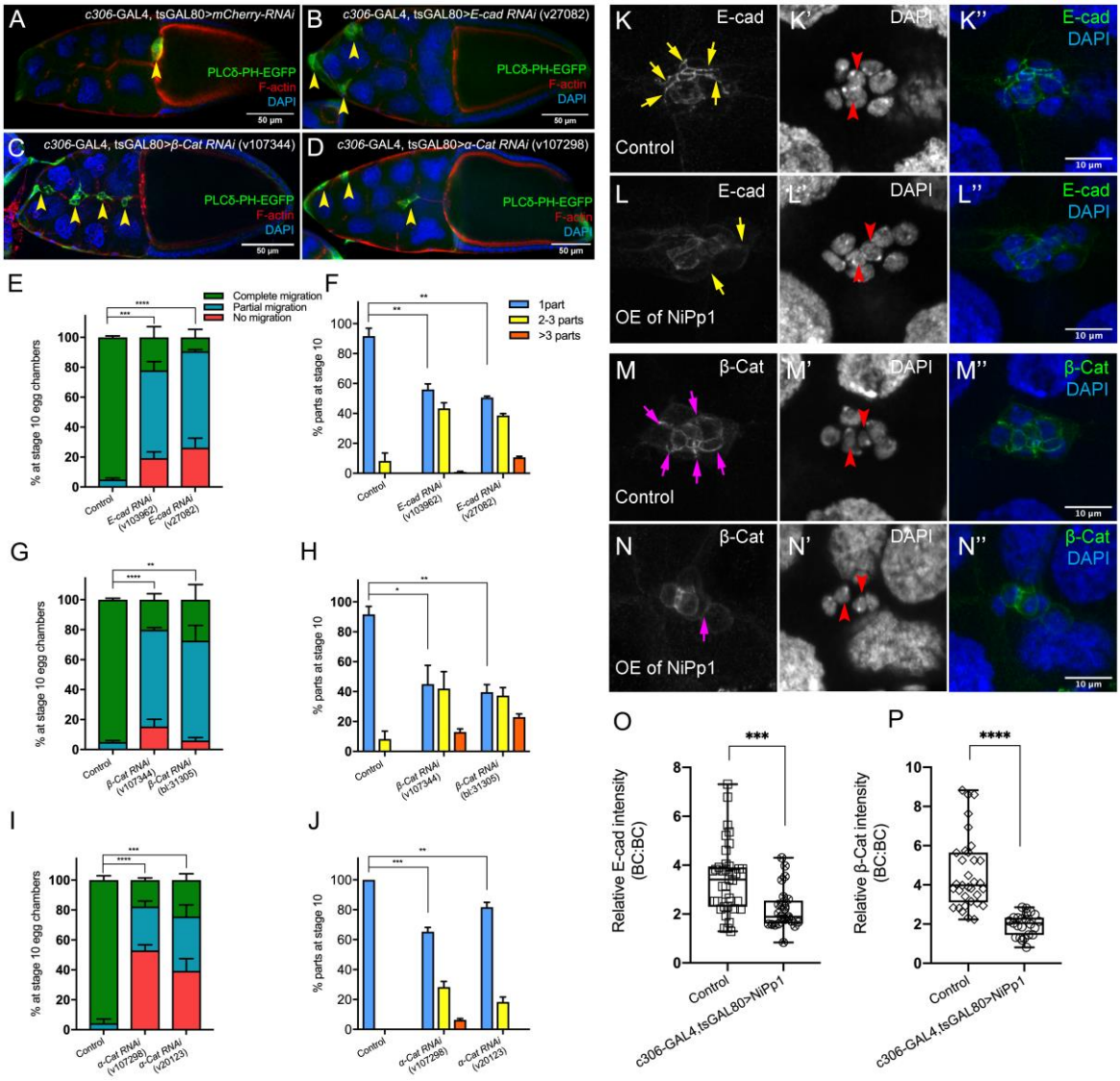

Figure 3.4 The cadherin-catenin complex is required for the collective cohesion of the migrating border cell cluster and is regulated by Pp1.

(**A-J**) Knocking down *E-Cad*, *β-Cat* or *α-Cat* by RNAi disrupts border cell cluster migration and cohesion. Images of stage 10 egg chambers stained for phalloidin to label F-actin (red) and DAPI to label nuclei (blue). Border cells (arrowheads) express the membrane marker PLCδ-PH-EGFP (green). (**E-J**) Quantification of border cell migration (E, G, I) and cluster cohesion (F, H, J) in stage 10 control and *E-Cad-RNAi* (E, F), *β-Cat-RNAi* (G, H) *and α-Cat-RNAi* (I, J) egg chambers. The controls for *E-Cad* and *β-Cat-RNAi* are identical, but shown on separate graphs (E-H) for

clarity; a separate matched control is shown for *α-Cat* RNAi (I, J). Error bars represent SEM in 3 experiments, each trial assayed n ≥ 27 egg chambers (total n ≥ 93 for *each genotype*). *p < 0.05; **p < 0.01; ***p < 0.001; ****p < 0.0001, unpaired two-tailed *t* test. (**E, G, I**) Quantification of border cell migration, shown as the percentage of egg chambers with complete (green), partial (blue), or no (red), border cell migration. (**F, H, J**) Quantification of cluster cohesion, shown as the percentage of border cells found as a single unit (1 part) or split into multiple parts (2-3 parts or >3 parts) in control versus RNAi egg chambers. (**K-N''**) Representative images showing the E-Cad (white in K, L; green in K", L") and β-cat (white in M, N; green in M", N") protein expression pattern in control and NiPp1 overexpressing (OE) border cells. Border cells were co-stained for DAPI to mark nuclei (white in K', L', M', N'; blue in K", L", M", N"). Images were generated from merged *z*-sections. The enriched levels of E-Cad (K, L) and β-cat (M, N) between border cells (border cell-border cell contacts) are marked by yellow and magenta arrows, respectively. The central polar cells are indicated by red arrowheads (K', L', M', N'). (**O, P**) Quantification of relative E-Cad (O) and β-Cat (P) protein intensity levels in control and NiPp1 overexpressing border cell clusters shown as box-and-whiskers plots (see Figure 3.1 legend for details of plot). For E-Cad, 39 border cell-border cell contacts from 8 matched control clusters and 24 border cell-border cell contacts from 16 NiPp1 clusters were measured. For β-Cat, 33 border cell-border cell contacts from 7 matched control clusters and 23 border cell-border cell contacts from 15 NiPp1 clusters were measured. ***p < 0.001, ****p < 0.0001, unpaired two-tailed *t* test. All genotypes are listed in Table 3.2.

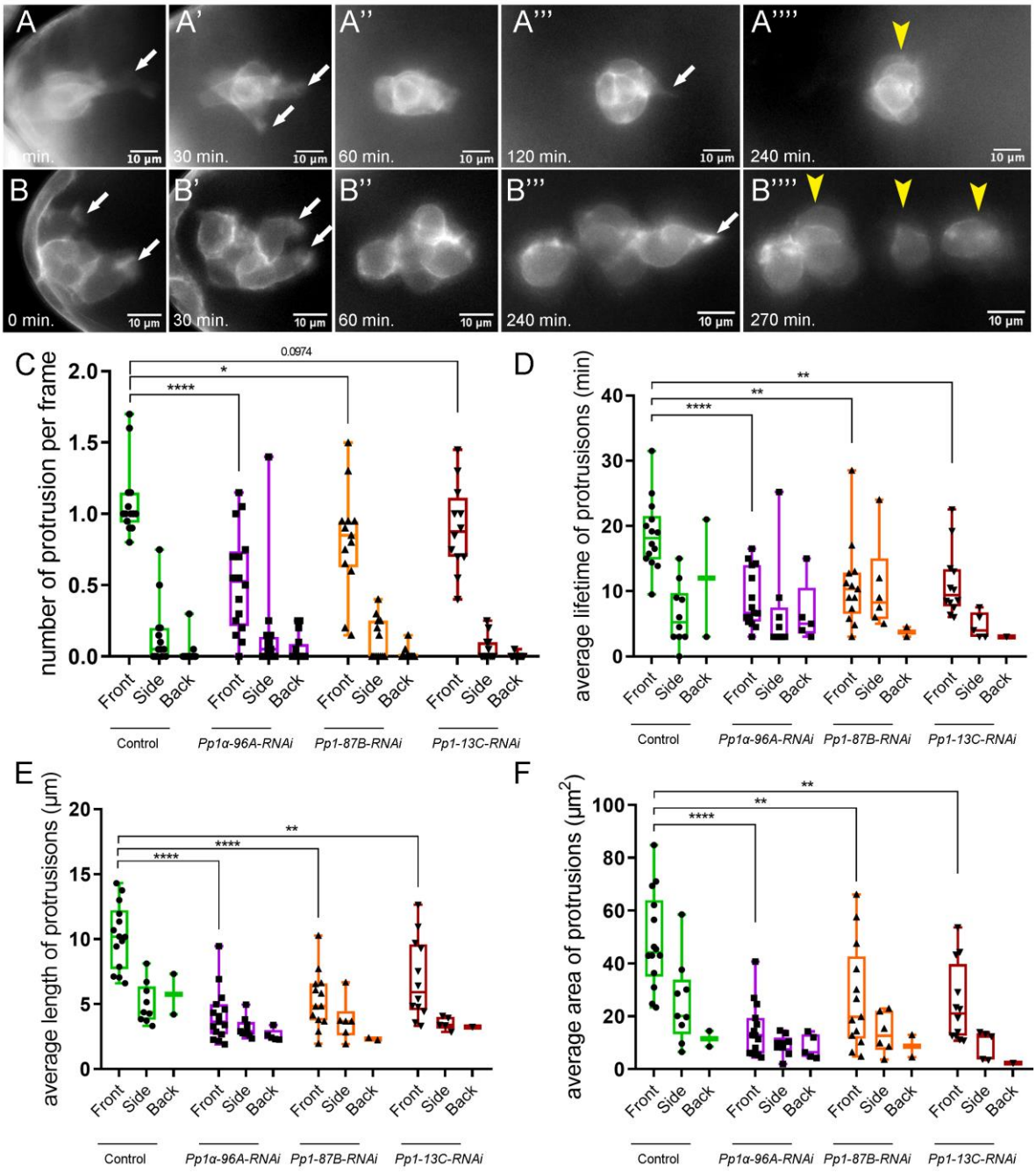

Figure 3.5 Pp1c is required for normal border cell protrusion dynamics.

(**A-B””**) Frames from a matched control (Video 6; A-A””) and a *Pp1alpha-96A-RNAi* (Video 8; B-B””) showing the migrating border cell cluster expressing the membrane marker PLCδ-PH-EGFP. Time in min. Arrows indicate protrusions, arrowheads indicate cluster “parts”. (**C-F**)

Quantification of the number of protrusions per frame (C), average protrusion lifetime (D), average protrusion length (E), and average protrusion area (F) from videos of the indicated genotypes. Protrusions were defined as in Figure 3.5 – figure supplement 1A and in the Materials and Methods. For control, protrusions were measured in 14 videos (n = 51 front-directed protrusions, n = 15 side-directed protrusions, n = 2 back-directed protrusions); for *Pp1alpha-96A-RNAi*, protrusions were measured in n = 16 videos (n = 59 front protrusions, n = 19 side protrusions, n = 9 for back protrusions), for *Pp1-87B-RNAi*, protrusions were measured in 13 videos (n = 67 for front protrusions, n=10 for side protrusions, n = 3 for back protrusions)*;* for *Pp1-13C-RNAi*, protrusions were measured in 12 videos (n = 61 front protrusions, n = 9 side protrusions, n = 1 back protrusion). Data are presented as box-and-whiskers plots (see Figure 3.1 legend for details of plot). *p < 0.05, **p < 0.01, ***p < 0.001, ****p < 0.0001, unpaired two-tailed *t* test. All genotypes are listed in Table 3.2.

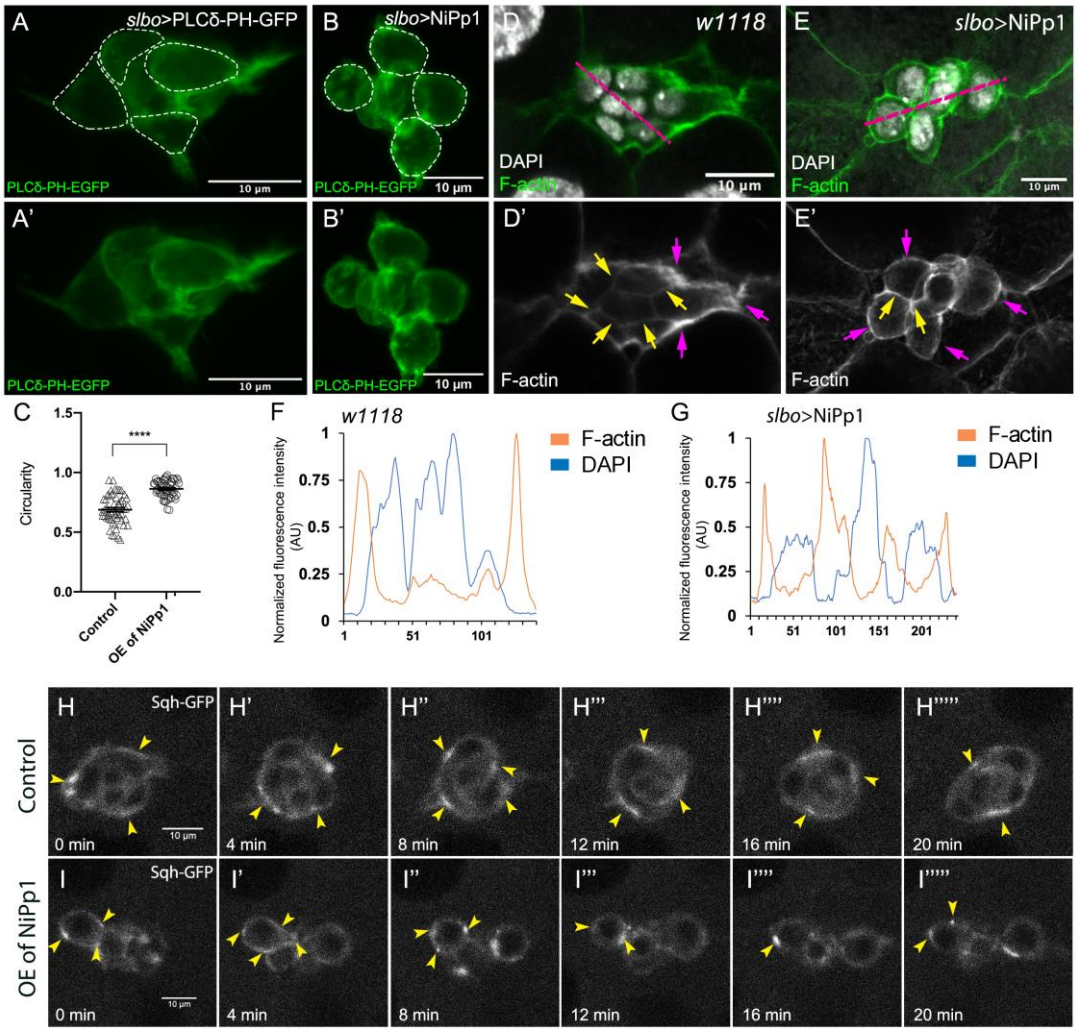

Figure 3.6 Pp1 activity promotes normal border cell shape and distribution of actomyosin in the border cell cluster.

(**A-C**) Pp1 is required for border cell shape. (**A-B'**) Examples of control (A, A') and NiPp1-expressing border cells (B, B'). Cell shape was visualized using the membrane marker PLCδ-PH-EGFP driven by *slbo*-GAL4 (green). Cells were outlined (A, B) and measured for circularity (C). (**C**) Control border cells are more elongated compared to NiPp1-expressing border cells (closer to 1.0, a perfect circle). Quantification of circularity, showing all data points and the mean; 51 control border cells and 57 NiPp1-expressing border cells were measured. ****$p < 0.0001$, unpaired two-tailed *t* test. (**D-G**) Pp1 restricts high levels of F-actin to the border cell cluster periphery. Egg

chambers were stained for phalloidin to detect F-actin (green in D, E; white in D', E') and DAPI to visualize nuclei (white in D, E). (**D, D'**) Control wild-type border cells (w^{1118}) have higher F-actin at the cluster perimeter (magenta arrows) and low levels at cell-cell contacts inside the cluster (yellow arrows). (**E, E'**) NiPp1 overexpression increases F-actin inside the cluster at cell contacts between border cells and at cell contacts between polar cells and border cells (yellow arrows). F-actin is relatively high on the outer surfaces of border cells (magenta arrows). (**F, G**) Plot profiles of normalized F-actin (orange) and DAPI (blue) fluorescence pixel intensity (AU, arbitrary units) measured along the lines shown in (D) and (E); similar results were obtained from additional border cell clusters (n = 11 for control and n = 8 for *slbo*>NiPp1). (**H-I'''''**) Pp1 restricts Myo-II, as visualized by Sqh-GFP, to the cluster periphery in live border cells. Stills from confocal videos of Sqh-GFP in mid-staged border cells over the course of 20 minutes. Enriched Sqh-GFP is marked by arrowheads. Imaging gain and other acquisition parameters were the same, except that the range of *z*-stacks vary slightly. Similar patterns were observed for control in n = 8 movies and n = 10 for NiPp1 overexpression. (**H-H''''**) Control border cells (video 16). (**I-I''''**) NiPp1 overexpression (video 17) changes the dynamics of Sqh-GFP, with more Sqh-GFP located in individual border cells and at cell contacts between border cells. All genotypes are listed in Table 3.2.

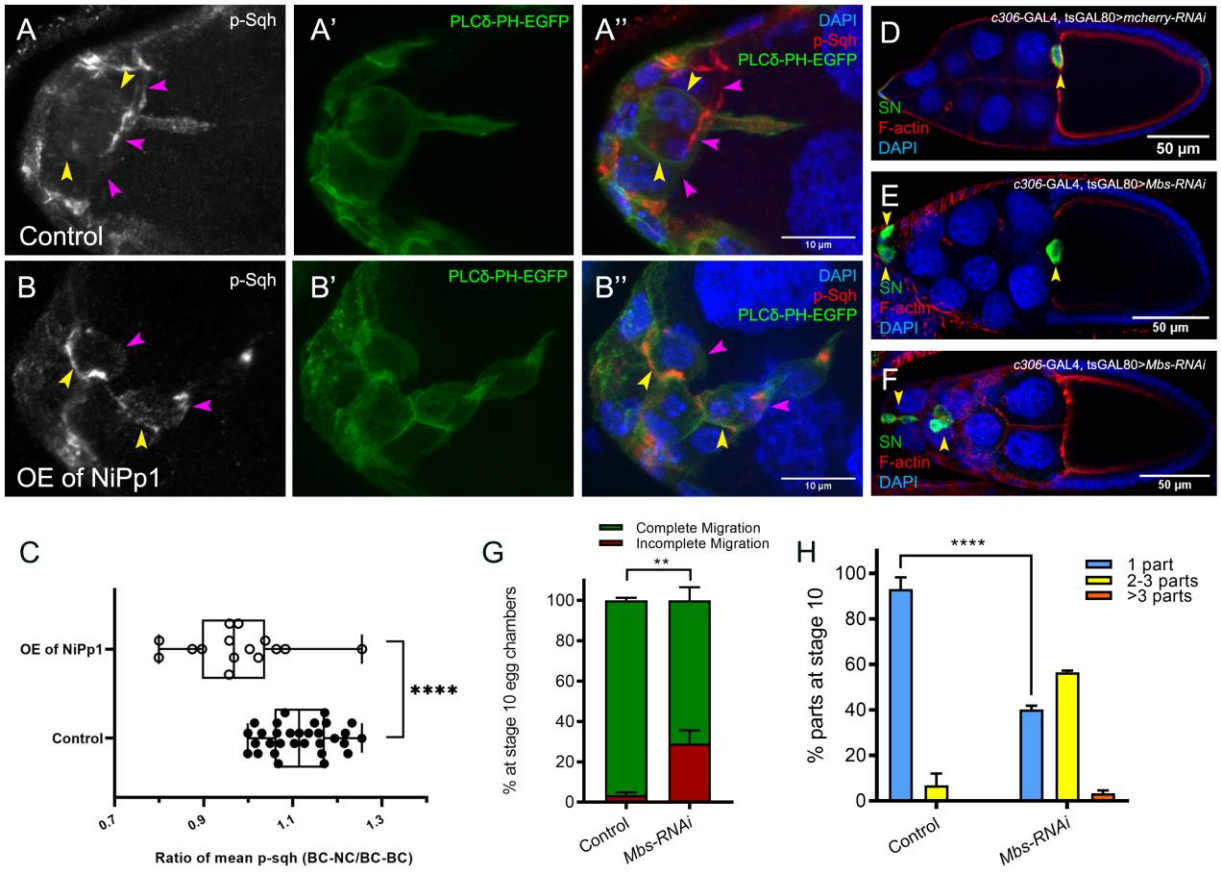

Figure 3.7 Pp1, through myosin phosphatase, promotes contractility of the cluster.

(A-B'') Pp1 restricts Myo-II activation to the cluster periphery. Representative images showing p-Sqh localization (white in A, B; red in A'', B'') and membrane GFP (PLCδ-PH-EGFP; green in A', A'', B', B'') in control (A-A'') and NiPp1 overexpressing (B-B'') border cells; DAPI labels nuclei (blue in A'', B''). There is an increase in p-Sqh levels (arrowheads) at the interface between border cells when NiPp1 is overexpressed. (C) Quantification of the mean pixel intensity of p-Sqh as a ratio of BC:NC/BC:BC. BC:NC stands for border cell-nurse cell interfaces, while BC:BC stands for border cell-border cell interfaces. N = 15 for control and n = 11 for NiPp1 overexpression. (D-H) Knocking down *Mbs* disrupts border cell migration and cluster cohesion. (D-F) Stage 10 control (D) and *Mbs* RNAi (E,F) egg chambers stained for SN to label border cells (green), phalloidin to label F-actin (red) and DAPI to label nuclei (blue). (G) Quantification of

border cell cluster migration for matched control and *Mbs-RNAi*, shown as the percentage that did not complete (red), or completed (green) their migration to the oocyte (see Figure 3.1I for egg chamber schematic). (H) Quantification of cluster cohesion at stage 10, shown as the percentage of border cells found as a single unit (1 part) or split into multiple parts (2 parts, 3 parts, >3 parts) in control versus *Mbs-RNAi* border cells. (G, H) Each trial assayed $n \geq 61$ egg chambers (total $n \geq 220$ per genotype). **$p < 0.01$; ****$p < 0.0001$; unpaired two-tailed *t* test. All genotypes are listed in Table 3.2.

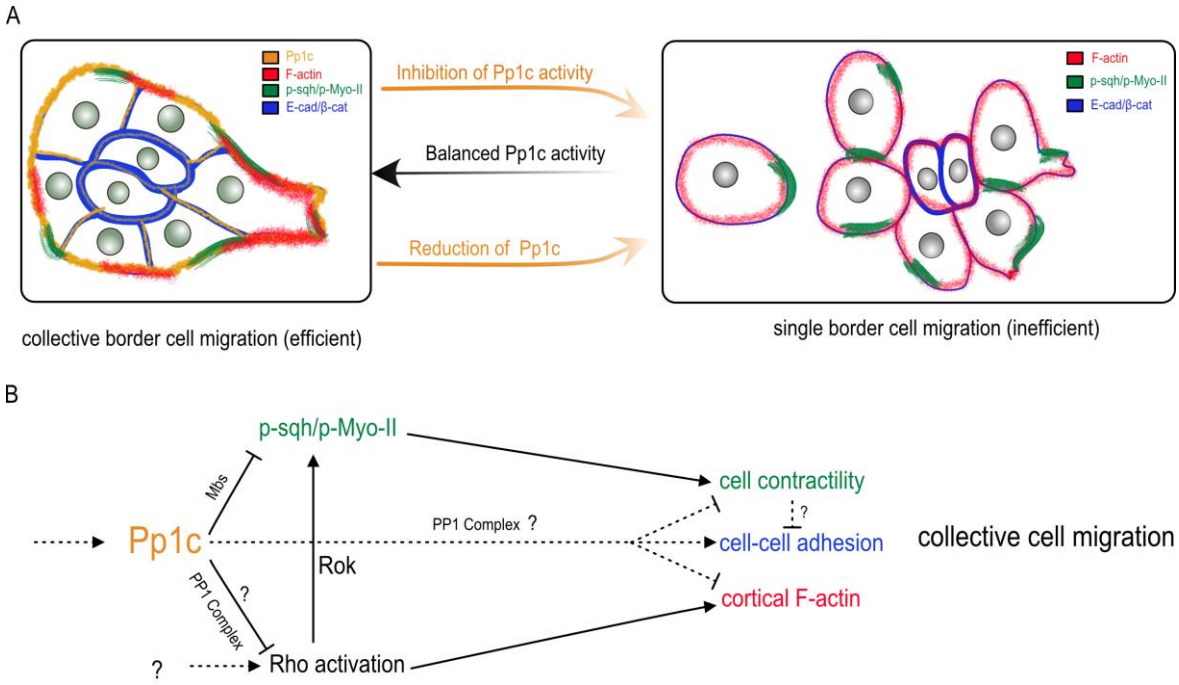

Figure 3.8 Model for the Pp1 function in border cell migration.

(**A**) Schematic of the phenotypes and the localizations of Pp1c, F-actin, p-Sqh, and the cadherin-catenin complex during normal and Pp1-inhibited (NiPp1 expression or *Pp1c-RNAi*) border cell cluster migration. (**B**) Proposed molecular pathways regulated by Pp1, which together promote cohesive collective border cell migration.

Tables

Gene Symbol	Annotation Symbol	RNAi line	Migration Defect (c306-Gal4)	Expression level in ovary (modENCODE)
Pp2B-14D	CG9842	BDSC:25929	No	moderate
		BDSC:40872	No	
		VDRC:46873	No	
mts	CG7109	BDSC:27723	Pupal lethal	moderate
		BDSC:38337	No	
		BDSC:57034	No	
		BDSC:60342	No	
Pp4-19C	CG32505	BDSC:27726	Pupal lethal	moderate
		BDSC:38372	No	
		BDSC:57823	Pupal lethal	
		VDRC:25317	Yes	
CanA-14F	CG9819	BDSC:38966	No	moderate
PpD3	CG8402	BDSC:57307	No	moderate
PpV	CG12217	BDSC:57765	No	moderate
NiPp1	CG8980	BDSC:23711	Yes	moderate
CanA1	CG1455	BDSC:25850	No	low
CG11597	CG11597	BDSC:57047	No	very low
		BDSC:61988	No	
rgdC	CG44746	BDSC:60076	No	very low

Table 3.1 Results of the targeted serine-threonine protein phosphatase RNAi screen.

Figure	Panel	Genotype
Figure 3.1	A-F	*w1118*
	G	*c306*-GAL4,tsGAL80/+
	H	*c306*-GAL4,tsGAL80/+;*UAS*-NiPp1/+
	K	*c306*-GAL4/+; *UAS*-Cherry:Jupiter / +
	L	*c306*-GAL4/+; *UAS*-Cherry:Jupiter / +;*UAS*-NiPp1/+
Figure 3.1-figure supplement 1	A	*c306*-GAL4,tsGAL80/+;*UAS*-GFP.nls/+
	B	*slbo*-GAL4/+;*UAS*-GFP.nls/+
Figure 3.1-figure supplement 2	B	*c306*-GAL4/+;*UAS*-PLCdelta-PH-EGFP/+
	D-G	*slbo*-GAL4,*UAS*-mCD8-GFP/+;
		slbo-GAL4,*UAS*-mCD8-GFP/+;*UAS*-NiPp1/+
	H-K	*upd*-GAL4/+;*UAS*-mCD8.ChRFP/+
		upd-GAL4/+;*UAS*-NiPp1/+
	L-N	*c306*-GAL4,tsGAL80/+
		c306-GAL4,tsGAL80/+;*UAS*-NiPp1/+
Figure 3.1-figure supplement 3	A	*c306*-GAL4/+ (WT)
	B	*c306*-GAL4,tsGAL80/+;*UAS*-NiPp1/+
Figure 3.2	A-C	FlyFos021765(pRedFlp-Hgr)(Pp1alpha-96A15346::2XTY1-SGFP-V5-preTEV-BLRP-3XFLAG)dFRT
	D-F	w[1118] PBac{681.P.FSVS-1}flw[CPTI002264]
	G-H	*c306*-GAL4,tsGAL80/+;*UAS*-NiPp1/*UAS*-mCD8.ChRFP
		c306-GAL4,tsGAL80/+;*UAS*-NiPp1/*UAS*-Pp1α-96A.HA
		c306-GAL4,tsGAL80/+;*UAS*-NiPp1/*UAS*-Pp1-87B.HA
		c306-GAL4,tsGAL80/+;*UAS*-NiPp1/*UAS*-Pp1-13C.HA
		c306-GAL4,tsGAL80/+;*UAS*-NiPp1/*UAS*-Flw.3xHA
		c306-GAL4,tsGAL80/+;*UAS*-hPPP1CC/+;*UAS*-NiPp1/
	A	*c306-GAL4/+;UAS*-Pp1α-96A.HA/+
	B	*c306-GAL4/+;UAS*-Pp1-87B.HA/+

Figure 3.2-figure supplement 1	C	*c306-GAL4/+;UAS*-Pp1-13C.HA/+
	D	*c306-GAL4/+;UAS*-Flw.3xHA/+
	E	*c306-GAL4/+;UAS*-hPPP1CC/+
	F-K	Same as Fig2. G-H
Figure 3.2-figure supplement 2	A	*c306*-GAL4,tsGAL80/+;*UAS*-NiPp1/+
	B	*slbo*-GAL4/+;*UAS*-NiPp1/Pp1alpha-96A-GFP
	C	w1118/Flw-YFP;*slbo*-GAL4/+;*UAS*-NiPp1/+
Figure 3.3	A-D	*c306*-GAL4/+;*UAS-mCherry RNAi*/+
		c306-GAL4/+;*UAS-Pp1α-96A RNAi*/+
		c306-GAL4/+;*UAS-Pp1-87B RNAi* /+
		c306-GAL4/+;*UAS-Pp1-13C RNAi*/+
	G	*c306*-GAL4,tsGAL80/+;*UAS*-mCherry RNAi/*UAS*-PLCdelta-PH-EGFP
		c306-GAL4,tsGAL80/+;UAS-Pp1α-96A RNAi/+;UAS-PLCdelta-PH-EGFP/+
		c306-GAL4,tsGAL80/+;UAS-Pp1-87B RNAi /+;UAS-PLCdelta-PH-EGFP/+
		c306-GAL4,tsGAL80/+;UAS-Pp1-13C RNAi/+;UAS-PLCdelta-PH-EGFP/+
	H-H"	*P{w[+mC]=Ubi-mRFP.nls}1, w[*], P{ry[+t7.2]=hsFLP}12 P{ry[+t7.2]=neoFRT}19A/flwFP41 FRT 19A*
Figure 3.3-figure supplement 1	A	Same as Fig3. G
	B	*P{w[+mC]=Ubi-mRFP.nls}1, w[*], P{ry[+t7.2]=hsFLP}12 P{ry[+t7.2]=neoFRT}19A/flwFP41 FRT 19A*
Figure 3.4	A-J	*c306*-GAL4,tsGAL80/+;*UAS-mCherry RNAi*/+
		c306-GAL4,tsGAL80/+;*UAS-E-cad RNAi(VDRC:103962)*/+
		c306-GAL4,tsGAL80/+;*UAS-E-cad RNAi(VDRC:27082)*/+
		c306-GAL4,tsGAL80/+;*UAS-β-Cat RNAi(VDRC:107344)*/+
		c306-GAL4,tsGAL80/+;*UAS-β-Cat RNAi(VDRC:31305)*/+
		c306-GAL4,tsGAL80/+;*UAS-α-Cat RNAi(VDRC:107298)*/+

		c306-GAL4,tsGAL80/+;*UAS-α-Cat RNAi(VDRC:20123)/+*
	K-P	*w1118(control)*
		c306-GAL4,tsGAL80/+;*UAS*-NiPp1/+
Figure 3.4-figure supplement 1	A,C,E,G	*c306*-GAL4/+;*UAS-mCherry RNAi/+*
	B	*c306*-GAL4/+;*UAS-E-cad RNAi(VDRC:103962)/+*
	D	*c306*-GAL4/+;*UAS-β-Cat RNAi(VDRC:107344)/+*
	F	*c306*-GAL4/+;*UAS-α-Cat RNAi(VDRC:107298)/+*
	G	*c306*-GAL4/+;*UAS-β-Cat RNAi(BDSC:31305)/+*
	I-J	*c306*-GAL4/+;*UAS-mCherry RNAi/+*
		upd-GAL4,tsGAL80/+;*UAS-α-Cat RNAi(VDRC:107298)/+*
		upd-GAL4/+;*UAS-α-Cat RNAi(VDRC:20123)/+*
Figure 3.5	A	*c306*-GAL4,tsGAL80/+;*UAS-mCherry RNAi/UAS*-PLCdelta-PH-EGFP
	B	*c306*-GAL4,*tsGAL80/+;UAS-Pp1α-96A RNAi/+;UAS-P*LCdelta-PH-EGFP/+
	C-F	Same as Fig3. G
Figure 3.5-supplement 1	B-C	Same as Fig3. G
	D-E	yw; *slbo*-GAL4/*UAS*-Rac FRET (WT) and *slbo*-GAL4/*UAS*-Rac FRET; +/*UAS*-NiPp1
	F-J	*c306*-GAL4,tsGAL80/+;*UAS-mCherry RNAi/UAS*-PLCdelta-PH-EGFP
		c306-GAL4,*tsGAL80/+;UAS-α-Cat RNAi(VDRC:107298);UAS-P*LCdelta-PH-EGFP/+
Figure 3.6	A	*slbo*-GAL4/+;*UAS*-PLCdelta-PH-EGFP/+
	B	*slbo*-GAL4/*+;UAS-NiPp1/UAS*-PLCdelta-PH-EGFP
	D,F	*w1118(control)*
	E,G	*slbo*-GAL4/+;*UAS*-NiPp1/+
	H	*c306-GAL4,tsGAL80*/+;+/sqh-GFP(VDRC:318484)
	I	*c306-GAL4,tsGAL80*/+;*UAS*-NiPp1/sqh-GFP(VDRC:318484)
	A	Same as Fig6. H

Figure 3.6-figure supplement 1	B	Same as Fig6. I
Figure 3.6-figure supplement 2	A,A',E,I	*c306*-GAL4,tsGAL80/+;*UAS-mCherry RNAi/+*
	B,B',F,J	*c306*-GAL4,tsGAL80/+;*UAS-E-cad RNAi(VDRC:103962)/+*
	C,C',G,K	*c306*-GAL4/+;*UAS-β-Cat RNAi(BDSC:31305)/+*
	D,D',H	*c306*-GAL4,tsGAL80/+;*UAS-sqh RNAi(VDRC:7916)/+*
Figure 3.6-figure supplement 3	A,C	*c306*-GAL4,tsGAL80/+;*UAS-mCherry RNAi/+*
	B,D	*c306*-GAL4,tsGAL80/+;*UAS-sqh RNAi(VDRC:7916)/+*
Figure 3.7	A-A'	*c306*-GAL4,tsGAL80/+;*UAS*-PLCdelta-PH-EGFP/+
	B-B'	*c306*-GAL4,tsGAL80/+;*UAS*-PLCdelta-PH-EGFP/UAS-NiPp1
	D-H	*c306*-GAL4,tsGAL80/+;*UAS*-mCherry RNAi/+
		c306-GAL4,tsGAL80/+;*UAS*-Mbs RNAi/+
Figure 3.7-figure supplement 1	D-F	*w1118*
	G-G"	FlyFos021765(pRedFlp-Hgr)(Pp1alpha-96A15346::2XTY1-SGFP-V5-preTEV-BLRP-3XFLAG)dFRT
	I-I"	w[1118] PBac{681.P.FSVS-1}flw[CPTI002264]
	K	*c306*-GAL4,tsGAL80/+;*UAS-mCherry RNAi/+*
	L	*c306*-GAL4,tsGAL80/+;*UAS-Mbs RNAi/+*
Figure 3.7-figure supplement 2	A-A'	*slbo*-GAL4/UAS-Rho FRET; +/*UAS*-Rho FRET
	B-B'	*slbo*-GAL4/UAS-Rho FRET;*UAS*-NiPp1/*UAS*-Rho FRET

Table 3.2 List of genotypes shown in the figures.

3.7 References

1. Friedl, P., Locker, J., Sahai, E. & Segall, J. E. Classifying collective cancer cell invasion. *Nat. Cell Biol.* **14,** 777–783 (2012).
2. Friedl, P. & Gilmour, D. Collective cell migration in morphogenesis, regeneration and cancer. *Nat. Rev. Mol. Cell Biol.* **10,** 445–457 (2009).
3. Wang, X., Enomoto, A., Asai, N., Kato, T. & Takahashi, M. Collective invasion of cancer: Perspectives from pathology and development. *Pathol. Int.* **66,** 183–192 (2016).
4. Cheung, K. J. & Ewald, A. J. A collective route to metastasis: Seeding by tumor cell clusters. *Science* **352,** 167–169 (2016).
5. Scarpa, E. & Mayor, R. Collective cell migration in development. *J. Cell Biol.* **212,** 143–155 (2016).
6. Huebner, R. J., Neumann, N. M. & Ewald, A. J. Mammary epithelial tubes elongate through MAPK-dependent coordination of cell migration. *Development* **143,** 983–993 (2016).
7. Shellard, A. & Mayor, R. Supracellular migration - beyond collective cell migration. *J. Cell Sci.* **132,** jcs226142 (2019).
8. Mayor, R. & Etienne-Manneville, S. The front and rear of collective cell migration. *Nat. Rev. Mol. Cell Biol.* **17,** 97–109 (2016).
9. Friedl, P. & Mayor, R. Tuning Collective Cell Migration by Cell-Cell Junction Regulation. *Cold Spring Harb. Perspect. Biol.* **9,** a029199 (2017).
10. Shellard, A., Szabó, A., Trepat, X. & Mayor, R. Supracellular contraction at the rear of neural crest cell groups drives collective chemotaxis. *Science* **362,** 339–343 (2018).

11. Hidalgo-Carcedo, C., Hooper, S., Chaudhry, S. I., Williamson, P., Harrington, K., Leitinger, B. & Sahai, E. Collective cell migration requires suppression of actomyosin at cell-cell contacts mediated by DDR1 and the cell polarity regulators Par3 and Par6. *Nat. Cell Biol.* **13,** 49–58 (2011).

12. Reffay, M., Parrini, M. C., Cochet-Escartin, O., Ladoux, B., Buguin, A., Coscoy, S., Amblard, F., Camonis, J. & Silberzan, P. Interplay of RhoA and mechanical forces in collective cell migration driven by leader cells. *Nat. Cell Biol.* **16,** 217–223 (2014).

13. Montell, D. J., Yoon, W. H. & Starz-Gaiano, M. Group choreography: mechanisms orchestrating the collective movement of border cells. *Nat. Rev. Mol. Cell Biol.* **13,** 631–645 (2012).

14. Saadin, A. & Starz-Gaiano, M. Circuitous Genetic Regulation Governs a Straightforward Cell Migration. *Trends Genet.* **32,** 660–673 (2016).

15. Llense, F. & Martín-Blanco, E. JNK signaling controls border cell cluster integrity and collective cell migration. *Curr. Biol.* **18,** 538–544 (2008).

16. Cai, D., Chen, S.-C., Prasad, M., He, L., Wang, X., Choesmel-Cadamuro, V., Sawyer, J. K., Danuser, G. & Montell, D. J. Mechanical Feedback through E-Cadherin Promotes Direction Sensing during Collective Cell Migration. *Cell* **157,** 1146–1159 (2014).

17. Prasad, M. & Montell, D. J. Cellular and Molecular Mechanisms of Border Cell Migration Analyzed Using Time-Lapse Live-Cell Imaging. *Dev. Cell* **12,** 997–1005 (2007).

18. Bianco, A., Poukkula, M., Cliffe, A., Mathieu, J., Luque, C. M., Fulga, T. A. & Rørth, P. Two distinct modes of guidance signalling during collective migration of border cells. *Nature* **448,** 362–365 (2007).

19. Poukkula, M., Cliffe, A., Changede, R. & Rørth, P. Cell behaviors regulated by guidance cues in collective migration of border cells. *J. Cell Biol.* **192,** 513–524 (2011).

20. Duchek, P., Somogyi, K., Jékely, G., Beccari, S. & Rørth, P. Guidance of cell migration by the *Drosophila* PDGF/VEGF receptor. *Cell* **107,** 17–26 (2001).

21. McDonald, J. A., Pinheiro, E. M., Kadlec, L., Schupbach, T. & Montell, D. J. Multiple EGFR ligands participate in guiding migrating border cells. *Dev. Biol.* **296,** 94–103 (2006).

22. Wang, X., He, L., Wu, Y. I., Hahn, K. M. & Montell, D. J. Light-mediated activation reveals a key role for Rac in collective guidance of cell movement *in vivo*. *Nat. Cell Biol.* **12,** 591–597 (2010).

23. Ramel, D., Wang, X., Laflamme, C., Montell, D. J. & Emery, G. Rab11 regulates cell-cell communication during collective cell movements. *Nat. Cell Biol.* **15,** 317–324 (2013).

24. Aranjuez, G., Burtscher, A., Sawant, K., Majumder, P. & McDonald, J. A. Dynamic myosin activation promotes collective morphology and migration by locally balancing oppositional forces from surrounding tissue. *Mol. Biol. Cell* **27,** 1898–1910 (2016).

25. Lucas, E. P., Khanal, I., Gaspar, P., Fletcher, G. C., Polesello, C., Tapon, N. & Thompson, B. J. The Hippo pathway polarizes the actin cytoskeleton during collective migration of *Drosophila* border cells. *J. Cell Biol.* **201,** 875–885 (2013).

26. Combedazou, A., Choesmel-Cadamuro, V., Gay, G., Liu, J., Dupré, L., Ramel, D. & Wang, X. Myosin II governs collective cell migration behaviour downstream of guidance receptor signalling. *J. Cell Sci.* **130,** 97–103 (2017).

27. Larsen, M., Tremblay, M. L. & Yamada, K. M. Phosphatases in cell–matrix adhesion and migration. *Nat. Rev. Mol. Cell Biol.* **4,** 700–711 (2003).

28. Majumder, P., Aranjuez, G., Amick, J. & McDonald, J. A. Par-1 controls myosin-II activity through myosin phosphatase to regulate border cell migration. *Curr. Biol.* **22,** 363–372 (2012).

29. Felix, M., Chayengia, M., Ghosh, R., Sharma, A. & Prasad, M. Pak3 regulates apical-basal polarity in migrating border cells during *Drosophila* oogenesis. *Development* **142,** 3692–3703 (2015).

30. Lin, Q., Buckler, E. S., Muse, S. V. & Walker, J. C. Molecular evolution of type 1 serine/threonine protein phosphatases. *Mol. Phylogenet. and Evol.* **12,** 57–66 (1999).

31. Verbinnen, I., Ferreira, M. & Bollen, M. Biogenesis and activity regulation of protein phosphatase 1. *Biochem. Soc. Trans* **45,** 89–99 (2017).

32. Heroes, E., Lesage, B., Görnemann, J., Beullens, M., Van Meervelt, L. & Bollen, M. The PP1 binding code: a molecular-lego strategy that governs specificity. *FEBS J.* **280,** 584–595 (2013).

33. Ceulemans, H. & Bollen, M. Functional diversity of protein phosphatase-1, a cellular economizer and reset button. *Physiol. Rev.* **84,** 1–39 (2004).

34. Ferreira, M., Beullens, M., Bollen, M. & Van Eynde, A. Functions and therapeutic potential of protein phosphatase 1: Insights from mouse genetics. *Biochim. Biophys. Acta –Mol. Cell Res.* **1866,** 16–30 (2019).

35. Miskei, M., Ádám, C., Kovács, L., Karányi, Z. & Dombrádi, V. Molecular Evolution of Phosphoprotein Phosphatases in *Drosophila*. *PLoS ONE* **6,** e22218 (2011).

36. Bennett, D., Szöor, B., Gross, S., Vereshchagina, N. & Alphey, L. Ectopic expression of inhibitors of protein phosphatase type 1 (PP1) can be used to analyze roles of PP1 in *Drosophila* development. *Genetics* **164,** 235–245 (2003).

37. Winkler, C., De Munter, S., Van Dessel, N., Lesage, B., Heroes, E., Boens, S., Beullens, M., Van Eynde, A. & Bollen, M. The selective inhibition of protein phosphatase-1 results in mitotic catastrophe and impaired tumor growth. *J. Cell Sci.* **128,** 4526–4537 (2015).

38. Parker, L., Gross, S., Beullens, M., Bollen, M., Bennett, D. & Alphey, L. Functional interaction between nuclear inhibitor of protein phosphatase type 1 (NIPP1) and protein phosphatase type 1 (PP1) in *Drosophila*: consequences of over-expression of NIPP1 in flies and suppression by co-expression of PP1. *Biochem. J.* **368,** 789–797 (2002).

39. Van Eynde, A., Wera, S., Beullens, M., Torrekens, S., Van Leuven, F., Stalmans, W. & Bollen, M. Molecular Cloning of NIPP-1, a Nuclear Inhibitor of Protein Phosphatase-1, Reveals Homology with Polypeptides Involved in RNA Processing. *J Biol. Chem.* **270,** 28068–28074 (1995).

40. Ghiglione, C., Devergne, O., Georgenthum, E., Carballès, F., Médioni, C., Cérézo, D. & Noselli, S. The *Drosophila* cytokine receptor Domeless controls border cell migration and epithelial polarization during oogenesis. *Development* **129,** 5437–5447 (2002).

41. Silver, D. L. & Montell, D. J. Paracrine Signaling through the JAK/STAT Pathway Activates Invasive Behavior of Ovarian Epithelial Cells in *Drosophila*. *Cell* **107,** 831–841 (2001).

42. Niewiadomska, P., Godt, D. & Tepass, U. DE-Cadherin is required for intercellular motility during *Drosophila* oogenesis. *J. Cell Biol.* **144,** 533–547 (1999).

43. Montell, D. J., Rørth, P. & Spradling, A. C. slow border cells, a locus required for a developmentally regulated cell migration during oogenesis, encodes *Drosophila* CEBP. *Cell* **71,** 51–62 (1992).

44. Starz-Gaiano, M., Melani, M., Wang, X., Meinhardt, H. & Montell, D. J. Feedback inhibition of Jak/STAT signaling by apontic is required to limit an invasive cell population. *Dev. Cell* **14,** 726–738 (2008).

45. Dai, W. & Montell, D. J. Live Imaging of Border Cell Migration in *Drosophila*. *Methods Mol. Biol.* **1407,** 153–168 (2016).

46. Dombrádi, V., Mann, D. J., Saunders, R. D. C. & Cohen, P. T. W. Cloning of the fourth functional gene for Protein Phosphatase 1 in *Drosophila* melanogaster from its chromosomal location. *Eur. J. Biochem.* **212,** 177–183 (1993).

47. Dombrádi, V., Axton, J. M., Brewis, N. D., Silva, E. F. D. C. E., Alphey, L. & Cohen, P. T. W. *Drosophila* contains three genes that encode distinct isoforms of protein phosphatase 1. *Eur. J. Biochem.* **194,** 739–745 (1990).

48. Graveley, B. R., Brooks, A. N., Carlson, J. W., Duff, M. O., Landolin, J. M., Yang, L., Artieri, C. G., van Baren, M. J., Boley, N., Booth, B. W., Brown, J. B., Cherbas, L., Davis, C. A., Dobin, A., Li, R., Lin, W., Malone, J. H., Mattiuzzo, N. R., Miller, D., Sturgill, D., Tuch, B. B., Zaleski, C., Zhang, D., Blanchette, M., Dudoit, S., Eads, B., Green, R. E., Hammonds, A., Jiang, L., Kapranov, P., Langton, L., Perrimon, N., Sandler, J. E., Wan, K. H., Willingham, A., Zhang, Y., Zou, Y., Andrews, J., Bickel, P. J., Brenner, S. E., Brent, M. R., Cherbas, P., Gingeras, T. R., Hoskins, R. A., Kaufman, T. C., Oliver, B. & Celniker, S. E. The developmental transcriptome of *Drosophila* melanogaster. *Nature* **471,** 473–479 (2011).

49. Sarov, M., Barz, C., Jambor, H., Hein, M. Y., Schmied, C., Suchold, D., Stender, B., Janosch, S., Kj, V. V., Krishnan, R. T., Krishnamoorthy, A., Ferreira, I. R., Ejsmont, R. K., Finkl, K., Hasse, S., Kämpfer, P., Plewka, N., Vinis, E., Schloissnig, S., Knust, E.,

Hartenstein, V., Mann, M., Ramaswami, M., VijayRaghavan, K., Tomancak, P. & Schnorrer, F. A genome-wide resource for the analysis of protein localisation in *Drosophila*. *Elife* **5,** e12068 (2016).

50. Yamamoto, S., Bayat, V., Bellen, H. J. & Tan, C. Protein Phosphatase 1ß Limits Ring Canal Constriction during *Drosophila* Germline Cyst Formation. *PLoS ONE* **8,** e70502 (2013).

51. Hu, Y., Flockhart, I., Vinayagam, A., Bergwitz, C., Berger, B., Perrimon, N. & Mohr, S. E. An integrative approach to ortholog prediction for disease-focused and other functional studies. *BMC Bioinformatics* **12,** 357–1100 (2011).

52. Trinkle-Mulcahy, L., Sleeman, J. E. & Lamond, A. I. Dynamic targeting of protein phosphatase 1 within the nuclei of living mammalian cells. *J. Cell Sci.* **114,** 4219–4228 (2001).

53. Mohr, S. E., Smith, J. A., Shamu, C. E., Neumüller, R. A. & Perrimon, N. RNAi screening comes of age: improved techniques and complementary approaches. *Nat. Rev. Mol. Cell Biol.* **15,** 591–600 (2014).

54. Sun, Y., Yan, Y., Denef, N. & Schupbach, T. Regulation of somatic myosin activity by protein phosphatase 1β controls *Drosophila* oocyte polarization. *Development* **138,** 1991–2001 (2011).

55. Collins, C. & Nelson, W. J. Running with neighbors: coordinating cell migration and cell–cell adhesion. *Curr. Opin. Cell Biol.* **36,** 62–70 (2015).

56. Sarpal, R., Pellikka, M., Patel, R. R., Hui, F. Y. W., Godt, D. & Tepass, U. Mutational analysis supports a core role for *Drosophila* α-catenin in adherens junction function. *J. Cell Sci.* **125,** 233–245 (2012).

57. Desai, R., Sarpal, R., Ishiyama, N., Pellikka, M., Ikura, M. & Tepass, U. Monomeric α-catenin links cadherin to the actin cytoskeleton. *Nat. Cell Biol.* **15,** 261–273 (2013).

58. Pacquelet, A. & Rørth, P. Regulatory mechanisms required for DE-cadherin function in cell migration and other types of adhesion. *J. Cell Biol.* **170,** 803–812 (2005).

59. Ridley, A. J. Life at the leading edge. *Cell* **145,** 1012–1022 (2011).

60. Caswell, P. T. & Zech, T. Actin-Based Cell Protrusion in a 3D Matrix. *Trends Cell Biol.* **28,** 823–834 (2018).

61. Boekhorst, Te, V., Preziosi, L. & Friedl, P. Plasticity of Cell Migration *In vivo* and In Silico. *Annu. Rev. Cell Dev. Biol.* **32,** 491–526 (2016).

62. Wang, H., Qiu, Z., Xu, Z., Chen, S. J., Luo, J., Wang, X. & Chen, J. aPKC is a key polarity determinant in coordinating the function of three distinct cell polarities during collective migration. *Development* **145,** dev158444 (2018).

63. Vicente-Manzanares, M., Ma, X., Adelstein, R. S. & Horwitz, A. R. Non-muscle myosin II takes centre stage in cell adhesion and migration. *Nat. Rev. Mol. Cell Biol.* **10,** 778–790 (2009).

64. Zeledon, C., Sun, X., Plutoni, C. & Emery, G. The ArfGAP Drongo Promotes Actomyosin Contractility during Collective Cell Migration by Releasing Myosin Phosphatase from the Trailing Edge. *Cell Rep.* **28,** 3238–3248.e3 (2019).

65. Plutoni, C., Keil, S., Zeledon, C., Delsin, L. E. A., Decelle, B., Roux, P. P. & Emery, G. Misshapen coordinates protrusion restriction and actomyosin contractility during collective cell migration. *Nature Comm.* **10,** 3940 (2019).

66. Grassie, M. E., Moffat, L. D., Walsh, M. P. & MacDonald, J. A. The myosin phosphatase targeting protein (MYPT) family: a regulated mechanism for achieving substrate

specificity of the catalytic subunit of protein phosphatase type 1δ. *Arch. Biochem. Biophys.* **510,** 147–159 (2011).

67. Qin, X., Park, B. O., Liu, J., Chen, B., Choesmel-Cadamuro, V., Belguise, K., Do Heo, W. & Wang, X. Cell-matrix adhesion and cell-cell adhesion differentially control basal myosin oscillation and *Drosophila* egg chamber elongation. *Nature Comm.* **8,** 14708 (2017).

68. Mège, R.-M. & Ishiyama, N. Integration of Cadherin Adhesion and Cytoskeleton at Adherens Junctions. *Cold Spring Harb. Perspect. Biol.* **9,** a028738 (2017).

69. Yap, A. S., Duszyc, K. & Viasnoff, V. Mechanosensing and Mechanotransduction at Cell-Cell Junctions. *Cold Spring Harb. Perspect. Biol.* **10,** a028761 (2018).

70. Priya, R., Gomez, G. A., Budnar, S., Verma, S., Cox, H. L., Hamilton, N. A. & Yap, A. S. Feedback regulation through myosin II confers robustness on RhoA signalling at E-cadherin junctions. *Nat. Cell Biol.* **17,** 1282–1293 (2015).

71. Ratheesh, A., Gomez, G. A., Priya, R., Verma, S., Kovacs, E. M., Jiang, K., Brown, N. H., Akhmanova, A., Stehbens, S. J. & Yap, A. S. Centralspindlin and α-catenin regulate Rho signalling at the epithelial zonula adherens. *Nat. Cell Biol.* **14,** 818–828 (2012).

72. le Duc, Q., Shi, Q., Blonk, I., Sonnenberg, A., Wang, N., Leckband, D. & de Rooij, J. Vinculin potentiates E-cadherin mechanosensing and is recruited to actin-anchored sites within adherens junctions in a myosin II-dependent manner. *J. Cell Biol.* **189,** 1107–1115 (2010).

73. Mishra, A. K., Mondo, J. A., Campanale, J. P. & Montell, D. J. Coordination of protrusion dynamics within and between collectively migrating border cells by myosin II. *Mol. Biol. Cell* **30,** 2490–2502 (2019).

74. Fulga, T. A. & Rørth, P. Invasive cell migration is initiated by guided growth of long cellular extensions. *Nat. Cell Biol.* **4,** 715–719 (2002).

75. Kimura, K., Ito, M., Amano, M., Chihara, K., Fukata, Y., Nakafuku, M., Yamamori, B., Feng, J., Nakano, T., Okawa, K., Iwamatsu, A. & Kaibuchi, K. Regulation of myosin phosphatase by Rho and Rho-associated kinase (Rho-kinase). *Science* **273,** 245–248 (1996).

76. Amano, M., Ito, M., Kimura, K., Fukata, Y., Chihara, K., Nakano, T., Matsuura, Y. & Kaibuchi, K. Phosphorylation and activation of myosin by Rho-associated kinase (Rho-kinase). *J Biol Chem* **271,** 20246–20249 (1996).

77. Matsui, T., Amano, M., Yamamoto, T., Chihara, K., Nakafuku, M., Ito, M., Nakano, T., Okawa, K., Iwamatsu, A. & Kaibuchi, K. Rho-associated kinase, a novel serine/threonine kinase, as a putative target for small GTP binding protein Rho. *EMBO J.* **15,** 2208–2216 (1996).

78. Julian, L. & Olson, M. F. Rho-associated coiled-coil containing kinases (ROCK). *Small GTPases* **5,** e29846 (2014).

79. Bravo-Cordero, J. J., Magalhaes, M. A. O., Eddy, R. J., Hodgson, L. & Condeelis, J. Functions of cofilin in cell locomotion and invasion. *Nat. Rev. Mol. Cell Biol.* **14,** (2013).

80. Zhang, L., Luo, J., Wan, P., Wu, J., Laski, F. & Chen, J. Regulation of cofilin phosphorylation and asymmetry in collective cell migration during morphogenesis. *Development* **138,** 455–464 (2011).

81. Huet, G., Rajakylä, E. K., Viita, T., Skarp, K.-P., Crivaro, M., Dopie, J. & Vartiainen, M. K. Actin-regulated feedback loop based on Phactr4, PP1 and cofilin maintains the actin monomer pool. *J. Cell Sci.* **126,** 497–507 (2013).

82. Ambach, A., Saunus, J., Konstandin, M., Wesselborg, S., Meuer, S. C. & Samstag, Y. The serine phosphatases PP1 and PP2A associate with and activate the actin-binding protein cofilin in human T lymphocytes. *Eur. J. Immunol.* **30,** 3422–3431 (2000).

83. Zhang, Y., Kim, T.-H. & Niswander, L. Phactr4 regulates directional migration of enteric neural crest through PP1, integrin signaling, and cofilin activity. *Genes Dev.* **26,** 69–81 (2012).

84. Oleinik, N. V., Krupenko, N. I. & Krupenko, S. A. ALDH1L1 inhibits cell motility via dephosphorylation of cofilin by PP1 and PP2A. *Oncogene* **29,** 6233–6244 (2010).

85. Kühn, S. & Geyer, M. Formins as effector proteins of Rho GTPases. *Small GTPases* **5,** e983876 (2014).

86. Melani, M., Simpson, K. J., Brugge, J. S. & Montell, D. Regulation of cell adhesion and collective cell migration by hindsight and its human homolog RREB1. *Curr. Biol.* **18,** 532–537 (2008).

87. Raza, Q., Choi, J. Y., Li, Y., O'Dowd, R. M., Watkins, S. C., Chikina, M., Hong, Y., Clark, N. L. & Kwiatkowski, A. V. Evolutionary rate covariation analysis of E-cadherin identifies Raskol as a regulator of cell adhesion and actin dynamics in *Drosophila*. *PLoS Genet.* **15,** e1007720 (2019).

88. Stappert, J. & Kemler, R. A short core region of E-cadherin is essential for catenin binding and is highly phosphorylated. *Cell Adhes. Commun.* **2,** 319–327 (1994).

89. McEwen, A. E., Maher, M. T., Mo, R. & Gottardi, C. J. E-cadherin phosphorylation occurs during its biosynthesis to promote its cell surface stability and adhesion. *Mol. Biol. Cell* **25,** 2365–2374 (2014).

90. Chen, Y.-J., Huang, J., Huang, L., Austin, E. & Hong, Y. Phosphorylation potential of *Drosophila* E-Cadherin intracellular domain is essential for development and adherens junction biosynthetic dynamics regulation. *Development* **144,** 1242–1248 (2017).

91. Escobar, D. J., Desai, R., Ishiyama, N., Folmsbee, S. S., Novak, M. N., Flozak, A. S., Daugherty, R. L., Mo, R., Nanavati, D., Sarpal, R., Leckband, D., Ikura, M., Tepass, U. & Gottardi, C. J. α-Catenin phosphorylation promotes intercellular adhesion through a dual-kinase mechanism. *J. Cell Sci.* **128,** 1150–1165 (2015).

92. Weiser, D. C., Row, R. H. & Kimelman, D. Rho-regulated Myosin phosphatase establishes the level of protrusive activity required for cell movements during zebrafish gastrulation. *Development* **136,** 2375–2384 (2009).

93. McGuire, S. E., Mao, Z. & Davis, R. L. Spatiotemporal Gene Expression Targeting with the TARGET and Gene-Switch Systems in *Drosophila*. *Sci. Signal.* **2004,** pl6 (2004).

94. Rørth, P., Szabo, K., Bailey, A., Laverty, T., Rehm, J., Rubin, G. M., Weigmann, K., Milán, M., Benes, V., Ansorge, W. & Cohen, S. M. Systematic gain-of-function genetics in *Drosophila*. *Development* **125,** 1049–1057 (1998).

95. Xu, T. & Rubin, G. M. Analysis of genetic mosaics in developing and adult *Drosophila* tissues. *Development* **117,** 1223–1237 (1993).

96. Bischof, J., Björklund, M., Furger, E., Schertel, C., Taipale, J. & Basler, K. A versatile platform for creating a comprehensive UAS-ORFeome library in *Drosophila*. *Development* **140,** 2434–2442 (2013).

97. Tootle, T. L. & Spradling, A. C. *Drosophila* Pxt: a cyclooxygenase-like facilitator of follicle maturation. *Development* **135,** 839–847 (2008).

98. Spracklen, A. J., Kelpsch, D. J., Chen, X., Spracklen, C. N. & Tootle, T. L. Prostaglandins temporally regulate cytoplasmic actin bundle formation during *Drosophila* oogenesis. *Mol. Biol. Cell* **25,** 397–411 (2014).

99. Schindelin, J., Arganda-Carreras, I., Frise, E., Kaynig, V., Longair, M., Pietzsch, T., Preibisch, S., Rueden, C., Saalfeld, S., Schmid, B., Tinevez, J.-Y., White, D. J., Hartenstein, V., Eliceiri, K., Tomancak, P. & Cardona, A. Fiji: an open-source platform for biological-image analysis. *Nat. Methods* **9,** 676–682 (2012).

100. Sawant, K., Chen, Y., Kotian, N., Preuss, K. M. & McDonald, J. A. Rap1 GTPase promotes coordinated collective cell migration *in vivo*. *Mol. Biol. Cell* **29,** 2656–2673 (2018).

101. Jambor, H., Surendranath, V., Kalinka, A. T., Mejstrik, P., Saalfeld, S. & Tomancak, P. Systematic imaging reveals features and changing localization of mRNAs in *Drosophila* development. *Elife* **4,** R106 (2015).

4 Rap1 GTPase promotes coordinated collective cell migration *in vivo*

Ketki Sawant[a,b,†], Yujun Chen[a,†], Nirupama Kotian[a,†], Kevin M. Preuss[a] and Jocelyn A. McDonald[a,*]

[a]Division of Biology, Kansas State University, Manhattan, KS, USA 66506; [b]Department of Biological, Geological, and Environmental Sciences, Cleveland State University, Cleveland, OH, USA 44115

[†]Co-first authors

Published in the Molecular Biology of the Cell, Vol. 29, No. 22 on 1 November 2018.

doi: 10.1091/mbc.E17-12-0752

Author contributions:

Nirupama Kotian performed experiments and analyzed data for Figure 4.3, Figure 4.4, Figure 4.5, Supplementary figures 4.1D, 4.3 and prepared the manuscript.

Ketki Sawant performed experiments for Figure 4.1, Figure 4.2, Figure 4.3, Supplementary figure 4.2 and prepared the manuscript.

Yujun Chen performed experiments and analyzed the data for Figure 4.6 and supplementary figure 4.4. prepared the manuscript.

4.1 Abstract

During development and in cancer, cells often move together in small to large collectives. In order to move as a unit, cells within collectives need to stay coupled together and coordinate their motility. How cell collectives remain interconnected and migratory, especially when moving through *in vivo* environments, is not well understood. The genetically tractable border cell group undergoes a highly polarized and cohesive cluster-type migration in the *Drosophila* ovary. Here we report that the small GTPase Rap1, through activation by PDZ-GEF, regulates border cell collective migration. We find that Rap1 maintains cell contacts within the cluster, at least in part by promoting the organized distribution of E-cadherin at specific cell-cell junctions. Rap1 also restricts migratory protrusions to the front of the border cell cluster and promotes the extension of protrusions with normal dynamics. Further, Rap1 is required in the outer migratory border cells but not in the central non-migratory polar cells. Such cell specificity correlates well with the spatial distribution of the inhibitory Rapgap1 protein, which is higher in polar cells than in border cells. We propose that precisely regulated Rap1 activity reinforces connections between cells and polarizes the cluster, thus facilitating the coordinated collective migration of border cells.

4.2 Introduction

Many cells that migrate to form and remodel tissues and organs during development move in small to large groups, known as collectives (Scarpa and Mayor, 2016). Collective cell movement also occurs in cancer and may contribute to invasion and metastasis (Yamamoto *et al.*, 1983; Friedl *et al.*, 1995; 2012; Cheung *et al.*, 2013; Cheung and Ewald, 2016; Khalil *et al.*, 2017). Both single cells and cells in collectives undergo a motility cycle that consists of several stereotypical steps (reviewed in Ridley *et al.*, 2003; Friedl and Gilmour, 2009). First, cells polarize to produce a major F-actin-enriched protrusion from the plasma membrane at the front, which helps pull the cell forward. Second, cells adhere to a migratory substrate, made up of either other cells or extracellular matrix (ECM). Finally, cells break rearward adhesions to retract the cell rear, allowing the cell body to move. In single cell movement, individual epithelial cells need to lose cell-cell adhesions with the adjacent epithelium to become motile (reviewed in Thiery *et al.*, 2009). In contrast, cells that migrate in collectives retain connections with neighboring cells to facilitate their movement as coordinated multicellular units (reviewed in Etienne-Manneville, 2014; Mayor and Etienne-Manneville, 2016; De Pascalis and Etienne-Manneville, 2017; Friedl and Mayor, 2017). Cell-cell contacts, typically through adherens junction (AJ) proteins such as E-cadherin, further facilitate transmission of information amongst the connected cells (Bazellières *et al.*, 2015; Collins and Nelson, 2015; Friedl and Mayor, 2017). Mechanical coupling of cell adhesions to the cytoskeleton in turn helps coordinate the entire cell group so that one (or more) cell at the front becomes the protrusive leader cell, while the cells at the back become non-protrusive followers (Etienne-Manneville, 2014; Llense and Etienne-Manneville, 2015; Mayor and Etienne-Manneville, 2016; Friedl and Mayor, 2017). The mechanisms that promote precise cell-cell communication within

collectives to establish and maintain this front-back polarity remain poorly understood, especially for those cells that migrate inside tissues.

The relatively simple *Drosophila* border cells provide a genetically-accessible model to investigate how cell collectives form and move *in vivo* (reviewed in Montell *et al.*, 2012; Saadin and Starz-Gaiano, 2016). Border cells migrate as a group in the developing egg chamber, which is the functional unit of the ovary (Montell *et al.*, 1992; Spradling, 1993). During late oogenesis, four to eight epithelial follicle cells at the anterior are specified to become motile border cells through activation of janus kinase/signal transducer and activator of transcription (JAK-STAT) signaling (Silver and Montell, 2001; Beccari *et al.*, 2002; Ghiglione *et al.*, 2002; Xi *et al.*, 2003). The border cells coalesce around the central pair of polar cells to form a migratory cluster. Subsequently, the border cell cluster detaches (delaminates) from the epithelium (Figure 4.1A). The timing of migration is regulated by a pulse of the ecdysone steroid hormone (Bai *et al.*, 2000; Jang *et al.*, 2009). Border cells then move between the large germline-derived nurse cells (Figure 4.1A). A combination of apical cell polarity proteins and adhesion proteins, including Par-3 (Bazooka; Baz), aPKC and E-cadherin, keep the border cells attached to the central polar cells and organized tightly into a cohesive cluster (Pinheiro *et al.*, 2004; Llense and Martín-Blanco, 2008; Cai *et al.*, 2014; Wang *et al.*, 2018). During migration, the border cell cluster is clearly polarized, producing a forward-directed protrusion that keeps the collective motile (Fulga and Rørth, 2002; Prasad and Montell, 2007; Poukkula *et al.*, 2011). Eventually the border cells reach the oocyte at the posterior (Figure 4.1A). Once there, border cells contribute to formation of the micropyle, the sperm-entry pore used for fertilization of the oocyte (Montell *et al.*, 1992; Spradling, 1993).

Recent work in border cells has produced critical insights into the cellular and molecular mechanisms that establish and reinforce the formation of leader and follower cells in collectives

(reviewed in Montell *et al.*, 2012; Mayor and Etienne-Manneville, 2016; Saadin and Starz-Gaiano, 2016). Signaling through two receptor tyrosine kinases (RTKs), epidermal growth factor receptor (EGFR) and platelet-derived growth factor/vascular-endothelial growth factor (PDGF/VEGF) receptor related (PVR), polarizes the border cell cluster in response to guidance ligands secreted by the oocyte (Duchek and Rørth, 2001; Duchek *et al.*, 2001; McDonald *et al.*, 2006; Prasad and Montell, 2007; Wang *et al.*, 2010). These RTKs activate the small GTPase Rac at the cluster front, thus promoting an enrichment of F-actin in the front ("leader") border cell, which then induces formation of a stable protrusion. Rab11, through the actin regulator Moesin, helps restrict Rac activity to the front, and communicates this information to the other cells so that non-leader ("follower") cells cannot form stable protrusions (Ramel *et al.*, 2013). The cell-cell adhesion protein E-cadherin, through its function in AJs and coupling to F-actin (Baum and Georgiou, 2011), further mechanically links border cells, stabilizing the lead protrusion and suppressing protrusions from the other cells, thus reinforcing their status as follower cells (Cai *et al.*, 2014). Jun amino-terminal kinase (JNK) signaling also promotes normal cell-cell contacts between border cells for cluster cohesion, as well as communication between cells (Llense and Martín-Blanco, 2008; Wang *et al.*, 2010). Protrusions thus restricted to the lead border cell help the cluster navigate its way to the oocyte. Currently, it is unclear whether additional molecular mechanisms work together with this RTK-mediated pathway, or in parallel, to polarize the cluster and help establish leader versus follower cells. In a screen to uncover new regulators of cell polarity and migration of border cells (Aranjuez *et al.*, 2012), we recently identified PDZ-GEF, a canonical guanine nucleotide exchange factor (GEF) for Rap1 (Raaijmakers and Bos, 2009).

Rap1, a highly conserved member of the Ras family of small GTPases, regulates many morphogenetic events during development through control of cell-cell and cell-extracellular

matrix (ECM) adhesion, cell polarity, and/or the actin cytoskeleton (reviewed in Kooistra *et al.*, 2007; Boettner and Van Aelst, 2009; Frische and Zwartkruis, 2010; Gloerich and Bos, 2011). Like all GTPases, Rap1 undergoes an activity cycle, consisting of activation by GEFs and inactivation by GTPase-activating proteins (GAPs). Highly specific functions of Rap1 occur through its downstream effectors, such as Canoe/Afadin, Riam, Rasip1, and others (Boettner *et al.*, 2003; Lafuente *et al.*, 2004; Kooistra *et al.*, 2007; Raaijmakers and Bos, 2009; Post *et al.*, 2013). In the early *Drosophila* embryo, Rap1 promotes establishment of epithelial polarity through positioning of AJs via Canoe (Choi *et al.*, 2013; Bonello *et al.*, 2018). Later in embryogenesis, differing levels of activated Rap1, through the spatially expressed GAP Rapgap1, positions where epithelia will fold and create invaginations (Wang *et al.*, 2013). Here Rap1 regulates adhesion strength and location by coupling AJs to F-actin. Similarly, in the developing wing, Rap1 stabilizes E-cadherin-containing AJs (Knox and Brown, 2002). Additional functions for Rap1 in fly development include invagination of the mesoderm, dorsal closure, anchoring of testis stem cells to their niche, neuroblast polarity, and eye morphogenesis (Asha *et al.*, 1999; Wang *et al.*, 2006; Sawyer *et al.*, 2009; Carmena *et al.*, 2011; Spahn *et al.*, 2012; Walther *et al.*, 2018). Developmental roles for Rap1 are conserved in vertebrates, where Rap1 participates in neural tube closure, convergent extension during gastrulation, as well as neuronal differentiation, polarity, and axon pathfinding (Haigo *et al.*, 2003; Tsai *et al.*, 2007; Shah and Püschel, 2016; Shah *et al.*, 2016; 2017). There is emerging evidence that Rap1-mediated signaling also regulates migration of single cells (Huelsmann *et al.*, 2006; Jossin and Cooper, 2011; Lee and Jeon, 2012; Magliozzi *et al.*, 2013; Zhang *et al.*, 2017). The function for Rap1 in collective cell migration, however, is relatively unexplored. Here we show that Rap1, activated by PDZ-GEF and inactivated by Rapgap1, is a major regulator of border cell collective movement. Specifically, Rap1 promotes the organization

of cell-cell contacts within the border cell cluster and facilitates the polarized extension of lead cell protrusions.

4.3 Results

PDZ-GEF is required for border cell migration

To identify new regulators of cell-cell junctions, cell polarity and other critical parameters of border cell collective migration, we previously performed an RNAi screen that targeted the majority of *Drosophila* PDZ (Psd95/Dlg/ZO-1) domain-containing proteins (Aranjuez *et al.*, 2012). One of the strongest candidates from the original screen was *PDZ-GEF* (also known as *dizzy* or *GEF26*). *PDZ-GEF* encodes a Rapgef1/2 homolog with single cyclic nucleotide monophosphate-binding (cNMP-binding), Ras-like guanine nucleotide exchange factor N-terminal (also called Ras exchanger motif or REM), PDZ, Ras-association (RA), and catalytic GEF domains (Lee *et al.*, 2002; Boettner and Van Aelst, 2007). To confirm a requirement in border cell migration, we first obtained additional independent UAS-RNAi lines that targeted *PDZ-GEF*. We drove UAS-RNAi knockdown in the entire border cell cluster using *c306*-GAL4, which drives expression early in anterior and posterior follicle cells, and maintains expression in both border cells and the central polar cells throughout their migration (Manseau *et al.*, 1997; Silver and Montell, 2001). Control border cells normally finish migrating to the oocyte by stage 10 (Figure 4.1, A and B). In contrast, each of the three *PDZ-GEF* RNAi lines consistently disrupted border cell migration when driven by *c306*-GAL4 (Figure 4.1B). Specifically, ~20-40% of border cells deficient for *PDZ-GEF* stopped along the migration pathway (Figure 4.1B). We also validated the ability of these RNAi lines to knock down *PDZ-GEF*. Each of the three *PDZ-GEF* RNAi lines reduced the levels of PDZ-GEF RNA when driven ubiquitously *in vivo* (Supplemental Figure 4.1A). We further verified the requirement for PDZ-GEF using two strong but viable trans-allelic combinations of *PDZ-GEF* mutant alleles, $PDZ\text{-}GEF^{1}/PDZ\text{-}GEF^{3}$ and $PDZ\text{-}GEF^{1}/PDZ\text{-}GEF^{6}$

(Figure 4.1, C-E) (see Materials and Methods; Singh *et al.*, 2006; Wang *et al.*, 2006). While control border cells (*PDZ-GEF*^{1}/+ heterozygotes) migrated to the oocyte, ~40-50% of border cells in *PDZ-GEF* mutant egg chambers failed to complete their migration (Figure 4.1, C and E). Similar to what we observed for *PDZ-GEF* RNAi, border cells mutant for *PDZ-GEF* initiated migration but stopped partway along the migration pathway (Figure 4.1, B, C and E).

We next confirmed that PDZ-GEF was expressed during the stages of border cell migration. A *lacZ* enhancer trap in the *PDZ-GEF* gene (*PDZ-GEF-lacZ*; genotype: *PDZ-GEF*^{1}/+) was ubiquitously expressed in all border cells during their entire migration, as well as in follicle cells and nurse cells (Supplemental Figure 4.1B). *PDZ-GEF* transcript was similarly detected in a ubiquitous pattern at these stages of ovarian development (Supplemental Figure 4.1C; Jambor *et al.*, 2015). Finally, PDZ-GEF protein, as visualized using a functional GFP-tagged transgene driven by the endogenous *PDZ-GEF* promoter (Boettner and Van Aelst, 2007; Spahn *et al.*, 2012), was present in all cells of the ovary, including border cells (Supplemental Figure 4.1D and D'). Together these data show that PDZ-GEF is expressed in and required for border cell migration.

Rap1 is regulated by PDZ-GEF and is required for border cell migration

PDZ-GEF typically functions as a GEF for the small GTPase Rap1 (de Rooij *et al.*, 1999; Liao *et al.*, 1999). Therefore, we next asked whether Rap1 was expressed in the ovary during the stages when border cells migrate (stages 9 to 10). We made use of a functional GFP-Rap1 transgene driven by the endogenous *Rap1* regulatory sequences (Knox and Brown, 2002). Rap1 was detected in all follicle cells and nurse cells in the ovary (Figure 4.2A). Moreover, Rap1 was expressed in border cells during initiation of cluster delamination/detachment (Supplemental Figure 4.2, A-A''), during migration (Figure 4.2, A and B), and at the end of migration. Specifically, Rap1 was enriched at the cell cortex of border cells and polar cells (Figure 4.2B), consistent with membrane-

recruited active Rap1 (Bivona *et al.*, 2004; Gloerich and Bos, 2011). Previous studies provided genetic evidence that *Drosophila* PDZ-GEF and Rap1 act in the same pathway and demonstrated that the two proteins could bind in a yeast two-hybrid assay (Lee *et al.*, 2002; Huelsmann *et al.*, 2006; Singh *et al.*, 2006; Wang *et al.*, 2006; Boettner and Van Aelst, 2007). We wanted to more directly test the extent to which PDZ-GEF regulates Rap1 activity in *Drosophila*. Therefore, we performed a GTPase activity assay in cultured S2 cells, designed to specifically pull down activated Rap1 (see Materials and Methods). When PDZ-GEF was knocked down by RNAi, using either of two double-stranded RNAs (dsRNAs; see Materials and Methods), the amount of activated Rap1 pulled down was markedly reduced compared to control dsRNA-treated cells (Figure 4.2C and Supplemental Figure 4.2B). Specifically, Rap1 activity was 63% and 31% of control levels (Figure 4.2C), closely matching the efficiency of the respective PDZ-GEF RNAi lines *in vivo* (Figure 4.1B and Supplemental Figure 4.1A). We independently repeated the experiment and observed a similar reduction in Rap1 activity due to PDZ-GEF dsRNA-mediated knockdown (Supplemental Figure 4.2B).

We next investigated Rap1 function in border cells using three different approaches: expression of dominant-negative- (DN-) $Rap1^{N17}$, Rap1 RNAi, and a *Rap1* loss-of-function mutant allele. Expression of $Rap1^{N17}$, using either of two different border cell GAL4 drivers, the earlier-expressing *c306*-GAL4 (Figure 4.2, D and H) and the later- (but generally higher) expressing *slbo*-GAL4 (Figure 4.2E), prevented 30-50% of border cells from reaching the oocyte by the correct stage. Rap1 RNAi driven by *c306*-GAL4 similarly disrupted border cell migration (Figure 4.2E). DN constructs and RNAi do not always represent true loss-of-function situations. Therefore, we next analyzed border cells mutant for a null allele of *Rap1* (*$Rap1^{CD3}$*, a deletion of the entire Rap1 gene) (Asha *et al.*, 1999). Because complete loss of *Rap1* is lethal, we used the mosaic FLP-FRT

system (Xu and Rubin, 1993) to generate clones consisting of homozygous *Rap1* mutant cells in an otherwise heterozygous animal. Here, wild-type cells were marked by the presence of nuclear Red Fluorescent Protein (RFP), while mutant cells were marked by absence of nuclear RFP. As with the other genetic manipulations, border cell clusters containing *Rap1* mosaic mutant cells fully delaminated (detached) from the epithelium but stopped along the migration pathway (Figure 4.2, F and G). Most phenotypic border cell clusters were comprised of both wild-type and mutant cells (Figure 4.2, F and F'). Nonetheless, 80% of clusters that contained a mix of *Rap1* mutant and wild-type border cells failed to reach the oocyte (Figure 4.2G). Taken together, these data demonstrate that the small GTPase *Rap1* is required for border cell migration.

The above-described migration defects caused by loss of *PDZ-GEF* and loss of *Rap1* were similar, and PDZ GEF is a known GEF for Rap1 (Boettner and Van Aelst, 2007; Raaijmakers and Bos, 2009; Spahn *et al.*, 2012). To test more directly whether PDZ-GEF was a major regulator of Rap1 in border cells, we next examined whether there was a genetic interaction between *Rap1* and *PDZ-GEF*. The $Rap1^{N17}$ mutation titrates away specific GEF activity for Rap1 in cells (Feig, 1999; Boettner *et al.*, 2003; Huelsmann *et al.*, 2006). In *Drosophila* embryonic hemocytes, co-expression of PDZ-GEF rescued the migration defects caused by $Rap1^{N17}$, likely due to overcoming the loss of GEF activity induced by DN-Rap1 (Huelsmann *et al.*, 2006). We drove expression of PDZ-GEF in border cells using *c306*-GAL4, either with a control UAS line (UAS-PLCΔPH-GFP, a neutral membrane GFP; Verstreken *et al.*, 2009) or with UAS-$Rap1^{N17}$ (Figure 4.2H). Expression of PDZ-GEF strongly inhibited border cell migration (Figure 4.2H, and below [see Figure 4.3, A and D]). Co-expression of PDZ-GEF with $Rap1^{N17}$, however, more closely resembled that found when $Rap1^{N17}$ was co-expressed with the control UAS-GFP transgene. Thus, expression of

Rap1^{N17} suppressed the migration defects caused by high levels of PDZ-GEF, likely by titrating away the exogenously expressed PDZ-GEF.

Although the data so far suggest that PDZ-GEF is a GEF for Rap1 in border cells, additional GEFs are known to regulate Rap1 activity (Raaijmakers and Bos, 2009; Gloerich and Bos, 2011). Two other Rap1 GEFs have been reported in *Drosophila*, Exchange protein directly activated by cAMP (Epac) and C3G guanyl-nucleotide exchange factor (C3G) (Dupuy *et al.*, 2005; Shirinian *et al.*, 2010). We obtained several RNAi lines for each gene and drove expression in border cells using *c306*-GAL4 (Supplemental Figure 4.2C). Decreased expression of *Epac* and *C3G* only mildly disrupted border cell migration, with ~5-15% of border cells failing to reach the oocyte. The strong phenotypes observed with both *PDZ-GEF* and *Rap1* mutants suggest that PDZ-GEF is the major GEF for Rap1 in border cells, but we do not rule out minor and/or redundant roles for Epac and C3G.

Defined levels of Rap1 activity promote border cell migration

Like other small GTPases, Rap1 activity levels are tightly regulated to produce distinct cellular outcomes (Gloerich and Bos, 2011). Therefore, we next tested the impact of elevated Rap1 activity on border cell migration. We increased the levels of activated Rap1 either by expressing a constitutively-active (CA) mutant Rap1 (Rap1^{V12}) or by overexpressing the activator PDZ-GEF in border cells and adjacent follicle cells using the *slbo*-GAL4 driver. Normally, at early stage 9, border cells detach from the anterior follicle cell epithelium before migrating between nurse cells and eventually reaching the oocyte (Figures 4.1A, 4.3A and 4.3B). In contrast, ~60% of border cells with higher Rap1 activity failed to complete their migration to the oocyte, with 30-40% of border cells remaining at the anterior tip of the egg chamber (Figure 4.3, A, C and D). Border cells retained at the anterior end appeared to be tightly connected to the neighboring epithelial follicle

cells (Figure 4.3, C and D, insets), suggesting a failure to detach from the epithelium. These data support the idea that precise levels of Rap1 activity are needed so that border cells can detach from the epithelium, initiate migration, and move between the nurse cells.

Cell-specific requirement for Rap1 in border cell migration

We next asked in which cells Rap1 activity was required for border cell migration. The border cell cluster consists of two cell types, the central polar cells and the outer migratory border cells (Figure 4.3E). In addition, border cells migrate upon and between nurse cells (Figure 4.1A and 4.3E). Several key regulatory genes and pathways function in more than one of these cell types to control distinct aspects of border cell movement. For example, E-cadherin has multiple cell-specific roles: 1) in polar cells, E-cadherin maintains adhesion of border cells to the cluster; 2) in border cells, E-cadherin transmits mechanical tension so that only the lead border cell forms a protrusion; and 3) in nurse cells, E-cadherin provides traction for border cell movement (Niewiadomska *et al.*, 1999; Fulga and Rørth, 2002; Cai *et al.*, 2014). Moreover, activation of JAK/STAT in border cells relies on secretion of the cytokine Unpaired from the polar cells, which then specifies and recruits epithelial follicle cells to become motile border cells (Silver and Montell, 2001; Beccari *et al.*, 2002; Ghiglione *et al.*, 2002; Xi *et al.*, 2003). Subsequently, JAK/STAT signaling is required in border cells for sustained migration (Silver *et al.*, 2005). Because Rap1 protein is uniformly expressed in border cells, polar cells, and nurse cells (Figure 4.2, A and B; Supplemental Figure 4.2A), this raised the possibility that Rap1 similarly functions in more than one cell type for successful migration.

To determine whether Rap1 was required in specific cells, we took advantage of two GAL4 drivers that have distinct expression patterns within the border cell cluster (Figure 4.3E); *upd*-GAL4 is expressed only in polar cells (Bai and Montell, 2002), whereas *slbo*-GAL4 is restricted

to border cells (Rørth *et al.*, 1998). We drove expression of UAS-Rap1^{N17} to inhibit Rap1 activity and UAS-Rap1^{V12} to activate Rap1. As described above, loss or gain of Rap1 activity in border cells using *slbo*-GAL4 strongly disrupted migration (Figures 4.2E and 4.3A). We next tested the requirement for Rap1 activity in polar cells using *upd*-GAL4. We included tsGAL80 to bypass potential lethality that could result from driving high expression of Rap1 mutants with *upd*-GAL4 during earlier stages of development (McGuire *et al.*, 2003; 2004; Xiang *et al.*, 2016; see Materials and Methods). We confirmed that under these experimental conditions the *upd*-GAL4 driver was functional. Expression of the transcriptional co-activator and protein tyrosine phosphatase Eyes Absent (Eya) caused frequent loss of anterior polar cells (not shown), in agreement with the role for Eya in suppressing polar cell specification (Bai and Montell, 2002). Loss of Rap1 activity in polar cells, however, did not affect cluster migration or the ability of border cells to attach to polar cells (Figure 4.3F). In contrast, increased Rap1 activity in polar cells by Rap1^{V12} mildly disrupted migration. Specifically, activated Rap1^{V12} expression in polar cells blocked border cell migration in ~15% of egg chambers (Figure 4.3F).

Finally, we tested whether Rap1 was required in nurse cells for border cell migration. We produced germline clones with the FLP-FRT method (Xu and Rubin, 1993) using a null allele of *Rap1*, *Rap1^{CD3}* (see Materials and Methods). As expected, control clones in nurse cells (FRT alone) had no effect on border cell migration (n = 19 egg chambers). Similarly, loss of *Rap1* in all nurse cells did not impair border cell movement (n = 31 egg chambers; Figure 4.3G). Rap1 function is thus required in border cells but does not appear to be necessary in polar cells or nurse cells for migration. However, having too much Rap1 activity, either in border cells alone, or in polar cells alone, prevents border cell migration.

Rapgap1 modulates Rap1 activity during border cell collective migration

The results described above indicate that active Rap1 primarily functions in border cells, but not in polar cells, whereas ectopic activation of Rap1 in polar cells can inhibit migration. These data thus raised the possibility that Rap1 activity was restricted in some way within the border cell cluster. Both Rap1 and its activator PDZ-GEF are broadly expressed in migrating border cells (Figure 4.2, A and B; Supplemental Figure 4.1, B-D'; Supplemental Figure 4.2A). Thus, another mechanism likely restricts Rap1 activity to border cells. We focused our attention on Rapgap1, which is a major GTPase-activating protein (GAP) for Rap1 in *Drosophila* (Chen *et al.*, 1997). GAPs hydrolyze guanosine triphosphate (GTP) to guanosine diphosphate (GDP), thus switching small GTPases from an active to an inactive state (Bos *et al.*, 2007). Notably, Rapgap1 protein was expressed in the developing ovary during the stages that border cells migrate (Figure 4.4, A-C'). Throughout oogenesis, Rapgap1 levels appeared to be high in both the anterior and posterior pairs of polar cells, and was expressed in border cells (Figure 4.4, A-C', and not shown). To confirm the polar cell staining of Rapgap1, we co-stained egg chambers with a specific marker of polar cells, Fasciclin III (FasIII; Ruohola *et al.*, 1991). Co-expression with FasIII confirmed that Rapgap1 was expressed in polar cells during the entire migration of border cells (Supplemental Figure 4.3, A-C'). Notably, prior to migration, we observed relatively lower levels of Rapgap1 protein in border cells compared to polar cells (Figure 4.4, A, A', D and D"). Once border cells moved into the egg chamber, Rapgap1 levels remained lower in border cells than in polar cells (Figure 4.4, B, B', E, E'', F and F''). However, Rapgap1 reached maximal levels in border cells by late phases of migration, particularly after the border cell cluster had reached the oocyte (Figure 4.4, C, C', G and G").

In other cells, Rapgap1 homologs are associated with a variety of subcellular compartments (Su *et al.*, 2003; Gloerich and Bos, 2011). Therefore, we examined the subcellular localization of Rapgap1 in border cells. We expressed a GFP-tagged membrane marker (UAS-PLCΔPH-GFP) in border cells and polar cells using *c306*-GAL4 (Figure 4.4, D-G"). Rapgap1 protein was detected in the cytoplasm of border cells and polar cells (e.g. Figure 4, D and D"). However, a fraction of Rapgap1 was also associated with the cell membrane (Figure 4.4, D-G"; Supplemental Figure 4.3, F and G). Additionally, Rapgap1 protein was detected at the cell cortex of nurse cells and the oocyte (Figure 4.4, A-C'). The membrane-associated Rapgap1, as well as differential polar cell versus border cell enrichment, suggests that Rapgap1 normally limits Rap1 activity in border cells and polar cells, although likely to different extents.

To test this idea further, we next raised and lowered the levels of Rapgap1 in border cells using the GAL4/UAS system. Overexpression of Rapgap1 prevented ~45% of border cell clusters from completing their migration (Figure 4.4H), consistent with a loss of Rap1 activity. Next, we knocked down Rapgap1 by RNAi only in border cells using *slbo*-GAL4 (Figure 4I). Rapgap1 RNAi significantly reduced the levels of Rapgap1 protein in border cells (Supplemental Figure 4.3, D-E'). Knockdown of Rapgap1 in border cells produced a mild, but significant impairment of border cell migration (~15%; Figure 4.4I). Together these results support the idea that Rapgap1 modulates Rap1 activity in border cells. Moreover, the polar cell-enrichment of Rapgap1 protein, along with the mild but reproducible disruption of border cell migration upon expression of activated Rap1 in polar cells (Figure 4.3F), supports a model in which Rapgap1 prevents Rap1 from being fully active in polar cells.

Rap1 promotes the distribution of junctional E-cadherin within the border cell collective

Rap1 promotes the formation and maturation of cell-cell junctions, and can regulate cell-extracellular matrix (ECM) adhesion (Bos, 2005; reviewed in Kooistra *et al.*, 2007; Boettner and Van Aelst, 2009; Pannekoek *et al.*, 2009). Maintaining integrity of junctional contacts between border cells is critical to coordinate their collective migration (Pinheiro *et al.*, 2004; Llense and Martín-Blanco, 2008; Melani *et al.*, 2008; Cai *et al.*, 2014; Felix *et al.*, 2015; Wang *et al.*, 2018). E-cadherin-containing adherens junctions (AJs) are established and/or stabilized by Rap1 in many cell types, including the *Drosophila* wing, embryo and eye (Knox and Brown, 2002; O'Keefe *et al.*, 2009; Spahn *et al.*, 2012; Choi *et al.*, 2013; Bonello *et al.*, 2018; Walther *et al.*, 2018). E-cadherin itself is a critical regulator of border cell movement, cell-cell communication, and stabilization of front-directed protrusions (Niewiadomska *et al.*, 1999; Fulga and Rørth, 2002; Cai *et al.*, 2014). Given the importance of having organized cell-cell contacts, which occurs at least partly through the proper distribution of E-cadherin during border cell collective migration, we next determined whether Rap1 activity regulates junctional E-cadherin.

High levels of E-cadherin are normally found at cell-cell contacts within the migrating border cell cluster (Niewiadomska *et al.*, 1999; Pinheiro *et al.*, 2004; Cai *et al.*, 2014), particularly at border cell-border cell (BC-BC) junctions, at junctions between the central polar cells and surrounding border cells (PC-BC), and between polar cells (PC-PC; Figure 4.5, A, A', D, F, and F'). Low levels of E-cadherin are found at junctions between border cells and nurse cells (BC-NC; Figure 4.5, A, A', D, F, and F'), where it provides traction for border cell movement upon nurse cells (Niewiadomska *et al.*, 1999; Fulga and Rørth, 2002; Cai *et al.*, 2014). Because of the similar migration defects observed upon using different genetic manipulations (Figure 4.2, D-G), we analyzed Rap1 function using the $Rap1^{N17}$ construct. To quantify changes to the levels and/or distribution of E-cadherin, we measured the fluorescence intensity at specific junctions in control

and Rap1^{N17} border cell clusters. Specifically, within the same cluster we quantified the E-cadherin fluorescence intensity ratio at BC-BC junctions compared to PC-PC junctions, and the ratio of BC-NC junctions compared to NC-NC junctions (Figure 4.5, A, A' and D). Rap1^{N17} border cell clusters on average accumulated higher E-cadherin levels at BC-BC junctions (Figure 4.5, B, B', and E), compared to control (Figure 4.5, A, A', and E). However, E-cadherin levels at BC-BC junctions were also quite variable, and sometimes were visibly lower than normal (Figure 4.5, B-C', and E). In contrast, E-cadherin was not generally altered at BC-NC contacts, although the overall levels of E-cadherin at BC-NC junctions were variable in both control and Rap1^{N17} border cell clusters (Figure 4.5E). Border cells were often rounder than normal (Figure 4.5, B-C'). Additionally, some border cells were less tightly-adhered to each other and appeared to partially separate (Figure 4.5, B and B').

We next examined the impact on E-cadherin and cell-cell junctions when Rap1 activity was elevated. E-cadherin levels at BC-BC junctions in Rap1^{V12} border cell clusters were overall unchanged, compared to control (Figure 4.5, F-I). However, there was a significant, though variable, elevation of E-cadherin at Rap1^{V12} BC-NC junctions (Figure 4.5I), ranging from quite high (Figure 4.5, G and G') to a more moderate increase (Figure 4.5, H and H'). Thus, increased Rap1 activity produced higher E-cadherin at the cluster periphery, where border cells contact the nurse cells. Taken together, these data support the idea that Rap1 controls the proper distribution and levels of E-cadherin at specific border cell junctions, as well as cell shape and cluster organization.

Rap1 coordinates protrusions in migrating border cells

The results described above indicate that having the correct levels of active Rap1 is critical for migration and the normal junctional E-cadherin distribution in border cells. To investigate why

border cells with altered Rap1 activity often could not complete their migration, we next performed live time-lapse imaging (Figure 4.6; Videos 1-7). We visualized border cells with *slbo*-LifeAct-GFP, which specifically labels F-actin in border cells and a few adjacent follicle cells (Cai *et al.*, 2014). This marker allowed us to examine border cell membranes and protrusions in more detail when Rap1 activity was inhibited (Figure 4.6, A-B’’’; Videos 1-3). At the start of migration, control border cells formed an organized cluster, with one or two prominent forward-directed protrusions that extended and retracted (Figure 4.6A; Video 1; n = 8 videos) (Bianco *et al.*, 2007; Prasad and Montell, 2007). During the remainder of migration, control border cell clusters stayed in a fairly tight group, with a leader cell continuing to extend and retract protrusions at the front (Figure 4.6A-A’’’; Video 1). $Rap1^{N17}$ border cells, in contrast, had trouble moving forward, which was reflected in decreased migration compared to control border cells (Figure 4.6B-C; Videos 2 and 3; n = 8 videos). Many $Rap1^{N17}$ border cell clusters extended protrusions, consistent with the ability of some mutant clusters to leave the follicular epithelium and begin migrating (Figure 4.6, B-D, Videos 2 and 3; n = 8 videos). When $Rap1^{N17}$ border cells were able to move into the egg chamber, they generally had a decreased migration speed compared to control (Figure 4.6C). $Rap1^{N17}$ border cell clusters often extended multiple protrusions (Videos 2 and 3; Figure 4.6D), rather than the typical single protrusion found in control border cell clusters (Video 1). Additionally, control border cells had significantly more front-directed protrusions than those at the “side” of the cluster (Figure 4.6D). In contrast, $Rap1^{N17}$ border cells had almost as many front and side protrusions (Figure 4.6D). Moreover, some $Rap1^{N17}$ border cell clusters stopped extending protrusions after migrating a short distance (Figure 4.6, B’’ and B’’’; Video 2). Further, $Rap1^{N17}$ border cells were rounder overall than normal (Figure 4.6, B’’ and B’’’; Videos 2 and 3). Consistent with a role in promoting cell-cell contacts (Figure 4.5, B and B’), $Rap1^{N17}$ border cells

often appeared to partially separate from each other, and were less tightly connected within the cluster compared to control (Figure 4.6B’’’; Video 2; not shown).

The formation of dynamic protrusions is critical for cells to successfully migrate (Ridley, 2011). Given that Rap1^{N17} border cells did not complete their migration, yet many clusters extended extra protrusions, we next analyzed how protrusions were affected by loss of Rap1 activity. We measured the length and area of protrusions produced by Rap1^{N17} border cell clusters compared to control (Figure 4.6, E and F; Supplemental Figure 4.4, A and B). Interestingly, we observed an increase in the average length of non-forward-directed protrusions (“side”), but an overall decrease in the maximum length of forward protrusions (Figure 4.6E; Supplemental Figure 4.4A). The size of protrusions was also altered, with forward protrusions decreasing and side protrusions increasing in area compared to control (Figure 4.6F; Supplemental Figure 4.4B). We further noticed that Rap1^{N17} side protrusions often resembled front protrusions (Figure 4.6B-B’’’; Video 2). Indeed, the length and area of Rap1^{N17} side protrusions were predominantly similar to the ones at the front, whereas in control the front and side protrusions were significantly different (Figure 4.6, E and F; Supplemental Figure 4.4B). These phenotypes together suggest that decreased Rap1 activity impairs the ability of border cells to produce productive lead protrusions and to suppress side protrusions.

Next, we analyzed the impact of elevated Rap1 activity on live border cells. We imaged matched control (Figure 4.6G-G’’’; Video 4; n = 13) and Rap1^{V12}-expressing border cell clusters (Figure 4.6H-H’’’; Video 5; n = 20) labeled with either mCD8::GFP (not shown) or *slbo*-LifeAct-GFP. In fixed egg chambers, ~35-40% of border cells with increased Rap1 activity (Rap1^{V12} or PDZ-GEF overexpression) did not migrate away from the anterior tip of the egg chamber (Figure 4.3A). Most live Rap1^{V12}-expressing border cells also did not move forward during imaging, in

contrast to control border cells that always completed their migration (Figure 4.6G-I; Videos 4 and 5). Border cells overexpressing PDZ-GEF also did not migrate and strongly resembled $Rap1^{V12}$ border cells (Video 7, n = 8; see Video 6 for matched control, n = 6). This lack of forward movement was despite the ability of $Rap1^{V12}$ (Figure 4.6J; Video 5) and PDZ-GEF-overexpressing (Video 7) border cells to extend front-directed protrusions.

Inclusion of *slbo*-LifeAct-GFP allowed us to further analyze protrusions in $Rap1^{V12}$ border cells compared to control (Figure 4.6J-L; Supplemental Figure 4.4, C and D; n = 7 videos for control; n = 12 videos for $Rap1^{V12}$). Notably, $Rap1^{V12}$ border cells extended more side-directed protrusions than control, with almost equal numbers of total protrusions produced at the side as at the front (Figure 4.6J). $Rap1^{V12}$ front- and side-directed protrusions were longer (Figure 4.6K; Supplemental Figure 4.4C), and had an increased area (Figure 4.6L; Supplemental Figure 4.4D), compared to control protrusions. These data together indicate that having the proper levels of activated Rap1 are necessary for producing front-directed protrusions with the correct length and size. The abnormal protrusions produced by both loss and gain of Rap1 activity, and the failure to restrict protrusions to the front, could account for the inability of these border cell clusters to complete their migration. Together, our data suggest that having an optimal level of Rap1 controls the shape of border cells, maintains cell-cell contacts within the cluster, and promotes the formation of polarized protrusions with normal dynamics.

4.4 Discussion

Rap1 is required for organ and tissue morphogenesis in developing organisms, often through its roles in modulating the cytoskeleton, cell polarity, and/or cell-cell or cell-matrix adhesions (Boettner and Van Aelst, 2009; Frische and Zwartkruis, 2010). While Rap1 has been implicated in the motility of some single cells (Huelsmann *et al.*, 2006; Jossin and Cooper, 2011; Lee and

Jeon, 2012; Magliozzi *et al.*, 2013; Zhang *et al.*, 2017), whether or how Rap1 regulates migration of cells that move as collectives is poorly understood. Here we report Rap1 as a new coordinator of *Drosophila* border cell collective migration. Specifically, Rap1 promotes connections between cells in the cluster, which occurs at least partly through regulation of the proper distribution of E-cadherin and potentially through maintenance of normal border cell shape. Rap1 further controls the extension of polarized, front-directed protrusions. Optimal levels of Rap1 activity restricts the number of protrusions produced by the cluster, and ensures that these protrusions have the proper length and size to sustain movement. Thus, we propose a model in which precise levels of activated Rap1, controlled by PDZ-GEF and Rapgap1, promotes the organization, shape, and polarity of the entire border cell cluster; this in turn drives the coordinated migration of the collective.

Our study indicates that Rap1 promotes the maintenance of cell-cell contacts within the border cell cluster during migration. Border cells, like other cell collectives, require tight cellular connections so that cells stay interconnected and move together *in vivo*. E-cadherin-based AJs are used by many epithelial-derived collectives to keep cells together during migration (reviewed in Collins and Nelson, 2015; Mayor and Etienne-Manneville, 2016; Friedl and Mayor, 2017). In border cells this is achieved through the proper localization and levels of multiple junctional proteins, including E-cadherin but also the apical polarity proteins aPKC, Par-3/Baz, and Par-6 (Niewiadomska *et al.*, 1999; Pinheiro *et al.*, 2004; Llense and Martín-Blanco, 2008; Melani *et al.*, 2008; Cai *et al.*, 2014; Wang *et al.*, 2018). Intriguingly, we found that either loss or gain of Rap1 activity was sufficient to disrupt the levels and distribution of E-cadherin at specific cell-cell junctions. Inhibition of Rap1 altered E-cadherin at BC-BC junctions, resulting in higher E-cadherin at some junctions and lower levels at others; in some cases, there was an apparent rounding and partial separation of the cells within the cluster. Border cells with activated Rap1, in

contrast, had elevated E-cadherin at BC-NC contacts, and many failed to detach from the epithelium. Low levels of E-cadherin at the BC-NC interface provides traction for border cells to migrate upon nurse cells (Niewiadomska *et al.*, 1999; Cai *et al.*, 2014). Elevation of E-cadherin at BC-NC contacts when Rap1 is constitutively-activated could prevent forward movement of border cells as seen in other mutants that disrupt distribution of E-cadherin within the cluster (Pinheiro *et al.*, 2004; Schober *et al.*, 2005; Anllo and Schupbach, 2016). Previous studies showed that abnormal elevation of apical polarity proteins and a failure to downregulate E-cadherin at junctions between border cells and follicle cells in turn prevents complete border cell detachment from the epithelium (Schober *et al.*, 2005; McDonald *et al.*, 2008; Anllo and Schupbach, 2016). Although not directly tested here, our results suggest that in order for border cells to detach from the epithelium, Rap1 activity must transiently be low so that junctions between border cells and follicle cells can be remodeled or broken.

Altogether our results suggest that having the correct levels of active Rap1 in border cells may impact E-cadherin junctional positioning, distribution and/or stability, similar to what has been seen in the wing and other epithelial tissues (Knox and Brown, 2002; Spahn *et al.*, 2012; Choi *et al.*, 2013; Wang *et al.*, 2013). Notably, loss of E-cadherin does not disrupt cell-cell contacts or the shape of cells within the border cell cluster (Niewiadomska *et al.*, 1999; Fulga and Rørth, 2002; Cai *et al.*, 2014). Instead, E-cadherin-deficient border cells fail to extend major protrusions but can migrate "off-track" for short distances, indicating that directional guidance to the oocyte is lost (Fulga and Rørth, 2002; Cai *et al.*, 2014). Thus, it is reasonable to predict that Rap1 promotes cell-cell contacts within the migrating border cell cluster through additional cell junction or cell polarity proteins. For example, Rap1 could more directly regulate connection of AJs to the F-actin cytoskeleton, possibly through junctional components such as alpha-Catenin, Vinculin, and/or

Canoe/Afadin (Mandai *et al.*, 2013; Lecuit and Yap, 2015). Further work will be needed to test these different possibilities.

We have shown that Rap1 promotes the formation of polarized protrusions within the border cell cluster. Increasing or decreasing Rap1 activity caused an overall increase in the number of protrusions, especially those produced by non-leading border cells. These results suggest that altering Rap1 activity disrupts polarization of the migrating cluster. Cells that migrate in collectives need to establish one or more cells that will become protrusive leaders, then reinforce this information among the group so that follower cells do not extend extra protrusions (Mayor and Etienne-Manneville, 2016). Such leader-follower orientation facilitates efficient directional movement. Border cells establish cluster polarity through a signaling cascade that begins with long-range secretion of chemoattractant guidance ligands from the oocyte (Duchek *et al.*, 2001; McDonald *et al.*, 2003; 2006). The border cell in front presumably receives the highest levels of ligands, triggering RTK-mediated activation of the Rac small GTPase and enrichment of F-actin, thus forming a stable lead protrusion (Duchek *et al.*, 2001; Wang *et al.*, 2010). This information is then communicated to follower cells through a combination of Rab11, Moesin, and JNK signaling, which prevent follower cells from extending protrusions (Llense and Martín-Blanco, 2008; Wang *et al.*, 2010; Ramel *et al.*, 2013). Loss of any one of these components results in all border cells, both leader and follower cells, extending protrusions (Prasad and Montell, 2007; Wang *et al.*, 2010; Ramel *et al.*, 2013), similar to what we observed when Rap1 activity was impaired.

Intra-collective adhesions also couple cells together to communicate and stabilize the front-rear polarity of the migrating collective (Bazellières *et al.*, 2015; Collins and Nelson, 2015; Mayor and Etienne-Manneville, 2016). In border cells, E-cadherin-based AJs facilitate this communication of leader-follower protrusion position in response to Rac GTPase signaling

through mechanical linkage of cells in the cluster (Cai *et al.*, 2014). We propose that Rap1 participates in this collective-wide communication of leader-follower protrusion formation, although the mechanism is currently unknown. Loss of Rap1 disrupted contacts between border cells and the normal distribution of E-cadherin. Thus, it is possible that Rap1 mediates reinforcement of protrusion extension from the front border cell through stabilization of cell-cell junctions. A recent study also found that Rap1 is required for the formation of a single leading border cell protrusion (Chang *et al.*, 2018), in agreement with our study. Supporting a role for Rap1 in border cell cluster polarization, Chang and colleagues (2018) found that disruption of Rap1 resulted in spatially uniform Rac activation. This depolarized Rac activity is consistent with a failure to restrict Rac-induced protrusions to the cluster front (Wang *et al.*, 2010). Whether Rap1 functions more directly as part of this canonical RTK-Rac-E-cadherin polarization pathway, however, remains to be determined.

Our data also demonstrate a role for Rap1 in protrusion formation. While many border cells deficient for Rap1 activity initially produced a burst of additional protrusions, eventually these protrusions retracted and did not reform. Notably, both loss and gain of Rap1 activity disrupted protrusion length and shape. Thus, having optimal levels of Rap1 activity is required for the proper morphology and dynamics of protrusions, which in turn is required for normal migration. Chang et al. (2018) further investigated the role for Rap1 in border cell protrusions. Similar to the findings reported here, Chang et al. (2018) found that Rap1 influenced protrusion formation and number. Moreover, Rap1 promoted the proper distribution of F-actin and myosin within the cluster. In this context, Rap1 inhibits the Hippo/Warts pathway (Chang *et al.*, 2018). Hippo suppresses F-actin enrichment in border cells through inhibition of Enabled (Ena), a regulator of F-actin polymerization (Lucas *et al.*, 2013). Rap1 binds to and suppresses Hippo activation, relieving

inhibition of Ena (Chang *et al.*, 2018), thus potentially accounting for the effects on protrusion dynamics (Gates *et al.*, 2009). The Hippo/Warts-Ena pathway also polarizes F-actin within the cluster (Lucas *et al.*, 2013). However, there are distinct differences in the effects on protrusions, and cluster polarity, caused by loss of Hippo/Warts versus gain of Rap1 activity (Lucas *et al.*, 2013; Chang *et al*, 2009; this study). Therefore, it is likely that Rap1 functions with additional downstream molecular targets in border cell migration.

Because Rap1 has multiple functions in border cells, an open question is where and when Rap1 is active. Both Rap1 and the major GEF, PDZ-GEF, are uniformly expressed during migration. Rap1 is required in border cells for migration, but its activity needs to be low or off in the central polar cells. These Rap1 functions correlate well with the expression pattern of Rapgap1, a GAP for Rap1 (Chen *et al.*, 1997). Rapgap1 protein is high in polar cells, but is expressed at lower levels in migrating border cells. However, Rapgap1 cannot simply turn off Rap1 activity in border cells as it likely does in polar cells, because this would be expected to block migration. Instead, Rapgap1 may induce rapid cycling of Rap1 in border cells, leading to dynamic or differential activation of this pathway. In *Drosophila* gastrulation, spatially different levels of Rapgap1 produces two distinct outcomes: 1) low Rapgap1 results in high Rap1 activation, which tightly links cell-cell junctions to F-actin, thus resulting in shallow invagination of the epithelium; and 2) high Rapgap1 results in rapid cycling of Rap1, which decouples cell-cell junctions from F-actin, thus allowing deeper invagination of the epithelium and further folding of the tissue (Wang *et al.*, 2013). More work, however, will be needed to determine whether Rapgap1 influences Rap1 activity in a similar manner in border cells versus polar cells. Further, it is unknown why Rapgap1 levels dramatically increase in border cells as they finish their migration, and what consequence this has, if any, for border cells once they arrive at the oocyte. In the future, development of a more

direct readout of Rap1 activity *in vivo* will help to clarify the spatial and temporal functions of Rap1. Likewise, identification of specific downstream effectors of Rap1 in border cells will be needed to further reveal the precise mechanisms by which Rap1 controls cluster organization, cell-cell contacts, and polarized protrusion extension. Given the molecular and cellular similarities found in diverse cells that migrate as collectives (Friedl and Gilmour, 2009; Mayor and Etienne-Manneville, 2016; Scarpa and Mayor, 2016), along with high conservation of the Rap1 protein (Frische and Zwartkruis, 2010), our study in border cells suggests that Rap1 may be a conserved regulator of collective cell movements *in vivo*.

4.5 Materials and Methods

Drosophila Genetics and Strains

Crosses were generally performed at 25°C. Crosses with temperature-sensitive GAL80 ("tsGAL80") were placed at 18°C to suppress GAL4/UAS during earlier developmental stages (McGuire *et al.*, 2003; 2004). For *slbo*-GAL4 or *c306*-GAL4 crosses, flies were incubated at 29°C for ≥ 14 h prior to dissection to produce optimal GAL4/UAS transgene expression and to inactivate tsGAL80. For *upd*-GAL4, flies were incubated at 29˚C for 3 d prior to dissection (Lin *et al.*, 2014). *c306*-GAL4 is expressed early in border cells, polar cells, and anterior follicle cells (Manseau *et al.*, 1997; Silver and Montell, 2001), and was used to drive UAS-RNAi and other UAS constructs earlier in oogenesis before border cells are specified. *c306*-GAL4 is generally more efficient at driving RNAi-dependent knock down, likely because of earlier expression than other drivers (Aranjuez *et al.*, 2012). *slbo*-GAL4 drives later, high expression in border cells, but not polar cells, after border cell cluster formation; it is also expressed in a few anterior and posterior follicle cells (Rørth *et al.*, 1998). *upd*-GAL4 drives expression solely in polar cells throughout oogenesis (Bai and Montell, 2002; Pinheiro *et al.*, 2004). GAL4 lines were generally outcrossed to w^{1118} to serve as controls.

Mosaic mutant clones of *Rap1*^{CD3} *FRT 2A*, and *FRT 2A* (control), were generated using the FLP-FRT system (Xu and Rubin, 1993). To produce somatic clones in border cells, flies were crossed to *hs*-FLP; *FRT 2A* His2Av-mRFP. Adult progeny of the correct genotype was heat shocked for 1 h at 37˚C, two to three times a day for 3 d, followed by 6 d at 25˚C prior to dissection. Mosaic mutant clones were marked by loss of the His2Av-mRFP (nuclear RFP) signal. For production of germline clones, *Rap1*^{CD3} *FRT 2A*, and *FRT 2A* (control), flies were mated to *hs*-FLP; *FRT 2A*, His2Av-mRFP flies and allowed to lay eggs for 2 d. The progeny was then heat shocked on days 3 and 4 (~2nd and 3rd instar larval stages), followed by incubation at 25˚C. Adult flies were dissected 5-7 d after eclosion. Dissected ovaries were analyzed for loss of nuclear RFP in the germline of individual egg chambers, indicating that clones had been made and nurse cells were mutant for *Rap1*.

The following *Drosophila* strains in this study were obtained from the Bloomington *Drosophila* Stock Center [BDSC], unless otherwise indicated: *tub*-GAL80^{ts} ("tsGAL80"), *hsp70*-GAL4 ("*hs*-GAL4"), *c306*-GAL4, *c306*-GAL4 tsGAL80 (Aranjuez *et al.*, 2016), *slbo*-GAL4, *slbo*-GAL4 UAS-mCD8::GFP (from D. Montell), *upd*-GAL4; tsGal80 (from D. Montell), UAS-GFP RNAi (dsRNA GFP; line 9331), UAS-mCherry RNAi (dsRNA mCherry; line 35785), UAS-*PDZ-GEF* RNAi (line 27017; Vienna *Drosophila* Resource Center [VDRC]), UAS-*PDZ-GEF* RNAi (line 27015; VDRC), UAS-*PDZ-GEF* RNAi (line TRiP.HM05139), UAS-*Epac* RNAi (line 50372; VDRC), UAS-*Epac* RNAi (line 50373; VDRC), UAS-*Epac* RNAi (line 110077; VDRC), UAS-*C3G* RNAi (line 21306; VDRC), UAS-*C3G* RNAi (line 21307; VDRC), UAS-*C3G* RNAi (line 105664; VDRC), UAS-*Rap1* RNAi (line 33437; VDRC), UAS-*Rapgap1* RNAi (line 102659; VDRC), *PDZ-GEF*^{1} (*PDZ-GEF*^{k13720}; P-element enhancer trap insertion line, from Kyoto Stock Center), *PDZ-GEF*^{3} (P-element insertion line, from S. Hou), *PDZ-GEF*^{6} (P-element excision line,

from S. Hou), FRT 2A, FRT 2A *Rap1*^{CD3} (deletes the entire Rap1 gene; from J. Curtiss), UAS-*PDZ-GEF* on 3rd (from B. Boettner), UAS-Rap1^{N17} (DN-Rap1 mutation; from B. Boettner), UAS-Rap1^{WT} (wild type Rap1; from B. Boettner), UAS-Rap1^{V12} (constitutively active- [CA-] Rap1; from B. Boettner), UASp-Rapgap1 (from Y.-C. Wang), UAS-Eya.II (Bai and Montell, 2002), UAS-PLCΔPH-GFP ("membrane GFP;" Verstreken *et al.*, 2009), *slbo*-LifeAct-GFP on 2nd (from D. Montell), *PDZ-GEF*-GFP-PDZ-GEF reporter ("GFP-PDZ-GEF;" from R. Reuter; Boettner and Van Aelst, 2007), and *Rap1*-GFP-Rap1 reporter ("GFP-Rap1;" from D. Siekhaus; Knox and Brown, 2002). Detailed information on *Drosophila* strains can be found at FlyBase (http://flybase.org/). The PDZ-GEF RNAi line TRiP.HM05139 targets independent *PDZ-GEF* sequences from PDZ-GEF RNAi lines 27015 and 27017 (construct GD14231). UAS-Rap1^{N17} and UAS-Rap1^{V12} mutations within the respective transgenic fly lines were PCR-amplified and sequence-verified using a UAS primer and a Rap1 gene-specific primer.

Immunostaining

Ovaries from 3-5 d old females were dissected in Schneider's media (Thermo Fisher Scientific) supplemented with 10% fetal bovine serum (FBS), and either kept whole or further dissected into individual ovarioles as described (McDonald and Montell, 2005). This was followed by fixation for 10 min with 4% methanol-free formaldehyde (Polysciences) in 0.1M Potassium Phosphate buffer, pH 7.4, and washes with NP40 block (50 mM Tris-HCl, pH 7.4, 150 mM NaCl, 0.5% NP40, 5 mg/mL BSA). All primary and secondary antibody incubations were performed in NP40 block. The following primary antibodies from the Developmental Studies Hybridoma Bank (DSHB) were used at the indicated concentrations: rat anti-E-cadherin 1:10 (DCAD2); mouse anti-GFP 1:10 (12A6); mouse anti-Fasciclin 3 1:10 (FasIII; 7G10); mouse anti-Fascin 1:25 (Sn7C). Additional antibodies used were rat anti-Rapgap1 1:1000 (a gift of Drs. Y.-C. Wang and E. Wieschaus) (Wang *et al.*, 2013); rabbit anti-phosphorylated c-Jun (p-Jun) 1:200 (KM-1; Santa

Cruz); rabbit anti-β-galactosidase 1:1000 (Cappel, MP Biomedicals); rabbit anti-GFP Tag polyclonal 1:1000-1:2000 (A-11122; Thermo Fisher Scientific). Alexa Fluor 488, 568 or 647 secondary antibodies (Thermo Fisher Scientific) were used at 1:400 dilution. Alexa Fluor 568 phalloidin and Alexa Fluor 488 phalloidin were used at 1:400 dilution. DAPI was used at 0.05 µg/ml. To amplify GFP signal in some experiments, GFP booster (ChromoTek) was used according to manufacturer's protocol. Dissected egg chambers were mounted on slides in Aqua-Poly/Mount (Polysciences) or FluorSave Reagent (Millipore Sigma) prior to imaging.

Live Time-Lapse Imaging

For live imaging of border cells inhibited for Rap1, *c306*-GAL4 tsGAL80 (control) and *c306*-GAL4 tsGAL80; UAS- $Rap1^{N17}$ stocks were each crossed to *slbo*-LifeAct-GFP. To obtain optimal GAL4/UAS expression, flies of the correct genotypes were incubated at 29˚C for ≥ 14 h prior to dissection. To image the overall effects of activated Rap1 on live border cell migration, w^{1118} (control), UAS- $Rap1^{V12}$ (CA-Rap1), and UAS-PDZ-GEF were each crossed to *slbo*-Gal4 UAS-mCD8:GFP. To image protrusion dynamics, *slbo*-GAL4; UAS-$Rap1^{V12}$ and *slbo*-GAL4 (control) were each crossed to *slbo*-LifeAct-GFP. Flies were incubated at 28-29˚C for ≥ 14 h prior to dissection. Live imaging was performed essentially as described (Prasad and Montell, 2007; Prasad *et al.*, 2007; Manning and Starz-Gaiano, 2015; Dai and Montell, 2016). Briefly, ovarioles were dissected in live imaging media (Schneider's media, pH 6.95, supplemented with 15-20% FBS and 0.2 µg/ml bovine insulin) and mounted on a lumox® Dish 50 (Sarstedt, cat. no. 94.6077.410), a gas-permeable culture dish. Fresh live imaging media was added to the sample just prior to imaging. For imaging cell membranes (Figure 4.1A), the lipophilic dye FM 4-64 (Thermo Fisher Scientific) was added at 9 µM concentration to dissected egg chambers in live imaging media as described (Bianco *et al.*, 2007; Prasad *et al.*, 2007). In all cases, time-lapse

images were acquired at intervals of 2-3 min for up to 4 h using a 20x Plan-Apochromat 0.75 NA objective, a Zeiss Colibri LED light source and either a Zeiss MRm or Axiocam 503 mono camera. Light intensity of the LED was adjusted to minimize phototoxicity of the sample. In some cases, multiple *z*-stacks were acquired and merged in Zeiss AxioVision, Zeiss ZEN or FIJI to produce a single in-focus time-lapse video of border cell migration.

Microscopy and Analyses

Images of fixed egg chambers were mainly acquired with an upright Zeiss AxioImager Z1 microscope using Apotome.2, an Axiocam 503 mono camera, and either a 20x Plan-Apochromat 0.75 numerical aperture (NA) or a 40x Plan-Neofluar 1.3 NA oil-immersion objective. Some images were acquired on a Zeiss LSM 880 confocal microscope using the 405, 488, 561 and/or 633 nm laser lines, and either a 20x 0.8 NA or 40x 1.3 NA oil-immersion objective (KSU-CVM Confocal Core). Image brightness/contrast and measurements were performed using Zeiss AxioVision 4.8, Zeiss ZEN or ImageJ (FIJI) (Schneider *et al.*, 2012). FIJI was used to merge *z*-stacks; maximum intensity projections are shown in the Figures, but were not used to measure fluorescence intensity.

Analyses of live border cell migration time-lapse videos was performed using Zeiss ZEN software. The migration speed was calculated from the duration of its movement. For protrusion quantification, a circle was drawn around the cell cluster, extensions greater than 4 µm were defined as protrusions (see Supplemental Figure 4A). Protrusions were classified into front (0° to 45° and 0° to 315°), side (45° to 135°and 225° to 315°), and back (135° to 225°), based on position within the cluster. The first 1h of each video was used for quantification.

Measurements of E-cadherin intensity at cell-cell junctions were performed on egg chambers stained using identical conditions for E-cadherin (Alexa-568), FasIII (Alexa-647), and DAPI. Identical confocal laser settings were used for each channel, based on a control border cell

cluster, and imaged with a 40x 1.3 NA objective. Acquired images were then processed in FIJI. First, the center of each *z*-stack was manually identified using the polar cells as a landmark. Two *z*-stacks above and below this central section (5 total) were then used to create a sum intensity projection. Cell-cell contacts (BC-BC, PC-PC, BC-NC, and NC-NC; see Figure 4.5D) were manually identified, a line drawn, and mean fluorescence intensity across the line was obtained using the "measure" tool. The PC-PC contact was defined by the FasIII staining, which is highest between polar cells. A ratio of BC-BC intensity versus PC-PC intensity was calculated to normalize "within-cluster" E-cadherin levels; a ratio of BC-NC intensity versus NC-NC (always a NC-NC contact in front of the cluster) was calculated to normalize the E-cadherin levels at the outer edge of the cluster.

To measure Rapgap1 colocalization with membrane GFP, at least one line was drawn using FIJI across each border cell cluster at clearly visible cell and polar cell membranes. The "plot profile" function was used to obtain graph curves for Rapgap1 pixel intensity and membrane-GFP pixel intensity across the line. Only a single *z*-section was measured for each border cell cluster (n = 7 border cell clusters). The values for each channel were normalized to the highest pixel value, and a scatter plot showing both channels was generated in Microsoft Excel (Supplemental Figure 4.3G). In most cases, the curves for Rapgap1 and membrane-GFP overlapped across all measured cell membranes within the border cell cluster.

RT-PCR

To measure RNAi efficiency of *PDZ-GEF* in flies, the three UAS-*PDZ-GEF* RNAi lines (v27017, v27015 and TRiP.HM05139) were each crossed to *hs*-GAL4. Adult progeny from this cross were heat shocked to achieve ubiquitous knockdown, followed by RNA extraction and cDNA synthesis, as described (Aranjuez *et al.*, 2012). Briefly, RNA from whole flies was extracted using Trizol (Thermo Fisher Scientific) and used for cDNA synthesis. RT-PCR was performed with the

Superscript III One-Step RT-PCR system (Thermo Fisher Scientific). PCR amplification was as follows: 50°C for 30 min during the cDNA synthesis step; 55°C for 30 s during the annealing step; 72°C for 1 min during the extension step. PCR was performed for 29 cycles to avoid the plateau phase of amplification. Band intensities of the RT-PCR products were measured using ImageJ (Schneider *et al.*, 2012) and compared to *GAPDH*, which was used as the reference gene. The gene-specific primers were: *PDZ-GEF* fwd, AGGAACGCGTCTCACTCAAG; *PDZ-GEF* rev, AGGAACGCGTCTCACTCAAG; *GAPDH* fwd, ACTCATCAACCCTCCCCCG; *GAPDH* rev, GCGGACGGTAAGATCCACAA.

Production of dsRNA for RNAi treatment of *Drosophila* S2 cells and Rap1 Activity Pull-Down

To make double-stranded RNA (dsRNA) for RNAi treatment of S2 cells, PCR primers were designed with the T7 RNA polymerase sequence at the 5' end (underlined, below) as described (Rogers and Rogers 2008). Templates for dsRNA were amplified by PCR using genomic DNA from w^{1118} flies. RNA was produced using the T7 MEGAscript kit (Thermo Fisher Scientific), followed by annealing and purification as described (Rogers and Rogers, 2008). PDZ-GEF primers were designed to match the sequences of the *in vivo* RNAi lines, v27017 (GD 14231) and TRiP.HM05139. The following primers were used: *gal80* fwd, TAATACGACTCACTATAGGGAGAATTAAGCGGCCGCAACATGGAC; *gal80* rev TAATACGACTCACTATAGGGAGAGCGTGTCTAGATTATAAACTAT; *PDZ-GEF* v27107 fwd, TAATACGACTCACTATAGGCGCGAATTCGTCGCCATCCAACGCTCTCTTCTC; *PDZ-GEF* v27107 rev, TAATACGACTCACTATAGGGCGTCTAGAGCTGCCTCCACCACCGCTTC; *PDZ-GEF* TRiP.HM05139 fwd, TAATACGACTCACTATAGGAAGAATTCACCGCGGATAACTACGTGAC; *PDZ-GEF*

TRiP.HM05139 rev,

TAATACGACTCACTATAGGAAGAATTCACCGCGGATAACTACGTGAC.

Drosophila S2 cells were treated with dsRNA designed to the two independent PDZ-GEF RNAi sequences (above). Cells were then treated with dsRNA for 4 d as described (Rogers and Rogers, 2008). Cells were harvested and lysates prepared according to manufacturer's instructions using the Active Rap1 Pull-Down and Detection Kit (Thermo Fisher Scientific, cat. no. 16120). Halt™ protease inhibitor cocktail (Thermo Fisher Scientific) was added to the lysis buffer. Lysates were incubated with GST-RalGDS-RBD purified protein and glutathione resin for 1 h followed by affinity precipitation. Western blot analysis was used to determine the amount of Rap1 present in the pull-down, bound to GST-RalGDS-RBD according to manufacturer's instructions. Briefly, samples were prepared for western blot analysis by addition of 2X SDS sample buffer, heated for 5 min at 100˚C, separated by SDS-PAGE on a 12% polyacrylamide gel, transferred to nitrocellulose membrane, and followed by incubation with anti-Rap1 antibody at 1:1000 dilution. A single band corresponding to ~24 kDa was recognized by anti-human Rap1A antibody, consistent with the predicted size of *Drosophila* Rap1 (22 kDa). *Drosophila* Rap1 and human Rap1A are 90% identical and 96% similar. Rap1 band intensities were measured using ImageJ.

Figures, Graphs and Statistics

Figures were assembled in Adobe Photoshop CS4 and CC 2018. Illustrations were created in Adobe Illustrator CC 2018. Videos were assembled in Zeiss AxioVision 4.8, Zeiss ZEN or FIJI (Schindelin *et al.*, 2012; 2015). Graphs and statistical tests were performed with GraphPad Prism 7. Statistical tests and *p*-values are listed in the Figure Legends.

4.6 Figure and tables

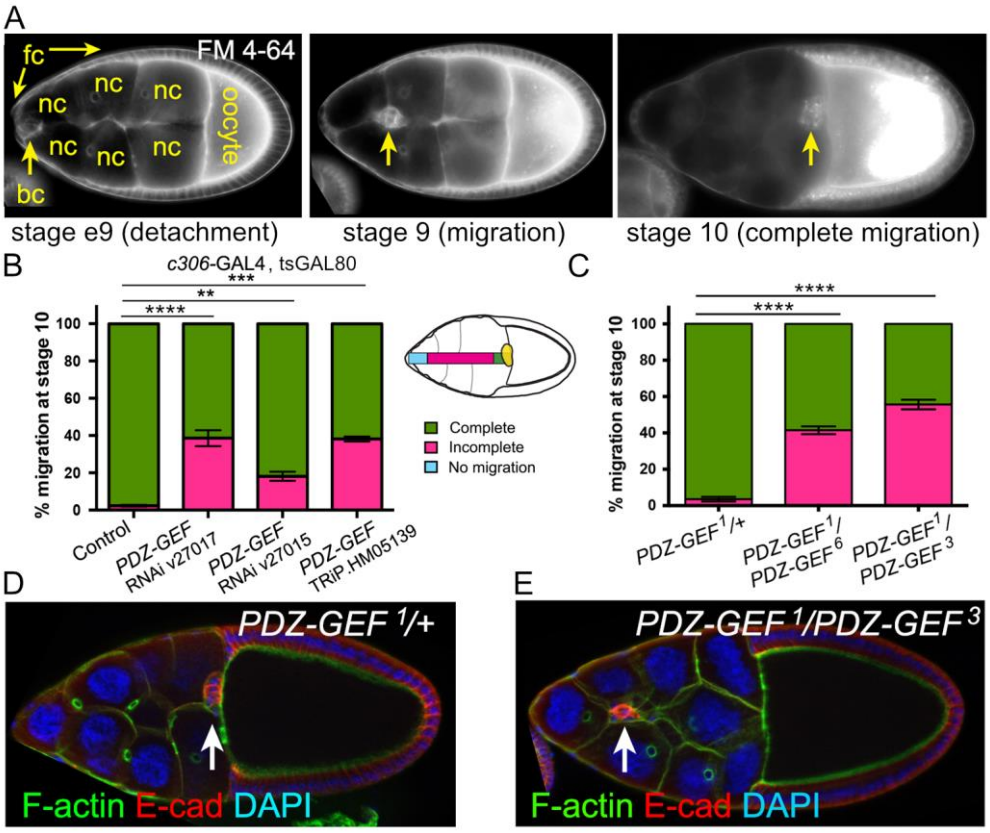

Figure 4.1 PDZ-GEF is required for border cell migration.

(A) Wild type border cell migration at the indicated ovarian developmental stages. Frames from live time-lapse videos of wild type egg chambers stained for the lipophilic dye FM 4-64. Border cells (bc; arrows) detach from the follicle cell (fc) epithelium at early stage 9 (e9), migrate between the 15 nurse cells (nc) at stage 9, and reach the large oocyte at the posterior by stage 10. (B) PDZ-GEF RNAi knockdown prevents border cell migration. Quantification of border cell migration at stage 10, shown as the percentage of complete (green), incomplete (pink), or no (blue) border cell migration in control (*c306*-GAL4, tsGAL80/+) and PDZ-GEF RNAi (*c306*-GAL4, tsGAL80/+; +/ PDZ-GEF RNAi) egg chambers, using three PDZ-GEF RNAi lines: 27017, 27105 and TRiP.HM05139. The egg chamber schematic illustrates the migration distance categories (no migration, incomplete, complete) of border cells (yellow). Values consist of four trials, with each

trial assaying n ≥ 75 egg chambers (total n ≥ 310 egg chambers per genotype); **, $p < 0.01$; ***, $p < 0.001$; ****, $p < 0.0001$; unpaired two-tailed *t* test comparing "complete" migration. (C) Loss of *PDZ-GEF*, using strong trans-allelic combinations of mutant alleles (Lee *et al.*, 2002; Singh *et al.*, 2006; Wang *et al.*, 2006), disrupts border cell migration. Quantification of migration at stage 10, as shown in panel B. Genotypes: $PDZ\text{-}GEF^{1}/+$ (control), $PDZ\text{-}GEF^{1}/PDZ\text{-}GEF^{6}$ and $PDZ\text{-}GEF^{1}/PDZ\text{-}GEF^{3}$. Values consist of five trials, with each trial assaying n ≥ 50 egg chambers (total n ≥ 255 egg chambers per genotype); ****, $p < 0.0001$; unpaired two-tailed *t* test comparing "complete" migration. Error bars in B and C: ± SEM. (D and E) Loss of *PDZ-GEF* impairs border cell migration. E-cadherin (E-cad; red) labels cell membranes of border cells (arrows) and follicle cells, phalloidin (green) labels F-actin and DAPI (blue) labels nuclear DNA in stage 10 $PDZ\text{-}GEF^{1}/+$ (control, D) and $PDZ\text{-}GEF^{1}/PDZ\text{-}GEF^{3}$ mutant (E) egg chambers. Anterior is to the left in this and all following figures.

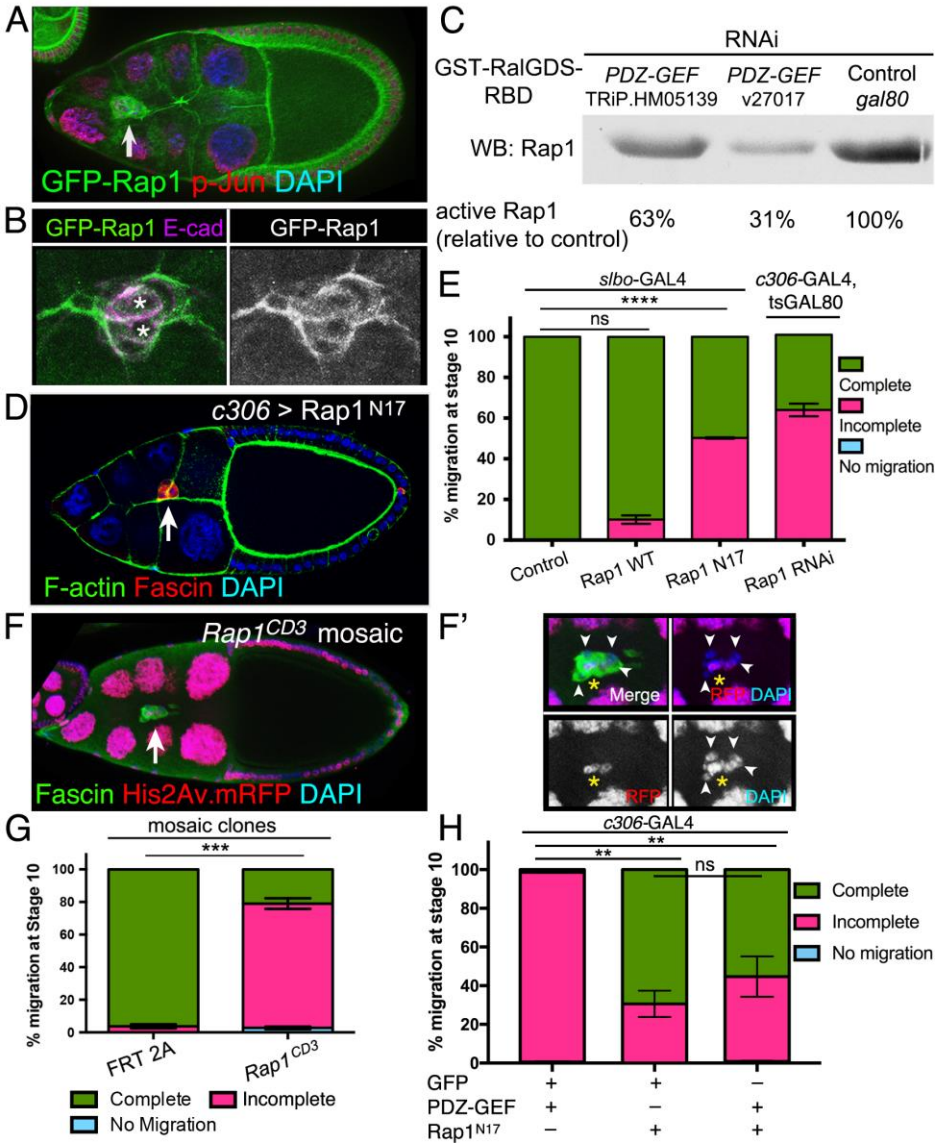

Figure 4.2 Rap1 is regulated by PDZ-GEF and is required for border cell migration.

(A and B) GFP-Rap1 is expressed in border cells. Representative examples of stage 9 egg chambers expressing GFP-Rap1 (green) and co-stained for DAPI (blue in A) to label nuclear DNA, phospho-Jun (red in A) to label nuclei, or E-cadherin (E-cad; magenta in B) to label cell membranes. (A) Arrow points to border cells. GFP-Rap1 is also expressed in follicle cells and nurse cells. (B) Close-up view of a border cell cluster showing that GFP-Rap1 is membrane-enriched and partly co-localizes with E-cadherin in border cells and polar cells (left panel: asterisks; co-localization in white). (C) Activity pulldown assay demonstrates that PDZ-GEF

regulates Rap1 activity in *Drosophila* S2 cells. GST-RalGDS-RBD beads were used to pull down GTP-bound active Rap1 from S2 cells in the presence of wild-type levels of PDZ-GEF (control *gal80* RNAi) or when PDZ-GEF was knocked down (v27107 and TRiP.HM05139 RNAi; see Materials and Methods). The relative amount of active Rap1 pulled down was identified by western blot using a Rap1 antibody. Relative band intensities were measured as a percentage of the control, which represents the amount of maximally-active Rap1 in this assay. (D and E) Inhibition of Rap1 activity by dominant-negative Rap1 ($Rap1^{N17}$) or knockdown by RNAi disrupts border cell migration. (D) Expression of $Rap1^{N17}$ disrupts border cell migration. Example of a stage 10 *c306*>$Rap1^{N17}$ egg chamber (*c306*-GAL4 tsGAL80/+; UAS-$Rap1^{N17}$/+) stained for Fascin (red) to label border cells (arrow), phalloidin to label F-actin (green) and DAPI (blue) to label nuclear DNA. (E) Quantification of complete (green), incomplete (pink), and no (blue) migration in stage 10 control (*slbo*-Gal4/+), $Rap1^{WT}$ (*slbo*-Gal4/+; +/UAS-$Rap1^{WT}$), $Rap1^{N17}$ (*slbo*-Gal4/UAS-$Rap1^{N17}$), and Rap1 RNAi (*c306*-Gal4 tsGAL80/+; +/UAS-Rap1 RNAi v33437) egg chambers. Migration distance as in Figure 4.1B. Values consist of five trials, with each trial assaying $n \geq 50$ egg chambers (total $n \geq 250$ egg chambers per genotype); ns, not significant, $p \geq 0.05$; ****, $p < 0.0001$; unpaired two-tailed *t* test comparing "complete" migration. (F and F') *Rap1* mosaic mutant border cells do not complete their migration to the oocyte. Stage 10 $Rap1^{CD3}$ mosaic mutant egg chamber stained for Fascin (green) to label the border cells (arrow) and DAPI (blue) to visualize nuclear DNA. His2Av.mRFP (red fluorescent protein, RFP; red) marks wild-type cells; co-localization with DAPI appears as magenta. Loss of RFP marks the homozygous mutant cells, including border cells (arrowheads in F'). (F') Magnified view of the $Rap1^{CD3}$ mosaic mutant border cell cluster from (F). Three cells, likely the pair of polar cells (yellow asterisk) and one border cell, are wild-type (red), while the remaining border cells are mutant (loss of red

fluorescence). (G) Extent of migration when border cells are mosaic mutant for a loss-of-function allele of *Rap1*. Quantification of complete (green), incomplete (pink), and no (blue) migration in stage 10 control (*FRT 2A*) and $Rap1^{CD3}$ *FRT 2A* mosaic mutant egg chambers. Migration distance as in Figure 4.1B. Values consist of four trials, with each trial assaying $n \geq 75$ egg chambers (total $n \geq 300$ egg chambers per genotype); ***, $p = 0.0001$; unpaired two-tailed *t* test comparing "complete" migration. (H) Expression of $Rap1^{N17}$ partially suppresses the migration defects caused by PDZ-GEF overexpression. Quantification of complete (green), incomplete (pink), and no (blue) migration in stage 10 egg chambers expressing PDZ-GEF and GFP (*c306*-GAL4/+; UAS-PLCΔPH-GFP/UAS-PDZ-GEF), $Rap1^{N17}$ and GFP (*c306*-GAL4/+; UAS-$Rap1^{N17}$/+; +/ UAS-PLCΔPH-GFP), or $Rap1^{N17}$ and PDZ-GEF (*c306*-GAL4/+; UAS-$Rap1^{N17}$/+; +/UAS-PDZ-GEF). Values consist of three trials, with each trial assaying $n \geq 42$ egg chambers per genotype (total $n \geq 176$ egg chambers per genotype); ns, $p \geq 0.05$; **, $p < 0.01$; one-way ANOVA comparing "incomplete" migration. Error bars in E, G, and H: ± SEM.

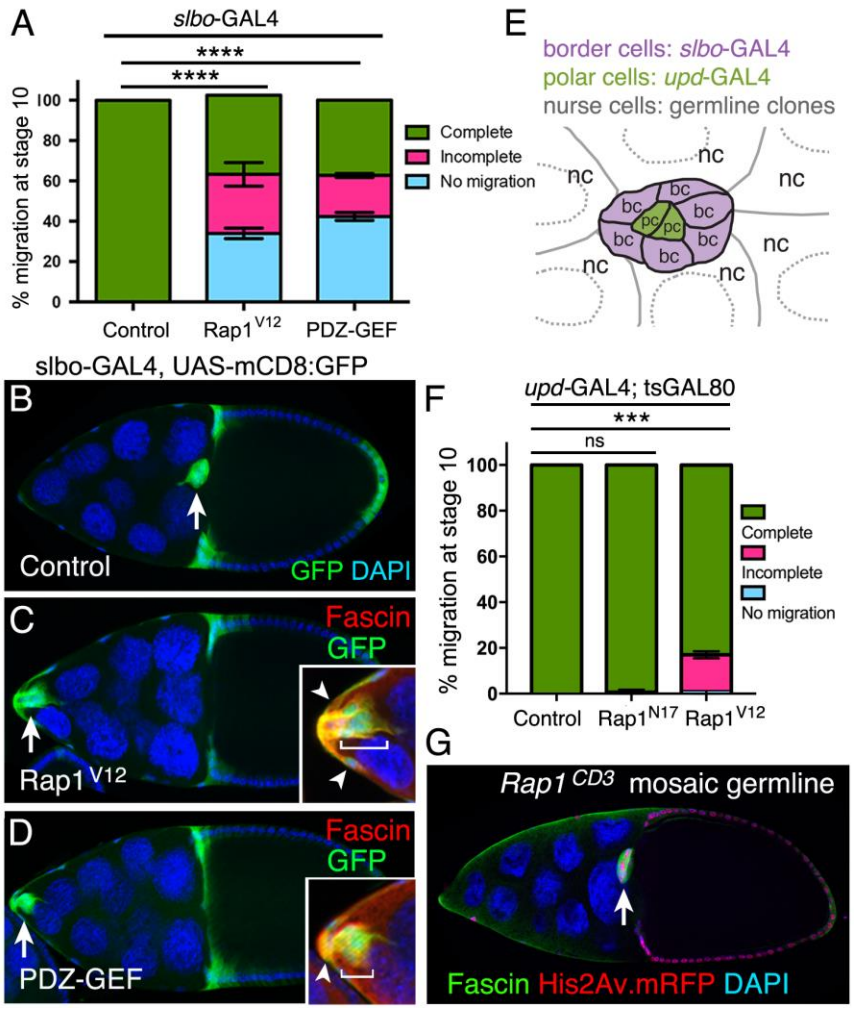

Figure 4.3 Defined levels of activated Rap1 are required in specific cells for border cell migration.

(A-D) Expression of constitutively-activated Rap1, or elevated activation of Rap1 through PDZ-GEF, in border cells impairs border cell migration. (A) Quantification of complete (green), incomplete (pink), and no (blue) migration in stage 10 control, $Rap1^{V12}$, and UAS-PDZ-GEF overexpression egg chambers. Genotypes: control (*slbo*-GAL4, UAS-mCD8:GFP/+), $Rap1^{V12}$ (*slbo*-GAL4 UAS-mCD8:GFP/+; +/UAS-$Rap1^{V12}$), PDZ-GEF (*slbo*-GAL4 UAS-mCD8:GFP/+; +/UAS-PDZ-GEF). Migration distance as in Figure 4.1B. Values consist of three trials, with each trial assaying n ≥ 100 egg chambers (total n ≥ 310 egg chambers per genotype); ****, $p < 0.0001$;

unpaired two-tailed *t* test, comparing "no migration". Error bars: ± SEM. (B-D) Stage 10 control (B), $Rap1^{V12}$ (C) and PDZ-GEF (D) overexpression egg chambers. *slbo*-GAL4 drives expression of UAS-$Rap1^{V12}$ and UAS-PDZ-GEF, along with UAS-mCD8:GFP (green), in border cells (arrow), adjacent follicle cells, and centripetal cells (cells at the anterior side of the oocyte). DAPI (blue) labels nuclear DNA. Genotypes as in A. Insets, magnified view of the same border cell cluster co-stained with Fascin (red) to further label border cells (brackets) and adjacent follicle cells (arrowheads). (E) Schematic drawing of the border cell cluster, with the central polar cells, and surrounding nurse cells. Different GAL4 drivers can be used to test gene function in border cells (bc) and central polar cells (pc). Germline mosaic mutant clones can be used to test function in nurse cells (nc). (F) Rap1 function in polar cells. Quantification of migration at stage 10 when the polar cells express a control GFP (*upd*-GAL4/+; tsGAL80/UAS-PLCΔPH-GFP), $Rap1^{N17}$ (*upd*-GAL4/+; +/UAS-$Rap1^{N17}$; tsGAL80/+) or $Rap1^{V12}$ (*upd*-GAL4/+; tsGAL80/UAS-$Rap1^{V12}$), shown as complete (green), incomplete (pink), and no (blue) border cell migration. Migration distance as in Figure 4.1B. Values consist of three trials, with each trial assaying $n \geq 27$ egg chambers per genotype (total $n \geq 134$ per genotype); ns, $p \geq 0.05$; ***, $p < 0.001$; unpaired two-tailed *t* test comparing "complete" migration. Error bars in A and F: ± SEM. (G) Border cells complete their migration to the oocyte when nurse cells are mutant for a loss-of-function allele of *Rap1*. Representative example of a stage 10 $Rap1^{CD3}$ mosaic mutant egg chamber stained for Fascin (green) to label the border cells (arrow) and DAPI (blue) to visualize nuclear DNA. His2Av.mRFP (red) marks the wild-type cells; loss of RFP marks homozygous mutant cells. In this egg chamber, all nurse cells are mutant (loss of red signal); the border cells and most follicle cells are wild-type (co-localization of DAPI in blue and RFP in red appears as magenta).

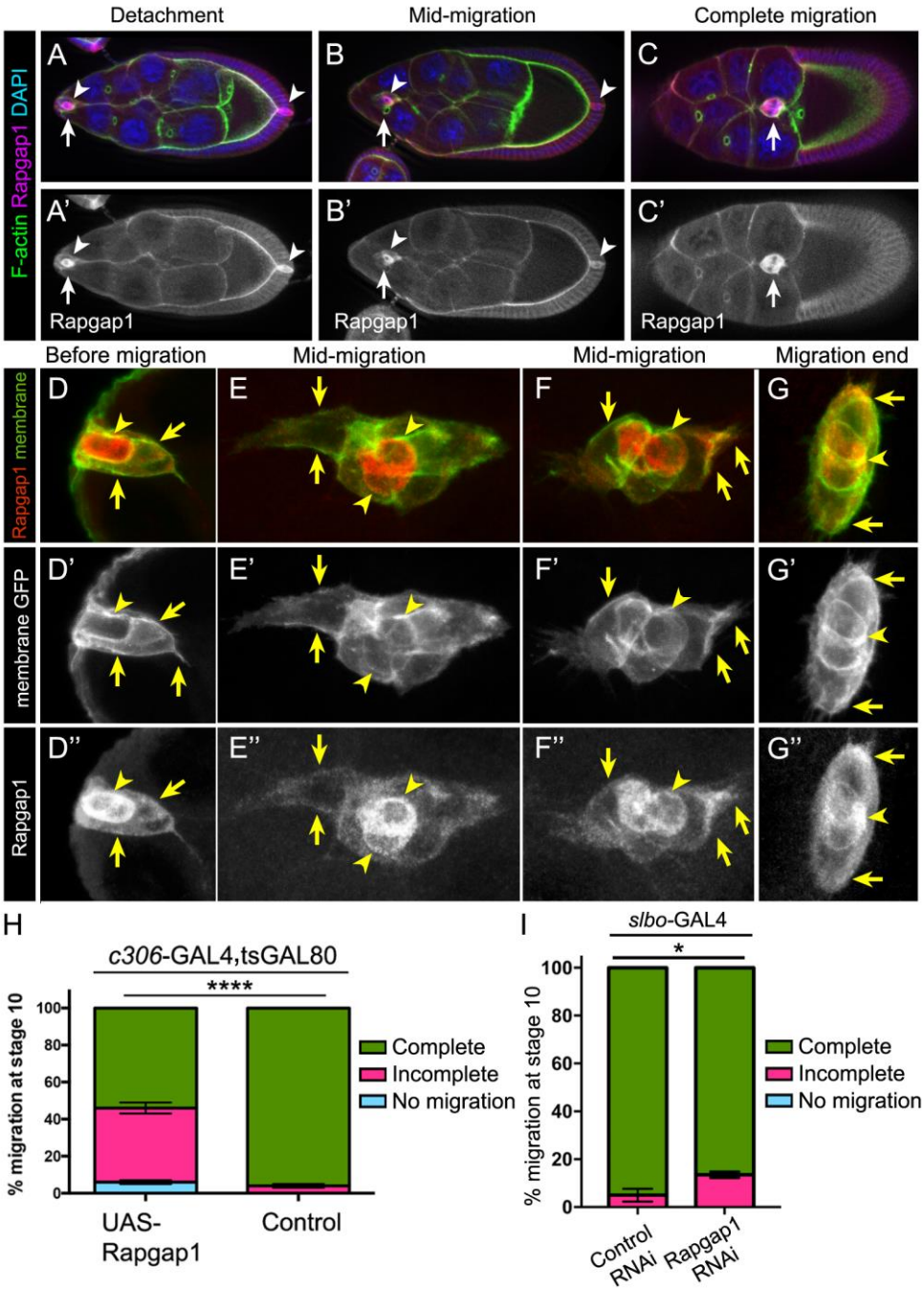

Figure 4.4 Rapgap1 is important for border cell migration.

(A-G") Rapgap1 protein expression and subcellular localization during the stages of oogenesis when border cells migrate. Wild-type egg chambers stained for Rapgap1 (magenta, A-C; red, D-G; white, A'-C', D"-G"), DAPI to visualize nuclear DNA (blue, A-C), and co-stained for phalloidin to label F-actin (green, A-C) or expressing UAS-PLCΔPH:GFP to visualize cell

membranes (green in D-G and white in D'-G'). (A-C') Rapgap1 is expressed in anterior and posterior polar cells (arrowheads), as well as border cells (arrows), throughout the stages when border cells migrate, from detachment to complete migration. (D-G") Close-up view of border cells co-expressing membrane-GFP and Rapgap1. Rapgap1 levels are highest in polar cells (arrowheads) at the start of migration (D and D") and at mid-migration stages (E, E", F, and F"). By the end of migration, polar cells and border cells exhibit more equivalent levels of Rapgap1 (G and G"). Rapgap1 exhibits diffuse subcellular localization in the cytoplasm and at cell membranes of border cells (arrows, D-G") and polar cells (arrowheads, D-G"). The co-localization of Rapgap1 with membrane-GFP was confirmed by measuring normalized pixel intensities across border cell (arrows) and polar cell (arrowheads) membranes using the "plot profile" feature of FIJI (see Materials and Methods and Supplemental Figure 4.3, F and G). Maximum intensity projections of 4-6 merged z-stack sections are shown here, but were not used for quantification. The direction of migration is to the right. (H and I) Raising or lowering the levels of Rapgap1 in border cells impairs migration. Quantification of complete (green), incomplete (pink), and no (blue) migration in stage 10 egg chambers. (H) Overexpression of Rapgap1 in border cells and polar cells driven by c306-GAL4. Genotypes are: control (c306-GAL4, tsGAL80/+) and UAS-Rapgap1 (c306-GAL4, tsGAL80/+; +/UAS-Rapgap1). Migration distance as in Figure 4.1B. Values consist of four trials, with each trial assaying $n \geq 50$ egg chambers (total $n \geq 230$ egg chambers per genotype); ****, $p < 0.0001$; unpaired two-tailed t test comparing "complete" migration. (I) Rapgap1 RNAi in border cells driven by slbo-GAL4. Genotypes are: control (slbo-GAL4/UAS-mCherry RNAi) and Rapgap1 RNAi (slbo-GAL4/UAS-Rapgap1 RNAi v102659, respectively). Values consist of three trials, with each trial assaying $n \geq 44$ egg chambers (total $n \geq 186$ egg chambers per genotype); *,

p = 0.016; unpaired two-tailed t test comparing “incomplete” migration. Error bars in H and I: ± SEM.

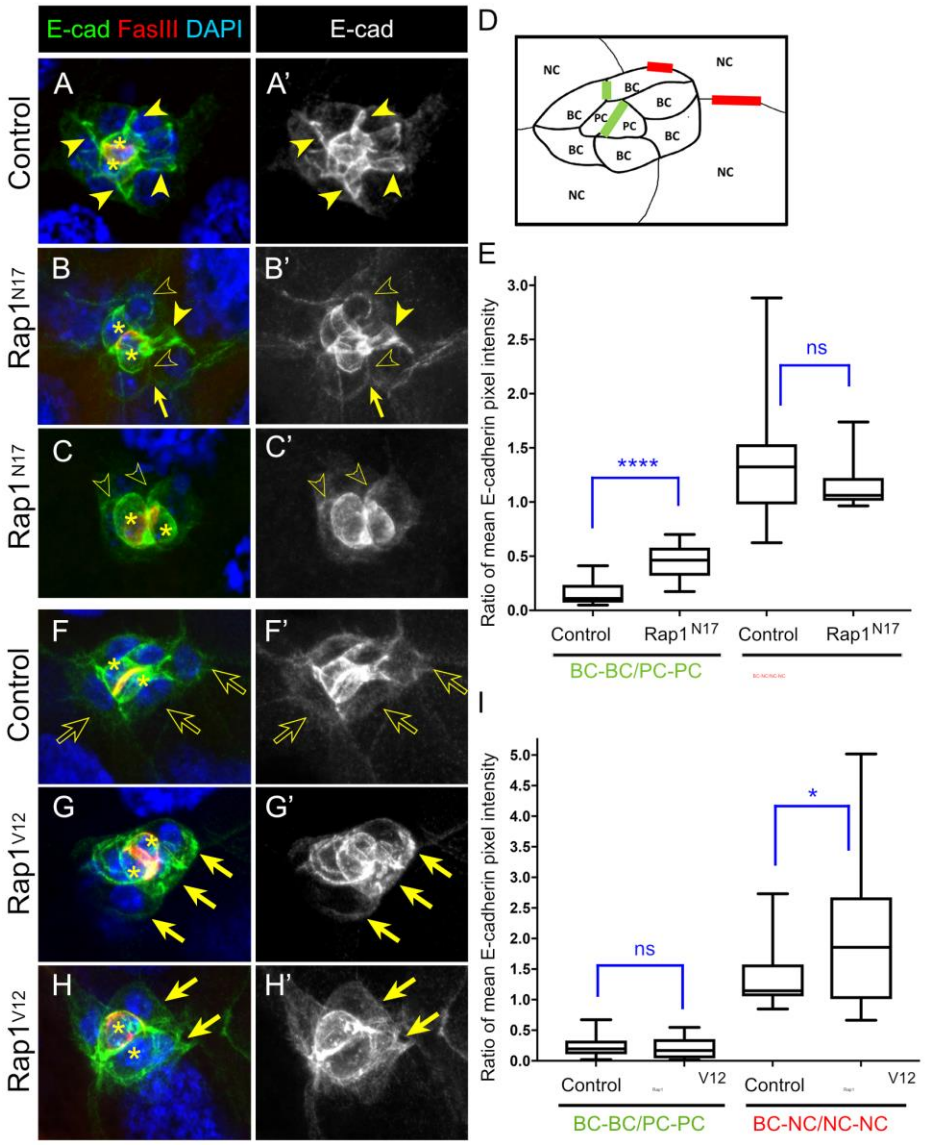

Figure 4.5 Rap1 regulates E-cadherin levels at specific cell-cell junctions.

(A-C', F-H') Representative stage 9 control (A, A', F, F'), stage 10 Rap1^{N17} (B-C'), and stage 10 Rap1^{V12} (G-H') border cell clusters stained for E-cadherin (green in A-C and F-H; white in A'-C' and F'-H'), Fas III to label the central polar cells (red in A-C and F-H; colocalization with E-cadherin appears yellow), and DAPI to visualize nuclear DNA (blue in A-C and F-H). Polar cells are marked with asterisks in A-C and F-H. The direction of migration is to the right in all panels. Maximum intensity projections of 5 merged *z*-stack sections are shown. (A-C') Solid arrowheads mark high E-cadherin expression at border cell-border cell (BC-BC) junctions; open arrowheads

indicate lower E-cadherin at BC-BC junctions. Arrows in B and B' indicate altered contacts between border cells. (F-H') Solid arrows mark high E-cadherin expression at BC-nurse cell (NC) junctions; open arrows indicate low E-cadherin at BC-NC junctions. (D) Schematic of a migrating border cell cluster showing cell-cell contacts measured for E-cadherin mean pixel fluorescence intensity in E and I; BC-BC and PC-PC (green) and BC-NC and NC-NC (red). (E, I) Quantification, represented as box-and-whisker plots, of the mean pixel intensity of E-cadherin as a ratio of BC-BC/PC-PC (green) and BC-NC/NC-NC (red) in matched control and $Rap1^{N17}$ egg chambers (E) and matched control and $Rap1^{V12}$ egg chambers (I). The whiskers represent the minimum and maximum pixel intensity; the box extends from the 25^{th} to the 75^{th} percentiles; the line indicates the median. ns, not significant ($p \geq 0.05$); *, $p < 0.05$; ****, $p < 0.0001$; two-tailed unpaired t-test. Genotypes are: matched controls (*c306*-GAL4 tsGal80/+; UAS-PLC-ΔPH-GFP/+ in A and A'; *slbo*-GAL4, UAS-mCD8-GFP/+ in D and D'); $Rap1^{N17}$ (*c306*-GAL4 tsGal80/+; +/UAS-$Rap1^{N17}$); $Rap1^{V12}$ (*slbo*-GAL4/+; UAS-$Rap1^{V12}$/+). (E) For control, 31 BC-BC contacts and 22 BC-NC contacts were measured from 15 border cell clusters. For $Rap1^{N17}$, 22 BC-BC contacts were measured from 12 border cell clusters and 24 BC-NC contacts were measured from 11 border cell clusters. (I) For control, 40 BC-BC contacts and 22 BC-NC contacts were measured from 20 border cell clusters. For $Rap1^{V12}$, 46 BC-BC contacts and 30 BC-NC contacts were measured from 25 border cell clusters.

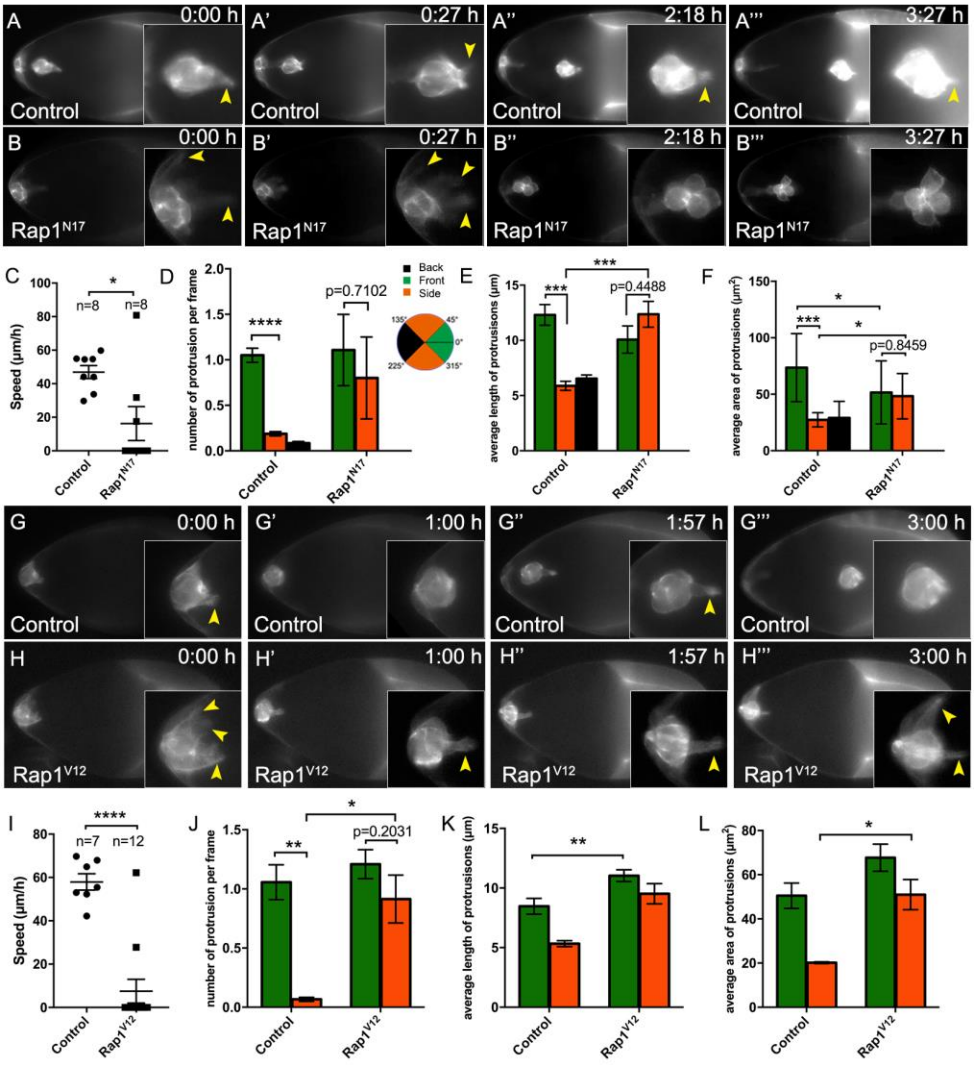

Figure 4.6 Rap1 promotes collective motility and the proper formation of a single lead protrusion.

(A-B’’’, and G-H’’’) Frames from matched control (A-A’’’; Video 1) and Rap1^{N17} (B-B’’’; Video 2), and matched control (G -G’’’; Video 4) and Rap1^{V12} (H-H’’’; Video 5) live time-lapse videos showing migrating border cells (*slbo*-LifeAct-GFP) at the indicated times (h:min). Insets, close-up views of the same border cell clusters from the indicated video frame. Arrowheads indicate protrusions. (A-A’’’ and G-G’’’) Representative control border cell clusters with major front protrusions. Cells within the cluster stay tightly cohesive throughout migration. (B-B’’’)

Representative Rap1^{N17} border cell cluster with multiple protrusions during early migration (B and B'). Later, the border cells become round (B'' and B'''). (H-H''') Representative Rap1^{V12} border cell cluster that failed to initiate migration. Border cells remain at the anterior of the egg chamber. Multiple "side" protrusions extend (H and H'''), in addition to prominent "front" protrusions (H' and H''). (C and I) Measurement of migration speed in individual videos. (C) Matched control (n = 8) and Rap1^{N17} (n = 8). (I) Matched control (n = 7) and Rap1^{V12} (n = 12). (D-F and J-L) Measurements of protrusions within the first hour of matched control and Rap1^{N17} (D-F) and matched control and Rap1^{V12} (J-L) videos. (D and J) Number of protrusions from migrating clusters, per frame of the video, at the front, back, or side of the cluster. (E, F, K, L) Quantification of the average length (E and K) and average area (F and L) of protrusions from time-lapse videos of the indicated genotypes. See Supplemental Figure 4A for a schematic showing how protrusion length and area were measured. (D-F) N = 8 videos for control: 22 front protrusions, 7 side protrusions, and 3 back protrusions were analyzed; n = 7 videos for Rap1^{N17}: 16 front protrusions and 3 side protrusions were analyzed; no back protrusions were observed. (J-L) N = 7 videos for control: 19 front protrusions and 3 side protrusions were analyzed; n = 12 videos for Rap1^{V12}: 26 front protrusions and 12 side protrusions. Error bars: SEM; *, $p < 0.05$; **, $p < 0.01$; ***, $p < 0.001$; all other values were not significant ($p \geq 0.05$) and not shown, with the exception of D, E, F, and J, where the *p* values are shown to compare front and side protrusions within the same genotype; unpaired two-tailed t test. (A-F) Genotypes: control (*c306*-GAL4, tsGal80/+; +/*slbo*-LifeAct-GFP) and Rap1^{N17} (*c306*-GAL4, tsGal80/+; UAS-Rap1^{N17}/*slbo*-LifeAct-GFP). (G-L) Genotypes: control (*slbo*-GAL4/*slbo*-LifeAct-GFP) and Rap1^{V12} (*slbo*-GAL4/*slbo*-LifeAct-GFP ; +/UAS-Rap1^{V12}).

4.7 References

Anllo, L., and Schupbach, T. (2016). Signaling through the G-protein-coupled receptor Rickets is important for polarity, detachment, and migration of the border cells in *Drosophila*. Dev Biol 414, 193–206.

Aranjuez, G., Burtscher, A., Sawant, K., Majumder, P., and McDonald, J. A. (2016). Dynamic myosin activation promotes collective morphology and migration by locally balancing oppositional forces from surrounding tissue. Mol Biol Cell 27, 1898–1910.

Aranjuez, G., Kudlaty, E., Longworth, M. S., and McDonald, J. A. (2012). On the role of PDZ domain-encoding genes in *Drosophila* border cell migration. G3 (Bethesda) 2, 1379–1391.

Asha, H., de Ruiter, N. D., Wang, M. G., and Hariharan, I. K. (1999). The Rap1 GTPase functions as a regulator of morphogenesis *in vivo*. EMBO J 18, 605–615.

Bai, J., and Montell, D. (2002). Eyes absent, a key repressor of polar cell fate during *Drosophila* oogenesis. Development 129, 5377–5388.

Bai, J., Uehara, Y., and Montell, D. J. (2000). Regulation of Invasive Cell Behavior by Taiman, a *Drosophila* Protein Related to AIB1, a Steroid Receptor Coactivator Amplified in Breast Cancer. Cell 103, 1047–1058.

Baum, B., and Georgiou, M. (2011). Dynamics of adherens junctions in epithelial establishment, maintenance, and remodeling. J Cell Biol 192, 907–917.

Bazellières, E., Conte, V., Elosegui-Artola, A., Serra-Picamal, X., Bintanel-Morcillo, M., Roca-Cusachs, P., Muñoz, J. J., Sales-Pardo, M., Guimerà, R., and Trepat, X. (2015). Control of cell–cell forces and collective cell dynamics by the intercellular adhesome. Nat Cell Biol 17, 409–420.

Beccari, S., Teixeira, L., and Rørth, P. (2002). The JAK/STAT pathway is required for border cell migration during *Drosophila* oogenesis. Mech Dev 111, 115–123.

Bianco, A., Poukkula, M., Cliffe, A., Mathieu, J., Luque, C. M., Fulga, T. A., and Rørth, P. (2007). Two distinct modes of guidance signalling during collective migration of border cells. Nature 448, 362–365.

Bivona, T. G., Wiener, H. H., Ahearn, I. M., Silletti, J., Chiu, V. K., and Philips, M. R. (2004). Rap1 up-regulation and activation on plasma membrane regulates T cell adhesion. J Cell Biol 164, 461–470.

Boettner, B., and Van Aelst, L. (2007). The Rap GTPase activator *Drosophila* PDZ-GEF regulates cell shape in epithelial migration and morphogenesis. Mol Cell Biol 27, 7966–7980.

Boettner, B., and Van Aelst, L. (2009). Control of cell adhesion dynamics by Rap1 signaling. Curr Opin Cell Biol 21, 684–693.

Boettner, B., Harjes, P., Ishimaru, S., Heke, M., Fan, H. Q., Qin, Y., Van Aelst, L., and Gaul, U. (2003). The AF-6 homolog canoe acts as a Rap1 effector during dorsal closure of the *Drosophila* embryo. Genetics 165, 159–169.

Bonello, T. T., Perez-Vale, K. Z., Sumigray, K. D., and Peifer, M. (2018). Rap1 acts via multiple mechanisms to position Canoe and adherens junctions and mediate apical-basal polarity establishment. Development 145, dev157941.

Bos, J. L. (2005). Linking Rap to cell adhesion. Curr Opin Cell Biol 17, 123–128.

Bos, J. L., Rehmann, H., and Wittinghofer, A. (2007). GEFs and GAPs: critical elements in the control of small G proteins. Cell 129, 865–877.

Cai, D., Chen, S.-C., Prasad, M., He, L., Wang, X., Choesmel-Cadamuro, V., Sawyer, J. K., Danuser, G., and Montell, D. J. (2014). Mechanical Feedback through E-Cadherin Promotes Direction Sensing during Collective Cell Migration. Cell 157, 1146–1159.

Carmena, A., Makarova, A., and Speicher, S. (2011). The Rap1-Rgl-Ral signaling network regulates neuroblast cortical polarity and spindle orientation. J Cell Biol 195, 553–562.

Chang, Y.-C., Wu, J.-W., Hsieh, Y.-C., Huang, T.-H., Liao, Z.-M., Huang, Y.-S., Mondo, J. A., Montell, D., and Jang, A. C.-C. (2018). Rap1 Negatively Regulates the Hippo Pathway to Polarize Directional Protrusions in Collective Cell Migration. Cell Rep 22, 2160–2175.

Chen, F. F., Barkett, M. M., Ram, K. T. K., Quintanilla, A. A., and Hariharan, I. K. I. (1997). Biological characterization of *Drosophila* Rapgap1, a GTPase activating protein for Rap1. Proc Natl Acad Sci U S A 94, 12485–12490.

Cheung, K. J., and Ewald, A. J. (2016). A collective route to metastasis: Seeding by tumor cell clusters. Science 352, 167–169.

Cheung, K. J., Gabrielson, E., Werb, Z., and Ewald, A. J. (2013). Collective Invasion in Breast Cancer Requires a Conserved Basal Epithelial Program. Cell 155, 1639–1651.

Choi, W., Harris, N. J., Sumigray, K. D., and Peifer, M. (2013). Rap1 and Canoe/afadin are essential for establishment of apical-basal polarity in the *Drosophila* embryo. Mol Biol Cell 24, 945–963.

Collins, C., and Nelson, W. J. (2015). Running with neighbors: coordinating cell migration and cell–cell adhesion. Curr Opin Cell Biol 36, 62–70.

Dai, W., and Montell, D. J. (2016). Live Imaging of Border Cell Migration in *Drosophila*. Methods Mol Biol 1407, 153–168.

De Pascalis, C., and Etienne-Manneville, S. (2017). Single and collective cell migration: the mechanics of adhesions. Mol Biol Cell 28, 1833–1846.

de Rooij, J., Boenink, N. M., van Triest, M., Cool, R. H., Wittinghofer, A., and Bos, J. L. (1999). PDZ-GEF1, a guanine nucleotide exchange factor specific for Rap1 and Rap2. J Biol Chem 274, 38125–38130.

Duchek, P., and Rørth, P. (2001). Guidance of cell migration by EGF receptor signaling during *Drosophila* oogenesis. Science 291, 131–133.

Duchek, P., Somogyi, K., Jékely, G., Beccari, S., and Rørth, P. (2001). Guidance of cell migration by the *Drosophila* PDGF/VEGF receptor. Cell 107, 17–26.

Dupuy, A. G., L'Hoste, S., Cherfils, J., Camonis, J., Gaudriault, G., and de Gunzburg, J. (2005). Novel Rap1 dominant-negative mutants interfere selectively with C3G and Epac. Oncogene 24, 4509–4520.

Etienne-Manneville, S. (2014). Neighborly relations during collective migration. Curr Opin Cell Biol 30, 51–59.

Feig, L. A. (1999). Tools of the trade: use of dominant-inhibitory mutants of Ras-family GTPases. Nat Cell Biol 1, E25–E27.

Felix, M., Chayengia, M., Ghosh, R., Sharma, A., and Prasad, M. (2015). Pak3 regulates apical-basal polarity in migrating border cells during *Drosophila* oogenesis. Development 142, 3692–3703.

Friedl, P., and Gilmour, D. (2009). Collective cell migration in morphogenesis, regeneration and cancer. Nat Rev Mol Cell Biol 10, 445–457.

Friedl, P., and Mayor, R. (2017). Tuning Collective Cell Migration by Cell-Cell Junction Regulation. Cold Spring Harb Perspect Biol 9, a029199.

Friedl, P., Locker, J., Sahai, E., and Segall, J. E. (2012). Classifying collective cancer cell invasion. Nat Cell Biol 14, 777–783.

Friedl, P., Noble, P. B., Walton, P. A., Laird, D. W., Chauvin, P. J., Tabah, R. J., Black, M., and Zänker, K. S. (1995). Migration of coordinated cell clusters in mesenchymal and epithelial cancer explants *in vitro*. Cancer Res. 55, 4557–4560.

Frische, E. W., and Zwartkruis, F. J. T. (2010). Rap1, a mercenary among the Ras-like GTPases. Dev. Biol. 340, 1–9.

Fulga, T. A., and Rørth, P. (2002). Invasive cell migration is initiated by guided growth of long cellular extensions. Nat Cell Biol 4, 715–719.

Gates, J., Nowotarski, S. H., Yin, H., Mahaffey, J. P., Bridges, T., Herrera, C., Homem, C. C. F., Janody, F., Montell, D. J., and Peifer, M. (2009). Enabled and Capping protein play important roles in shaping cell behavior during *Drosophila* oogenesis. Dev Biol 333, 90–107.

Ghiglione, C., Devergne, O., Georgenthum, E., Carballès, F., Médioni, C., Cérézo, D., and Noselli, S. (2002). The *Drosophila* cytokine receptor Domeless controls border cell migration and epithelial polarization during oogenesis. Development 129, 5437–5447.

Gloerich, M., and Bos, J. L. (2011). Regulating Rap small G-proteins in time and space. Trends Cell Biol 21, 615–623.

Haigo, S. L., Hildebrand, J. D., Harland, R. M., and Wallingford, J. B. (2003). Shroom Induces Apical Constriction and Is Required for Hingepoint Formation during Neural Tube Closure. Curr Biol 13, 2125–2137.

Huelsmann, S., Hepper, C., Marchese, D., Knöll, C., and Reuter, R. (2006). The PDZ-GEF dizzy regulates cell shape of migrating macrophages via Rap1 and integrins in the *Drosophila* embryo. Development 133, 2915–2924.

Jambor, H., Surendranath, V., Kalinka, A. T., Mejstrik, P., Saalfeld, S., and Tomancak, P. (2015). Systematic imaging reveals features and changing localization of mRNAs in *Drosophila* development. Elife 4, R106.

Jang, A. C.-C., Chang, Y.-C., Bai, J., and Montell, D. (2009). Border-cell migration requires integration of spatial and temporal signals by the BTB protein Abrupt. Nat Cell Biol 11, 569–579.

Jossin, Y., and Cooper, J. A. (2011). Reelin, Rap1 and N-cadherin orient the migration of multipolar neurons in the developing neocortex. Nat Neurosci 14, 697–703.

Khalil, A. A., Ilina, O., Gritsenko, P. G., Bult, P., Span, P. N., and Friedl, P. (2017). Collective invasion in ductal and lobular breast cancer associates with distant metastasis. Clin Exp Metastasis 34, 421-429.

Knox, A. L., and Brown, N. H. (2002). Rap1 GTPase regulation of adherens junction positioning and cell adhesion. Science 295, 1285–1288.

Kooistra, M. R. H., Dubé, N., and Bos, J. L. (2007). Rap1: a key regulator in cell-cell junction formation. J Cell Sci 120, 17–22.

Lafuente, E. M., van Puijenbroek, A. A. F. L., Krause, M., Carman, C. V., Freeman, G. J., Berezovskaya, A., Constantine, E., Springer, T. A., Gertler, F. B., and Boussiotis, V. A. (2004). RIAM, an Ena/VASP and Profilin Ligand, Interacts with Rap1-GTP and Mediates Rap1-Induced Adhesion. Dev Cell 7, 585–595.

Lecuit, T., and Yap, A. S. (2015). E-cadherin junctions as active mechanical integrators in tissue dynamics. Nat Cell Biol 17, 533–539.

Lee, J. H., Cho, K. S., Lee, J., Kim, D., Lee, S. B., Yoo, J., Cha, G. H., and Chung, J. (2002). *Drosophila* PDZ-GEF, a guanine nucleotide exchange factor for Rap1 GTPase, reveals a novel upstream regulatory mechanism in the mitogen-activated protein kinase signaling pathway. Mol Cell Biol 22, 7658–7666.

Lee, M.-R., and Jeon, T. J. (2012). Cell migration: regulation of cytoskeleton by Rap1 in Dictyostelium discoideum. J. Microbiol. 50, 555–561.

Liao, Y., Kariya, K.-I., Hu, C.-D., Shibatohge, M., Goshima, M., Okada, T., Watari, Y., Gao, X., Jin, T.-G., Yamawaki-Kataoka, Y., et al. (1999). RA-GEF, a novel Rap1A guanine nucleotide exchange factor containing a Ras/Rap1A-associating domain, is conserved between nematode and humans. J Biol Chem 274, 37815–37820.

Lin, T.-H., Yeh, T.-H., Wang, T.-W., and Yu, J.-Y. (2014). The Hippo Pathway Controls Border Cell Migration Through Distinct Mechanisms in Outer Border Cells and Polar Cells of the *Drosophila* Ovary. Genetics 198, 1087–1099.

Llense, F., and Etienne-Manneville, S. (2015). Front-to-Rear Polarity in Migrating Cells. In: Ebnet K. (eds) Cell Polarity 1. Springer, Cham.

Llense, F., and Martín-Blanco, E. (2008). JNK signaling controls border cell cluster integrity and collective cell migration. Curr Biol 18, 538–544.

Lucas, E. P., Khanal, I., Gaspar, P., Fletcher, G. C., Polesello, C., Tapon, N., and Thompson, B. J. (2013). The Hippo pathway polarizes the actin cytoskeleton during collective migration of *Drosophila* border cells. J Cell Biol 201, 875–885.

Magliozzi, R., Low, T. Y., Weijts, B. G. M. W., Cheng, T., Spanjaard, E., Mohammed, S., van Veen, A., Ovaa, H., de Rooij, J., Zwartkruis, F. J. T., et al. (2013). Control of epithelial cell migration and invasion by the IKKβ- and CK1α-mediated degradation of RAPGEF2. Dev Cell 27, 574–585.

Mandai, K., Rikitake, Y., Shimono, Y., and Takai, Y. (2013). Afadin/AF-6 and canoe: roles in cell adhesion and beyond. Prog Mol Biol Transl Sci 116, 433–454.

Manning, L., and Starz-Gaiano, M. (2015). Culturing *Drosophila* Egg Chambers and Investigating Developmental Processes Through Live Imaging. Methods Mol Biol 1328, 73–88.

Manseau, L., Baradaran, A., Brower, D., Budhu, A., Elefant, F., Phan, H., Philp, A. V., Yang, M., Glover, D., Kaiser, K., et al. (1997). GAL4 enhancer traps expressed in the embryo, larval brain, imaginal discs, and ovary of *Drosophila*. Dev Dyn 209, 310–322.

Mayor, R., and Etienne-Manneville, S. (2016). The front and rear of collective cell migration. Nat Rev Mol Cell Biol 17, 97–109.

McDonald, J. A., and Montell, D. J. (2005). Analysis of cell migration using *Drosophila* as a model system. Methods Mol Biol 294, 175–202.

McDonald, J. A., Khodyakova, A., Aranjuez, G., Dudley, C., and Montell, D. J. (2008). PAR-1 kinase regulates epithelial detachment and directional protrusion of migrating border cells. Curr Biol 18, 1659–1667.

McDonald, J. A., Pinheiro, E. M., and Montell, D. J. (2003). PVF1, a PDGF/VEGF homolog, is sufficient to guide border cells and interacts genetically with Taiman. Development 130, 3469–3478.

McDonald, J. A., Pinheiro, E. M., Kadlec, L., Schupbach, T., and Montell, D. J. (2006). Multiple EGFR ligands participate in guiding migrating border cells. Dev Biol 296, 94–103.

McGuire, S. E., Le, P. T., Osborn, A. J., Matsumoto, K., and Davis, R. L. (2003). Spatiotemporal Rescue of Memory Dysfunction in *Drosophila*. Science 302, 1765–1768.

McGuire, S. E., Mao, Z., and Davis, R. L. (2004). Spatiotemporal Gene Expression Targeting with the TARGET and Gene-Switch Systems in *Drosophila*. Sci Signal 2004, pl6.

Melani, M., Simpson, K. J., Brugge, J. S., and Montell, D. (2008). Regulation of cell adhesion and collective cell migration by hindsight and its human homolog RREB1. Curr Biol 18, 532–537.

Montell, D. J., Rørth, P., and Spradling, A. C. (1992). slow border cells, a locus required for a developmentally regulated cell migration during oogenesis, encodes *Drosophila* CEBP. Cell 71, 51–62.

Montell, D. J., Yoon, W. H., and Starz-Gaiano, M. (2012). Group choreography: mechanisms orchestrating the collective movement of border cells. Nat Rev Mol Cell Biol 13, 631–645.

Niewiadomska, P., Godt, D., and Tepass, U. (1999). DE-Cadherin is required for intercellular motility during *Drosophila* oogenesis. J Cell Biol 144, 533–547.

O'Keefe, D. D., Gonzalez-Niño, E., Burnett, M., Dylla, L., Lambeth, S. M., Licon, E., Amesoli, C., Edgar, B. A., and Curtiss, J. (2009). Rap1 maintains adhesion between cells to affect Egfr signaling and planar cell polarity in *Drosophila*. Dev Biol 333, 143–160.

Pannekoek, W.-J., Kooistra, M. R. H., Zwartkruis, F. J. T., and Bos, J. L. (2009). Cell-cell junction formation: the role of Rap1 and Rap1 guanine nucleotide exchange factors. Biochim. Biophys. Acta 1788, 790–796.

Pinheiro, E. M., and Montell, D. J. (2004). Requirement for Par-6 and Bazooka in *Drosophila* border cell migration. Development 131, 5243–5251.

Post, A., Pannekoek, W.-J., Ross, S. H., Verlaan, I., Brouwer, P. M., and Bos, J. L. (2013). Rasip1 mediates Rap1 regulation of Rho in endothelial barrier function through ArhGAP29. Proc Natl Acad Sci U S A 110, 11427–11432.

Poukkula, M., Cliffe, A., Changede, R., and Rørth, P. (2011). Cell behaviors regulated by guidance cues in collective migration of border cells. J Cell Biol 192, 513–524.

Prasad, M., and Montell, D. J. (2007). Cellular and Molecular Mechanisms of Border Cell Migration Analyzed Using Time-Lapse Live-Cell Imaging. Dev Cell 12, 997–1005.

Prasad, M., Jang, A. C.-C., Starz-Gaiano, M., Melani, M., and Montell, D. J. (2007). A protocol for culturing *Drosophila* melanogaster stage 9 egg chambers for live imaging. Nat Protoc 2, 2467–2473.

Raaijmakers, J. H., and Bos, J. L. (2009). Specificity in Ras and Rap signaling. J Biol Chem 284, 10995–10999.

Ramel, D., Wang, X., Laflamme, C., Montell, D. J., and Emery, G. (2013). Rab11 regulates cell-cell communication during collective cell movements. Nat Cell Biol 15, 317–324.

Ridley, A. J. (2011). Life at the leading edge. Cell 145, 1012–1022.

Ridley, A. J., Schwartz, M. A., Burridge, K., Firtel, R. A., Ginsberg, M. H., Borisy, G., Parsons, J. T., and Horwitz, A. R. (2003). Cell migration: integrating signals from front to back. Science 302, 1704–1709.

Rogers, S. L., and Rogers, G. C. (2008). Culture of *Drosophila* S2 cells and their use for RNAi-mediated loss-of-function studies and immunofluorescence microscopy. Nat Protoc 3, 606–611.

Ruohola, H., Bremer, K. A., Baker, D., Swedlow, J. R., Jan, L. Y., and Jan, Y. N. (1991). Role of neurogenic genes in establishment of follicle cell fate and oocyte polarity during oogenesis in *Drosophila*. Cell 66, 433–449.

Rørth, P., Szabo, K., Bailey, A., Laverty, T., Rehm, J., Rubin, G. M., Weigmann, K., Milán, M., Benes, V., Ansorge, W., et al. (1998). Systematic gain-of-function genetics in *Drosophila*. Development 125, 1049–1057.

Saadin, A., and Starz-Gaiano, M. (2016). Circuitous Genetic Regulation Governs a Straightforward Cell Migration. Trends Genet. 32, 660–673.

Sawyer, J. K., Harris, N. J., Slep, K. C., Gaul, U., and Peifer, M. (2009). The *Drosophila* afadin homologue Canoe regulates linkage of the actin cytoskeleton to adherens junctions during apical constriction. J Cell Biol 186, 57–73.

Scarpa, E., and Mayor, R. (2016). Collective cell migration in development. J Cell Biol 212, 143–155.

Schindelin, J., Arganda-Carreras, I., Frise, E., Kaynig, V., Longair, M., Pietzsch, T., Preibisch, S., Rueden, C., Saalfeld, S., Schmid, B., et al. (2012). Fiji: an open-source platform for biological-image analysis. Nat Methods 9, 676–682.

Schindelin, J., Rueden, C. T., Hiner, M. C., and Eliceiri, K. W. (2015). The ImageJ ecosystem: An open platform for biomedical image analysis. Mol Reprod Dev 82, 518–529.

Schneider, C. A., Rasband, W. S., and Eliceiri, K. W. (2012). NIH Image to ImageJ: 25 years of image analysis. Nat Methods 9, 671–675.

Schober, M., Rebay, I., and Perrimon, N. (2005). Function of the ETS transcription factor Yan in border cell migration. Development 132, 3493–3504.

Shah, B., and Püschel, A. W. (2016). Regulation of Rap GTPases in mammalian neurons. Biol Chem 397, 1055–1069.

Shah, B., Lutter, D., Bochenek, M. L., Kato, K., Tsytsyura, Y., Glyvuk, N., Sakakibara, A., Klingauf, J., Adams, R. H., and Püschel, A. W. (2016). C3G/Rapgef1 Is Required in Multipolar Neurons for the Transition to a Bipolar Morphology during Cortical Development. PLoS ONE 11, e0154174.

Shah, B., Lutter, D., Tsytsyura, Y., Glyvuk, N., Sakakibara, A., Klingauf, J., and Püschel, A. W. (2017). Rap1 GTPases Are Master Regulators of Neural Cell Polarity in the Developing Neocortex. Cereb Cortex 27, 1253–1269.

Shirinian, M., Grabbe, C., Popovic, M., Varshney, G., Hugosson, F., Bos, H., Rehmann, H., and Palmer, R. H. (2010). The Rap1 Guanine Nucleotide Exchange Factor C3G Is Required for Preservation of Larval Muscle Integrity in *Drosophila* melanogaster. PLoS ONE 5, e9403.

Silver, D. L., and Montell, D. J. (2001). Paracrine Signaling through the JAK/STAT Pathway Activates Invasive Behavior of Ovarian Epithelial Cells in *Drosophila*. Cell 107, 831–841.

Silver, D. L., Geisbrecht, E. R., and Montell, D. J. (2005). Requirement for JAK/STAT signaling throughout border cell migration in *Drosophila*. Development 132, 3483–3492.

Singh, S. R., Oh, S.-W., Liu, W., Chen, X., Zheng, Z., and Hou, S. X. (2006). Rap-GEF/Rap signaling restricts the formation of supernumerary spermathecae in *Drosophila* melanogaster. Dev Growth Differ 48, 169–175.

Spahn, P., Ott, A., and Reuter, R. (2012). The PDZ-GEF protein Dizzy regulates the establishment of adherens junctions required for ventral furrow formation in *Drosophila*. J Cell Sci 125, 3801–3812.

Spradling, A. C. (1993). Developmental Genetics of Oogenesis. In: The Development of *Drosophila* Melanogaster, M. Bate, and A. Martinez-Arias, Cold Spring Harbor: Cold Spring Harbor Laboratory Press, 1–70.

Su, L., Hattori, M., Moriyama, M., Murata, N., Harazaki, M., Kaibuchi, K., and Minato, N. (2003). AF-6 controls integrin-mediated cell adhesion by regulating Rap1 activation through the specific recruitment of Rap1GTP and SPA-1. J Biol Chem 278, 15232–15238.

Thiery, J. P., Acloque, H., Huang, R. Y. J., and Nieto, M. A. (2009). Epithelial-mesenchymal transitions in development and disease. Cell 139, 871–890.

Tsai, I.-C., Amack, J. D., Gao, Z.-H., Band, V., Yost, H. J., and Virshup, D. M. (2007). A Wnt-CKIvarepsilon-Rap1 pathway regulates gastrulation by modulating SIPA1L1, a Rap GTPase activating protein. Dev Cell 12, 335–347.

Verstreken, P., Ohyama, T., Haueter, C., Habets, R. L. P., Lin, Y. Q., Swan, L. E., Ly, C. V., Venken, K. J. T., De Camilli, P., and Bellen, H. J. (2009). Tweek, an Evolutionarily Conserved Protein, Is Required for Synaptic Vesicle Recycling. Neuron 63, 203–215.

Walther, R. F., Burki, M., Pinal, N., Rogerson, C., and Pichaud, F. (2018). Rap1, Canoe and Mbt cooperate with Bazooka to promote zonula adherens assembly in the fly photoreceptor. J Cell Sci 131, jcs207779.

Wang, H., Qiu, Z., Xu, Z., Chen, S. J., Luo, J., Wang, X., and Chen, J. (2018). aPKC is a key polarity determinant in coordinating the function of three distinct cell polarities during collective migration. Development 145, dev158444.

Wang, H., Singh, S. R., Zheng, Z., Oh, S.-W., Chen, X., Edwards, K., and Hou, S. X. (2006). Rap-GEF Signaling Controls Stem Cell Anchoring to Their Niche through Regulating DE-Cadherin-Mediated Cell Adhesion in the *Drosophila* Testis. Dev Cell 10, 117–126.

Wang, X., He, L., Wu, Y. I., Hahn, K. M., and Montell, D. J. (2010). Light-mediated activation reveals a key role for Rac in collective guidance of cell movement *in vivo*. Nat Cell Biol 12, 591–597.

Wang, Y.-C., Khan, Z., and Wieschaus, E. F. (2013). Distinct Rap1 activity states control the extent of epithelial invagination via α-catenin. Dev Cell 25, 299–309.

Xi, R., McGregor, J. R., and Harrison, D. A. (2003). A Gradient of JAK Pathway Activity Patterns the Anterior-Posterior Axis of the Follicular Epithelium. Dev Cell 4, 167–177.

Xiang, W., Zhang, D., and Montell, D. J. (2016). Tousled-like kinase regulates cytokine-mediated communication between cooperating cell types during collective border cell migration. Mol Biol Cell 27, 12–19.

Xu, T., and Rubin, G. M. (1993). Analysis of genetic mosaics in developing and adult *Drosophila* tissues. Development 117, 1223–1237.

Yamamoto, E., Kohama, G.-I., Sunakawa, H., Iwai, M., and Hiratsuka, H. (1983). Mode of invasion, bleomycin sensitivity, and clinical course in squamous cell carcinoma of the oral cavity. Cancer 51, 2175–2180.

Zhang, Y.-L., Wang, R.-C., Cheng, K., Ring, B. Z., and Su, L. (2017). Roles of Rap1 signaling in tumor cell migration and invasion. Cancer Biol Med 14, 90–99.

5 Quantitative image analysis of dynamic cell behaviors during border cell migration

Yujun Chen, Nirupama Kotian, and Jocelyn A. McDonald
Division of Biology, Kansas State University, Manhattan, KS 66506, USA

Submitted to the Springer Nature's Methods in Molecular Biology: *Drosophila* oogenesis on 14th February 2022.

Author contributions:

Nirupama Kotian performed experiments for Figure 5.1, Figure 5.2 B,C, G, live time-lapse videos for analysis (performed by Yujun Chen) in Figures 5.4 and wrote the manuscript with Yujun Chen and Jocelyn McDonald.

5.1 Abstract

Drosophila border cells have emerged as a genetically tractable model to investigate dynamic collective cell migration within the context of a developing organ. Studies of live border cell cluster migration have revealed similarities with other migrating collectives, including formation and restriction of cellular protrusions to the front of the cluster, supracellular actomyosin contractility of the entire collective, and intra-collective cell motility. Here we describe protocols to prepare *ex vivo* cultures of stage 9 egg chambers followed by live time-lapse imaging of fluorescently-labeled border cells to image dynamic cell behaviors. We provide options to perform live imaging using either a widefield epifluorescent microscope or a confocal microscope. We further outline steps to quantify various cellular behaviors and protein dynamics of live migrating border cells using the Fiji image processing package of ImageJ. These methods can be adapted to other migrating cell collectives in cultured tissues and organs.

5.2 Introduction

Small to large groups of cells coordinate their movement in a process termed collective cell migration. Migrating cell collectives are essential for the proper development of many tissues and organs and contribute to pathological processes such as tumor invasion and metastasis [1, 2]. To better understand the conserved developmental, cellular, and molecular mechanisms that underlie collective cell migration, a number of *in vivo* models have been used, including the zebrafish lateral line, *Xenopus* neural crest cells, *Drosophila* embryonic tracheal branching and dorsal closure, and *Drosophila* ovarian border cells [2, 3]. Border cells are a small group of epithelial-derived cells that migrate collectively during mid-to-late oogenesis [4]. Importantly, border cells can be genetically manipulated and imaged over several hours in live *ex vivo* cultured egg chambers [4, 5]. Studies using border cells have revealed mechanisms that control collective cell polarization, cell-cell communication and adhesion for cooperative movement, and interactions with the surrounding tissue environment [4, 6–12].

Border cells migrate as a cohesive cluster of 6-10 cells, navigating the surrounding germline-derived nurse cells to reach the oocyte at the anterior end of the egg chamber, the functional unit of the ovary. At late stage 8, a pair of non-motile polar cells at the posterior end of the egg chamber specifies and recruits surrounding follicle cells to become the migratory border cells (Fig. 5.1A). Border cells delaminate as a cluster from the follicular epithelium at early stage 9 (Fig. 5.1F), then move between the 15 large nurse cells (Fig. 5.1G). At late stage 9, border cells stop migrating when they arrive at the anterior border of the oocyte (Fig. 5.1H). By mid-stage 10, border cells align with the dorsal-anterior corner of the oocyte. Later, border cells contribute to formation of the micropyle, the sperm entry pore into the oocyte. The entire ~150 μm border cell migration occurs over the course of 3- to 4-hours. The development of robust methods of *ex vivo*

live culturing of stage 9 egg chambers along with time-lapse imaging has revealed complex dynamic cellular behaviors of border cells [5, 13, 14]. The border cell cluster initially undergoes fast polarized migration with one or two cellular protrusions that extend and retract from the leading border cells [15, 16]. This is followed by a slower migration phase in which the cluster 'tumbles' or 'rotates' and extends multiple protrusions prior to reaching the oocyte [15–17]. Protrusions help border cells crawl between nurse cells and sense signals in the environment [14, 15]. During migration, border cells maintain adhesions to the polar cells and to each other yet are able to exchange positions within the cluster [12, 17]. Individual border cells, and the cluster itself, have specific cellular shapes, which help the group navigate the egg chamber [7, 8, 11]. Visualization of fluorescently labeled proteins and biosensors have revealed the dynamics of non-muscle myosin II (myosin II), F-actin, and E-cadherin proteins and the activity of the small GTPase Rac in live migrating border cell clusters [8, 11, 18, 19]. This includes a supracellular organization of actomyosin in the border cell cluster [8, 10, 11].

Here we describe a protocol to culture stage 9 egg chambers and perform live time-lapse imaging of fluorescently labeled border cells followed by quantification of cellular behaviors or protein dynamics. We describe flexible imaging options using either an epifluorescent microscope or a confocal microscope. We include a recently described strategy to immobilize egg chambers during time-lapse imaging using a fibrinogen-thrombin clot [20], which is useful in imaging and analyzing live border cell migration. Depending on which cellular or protein behaviors are of interest, imaging can be done on timescales of minutes to hours (e.g. 15 minutes for protein dynamics; 4-6 hours for protrusions). We outline steps to process images from time-lapse imaging using the open-source Fiji software [21]. We further describe quantification methods to measure and analyze border cell cluster migration speed, cluster and cell shapes, protrusion dynamics, and

protein localization and dynamics using Fiji [21]. While for simplicity we focus on wild type border cell migration, many options exist to genetically manipulate border cells in the developing egg chamber. The GAL4-UAS system can be used to knock down genes using RNA interference (RNAi), to overexpress proteins, or to manipulate protein levels or activity with various available optogenetic tools (e.g., [7, 8, 19, 22, 23]). Alternatively, researchers can perform classical genetic analyses using homozygous mutant alleles or mosaic mutant analyses [24, 25].

5.3 Materials

Preparation of Fly Stocks for Time Lapse Imaging

1. Select an appropriate fluorescent reporter fly stock for live imaging. Table 5.1 has a list of commonly used reporters and GAL4/UAS lines used for live time lapse imaging of border cell migration (*see* **Note 1**). As needed, set up a genetic cross to obtain flies of the correct genotype to express the fluorescent reporter in the desired cell types.
2. Dry (active) yeast (e.g. Red Star active yeast). To make a wet yeast paste for fattening females prior to dissection, dissolve dry yeast with water and mix to produce a spreadable paste that is not too runny but also will not dry out too quickly.
3. Fly food vials.

Ovary Dissection

1. Two pairs of dissecting forceps, Dumont #5, 0.1 x 0.06 mm tips, Inox (Electron Microscopy Sciences, cat. no. 0302-5-PO).
2. One two-well glass concavity (‘depression’) slide, thickness 3.12 - 3.22 mm (e.g., Electron Microscopy Sciences, cat. no. 71878-08).
3. Stereo microscope with good illumination (e.g., a ring light; a polarizer can be added to reduce glare).

4. CO_2 to anesthetize flies for dissection.
5. Dissection media (Preparation of Live Imaging Media).
6. Transfer pipettes to move egg chambers and dissection or live imaging media (e.g., 1 mL ultra-fine tip, Sarstedt cat. no. 86.1180).

Preparation of Dissection and Live Imaging Media

1. Fetal bovine serum (FBS; e.g., Avantor Seradigm Premium Grade Fetal Bovine Serum, cat. no. 97068-085).
2. Insulin, recombinant human (Millipore Sigma, cat. no. 91077C-250MG). To prepare a stock solution of insulin, first prepare acidified water. Add 1.2 mL 1 N HCl to 100 mL of dH2O; store at room temperature. Add 5 mg insulin powder to 500 µL acidified water and aliquot 10 µL into separate 0.6 mL microcentrifuge tubes (to a final concentration of 10 mg/mL). The insulin stock solution can be stored at -80˚C for at least 6 months.
3. 100X antibacterial-antimycotic solution, Gibco (Thermo Fisher Scientific, cat. no. 15240062)
4. Schneider's *Drosophila* Medium (Thermo Fisher Scientific, cat. no. 21720024).
5. pH meter.
6. 50mL centrifuge tube filtration system, PES, 0.22µm filter (Celltreat Scientific Products, cat. no. 229710).
7. Dissection medium: 1X Schneider's *Drosophila* Medium, 20% FBS, 1X antibacterial-antimycotic solution. To make, aliquot 39.5 mL of Schneider's medium into a 50 mL tube. To the same tube, add 10 mL of FBS and 0.5 mL of the 100X antibiotic-antimycotic solution. Bring the medium to room temperature, calibrate the pH meter and measure the pH of the solution. Adjust the pH to 6.95 (*see* **Note 2**). Filter sterilize using a 50mL tube

top vacuum filter. Aliquot into 1.5 mL microcentrifuge tubes. Store at 4˚C. Bring to room temperature before dissection.

8. Live imaging medium: 1X Schneider's *Drosophila* Medium, 20% FBS, 0.2 mg/mL insulin, 1X antibacterial-antimycotic solution. To prepare, add 490 μL dissection medium to a microcentrifuge tube containing 10 μL of 10 mg/ml insulin. Bring to room temperature before mounting egg chambers.

Mounting Egg Chambers for Live Imaging

1. Lumox dish 50 tissue culture dish, 50 mm, adherent (Sarstedt, cat. no. 94.6077.410). These dishes are oxygen-permeable, making them ideal for live imaging of border cells (*see* **Note 3**).
2. 22 x 22 mm^2 coverslip (no. 1 thickness).
3. 22 x 40 mm^2 coverslip (no. 1 thickness).
4. Halocarbon oil 27 (Millipore Sigma, cat. no. H8773-100ML).
5. Fibrinogen, Bovine Plasma (Millipore Sigma, cat. No. 341573-1GM; *see* **Note 4**).
6. Thrombin (Cytiva, cat. no. 27084601; *see* **Note 4**).

Live Time-lapse Imaging and Quantitative Analysis of Live Migrating Border Cells

1. Motorized microscope with an upright or inverted set up (Fig. 5.2) and either widefield epifluorescence or confocal imaging modality (*see* **Note 5**). We have successfully imaged border cells using a Zeiss Axio Imager Z1 upright epifluorescence microscope, which has a motorized z-focus drive, and a Zeiss 880 confocal with inverted microscope and motorized scanning x-y stage.
2. Objective: e.g. Plan-Apochromat 20× 0.75 Numerical Aperture (NA) air or 40× 1.2 NA water immersion.

3. Fiji (https://fiji.sc/) open source image processing package based on ImageJ2 [21].
4. Zen software (Zeiss), or similar microscope software.

5.4 Methods

Prepare Flies for Dissection

1. Obtain fly stocks with fluorescent markers and/or set up a genetic cross to express the fluorescent marker using the GAL4/UAS system (Table 5.1; see Note 1).
2. Collect 8-10 newly eclosed females (3-5 day old) of the correct genotype, along with 2-3 males to ensure the females have mated.
3. Transfer flies to a fresh food vial with wet yeast paste for 18-20 hours at 25°C or 29°C prior to ovary dissection. For maximal expression of GAL4/UAS, and inactivation of ts-GAL80 (as needed), incubation at 29˚C is often required.
4. A properly mated and fattened female will have a swollen abdomen that is filled by the enlarged ovary pair. The ovaries should contain ovarioles with most stages of oogenesis represented.

Dissection of ovaries for live imaging

1. Pull out whole ovaries
2. Allow the dissection medium to warm up to room temperature.
3. Prepare the dissection station by cleaning with 70% ethanol. Prepare a Kimwipe for disposal of fly tissue debris, and to wipe off forceps, during dissection.
4. Transfer a small amount of dissection medium to both wells of the glass concavity slide and focus on the slide under the stereomicroscope.
5. Anesthetize the flies and place onto a CO_2 pad (males can be discarded). Using the non-dominant hand, pick up one female using one forceps. Place the fly in one depression well

while simultaneously pressing down gently on the thorax and the top of the abdomen to make sure the fly is fully submerged under the medium. With the forceps in the dominant hand, grasp the dorsal posterior end of the abdominal cuticle and pierce it (*see* **Note 6**). Pull the cuticle gently away, which will cause the pair of ovaries to be released (Fig. 5.1B, C). Pull the ovary pair completely away from the rest of the fly carcass (Fig. 5.1C).

6. Remove the fly carcass by cleaning the forceps on a wet Kimwipe. Remove any other tissue debris that may be attached to the ovary using the forceps. Transfer the whole ovary to another well with fresh dissecting media. Repeat these steps until you obtain three to four pairs of whole ovaries.

Further dissect ovaries into ovarioles

1. Ovarioles need to be removed from the whole ovary. This allows imaging of the specific egg chamber stages for border cell migration as well as removal of the overlying muscle sheath (*see* **Note 6**). To further dissect the ovary into ovarioles, grasp one ovary from the pair with your non-dominant forceps at the larger posterior end (Fig. 5.1D). Push down to anchor the ovary at the bottom of the dissecting well. While continuing to hold a gentle grip on the older egg chambers of the whole ovary, use the other forceps (dominant hand) to grasp the early egg chambers at the anterior end. Slowly and carefully pull out 1-2 ovariole chains at a time (Fig. 5.1E). Repeat, until you are confident you have obtained at least 5-10 stage 9 egg chambers from approximately 10-15 dissected ovarioles (Fig. 5.1F).
2. Once the ovarioles are pulled out, remove late staged egg chambers (anything older than stage 9, typically egg chambers with the oocyte filling >50% of the length of the egg chamber) and other unwanted ovarian tissue using the forceps (*see* **Note 6**). Clean the forceps on a wet Kimwipe.

3. Carefully aspirate excess media from the well that has the dissected egg chambers by looking through the stereo microscope**.** Leave behind enough media to prevent the ovarioles from drying up. Add 100µL of live imaging medium to the same well. Aspirate the egg chambers along with the medium using a fine transfer pipette or a P200 pipettor with the tip cut off. Transfer the egg chambers to a 0.6 mL tube and wait for the egg chambers to settle to the bottom. Remove media from the tube with a fine pipette tip or transfer pipette, leaving behind a few microliters of media. Add 100 µL of fresh live imaging medium (*see* **Note 7**).

Mounting egg chambers for live imaging

Mount egg chambers for upright microscope live imaging

1. Prepare a Lumox culture dish (new or reused; *see* **Note 8**). Use the blunt end of a forceps (or a diamond glass cutter) to break a 22 × 22 mm coverslip into half in a petri dish; these will be used to support the overlying coverslip as a bridge to prevent crushing of egg chambers.
2. Pipet two 6 µL drops of fresh live imaging medium onto the inner membrane of the Lumox dish (Fig. 5.2F). Place the drops about 18 mm apart. Place the broken coverslip halves onto each drop, with the smooth edge facing the center (Fig. 5.2A).
3. Take the microcentrifuge tube containing the dissected egg chambers and gently aspirate to mix the egg chambers with the live imaging media.
4. Pipette 88 µL of the egg chambers with live imaging media and dispense the mixture to the Lumox dish in the center between the coverslip bridges. Use a circular motion to avoid overcrowding of egg chambers (Fig. 5.2B). Only a few egg chambers should be in the field

of view (Fig. 5.2C). Avoid any bubbles while pipetting the mixture onto the dish (*see* **Note 9**).

5. Pick up a 22 × 40 coverslip using a forceps. Gently place the coverslip on top of the broken coverslips and the dissected egg chambers, such that the coverslip fragments form a bridge between the egg chambers and the overlying coverslip. Gently tap the dish using your hand or on the bench to allow even spread of the egg chambers and live imaging medium. Remove any excess media using a torn off Kimwipe, wicking away liquid near the broken coverslip bridges.
6. Finally, apply 6 to 9 small drops of halocarbon oil using a P20 pipettor (~ three drops of oil each on the long sides and one drop on each of the short sides). Pipette the oil around the coverslip to form a thin layer that will prevent drying of the live imaging medium during imaging (Fig. 5.2A). Avoid excess halocarbon oil as this can interfere with imaging.

Mount egg chambers for inverted microscope live imaging and immobilize egg chambers with a fibrinogen-thrombin clot

1. Prepare a Lumox culture dish (new or reused; *see* **Note 8**). Use the blunt end of a forceps (or a diamond glass cutter) to break a 22 × 22 mm^2 coverslip into half in a petri dish; these will be used to support the overlying coverslip as a bridge to prevent crushing of egg chambers.
2. To the bottom side of the Lumox dish membrane (Fig. 5.2D), pipette 6 µL of fresh live imaging medium on the membrane about 18 mm apart. Place the broken coverslip halves onto each drop, with the smooth edge facing the center (Fig. 5.2A).
3. Rinse the egg chambers one time with 100 µL of live imaging medium. Remove as much live imaging medium as possible.

4. A fibrinogen-thrombin clot can be used to immobilize egg chambers [20, 26], which is especially helpful when using a 40x water-immersion objective (Fig. 5.2A; see **Note 4**). Otherwise, follow the procedure for upright microscope egg chamber mounting (*see* 3.3.1), but mount the egg chambers in live imaging media on the bottom side of the dish (Fig. 5.2D). To make the clot, add 10 µL fibrinogen (10 mg/mL) to the egg chambers in the tube. Next, transfer the egg chambers with fibrinogen to the bottom side of the Lumox dish onto the membrane between the broken coverslips. Quickly add 1 µL thrombin (10 U/mL), then wait 5-10 min to allow the fibrinogen-thrombin clot to form.
5. Add 78 µL of live imaging medium to the egg chambers with the fibrinogen-thrombin clot.
6. Gently place a 22 × 40 mm^2 coverslip on top of the broken coverslips, medium and egg chambers, using a forceps to guide the covering process as needed (*see* **Note 9**).
7. If needed, slowly add additional live imaging medium under one side of the coverslip until the entire gap under the coverslip is filled.
8. Finally, apply 6 to 9 small drops of halocarbon oil using a P20 pipettor (~ three drops of oil each on the long sides and one drop on each of the short sides). Pipette the oil around the coverslip to form a thin layer that will prevent drying of the live imaging medium during imaging (Fig. 5.2A). Avoid excess halocarbon oil as this can interfere with imaging.

Live time-lapse imaging

Live imaging using a widefield epifluorescent microscope

1. Place the mounted egg chambers on the Lumox dish onto the stage of a widefield epifluorescent microscope (*see* **Note 5**). If using an inverted microscope, your sample will be on the bottom of the dish (Fig. 5.2D, E); if using an upright microscope, your sample will be mounted on the inside of the dish (Fig. 5.2F, G).

2. Choose an egg chamber to image (Fig. 5.1F, Fig. 5.2C). Place the Lumox dish on the stage of a widefield epifluorescent microscope (Fig. 5.2E, G). Move the 10× objective into place and bring the egg chambers on the dish into focus (*see* **Note 10**).
3. Using either brightfield, or the fluorescence channel of interest, scan the dish to find an egg chamber at the appropriate stage (Fig. 5.1F). Egg chambers should be avoided that are visibly damaged, look abnormal in overall shape, or show a migration defect when not expected (*see* **Note 11**). Avoid egg chambers that are too early (e.g., border cells not yet rounded up or are not ready to delaminate) or are too late (Fig. 5.1H; border cells finished migrating). Selection of mid-stage 9 egg chambers (Fig. 5.1G; border cells in mid-migration) is sometimes appropriate when focusing on specific cellular phenomena such as protrusions, cell exchange, and/or cell shape.
4. After finalizing the egg chamber to be imaged, switch to the 20× objective and manually refocus.

Set up the widefield epifluorescent time-lapse experiment

1. Using the microscope software (e.g., Zeiss Zen), check the box for the time series function on the Acquisition tab. Set the time interval and duration of the experiment as prefered. Check the exposure for your channel of interest. (*see* **Note 12**)
2. To be able to capture different slices of the border cell cluster as it migrates, set up a Z-stack for the sample (*see* **Note 13**).
3. Start the time-lapse imaging experiment. Check the status of the experiment every 15-30 minutes. Check if the border cell cluster is still in focus and that the egg chamber continues to develop. Pause the experiment in the software, if needed, readjust the focus and/or exposure, then continue with the experiment. If the egg chambers are not developing

correctly (e.g., no growth of oocyte or no movement of the outer follicle cells towards the oocyte) or begin to appear abnormal as the experiment proceeds, either find a new egg chamber or start over with a new live imaging prep (*see* **Note 11**).

Live confocal microscopy

1. After turning on the confocal microscope, open the software (e.g. Zen software on a Zeiss confocal), then load the Lumox dish with the mounted egg chambers onto the stage (*see* **Note 5**).
2. Locate positions using a scanning x-y stage (optional): Switch the objective lens to 10×. Under “Locate” mode, use brightfield to adjust the focal plane, scan through the egg chambers and search for ones at the right stage (*see* **Note 10**). Use the desired fluorescent channel to check the fluorescence intensity in the border cell cluster to help choose the sample(s) to image. Click ‘‘Add’’ in the ‘‘position’’ box; scan the slide and repeat to select up to 10 egg chambers.
3. Switch to the 20× objective and make fine focus adjustments. Add water to the 40× lens (if using a water-immersion objective) and move the 40× objective into place on the sample.
4. Set the Scan Area: Change the scan area to "0.6", then click the “live” button, and move the border cluster to the center. Set the frame size to “512 x 512” and set the scan line speed, increasing the scan line speed for faster scanning time. For imaging the fast dynamics of proteins, increase the scanning speed accordingly. It is best to adjust the frame size and scan speed to meet the purpose of the specific experiment.
5. Set Channels and Intensity: Adjust the laser intensity (usually ranging from 0.1%~3%), pinhole, and the gain (master) with the range indicator to the appropriate level (bright

enough but not oversaturated). Click the “snap” button and take an image, then crop the image and modify the scan area and rotate the orientation of the egg chamber (anterior to the left and posterior to the right). Including unnecessary scanning areas in the field of view will increase acquisition time.

6. Set Z-Stack: For cell shape and protrusion analysis, find the top and bottom of the cluster, then set the interval of the z-stack as 1 µm to optimize for speed of acquisition (*see* **Note 13**). For analyses of protein dynamics, we typically image a single focal plane.
7. Set Time Series: For cell shape and protrusion analysis, the interval time should be set at 3 min and the duration time for 4-6h; stop the imaging early if needed. For protein dynamics, the interval time should be set at 15 sec and the duration time for 10-15 min (*see* **Note 12**).
8. Start the time-lapse movie experiment. Once finished, save the file in “.czi” or other native software file format. Move to the next egg chamber position, then repeat steps 3–6 to finish time-lapse imaging of all egg chambers (*see* **Notes 11 and 12**).

Quantitative analysis of live migrating border cells

General Image processing

1. Open the “.czi” movie in Fiji with “Bio-Formats Import Options” (Fig. 5.3A).
2. Create a maximum z-stack projection as needed: Use “Image › Stacks › Z Project” (Fig. 5.3B). For tracking protein dynamics, in which a single focal plane is imaged, skip to step 3.
3. Crop the region of interest: Use “Image › Crop” (Fig. 5.3C). Be sure to duplicate the image; this will ensure that the image can be re-edited as needed.

4. Change the visualization to invert the fluorescence image (*see* **Note 14**): Use “Image › Lookup Tables › Invert LUT” (Fig. 5.3D). As needed, adjust the image to best display the range of the signals: Use “Image › Adjust › Brightness/Contrast”.
5. Add a scale bar: Use “Analyze › Tools › Scale Bar” (Fig. 5.3E).
6. Add a timestamp: Use “Image › Stacks › Time Stamper” (Fig. 5.3F).
7. Convert the image to RGB mode and save it in “.avi” format for a movie or in “.tif” format for still images. Still frames from several successful live time-lapse border cell movies, with dynamic protrusion extension and retraction, are shown in Fig. 5.4 (widefield epifluorescence long time-lapse, Fig. 5.4A-B’’’’’; confocal short time-lapse, Fig. 5.4C-C’’’’’).

Measurements of cellular behaviors in Fiji

1. Migration speed: The migration speed is calculated from the duration of its movement. Use the "Straight line" tool from the main toolbar to draw a line from the anterior to posterior along the length of the egg chamber. Use the "Analyze › Measure" to measure the length of the migration, then divide the length by the time of the movie.
2. Cluster and cell shape: Use "Freehand selections" to select the main body of the cluster or a single cell (see Fig. 5.5A, B). Use "Analyze › Measure" to measure the area, circularity, and aspect ratio. Before measuring, make sure the "Area" and "Shape descriptors" are selected under "Analyze › Set Measurements".
3. Size, length, direction, and lifetime of the protrusion: Hold the shift key and use the “Oval” function to draw a circle surrounding the cell cluster (Fig. 5.5C). Any cellular extensions greater than 4 μm are defined as major (also termed ‘prominent’) protrusions [7, 8, 27] (*see* **Note 15**). Use “Freehand selections" to select the protrusion and use “Analyze › Measure”

to measure the area. Select the "Area" box under "Analyze › Set Measurements" before measuring. Use the "Straight Line" function and "Analyze › Measure" to measure the length of the protrusion (Fig. 5.5D). Use "Angle Tool" (found on the main toolbar) to measure the angle of the protrusion (Fig. 5.5E). With the anterior-posterior axis of the egg chamber aligned with the anterior at the left, measure the protrusion angles off a centerline that cuts through that axis. Protrusions are classified into the front (0° to 45° and 0° to 315°), side (45° to 135°and 225° to 315°), and back (135° to 225°) based on position within the cluster (Fig. 5.5F). The protrusion lifetime is calculated by noting the frame in which the protrusion starts to extend until the protrusion fully retracts.

Measurements of protein localization and dynamics

1. Measurements and analyses for each specific fluorescently labeled protein need to be empirically determined. Here, we focus on myosin II and F-actin, for which we have extensive experience imaging and quantifying [8, 11, 28]. GFP-tagged Spaghetti Squash (Sqh:GFP) labels the *Drosophila* non-muscle myosin II regulatory subunit (MRLC) and thus visualizes the dynamics of myosin II, particularly at cell membranes. LifeAct:GFP detects F-actin and has been used extensively in border cells (Table 5.1; [7, 8, 18]).
2. During border cell migration, Sqh:GFP accumulation occurs mostly at the outer periphery of the border cell cluster (supracellular localization), with occasional accumulation observed inside the cluster at contacts between border cells in some movie frames (Fig. 5.5G). Accumulation of LifeAct:GFP can be found at the protrusion and the periphery of the border cell cluster (Fig. 5.5H).
3. To quantify protein distribution and levels, the number of spots (“foci”) of Sqh:GFP or LifeAct:GFP can be manually counted for the entire movie. To identify the foci of

fluorescent protein (region of interest), use “Freehand selections" to manually select. To measure the intensity of each focal accumulation of the fluorescently labeled protein, under "Analyze › Set Measurements", select the "Mean gray value", then use the “Analyze › Measure” function. To obtain the average number of fluorescent protein foci, divide the total number of fluorescent focal accumulations by the total number of movie frames. Alternatively, or in addition, the number and average intensity of foci at the periphery of the cluster versus inside the cluster (internal cell membranes) can be calculated. Both Sqh-GFP and LifeAct-GFP foci at the periphery should be dynamic at cell membranes while the cluster is migrating. The average intensity of fluorescent signals can be compared between control clusters and genetically manipulated clusters. These measurements can provide useful insights into the mechanical forces and other cellular behaviors regulating border cell migration.

Notes

1. Selecting an appropriate reporter (and GAL4 driver, if required) is crucial for setting up a successful time-lapse imaging experiment (Table 5.1). *slbo*-GAL4 and c306-GAL4 are the two most commonly used GAL4 lines for time-lapse imaging of border cell migration. If driving RNAi, *c306*-GAL4 is often used; however, because *c306*-GAL4 drives expression during early oogenesis, ts-Gal80 should be employed to block early GAL4/UAS expression. All genotypes should be tested prior to scaling up experiments to make sure no unexpected defects in border cell migration occur. For example, *c306*-GAL4, tsGal80; UAS-PLCδPH:GFP (Table 5.1; Fig. 5.4) is typically outcrossed to a control fly stock (e.g., w^{1118}) to ensure normal migration; two copies of *c306*-GAL4 in this stock can cause developmental defects, whereas outcrossing eliminates these defects. Prior to using a new fluorescent reporter, or GAL4/UAS combination, it is important to determine if border cell

migration occurs properly in fixed egg chambers. See Table 5.1 for additional known advantages and disadvantages for different fluorescent reporters and GAL4/UAS combinations that have been used to image migrating border cells. When performing genetic manipulations (e.g. using RNAi, mutant alleles, overexpression), be sure to have controls for live imaging. This will ensure that any defect observed in border cells is a real phenotype and not due to any extraneous issues such as reagents that have gone bad, issues with dissecting or mounting the samples, or phototoxicity during imaging.

2. The pH of the live imaging medium is one of the most crucial factors for time lapse imaging of border cells [5]. Ideally, the pH should be between 6.85-6.95. Egg chambers tend to show developmental defects and/or border cell migration defects in media with pH outside this range. Before using the dissection or live imaging medium, check for any signs of contamination or growth, such as cloudiness. It is best to prepare fresh batches of media or enough to last 1-2 months.
3. Oxygen is very important for live imaging of border cells, thus use of the Lumox dish with its oxygen-permeable membrane is ideal. Other types of preps can be used [28–30], including use of MatTek glass bottom dishes (e.g., cat. no. P50G-1.5-14-F [50 mm uncoated dish, no. 1.5 coverslip], or cat. no. P50GC-1.5-14-F [50 mm Poly-D-Lysine coated, no. 1.5 coverslip). However, special care with these other types of preps must be made to prevent drying out of the imaging media, and thus the egg chambers, during imaging.
4. Mounting in a fibrinogen-thrombin clot is an optional step but is useful when using objectives with small working distances, such as the 40× water immersion objective. Fibrinogen and thrombin together form a clot that immobilizes the egg chambers [20].

5. The choice between widefield epifluorescence and confocal imaging will depend on the goal of the experiment and the availability of microscopes. Widefield epifluorescent microscopes are widely available and easy to use. While different light sources can be used, LED illuminators (e.g. Zeiss Colibri) offer significant benefits for time-lapse imaging. LED light sources provide gentle light for live imaging due to the precise control of light intensity and wavelength, and ability to be precisely switched on and off. We often use widefield epifluorescence to perform longer time-lapse imaging (3-4 hours) that allows analysis of migration speed, protrusion dynamics, and general protein localization [8, 27, 31]. Confocal microscopy offers significant advantages by reducing out-of-focus illumination and allowing acquisition of images at high speed, which allows for shorter time-lapse intervals and faster z-stack acquisition, both of which are needed for detailed analysis of cellular and protein dynamics. However, even with lower laser intensity, care must be made with confocal time-lapse imaging to reduce phototoxicity and potential photobleaching of fluorescent proteins. We typically use confocal imaging to perform shorter time-lapse imaging (30 minutes to 2 hours), which is useful for analysis of faster protein dynamics and cellular behaviors.
6. Handling the ovaries too much increases the risk of tissue damage and potential failure of egg chamber development and/or impairment of border cell migration during live imaging. Likewise, leaving behind excess tissue can result in unwanted movement of egg chambers during imaging or depletion of nutrients in the medium by older egg chambers. It is important to very slowly and gently pull out only one or two ovarioles to allow full removal of the ovarioles from the overlying muscle sheath. Failure to remove the muscle sheath will

potentially cause unwanted movement of the egg chamber due to the muscle contracting during imaging.

7. Minimize the time it takes to dissect the ovarioles and mount the egg chambers. We try to limit dissection and mounting to ~30 minutes from start to finish.
8. The Lumox dish can be reused multiple times but discard the dish if the membrane tears. To reuse the Lumox dish, remove the cover glass and cover glass shards after imaging. Immerse and soak the dish in "Windex Glass Cleaner" overnight while shaking to remove the halocarbon oil. While wearing gloves, gently rub the membrane with your fingers under running tap water to ensure no residual halocarbon oil remains. Rinse the dish with deionized water and air dry the dish. Store the cleaned Lumox dish in a closable container to avoid dust or disturbance.
9. There should be no air bubbles between the dish and coverslip. As needed, gently nudge the coverslip to push any bubbles out.
10. When scanning the dish to find a desired egg chamber to image, it is best to start from the center of the coverslip instead of the sides. Avoid egg chambers that are near the edge of the coverslip if you are imaging with a 20× objective, or another objective with a short working distance, so that the halocarbon oil does not come into contact with the objective lens.
11. Sometimes egg chambers only show defects during imaging. Some egg chambers are either developmentally behind, show migration defects when not expected, or the egg chamber simply moves out of the frame of view during imaging. Normal development of the egg chamber includes the growth of the oocyte, movement of the follicle cell layer towards the oocyte, and cytoplasmic flow within the oocyte (visualized by yolk granule movement in

the brightfield channel). If defects are observed, the best solution is either to find another egg chamber within the dish, being sure to avoid any egg chambers that might be even slightly damaged, or to start over and prepare a fresh sample. If you encounter too many problems during imaging, it is a good idea to recheck the pH of the live imaging media.

12. The mounted live imaging prep is generally good for 4-6 hours. Time and phototoxicity are correlated when it comes to setting up time intervals for the experiment. An optimal combination of time intervals and speed of acquisition is key to this process. Shorter time intervals can lead to defects caused by phototoxicity due to continuous exposure while capturing the slices. However, longer time intervals allow the entire cluster to be imaged using z-stacks while also decreasing the chance for phototoxicity to occur. Short intervals (15-30 seconds) allow the capture of more cellular details and dynamics but increases the chances of photobleaching and phototoxicity. Long intervals (e.g. 2-3 minutes), on the other hand, capture fewer cellular details and dynamics but with less chance of phototoxicity. Using a widefield epifluorescent microscope, an LED light source, and 2–3-minute intervals, we typically image one egg chamber for 2-4 hours. Depending on the time interval, live imaging on a confocal can be done for 1-4 hours. Signs of phototoxicity include shrinking of the egg chamber and/or loss of yolk granule movement in the oocyte. If this is observed, move to a new sample and adjust the light levels and/or time interval.
13. The border cell cluster can sometimes go out of focus during migration, either because of sample drift or the border cell migration path between nurse cells. Therefore, it is important to consider the thickness of the border cell cluster when setting up z-stacks. We recommend setting a z-stack of at least 20 μm with 10 slices (or 1 μm interval between z-slices) to

ensure that most of the entire cluster height (estimated to be ~30-50 µm) is captured. Alternatively, manually set the top and the bottom of the cluster *z*-positions.

14. We often find it easier to invert the fluorescence image, which allows for better contrast when visualizing and measuring cellular behaviors and protein localization. As preferred, leave the image as acquired. Alternatively, use "Image › Lookup Tables" to change the color and/or use a color range such as "Rainbow RGB", or other appropriate LUT, to visualize pixel intensity of fluorescent proteins.
15. We define major protrusions as those cellular extensions that project away from the cell body and are greater than 4 µm in length from the base of the protrusion to the tip. Other studies use the same method to identify where in the cluster protrusions form but use different criteria to identify major protrusions. These criteria include any cellular extension greater than 2 µm [19], any protrusion greater than 3 µm long (base to tip) and 3 µm wide at the base of the protrusion [32], or any cellular extension that is thinner in diameter than the cell body [17].

5.5 Figures and tables

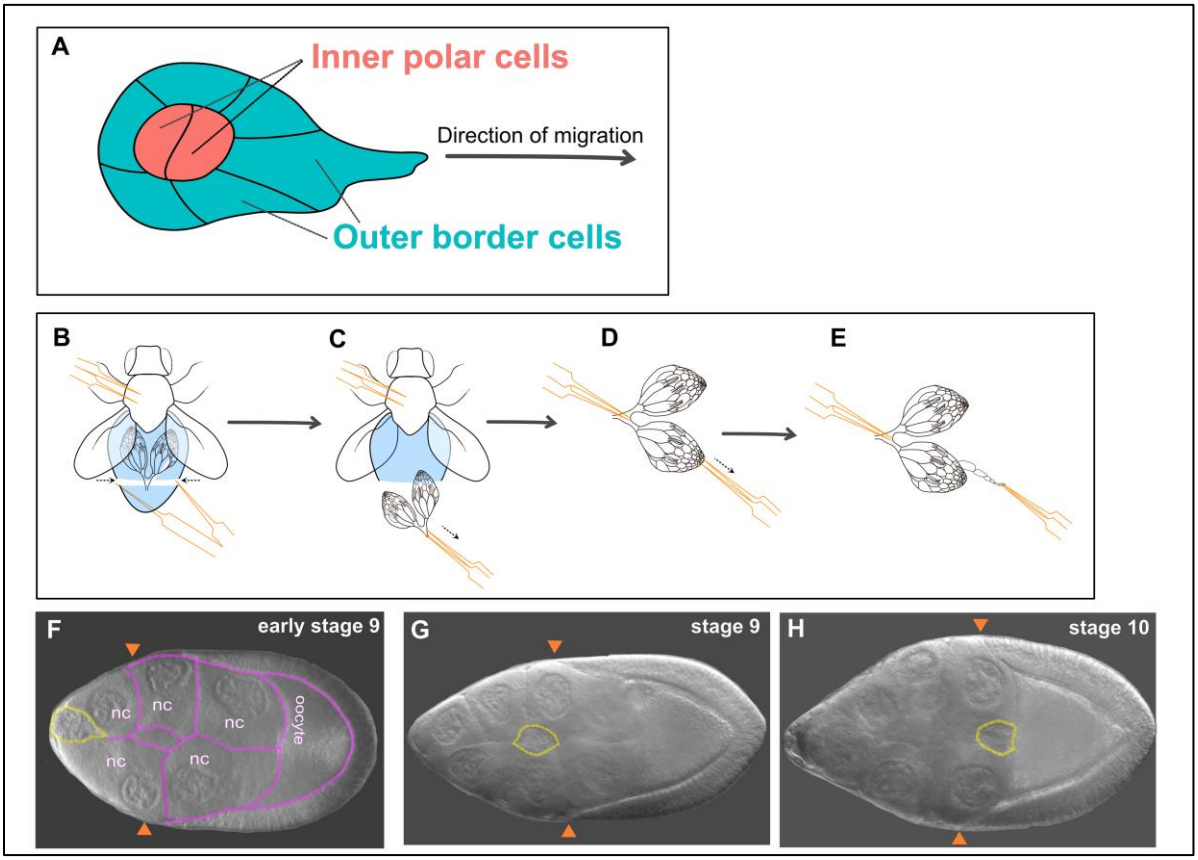

Figure 5.1 Illustration of ovary dissection and staging of egg chambers for imaging border cell migration.

(A) Schematic of a border cell cluster. Shown in the drawing are inner polar cells in pink and outer border cells in blue with an arrow pointing towards the direction of migration of the cluster. (B-E) Illustrated stepwise instructions for ovary dissection from flies and further ovariole dissection from a pair of whole ovaries. In all drawings, the dominant forceps are on the right and the non-dominant forceps are on the left. (F-H) DIC images of *Drosophila* egg chambers from early stage 9 (F), mid-migration (G) and stage 10 (H) with yellow line outlining the border cell cluster in each egg chamber and orange arrowheads showing the movement of outer follicle cells around the

oocyte as egg chamber maturation progresses. In F, nurse cells are labeled “nc”; both the oocyte and nurse cells are outlined in magenta. Anterior is to the left (A, F-G).

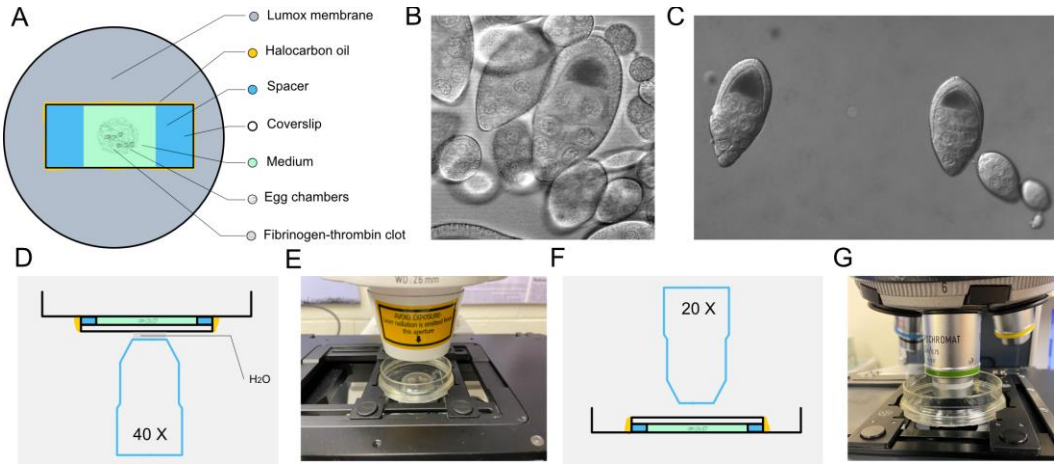

Figure 5.2 Sample mounting.

(A) Illustration of the mounted egg chambers ready for imaging. Shown is the sample prep with the optional fibrinogen-thrombin clot. (B) DIC image of an overcrowded field of view of a sample prep with egg chambers too close to each other. (C) DIC image of a well-spaced field of view of a sample prep with egg chambers at an ideal density for imaging. (D) Illustration of the sample setup for a confocal microscope with the sample mounted on the bottom of the dish. (E) Image of the setup on an inverted confocal microscope, the Zeiss LSM-800. (F) Illustration of the imaging setup for a widefield microscope with the sample mounted on the inside of the dish. (F) Image of the setup on an upright microscope, the Zeiss Axio Imager.

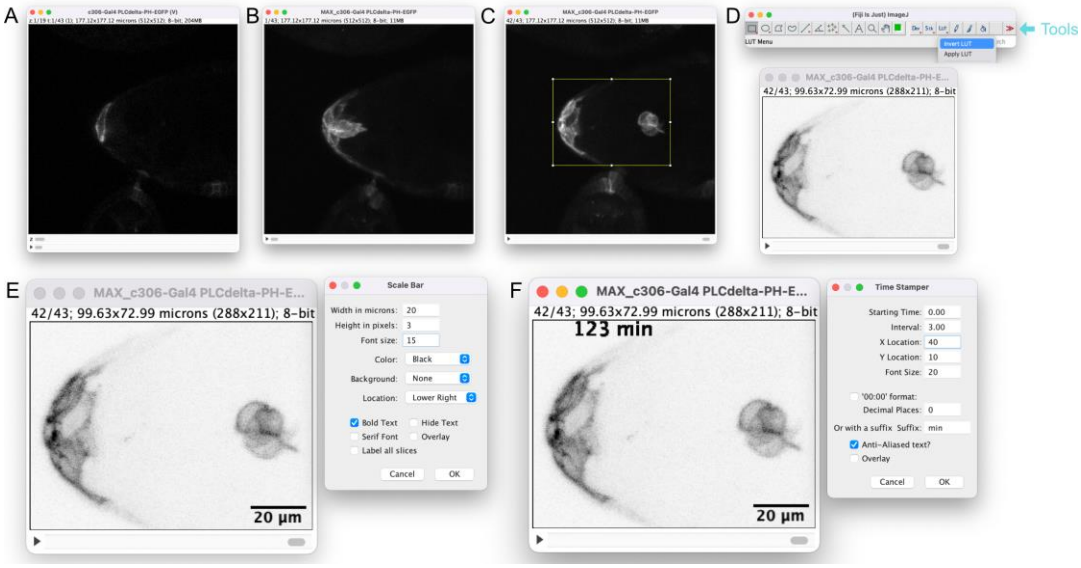

Figure 5.3 Overview of steps in Fiji to process a time-lapse movie. Screen captures to illustrate how to process time-lapse imaging files in Fiji.

(A) Open the movie in Fiji. (B) Create a maximum z-stack projection. (C) Crop the image as needed. (D) Invert the LUT; the tool bar is shown. (E) Add a scale bar. (F) Add the time using the time stamper tool.

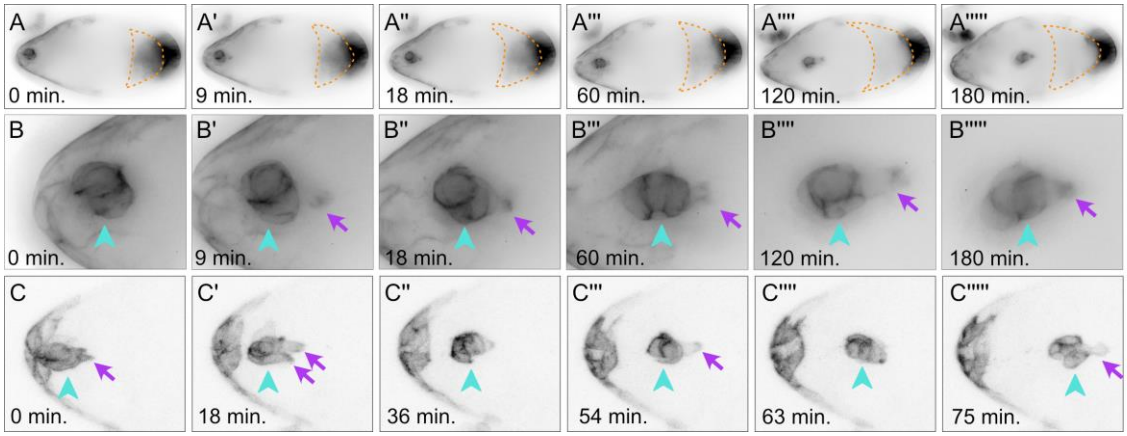

Figure 5.4 Time-lapse images showing key stages of border cell migration.

(A-A’’’’’) Still images from a 240 minute (imaged at 3-minute intervals) time-lapse movie of a *c306*-GAL4/+; UAS- PLCδ-PH-EGFP/+ egg chamber generated using a widefield epifluorescent microscope. Six time points, from 0-180 minutes, show the border cell cluster as it migrates to the oocyte anterior border. (B-B’’’’’) Magnified views of the same border cell cluster (arrowhead) from (A-A’’’’’), showing a protrusion (arrow) at various time points. (C-C’’’’’) Still images of a 129 minute (imaged at 3-minute intervals) time-lapse movie of a *c306*-GAL4/+; UAS- PLCδ-PH-EGFP/+ generated using a confocal microscope. Six time points are shown. The border cell cluster (arrowhead) delaminated from the epithelium (C; 0 min) and migrated (C’-C’’’’’; 18-75 min), with protrusions (arrows) extending and retracting during this time. Anterior is to the left in all panels.

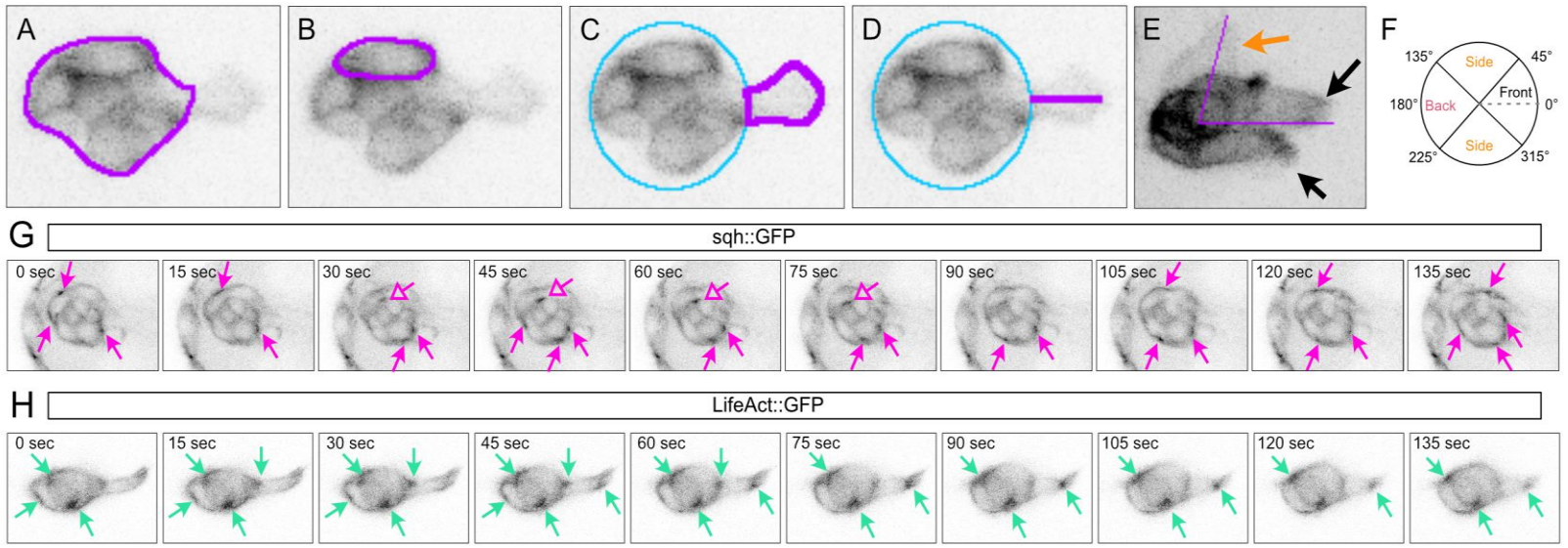

Figure 5.5 Analysis of protrusion and protein dynamics in live border cells.

(A-F) Measurement and selection of live border cell cellular features using Fiji: (A) cluster shape; (B) single border cell shape; (C) area of the major protrusion; (D) length of the major protrusion; and (E-F) the direction of the major protrusion. (A-D) A still image of the same *c306*-GAL4/+; UAS- PLCδ-PH-EGFP/+ border cell cluster shown at high magnification. (E) A still image of a different c306-GAL4/+; UAS-PLCδ-PH-EGFP/+ border cell cluster shown at high magnification. (G-H) Measurement of enriched accumulations of proteins in live border cells using fluorescent markers of myosin II (G; sqh::GFP) and F-actin (H; LifeAct::GFP). (G) Accumulation of sqh::GFP (fTRG Line; Table 5.1) at the cluster perimeter (solid pink arrows) and inside the cluster (hollow pink arrows) at the indicated times (in seconds). (H) Accumulation of LifeAct::GFP (driven directly by the *slbo* enhancer; Table 5.1) at the cluster perimeter (light blue arrows) at the indicated times (in seconds). Anterior is to the left in all panels.

Tables

Table 5.1 Commonly used fluorescent reporters and other fly stocks useful for live imaging of border cells

Stock Genotype	Source (stock number)	Advantages	Disadvantages	Live Imaging References (PMID)
UAS-PLCδPH::EGFP	BDSC (39693)	Marks cell membranes with almost no cytoplasmic signal; bright with very good signal to noise; use to label cell shapes, cluster shape, and protrusions		[8]
slbo-LifeAct::GFP [2M]	BDSC (58364)	Labels F-actin; LifeAct-GFP driven directly by the *slbo* enhancer; specific to border cells and a few follicle cells; very good signal to noise; can be used to measure protrusions and actin dynamics; independent of GAL4/UAS system	Strong expression of LifeAct can cause severe F-actin defects in some cells and tissues, for example the germline [40]; live imaging conditions should be optimized to avoid artifacts induced by LifeAct overexpression	[8, 12]
UAS-LifeAct::GFP	BDSC (35544)	Labels F-actin; UAS-driven LifAct-GFP;	Strong expression of LifeAct can cause severe	[7]

Stock Genotype	Source (stock number)	Advantages	Disadvantages	Live Imaging References (PMID)
		excellent signal to noise; can be used to measure protrusions and actin dynamics	F-actin defects in some cells and tissues, for example the germline [40]; choice of GAL4 is crucial; live imaging conditions should be optimized to avoid artifacts induced by LifeAct overexpression	
sqh fTRG library (sqh$^{fTRG00600.sfGFP-TVPTBF}$)	VDRC (318484)	Labels non-muscle myosin II; bright with very good signal to noise; tagged FlyFos transgene; can be used as a heterozygote		[8]
sqh^{AX3}; sqh::GFP	BDSC (57144)	Labels myosin II; bright with good signal to noise; rescue transgene in mutant background so is the only source of MRLC		[28, 33]
c306-GAL4; sqh::GFP	J. McDonald	Labels myosin II; bright with good signal		[28]

Stock Genotype	Source (stock number)	Advantages	Disadvantages	Live Imaging References (PMID)
	(derived from BDSC 57144)	to noise; rescue transgene, can be used as a heterozygote		
sqh-mCherry	BDSC (59024)	Labels myosin II; good signal; rescue transgene	mCherry can sometimes aggregate into abnormal punctae; brighter at central polar cells	[18, 34, 35]
UAS-mCherry::Jupiter	C.Q. Doe	Labels microtubules and cytoplasm; bright with good signal to noise	Mostly cytoplasmic in border cells; does not visibly label distinct microtubules in live border cells; occasional aggregated mCherry punctae are observed	[28, 36, 37]
c306-GAL4;UAS-mCherry::Jupiter	J.A. McDonald	Stock carrying mCherry-Jupiter to express in border cells	Best to outcross to wild-type chromosome and image as a heterozygote	
UAS-mCD8::GFP or UAS-mCD8::ChRFP	Various stocks, BDSC (e.g., 5136, 27392)	General membrane marker; bright with good signal to noise; labels protrusions and general cell and cluster shape	Can appear mostly cytoplasmic in border cells with less enrichment at the cell membrane	

Stock Genotype	Source (stock number)	Advantages	Disadvantages	Live Imaging References (PMID)
UAS-nuclear::GFP or UAS-nuclear::ChRFP	Various stocks, BDSC (e.g., 4776, 38425)	Use to label nuclei; especially good for tracking positions of border cells within the cluster		[18]
E-cad::GFP (TI{TI}shg[GFP])	BDSC (60584)	Labels endogenous E-cadherin (Shg) in border cells; GFP engineered into the *shg* gene locus		[18, 38]
UAS-GMA	Various stocks, BDSC (e.g., 31775)	Moesin actin-binding domain tagged with GFP; enriched at cell membranes; good signal to noise		[14, 39]

Stock Genotype	Source (stock number)	Advantages	Disadvantages	Live Imaging References (PMID)
c306-GAL4	BDSC (3743)	GAL4 driver that turns on early in border cells and maintains expression; especially useful for effective RNAi-mediated knockdown in border cells	Occasional slow border cell delamination and/or mild cluster splitting; somewhat heterogeneous expression in border cells; use outcrossed to UAS or to a wild-type chromosome; expressed in other follicle cells; expressed at earlier stages of development so is often used in combination with ts-GAL80	
slbo-GAL4	D. Montell (insertion on II without UAS-GFP); BDSC (58435; insertion on III)	GAL4 driver that turns on in border cells just prior to delamination; strong expression in border cells; not expressed during earlier stages of oogenesis	Not expressed in the central polar cells; expressed in a few anterior and posterior follicle cells in addition to the border cells	
ts-GAL80	BDSC various	Used to suppress GAL4/UAS expression	Flies carrying ts-GAL80 need to be incubated at	

Stock Genotype	Source (stock number)	Advantages	Disadvantages	Live Imaging References (PMID)
	stocks (e.g., 7019)	at earlier stages of development	29˚C for at least 14 h prior to ovary dissection to ensure GAL80 is off and GAL4/UAS is on	
w^{1118} or Oregon R	BDSC various stocks (e.g., 3605, 5)	Stocks used to outcross GAL4-driven fluorescent reporter stocks; many P-element stocks are made in a *w* background making w^{1118} a good control		

Bolded text: stocks used in this chapter.

5.6 References

1. Nagai T, Ishikawa T, Minami Y, Nishita M (2020) Tactics of cancer invasion: solitary and collective invasion. J Biochem 167:347–355
2. Scarpa E, Mayor R (2016) Collective cell migration in development. J Cell Biol 212:143–155
3. Friedl P, Gilmour D (2009) Collective cell migration in morphogenesis, regeneration and cancer. Nat Rev Mol Cell Biol 10:445–457
4. Saadin A, Starz-Gaiano M (2016) Circuitous Genetic Regulation Governs a Straightforward Cell Migration. Trends Genet 32:660–673
5. Prasad M, Jang AC-C, Starz-Gaiano M, et al (2007) A protocol for culturing *Drosophila* melanogaster stage 9 egg chambers for live imaging. Nat Protoc 2:2467–2473
6. Dai W, Guo X, Cao Y, et al (2020) Tissue topography steers migrating *Drosophila* border cells. Science 370:987–990
7. Plutoni C, Keil S, Zeledon C, et al (2019) Misshapen coordinates protrusion restriction and actomyosin contractility during collective cell migration. Nat Commun 10:1–16
8. Chen Y, Kotian N, Aranjuez G, et al (2020) Protein phosphatase 1 activity controls a balance between collective and single cell modes of migration. eLife 9:e52979
9. Ramel D, Wang X, Laflamme C, et al (2013) Rab11 regulates cell-cell communication during collective cell movements. Nat Cell Biol 15:317–324
10. Lamb MC, Kaluarachchi CP, Lansakara TI, et al (2021) Fascin limits Myosin activity within *Drosophila* border cells to control substrate stiffness and promote migration. Elife 10:e69836
11. Aranjuez G, Burtscher A, Sawant K, et al (2016) Dynamic myosin activation promotes collective morphology and migration by locally balancing oppositional forces from surrounding tissue. Mol Biol Cell 27:1898–1910

12. Cai D, Chen S-C, Prasad M, et al (2014) Mechanical feedback through E-cadherin promotes direction sensing during collective cell migration. Cell 157:1146–1159
13. Bianco A, Poukkula M, Cliffe A, et al (2007) Two distinct modes of guidance signalling during collective migration of border cells. Nature 448:362–365
14. Prasad M, Montell DJ (2007) Cellular and molecular mechanisms of border cell migration analyzed using time-lapse live-cell imaging. Dev Cell 12:997–1005
15. Poukkula M, Cliffe A, Changede R, Rorth P (2011) Cell behaviors regulated by guidance cues in collective migration of border cells. J Cell Biol 192:513–524
16. Combedazou A, Choesmel-Cadamuro V, Gay G, et al (2017) Myosin II governs collective cell migration behaviour downstream of guidance receptor signalling. J Cell Sci 130:97–103
17. Cliffe A, Doupé DP, Sung H, et al (2017) Quantitative 3D analysis of complex single border cell behaviors in coordinated collective cell migration. Nat Commun 8:14905
18. Mishra AK, Mondo JA, Campanale JP, Montell DJ (2019) Coordination of protrusion dynamics within and between collectively migrating border cells by myosin II. MBoC 30:2490–2502
19. Wang X, He L, Wu YI, et al (2010) Light-mediated activation reveals a key role for Rac in collective guidance of cell movement *in vivo*. 12:1133-1142
20. Wilcockson SG, Ashe HL (2021) Live imaging of the *Drosophila* ovarian germline stem cell niche. STAR Protocols 2:100371
21. Schindelin J, Arganda-Carreras I, Frise E, et al (2012) Fiji: an open-source platform for biological-image analysis. Nat Methods 9:676–682
22. Wang H, Guo X, Wang X, et al (2020) Supracellular Actomyosin Mediates Cell-Cell Communication and Shapes Collective Migratory Morphology. iScience 23:101204

23. Zeledon C, Sun X, Plutoni C, Emery G (2019) The ArfGAP Drongo Promotes Actomyosin Contractility during Collective Cell Migration by Releasing Myosin Phosphatase from the Trailing Edge. Cell Reports 28:3238-3248.e3
24. Lamb MC, Anliker KK, Tootle TL (2020) Fascin regulates protrusions and delamination to mediate invasive, collective cell migration *in vivo*. Dev Dyn 249:961–982
25. Badmos H, Cobbe N, Campbell A, et al (2021) *Drosophila* USP22/nonstop polarizes the actin cytoskeleton during collective border cell migration. J Cell Biol 220:e202007005
26. Wilcockson SG, Ashe HL (2019) *Drosophila* Ovarian Germline Stem Cell Cytocensor Projections Dynamically Receive and Attenuate BMP Signaling. Developmental Cell 50:296-312.e5
27. Sawant K, Chen Y, Kotian N, et al (2018) Rap1 GTPase promotes coordinated collective cell migration *in vivo*. Mol Biol Cell 29:2656–2673
28. Majumder P, Aranjuez G, Amick J, McDonald JA (2012) Par-1 controls myosin-II activity through myosin phosphatase to regulate border cell migration. Curr Biol 22:363–372
29. Manning L, Starz-Gaiano M (2015) Culturing *Drosophila* Egg Chambers and Investigating Developmental Processes Through Live Imaging. Methods Mol Biol 1328:73–88
30. Cetera M, Lewellyn L, Horne-Badovinac S (2016) Cultivation and Live Imaging of *Drosophila* Ovaries. Methods Mol Biol 1478:215–226
31. Starz-Gaiano M, Melani M, Wang X, et al (2008) Feedback Inhibition of JAK/STAT Signaling by Apontic Is Required to Limit an Invasive Cell Population. Dev Cell 14:726-38
32. Wang H, Qiu Z, Xu Z, et al (2018) aPKC is a key polarity determinant in coordinating the function of three distinct cell polarities during collective migration. Development 145:dev158444

33. Royou A, Field C, Sisson JC, et al (2004) Reassessing the role and dynamics of nonmuscle myosin II during furrow formation in early *Drosophila* embryos. Mol Biol Cell 15:838–850
34. Chang Y-C, Wu J-W, Hsieh Y-C, et al (2018) Rap1 Negatively Regulates the Hippo Pathway to Polarize Directional Protrusions in Collective Cell Migration. Cell Reports 22:2160–2175
35. Rauzi M, Lenne P-F, Lecuit T (2010) Planar polarized actomyosin contractile flows control epithelial junction remodelling. Nature 468:1110–1114
36. Cabernard C, Doe CQ (2009) Apical/basal spindle orientation is required for neuroblast homeostasis and neuronal differentiation in *Drosophila*. Dev Cell 17:134–141
37. McDonald JA, Khodyakova A, Aranjuez G, et al (2008) PAR-1 Kinase Regulates Epithelial Detachment and Directional Protrusion of Migrating Border Cells. Curr Biol 18:1659–1667
38. Huang J, Zhou W, Dong W, et al (2009) From the Cover: Directed, efficient, and versatile modifications of the *Drosophila* genome by genomic engineering. Proc Natl Acad Sci U S A 106:8284–8289
39. Sharma A, Halder S, Felix M, et al (2018) Insulin signaling modulates border cell movement in *Drosophila* Oogenesis. Development 145:dev166165-43
40. Spracklen AJ, Fagan TN, Lovander KE, et al (2014) The pros and cons of common actin labeling tools for visualizing actin dynamics during *Drosophila* oogenesis. Developmental Biology 393:209-226

6 Discussion and future directions

6.1 Discussion

To orchestrate the movement of collectives on a supracellular level, multiple cellular and molecular mechanisms work together to regulate this dynamic process. Cell-cell adhesion is a shared mechanism seen in different variants and modes of collective cell migration. Focusing on conserved cell adhesion-based mechanisms that connect the cells and relay the mechanical signals during collective cell migration can provide a starting point to determine a therapeutic target for invasive cancers. Our work revealed key findings involving the role of adhesion-related proteins during collective cell migration and collective cell invasion. Using a novel glioblastoma-informed approach, we identified conserved adhesion genes essential for collective border cell migration. These adhesion genes were members of well-categorized adhesion systems like the Cadherin-catenin complex, IgCAMs, protocadherins and the septate junction family of adhesion proteins. Analyzing the regional expression of human orthologs of border cell screen hits in a glioblastoma tumor database uncovered subsets of orthologous genes that were enriched in the invasive edge of patient glioblastoma tumors. Through this methodology, we were able to find genes that caused migration defects in the border cell model and caused regional gene expression changes in human GBM patient tumors (Fig. 6.1A). Therefore, we utilized a human disease informed approach to study conserved regulators of collective cell migration in an *in vivo* fly ovary model. This approach will further inform the development of effective treatment strategies by finding new potential genes involved in driving GBM tumor invasion.

Further, we uncovered two mechanisms that regulate E-cadherin mediated cell adhesion in border cell collective migration. Fast turnover and organization of cell adhesion proteins is crucial for the movement of cell collectives. First, we showed that downregulating members of the

cadherin-catenin complex such as α-Catenin, β-Catenin and E-cadherin, in the border cell cluster causes cohesion and migration defects. After knocking down these adhesion proteins, the border cell cluster which is otherwise tightly connected, falls apart during migration. Interestingly, knocking down Protein serine-threonine phosphatase 1 (PP1) through a nuclear inhibitor of PP1 (NiPP1) also led to similar cohesion defects in border cells (Chen *et al*. 2020). PP1 is a conserved phosphatase required in a range of cellular processes like cell division, RNA splicing and individual cell migration of cancer cells (Martin-Granados *et al.* 2012; Ceulemans and Bollen 2004). We present proof that PP1 keeps border cells connected by regulating cadherin-catenin protein levels at cell-cell contacts.

Next, we also discovered the role of Rap1 in organizing E-cadherin distribution between cell-cell contacts in the border cell cluster (Sawant *et al.* 2018). Constitutively active or dominant negative mutants of Rap1 showed disorganized accumulation of E-cadherin between border cells and border cell-nurse cell contacts. Disorganization of these cell-cell contacts leads to severe migration defects and cluster shape changes confirming the role of Rap1 in this process. Further, Rap1 is spatially regulated in the border cell cluster by its inhibiting GAP, Rapgap1 during migration. Together, we showed that regulated Rap1 activity through Rapgap1 is required for collective border cell migration. Our study also showed that Rap1 activity is required for generation of protrusions in border cells. Chang and others (2018) in an independent study showed that Rap1 interacts with the Hippo/Warts pathway to regulate polarization of actomyosin protrusion in border cells (Chang *et al.* 2018). Rap1 binds to and inhibits Hippo, thereby relieving Enabled (Ena) from Hippo suppression and regulating actin assembly. While the Rap1-Hippo pathway actively contributes to actin polarization and protrusion generation in border cells, additional experiments will be needed to identify additional molecular targets of Rap1 in border

cells. Whether PP1 and Rap1 have a direct or indirect role in maintaining cell-cell adhesion in border cells and other cell collectives is still unknown. Further work to determine a direct role of these conserved adhesion proteins using fly and human tumor model systems will therefore answer many open questions in the field (Fig. 6.1 A).

6.2 Future directions

How do we identify a direct role of cell adhesion genes and PP1 in collective tumor cell invasion?

In cancers, the characteristic invasion and spreading of tumor cells from the primary site to a local or secondary site is one of the leading causes of mortality (Wang *et al.* 2016). Collectively invading tumor cells are one of the multiple modes of tumor spreading that depend on cell-cell contacts through dynamic cell adhesion proteins (Friedl and Wolf 2003; Friedl *et al.* 2012). From the glioblastoma-informed targeted RNAi screen, we identified eight adhesion and adhesion regulatory genes that disrupted collective border cell migration and were also enriched in invasive edge of human glioblastoma patient tumors. Future experiments using *in vivo* fly larval tumor models and human glioblastoma models will further help explain the direct roles of these adhesion-related genes in tumor invasion (Fig. 6.1 A and B).

Fly models of tumor invasion and metastasis have provided scientists with essential tools to study classical molecular pathways that contribute to tumor growth and spreading *in vivo*. One such model is the powerful RasV12 tumor model in the *Drosophila* larval eye neural epithelium. This model shows invasion of tumor cells from the eye disc to the ventral nerve cord (VNC) (Miles *et al*. 2012; Fig. 6.1B). This system uses the MARCM technique to overexpress UAS-transgenes in the eye disc under eye-specific flippase and produce mosaic clones marked with GFP or RFP. Altering oncogenes like *scrib* and *lgl* in this model along with overexpressed RasV12 makes the tumor cells highly invasive and metastatic, which can be monitored *in vivo* using fixed and live imaging approaches (Miles *et al*. 2012; Pagliarini and Xu 2003). Using the GFP+ *RasV12; scrib-/-* (or *RasV12; lgl-/-*) model, we will co-express UAS- RNAi targeting cell adhesion hits from the GBM screen. We will then assess if metastatic potential of these brain tumor cells is enhanced or

suppressed by disrupting cell adhesion genes (Fig 6.1B). We anticipate that due to collective cell invasion of these tumor cells, reducing essential cell adhesion junctions will suppress the invasion and metastasis of tumor cells to the ventral nerve cord from the eye disc. We will investigate tumor size and measure the grade of invasion to the nerve cord (Fig 6.1B), which help us confirm if these adhesion genes contribute to collective tumor cell invasion. Additionally, expression of UAS-NiPP1 in the border cell cluster causes the cells to split apart by decreasing cadherin-catenin adhesion (Chapter 3). Therefore, we will also test NiPP1 in this model to examine if adhesion of collectively invading tumor cells can be reduced. We have prepared transgenic flies for UAS-NiPP1, α-catenin RNAi and Symplekin RNAi and are in the process of obtaining RNAi lines for other genes ready for testing in this model.

While the RasV12 tumor model is an excellent system to study tumor invasion and metastasis, the experimental challenges associated with generating genetic mosaics in this model are complicated. Therefore, we decided to also use a relatively simple wing disc model in parallel with the RasV12 model to identify adhesion dependent regulators of collective tumor cell invasion. We will use a similar approach with another larval tumor model in the wing disc (Fig 6.1C). Activating Src in the A-P (anterior-posterior) boundary by specific GAL4 (ptc-GAL4) leads to detachment of cells from the boundary and further invasion to the posterior side of the wing disc (Fig 6.1C). Coexpressing UAS-trangenes will help us determine if the gene of interest suppresses or enhances invasion by tracking fluorescently labelled invading cells from the A-P boundary. Measuring the volume of A-P boundary in both Src activated and Src activated cells coexpressing UAS-RNAi will help determine the extent of invasion. Testing the tumor invasion potential first in the larval tumor models will help validate the phenotypes and confirm their more direct role in collective tumor cell invasion.

Next, once we identify and confirm candidate adhesion genes from the larval tumor model, our collaborator, Dr. Lathia will use the glioblastoma tumor models to analyze GBM collective cell invasion (Fig. 6.1D). In GBM, self-renewing population of cancer stem cells (CSC) were shown to collectively invade *in vitro* (Volovetz *et al.* 2020). We will use the 3D- ECM invasion model and exit sphere assays to test if siRNA knockdown of human orthologs of adhesion genes and NiPP1 disrupts collective GBM CSC invasion (Fig. 6.1D). Additionally, we will determine if protein levels of adhesion gene hits are upregulated using western blots of GBM CSC. Overall, combining the tumor models in both the human and fly systems will reveal mechanisms that govern collective tumor cell invasion and to develop therapeutic targets for highly invasive cancers.

How does identifying conserved mechanisms regulating collective cell invasion impact cancer outcome?

The common signaling pathways between collective cell invasion leading to metastasis in cancers and collective migration during development have been studied across multiple systems using both *in vivo* and *in vitro* models. Research in the last three decades focusing on multiple signaling networks has shown ample evidence about the molecular similarities between *in vivo* developmental models and the cancer systems including the border cell model used in this study (Scarpa and Mayor 2016; Stuelten *et al.* 2018). The striking similarities between the invasive edge of tumors and the border cell model, for example the requirement of cell adhesion-based mechanisms to keep the cells intact, was used in this dissertation to reveal mechanisms that favor collective cancer cell invasion. This dual system approach successfully identified human orthologs of adhesion proteins that were upregulated in invasive regions of human GBM tumors. A previous study in the lab used a similar approach to identify a gene required in collective invasion of GBM

cells (Volovetz *et al.* 2020). These studies together support dissecting conserved key mechanisms required in cancers through model organisms, which can reveal potential therapeutic targets. Experiments involving advanced high resolution live-imaging techniques can help elucidate cluster dynamics and allow scientists to understand the fundamental processes that govern collective cell migration. Essential gene networks identified in such studies may not necessarily be limited to developing anti-tumor invasion therapies in highly invasive cancers but can also be extended to correlate gene signatures from clinical samples during early diagnosis across different invasive cancer types. The molecular signatures derived from such diagnostic samples may reveal patient outcomes and prognosis depending on the expression in the invasive edges and the metastatic potential of the tumors. This could further help determine treatment strategies and provide a framework for personalized medicine in malignant cancers especially those known to cause high recurrence.

While these future prospects in application of targeted therapies is hopeful, there are some limitations to this approach. Model organisms like *Drosophila* offer elegant and simple genetically accessible systems that have been used for decades for exploring fundamental developmental pathways which can translate to mammalian cells. However, invertebrates such as flies often only have single orthologs for essential genes whereas mammals often have multiple orthologs. Additionally, the tumor microenvironment is complex and extremely difficult to mimic in these model organisms. Therefore, combined efforts of researchers and oncologists in using *in vivo* developmental and tumor models along with *in vitro* mammalian systems are required to determine the overall function of a gene target. 3D tumor cell invasion studied by observing *in vitro* movement of invasive tumor cells on a layer of ECM or 3D exit sphere assays that lead to horizontal invasion of tumor cells from a tumor spheroid on an ECM are excellent examples of *in*

vitro mammalian cell systems to assess tumor invasion potential of both tumor cells and the tumor microenvironment (Fig. 6.1D). Further, 3D organ explants of primary tumor tissues, in which scientists transfer live tumor tissue on an ECM layer, are a powerful method to analyze the migration of tumor cells on matrix (Friedl and Gilmour 2009). These models are somewhat comparable to *in vivo* models since the effects of tumor stroma and cell invasion can be studied using live imaging. On the other hand, 2D scratch wound assays help in understanding mechanisms related to sheet migration of epithelial cells on 2D surfaces after initiating a wound in the center of the cell monolayer. 2D models generally do not include an ECM and are therefore not as suitable to assess the effects of *in vivo* tumor cell invasion. Nevertheless, the approach used in this dissertation provides a starting point to develop future experimental strategies in the hopes of providing insights and treatment strategies for invasive cancer clusters promoting metastasis.

What are the mechanisms employed by Rap1 to regulate cell adhesion in collectively migrating border cells? Does Rap1 interact with Canoe/Afadin to organize E-cadherin distribution?

In my dissertation, we showed that Rap1 was required to organize E-cadherin distribution between border cell contacts during collective border cell migration (Chapter 4). The exact mechanism of action of Rap1 in regulating E-cadherin distribution is still unknown. Evidence shows that Canoe, an F-actin binding protein and fly ortholog of Afadin6 is required during dorsal closure of *Drosophila* embryo by acting as an effector of Rap1 (Boettner *et al.* 2003; Boettner and Van Aelst 2009; Bonello *et al.* 2018). Future experiments will thus focus on identifying whether Canoe acts as a Rap1 effector during border cell migration to localize to cell adhesion proteins and organize E-cadherin distribution. Canoe is a highly conserved multidomain protein and its domains include

two Ras Association (RA) domains and one PDZ domain (Boettner and Aelst, 2009). Cno binds to Rap1 through the RA1 domain (Linnemann *et al.* 1999; Boettner *et al.* 2003) and to E-cadherin through the PDZ domain (Sawyer *et al.* 2009). Expression of dominant negative mutant, $Rap1N^{17}$ or constitutively active Rap1 mutant, $Rap1V^{12}$ in the border cell cluster changes E-cadherin distribution in the border cell cluster (Sawant *et al.* 2018). Therefore, we will first coexpress UAS-cno (Canoe) with UAS-$Rap1N^{17}$ or UAS-$Rap1V^{12}$ under c306-GAL4 and analyze if we can rescue the E-cadherin distribution defects and thereby the migration defects. From Chapter 4, we know that UAS-GFP-Rap1 (active Rap1) is enriched at the cell cortex of border cells and polar cells. To analyze if Rap1 is mislocalized in Cno mutants, we can express UAS-GFP-Rap1 in Cno mutants egg chambers. Cno mutants such as $cno^{\Delta N}$ with deleted RA domains or $Cno^{RA1*+RA2*}$ with point mutations in RA domains that hinders binding can be used in these experiments (Boettner *et al.* 2003). With deficient binding sites for Rap1 in Cno mutants, will GFP:Rap1 accumulate or mislocalize in the cno mutant border cell cluster? These experiments can be a starting point to test if Rap1 functions through junctional proteins to regulate E-cadherin distribution in border cell cluster and eventually in different collective cell migration modes.

Rap1 mutants also caused protrusion defects in the border cell cluster (Chapter 4), but the nature of this phenotype is less well understood. Loss of Rap1 also caused uniform Rac expression in the cluster causing severe leader cell protrusion defects, suggesting that Rap1 polarizes Rac for actin-rich protrusions at the front of the cluster (Chang *et al.* 2018). E-cadherin functions in a positive feedback loop with the RTK-Rac pathway to develop an actin-rich protrusion in the lead cell (Cai *et al.* 2014). Does Rap1 additionally regulate protrusion formation by working directly or indirectly with the RTK-Rac-E-cadherin pathway? Elmo, an upstream regulator of Rac functions in a complex with RacGEF Myoblast city (Mbc) and is required in border cell migration

(Geisbrecht *et al.* 2008; Bianco *et al.* 2007). To determine if Rap1 works upstream of Rac by regulating the Elmo/Mbc complex during border cell migration, we can first use Rap1 pulldown to test if Elmo and Mbc bind to active Rap1. Next, if Rap1 binds to Elmo and Mbc, we can overexpress Elmo in $Rap1^{N17}$ (DN-Rap1) mutants and use Rac FRET analysis to determine if Rac is polarized in the border cell cluster and test if the protrusion defects are rescued. Additional experiments coexpressing CA-Rap1 in *elmo* knockout alleles will also be required to test if Rap1 functions upstream of Rac. Subcellularly, Elmo is ubiquitously expressed like Rap1 in follicle cells and border cells (Geisbrecht *et al.* 2008). Determining the subcellular localization of Elmo in Rap1 mutants will be crucial to provide evidence for an additional Rap-1 dependent role of Elmo in protrusion formation and stabilization.

In conclusion, collective cell migration is a highly dynamic process that is essential during development and cancer invasion. Using the *in vivo Drosophila* ovary border cell model will help reveal molecular and cellular mechanisms that govern conserved collective cell migration and invasion. In my thesis, I determined the roles of adhesion-based mechanisms that regulate collective border cell migration and collective cancer cell invasion by maintaining cluster cohesion and cluster shape. Future experiments will provide insight into conserved mechanisms that drive collective cancer cell invasion and provide potential therapeutic targets for invasive cancers like GBM.

6.3 Figures

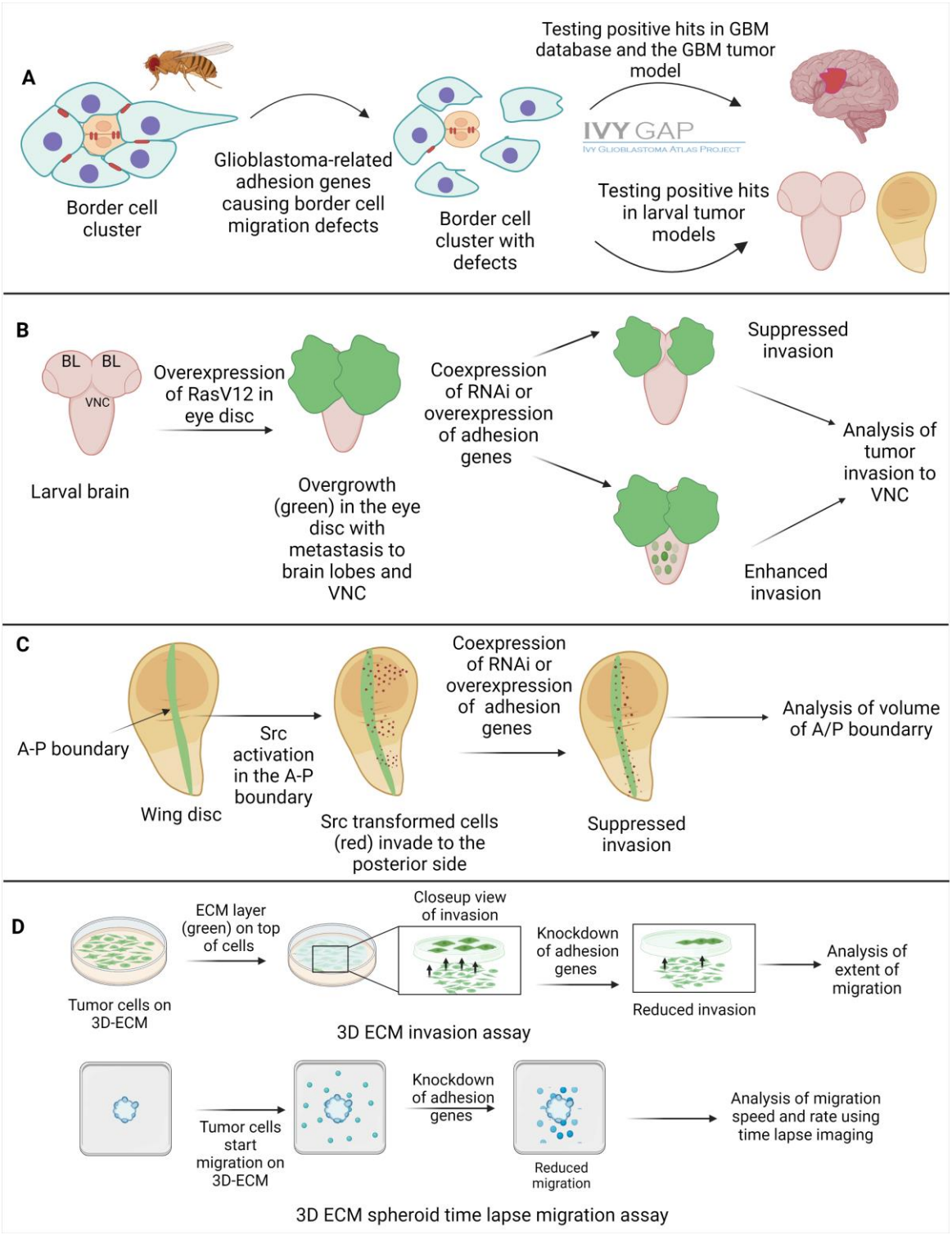
A
Border cell cluster
Glioblastoma-related adhesion genes causing border cell migration defects
Border cell cluster with defects
Testing positive hits in GBM database and the GBM tumor model
IVY GAP
Testing positive hits in larval tumor models
B
BL
BL
VNC
Larval brain
Overexpression of RasV12 in eye disc
Overgrowth (green) in the eye disc with metastasis to brain lobes and VNC
Coexpression of RNAi or overexpression of adhesion genes
Suppressed invasion
Analysis of tumor invasion to VNC
Enhanced invasion
C
A-P boundary
Wing disc
Src activation in the A-P boundary
Src transformed cells (red) invade to the posterior side
Coexpression of RNAi or overexpression of adhesion genes
Suppressed invasion
Analysis of volume of A/P boundarry
D
Tumor cells on 3D-ECM
ECM layer (green) on top of cells
Closeup view of invasion
Knockdown of adhesion genes
Reduced invasion
Analysis of extent of migration
3D ECM invasion assay
Tumor cells start migration on 3D-ECM
Knockdown of adhesion genes
Reduced migration
Analysis of migration speed and rate using time lapse imaging
3D ECM spheroid time lapse migration assay

Figure 6.1 Schematic showing experimental approach and future experiments with tumor mode.

A). Overview of the human brain-tumor related adhesion screen in border cell that identified adhesion genes required for border cell migration. Potential role in collective cell invasion was determined using the IVY GAP database to look at regional gene expression data of adhesion genes in patient tumors. B and C). Two larval tumor models, the RasV12 eye-neural epithelium model and the wing disc model to study invasion and metastasis. These models will be used to determine a more direct role of the adhesion genes in collective tumor cell epithelium. D) GBM assays to test if disrupting cell junctions alters collective invasion of GBM cells. In the 3D ECM invasion assay (top panel), a matrix layer (green) is placed on top of the adherent cells on the plate and movement of live labeled cells through the matrix layer is measured. An inset showing a closeup view of cells invading through the matrix layer above. In the tumor sphere exit assay (bottom panel), tumor spheres are transferred to a plate and cells migrating away from the sphere are analyzed using time lapse imaging. Created with Biorender.com.

6.4 References

Bianco, A., M. Poukkula, A. Cliffe, J. Mathieu, C. M. Luque *et al.*, 2007 Two distinct modes of guidance signalling during collective migration of border cells. Nature 448: 362–365.

Boettner, B., P. Harjes, S. Ishimaru, M. Heke, H. Q. Fan *et al.*, 2003 The AF-6 Homolog Canoe Acts as a Rap1 Effector During Dorsal Closure of the *Drosophila* Embryo. Genetics 165: 159–169.

Boettner, B., and L. Van Aelst, 2009 Control of cell adhesion dynamics by Rap1 signaling. Curr Opin Cell Biol 21: 684–693.

Bonello, T. T., K. Z. Perez-Vale, K. D. Sumigray, and M. Peifer, 2018 Rap1 acts via multiple mechanisms to position Canoe and adherens junctions and mediate apical-basal polarity establishment. Development 145: dev157941.

Cai, D., S.-C. Chen, M. Prasad, L. He, X. Wang *et al.*, 2014 Mechanical feedback through E-cadherin promotes direction sensing during collective cell migration. Cell 157: 1146–1159.

Ceulemans, H., and M. Bollen, 2004 Functional diversity of protein phosphatase-1, a cellular economizer and reset button. Physiol Rev 84: 1–39.

Chang, Y.-C., J.-W. Wu, Y.-C. Hsieh, T.-H. Huang, Z.-M. Liao *et al.*, 2018 Rap1 Negatively Regulates the Hippo Pathway to Polarize Directional Protrusions in Collective Cell Migration. Cell Rep 22: 2160–2175.

Chen, Y., N. Kotian, G. Aranjuez, L. Chen, C. L. Messer *et al.*, 2020. Protein phosphatase 1 activity controls a balance between collective and single cell modes of migration (T. Piotrowski & U. Banerjee, Eds.). eLife 9: e52979.

Friedl, P., and K. Wolf, 2003 Tumour-cell invasion and migration: diversity and escape mechanisms. Nat Rev Cancer 3: 362–374.

Friedl, P., and D. Gilmour, 2009 Collective cell migration in morphogenesis, regeneration and cancer. Nat Rev Mol Cell Biol 10: 445–457.

Friedl, P., J. Locker, E. Sahai, and J. E. Segall, 2012 Classifying collective cancer cell invasion. Nat Cell Biol 14: 777–783.

Geisbrecht, E. R., S. Haralalka, S. K. Swanson, L. Florens, M. P. Washburn *et al.*, 2008 Drosophila ELMO/CED-12 interacts with Myoblast city to direct myoblast fusion and ommatidial organization. Dev Biol 314: 137–149.

Linnemann, T., M. Geyer, B. K. Jaitner, C. Block, H. R. Kalbitzer *et al.*, 1999 Thermodynamic and Kinetic Characterization of the Interaction between the Ras Binding Domain of AF6 and Members of the Ras Subfamily *. Journal of Biological Chemistry 274: 13556–13562.

Martin-Granados, C., A. R. Prescott, N. V. Dessel, A. V. Eynde, M. Arocena *et al.*, 2012 A Role for PP1/NIPP1 in Steering Migration of Human Cancer Cells. PLOS ONE 7: e40769.

Miles, W. O., N. J. Dyson, and J. A. Walker, 2011 Modeling tumor invasion and metastasis in *Drosophila*. Dis Model Mech 4: 753–761.

Pagliarini, R. A., and T. Xu, 2003 A genetic screen in *Drosophila* for metastatic behavior. Science 302: 1227–1231.

Sawant, K., Y. Chen, N. Kotian, K. M. Preuss, and J. A. McDonald, 2018 Rap1 GTPase promotes coordinated collective cell migration *in vivo*. MBoC 29: 2656–2673.

Sawyer, J. K., N. J. Harris, K. C. Slep, U. Gaul, and M. Peifer, 2009 The Drosophila afadin homologue Canoe regulates linkage of the actin cytoskeleton to adherens junctions during apical constriction. Journal of Cell Biology 186: 57–73.

Scarpa, E., and R. Mayor, 2016 Collective cell migration in development. J Cell Biol 212: 143–155.

Stuelten, C. H., C. A. Parent, and D. J. Montell, 2018 Cell motility in cancer invasion and metastasis: insights from simple model organisms. Nat Rev Cancer 18: 296–312.

Volovetz, J., A. D. Berezovsky, T. Alban, Y. Chen, A. Lauko *et al.*, 2020 Identifying conserved molecular targets required for cell migration of glioblastoma cancer stem cells. Cell Death Dis 11: 152.

Wang, X., A. Enomoto, N. Asai, T. Kato, and M. Takahashi, 2016 Collective invasion of cancer: Perspectives from pathology and development. Pathol Int 66: 183–192.

Appendix A- Chapter 2 Supplemental Materials

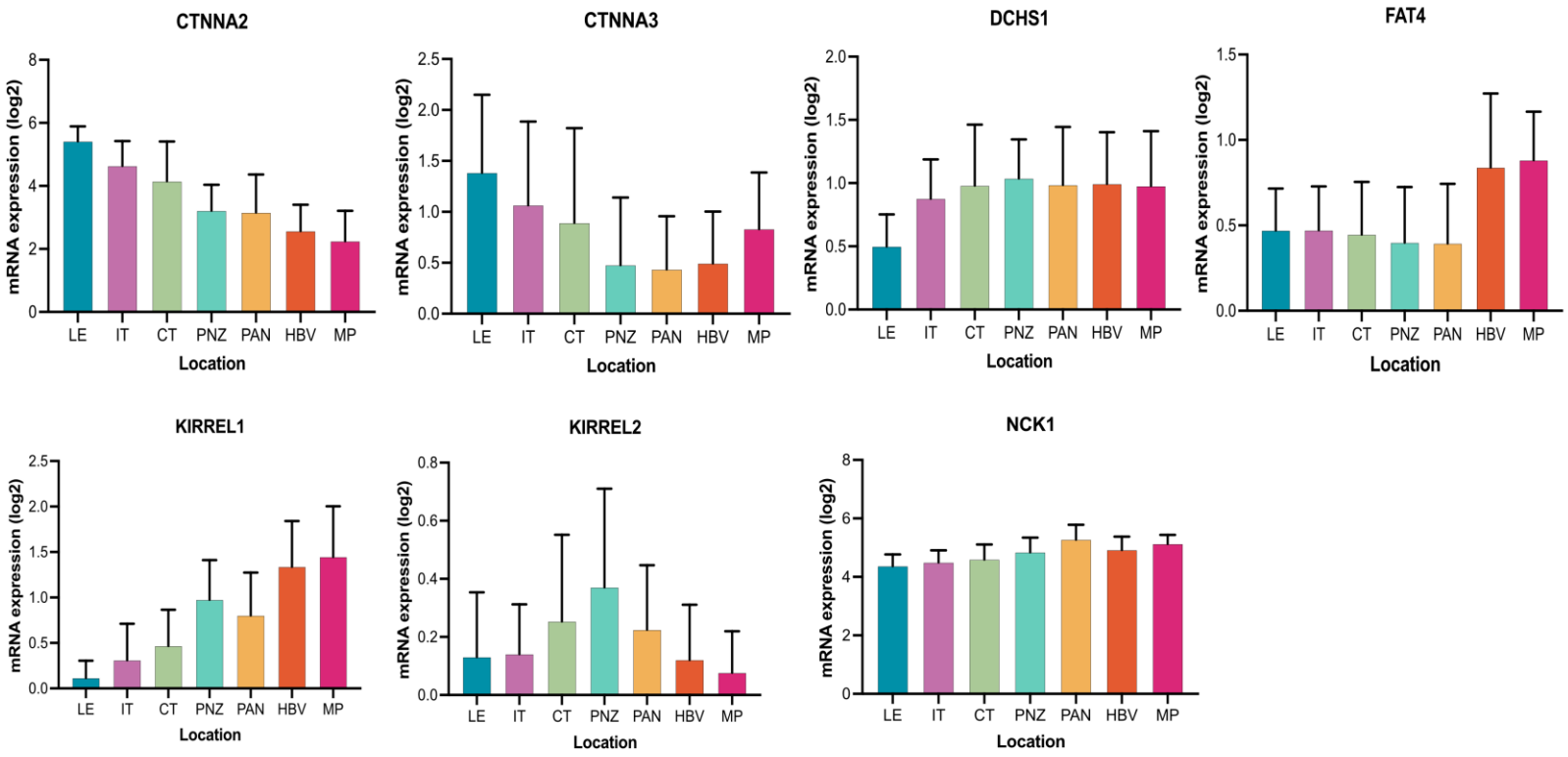

Supplementary figure 2.1. Regional expression of human ortholog adhesion genes in GBM patient tumors for additional human genes. See Figure 2.4 legend for abbreviations of the tumor regions. Data from the Ivy GAP are shown as mean expression +/- SD across GBM tumor regions. Statistics are shown in Supplementary Table 2.2: *p<0.05; **p<0.01; ***p<0.001, one way ANOVA with Tukey HSD.

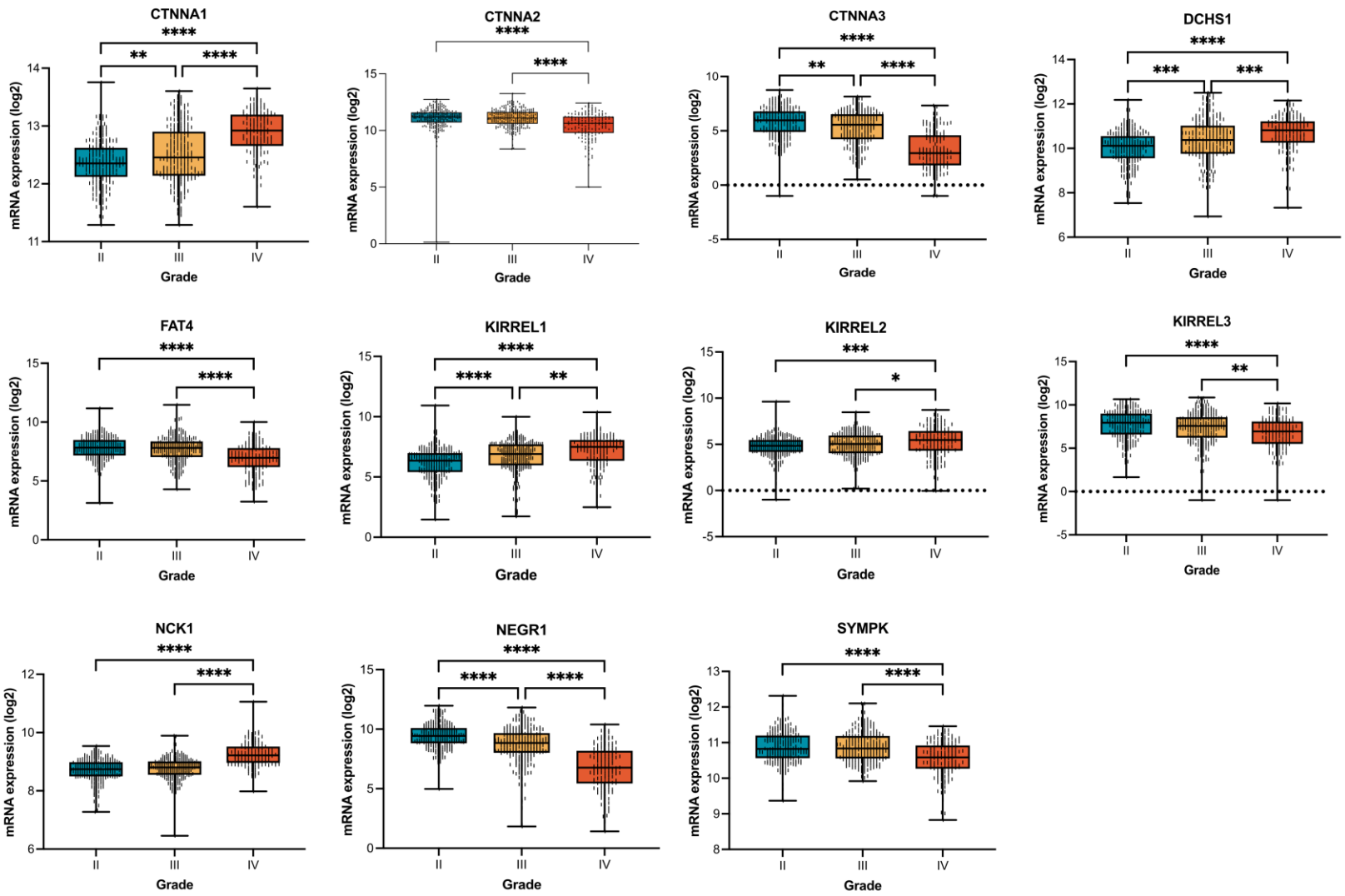
CTNNA1
CTNNA2
CTNNA3
DCHS1
FAT4
KIRREL1
KIRREL2
KIRREL3
NCK1
NEGR1
SYMPK
mRNA expression (log2)
Grade
II
III
IV

Supplementary Figure 2.2. Expression of human ortholog adhesion genes across glioma tumor grade. Box plots of mRNA expression obtained from the TCGA database in grade II (n=226), grade III (n=244), and grade IV (n=150) patient gliomas. *p<0.05; **p<0.01; ***p<0.001, one way ANOVA with Tukey HSD.

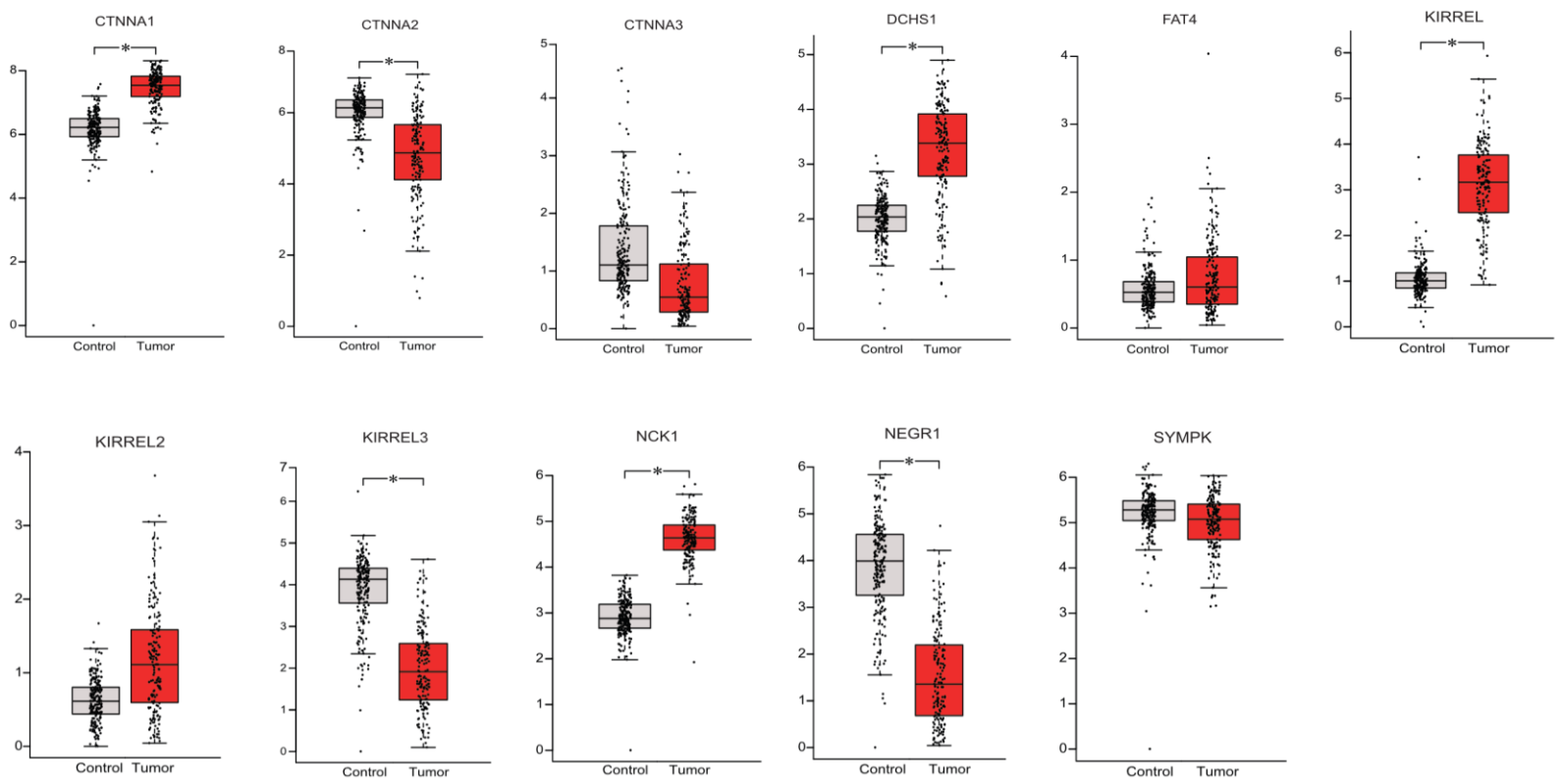

Supplementary figure 2.3. Expression of human ortholog adhesion genes in GBM compared to non-tumor brain tissue. Box plots of mRNA expression obtained from the GEPIA database in non-tumor (n=207) and GBM tumor (n=163). *p<0.01.

Supplementary Table 2.1 List of *Drosophila* RNAi lines with various phenotypes in other studies.

Gene	RNAi	Stock center	Construct ID	Other systems
alpha-catenin (α-cat)	20123	VDRC	GD8808	Pupal lethal under pnr-GAL4 and lethal under tubulin driver[1,2]
	40882	VDRC	GD8808	Pupal lethal under pnr-GAL4[1]; rotation defects in male genitalia[4]; epithelial defects in the ovaries when driven by *traffic jam*-Gal4[7]
	107298	VDRC	KK107916	Epithelial defects in the ovaries when driven by *escargot (esg)*-GAL4 and *traffic jam*-Gal4[3,7]; rotation defects in male genitalia[4]
Dachsous (ds)	36219	VDRC	GD14350	Genome-wide bristle screen[1]; larval hindgut in LR asymmetry[5]; size defect, wing imaginal disc and adult wing[6,8,9,13]; cardiac cells[10]; wing shape and local hair polarity[11]; lethal under esg-GAL4[17]
	4313	VDRC	GD2646	Adult wing and wing disc abnormality[12,13,14]; larval hindgut in LR asymmetry[5]; reduced escort cell extension[66]

Gene	RNAi	Stock center	Construct ID	Other systems
	32964	BL	HMS00759	Larval ventral nerve cord[15]; anterior wing margin bristle apical rotation[16], abdomen PCP[18]; lethal under Act5C-GAL4[17]; larval/pupal lethal and flight muscle defect under c587 and nos-GAL4s[20,67]
Dreadlocks (dock)	37524	VDRC	GD4034	Agglutination of larval nephrocytes[19]
	27728	BL	JF02810	Embryonic CNS (anterior corner cell) and adult CNS[21]; lethal under Act5C-GAL4, nos-GAL4 and c587-GAL4[17,20]
Fat	108863	VDRC	KK101190	Larval hindgut in LR asymmetry[5]; abnormal adult wing and wing disc[23,24]; reduced escort cell extension[66]
	9396	VDRC	GD881	Genome-wide bristle screen[1]; larval hindgut in LR asymmetry[5]; wing disc and adult wing[6,11,12,25,26,27,28]; enterocytes[29]; larval brain and eye disc[31]
	40890	BL	HMS02138	ECM defects in 3rd instar larvae[30]

Gene	RNAi	Stock center	Construct ID	Other systems
G protein alpha i subunit	28150	VDRC	GD12576	Genome-wide bristle screen[1]; fly antennae for olfaction[33]
G protein alpha o subunit	34653	BL	HMS01129	Larval and adult brain[35,36]; lethal under Act5C-GAL4 and MTD-GAL4[17,37]
	110552	VDRC	KK109018	Octopaminergic neurons[32]
	19124	VDRC	GD8640	Genome-wide bristle screen[1]; embryonic lethal under elav-GAL4[38]; Anterior Paired Lateral (APL) neurons and adult brain[40,32]; gustatory receptors[34]; wing and notum[41,42]; male courtship[43]
Gliotactin	37115	VDRC	GD1735	Genome-wide bristle screen[1]
	37116	VDRC	GD1735	Genome-wide bristle screen[1]
	35524	VDRC	GD12649	pupal lethal under pnr-GAL4[1]

Gene	RNAi	Stock center	Construct ID	Other systems
Lachesin (Lac)	107450	VDRC	KK107469	Epithelial defects during oogenesis[3,39]; enhanced astrocyte seizure activity[44];
	28940	BL	HM05151	lethal under Act5C-GAL4[17]
Liprin-alpha	106588	VDRC	KK10116	Fly eye tumor model (overexpression of a Notch ligand leads to benign overgrowths in the eyes)[45]; adult mechanosensory neurons[46]; neuronal defects[47]
Mesh	6867	VDRC	GD3140	Pupal lethal under pnrGAL4[1]
Parvin	105356	VDRC	KK102567	Larval wing disc[49]; larval lethal under MEf2-GAL4[51]
Roughest (rst)	27223	VDRC	GD14475	Genome-wide bristle screen[1], wing margin hair[49]
	27225	VDRC	GD14475	Larval optic lobe[50]

Gene	RNAi	Stock center	Construct ID	Other systems
	951	VDRC	GD86	Genome-wide bristle screen[1], male genital disc and myoblasts around adult male genitalia[52]
Schizo	36625	VDRC	GD14895	Patterning of the eye[53]
	36627	VDRC	GD14895	Patterning of the eye[53;] flight defective[54]; suppression of larval eye disc tumors[65]
	106168	VDRC	KK103616	Neurons under elav-GAL4[55]; suppression of larval eye disc tumors[65]
	39060	BL	HMS01980	Neurons under elav-GAL4[55]; suppression of larval eye disc tumors[65]; pupal lethal under c587-GAL4[20]
Shroom	47147	VDRC	GD16363	Retinal degeneration[58]
	100672	VDRC	KK106863	Wing imaginal disc[56]
	33469	VDRC	GD9722	Pupal lethal under pnrGAL4[1]

Gene	RNAi	Stock center	Construct ID	Other systems
Symplekin (Sym)	33470	VDRC	GD9722	Pupal lethal under pnrGAL4[1]; partial lethal under elav-GAL4 and lethal under Mef2-GAL4[38,54]
	39041	BL	HMS01961	Mitotic spermatogonia[57]
Vulcan	46230	VDRC	GD16319	Increased astrocyte seizure activity[44]
Wnt4	38011	VDRC	GD5347	Pain response defects[38]
	38010	VDRC	GD5347	Larval cardiac cells[10]
	104671	VDRC	KK102348	Larval cardiac cells[10]; ostia progenitor cells[59]; egg chamber defects during oogenesis under traffic jam-GAL4[3]
	29442	BL	JF03378	Wing disc and adult wing[60]; germline stem cell defects in ovaries under c587-GAL4[61]

Gene	RNAi	Stock center	Construct ID	Other systems
Wunen	6446	VDRC	GD1640	Caudal visceral mesoderm cell migration (weak phenotype)[62]; bacterial infection induced *drosomycin* expression[63]; suppression of dystrophic muscle phenotype[64]

Supplementary file 2.1. List of references for Table 2.1.

1. Benjamin, J. M., A. V. Kwiatkowski, C. Yang, F. Korobova, S. Pokutta *et al*., 2010 AlphaE-catenin regulates actin dynamics independently of cadherin-mediated cell-cell adhesion. J Cell Biol 189: 339–352.
2. Bunker, E. N., G. E. Wheeler, D. A. Chapnick, and X. Liu, 2021 Suppression of α-catenin and adherens junctions enhances epithelial cell proliferation and motility via TACE-mediated TGF-α autocrine/paracrine signaling. Mol Biol Cell 32: 348–361.
3. Matsuzawa, K., T. Himoto, Y. Mochizuki, and J. Ikenouchi, 2018 α-Catenin Controls the Anisotropy of Force Distribution at Cell-Cell Junctions during Collective Cell Migration. Cell Rep 23: 3447–3456.
4. Seddiki, R., G. H. N. S. Narayana, P.-O. Strale, H. E. Balcioglu, G. Peyret *et al*., 2018 Force-dependent binding of vinculin to α-catenin regulates cell-cell contact stability and collective cell behavior. Mol Biol Cell 29: 380–388.
5. Vassilev, V., A. Platek, S. Hiver, H. Enomoto, and M. Takeichi, 2017 Catenins Steer Cell Migration via Stabilization of Front-Rear Polarity. Developmental Cell 43: 463-479.e5.
6. Carvalho, J. R., I. C. Fortunato, C. G. Fonseca, A. Pezzarossa, P. Barbacena *et al*., 2019 Non-canonical Wnt signaling regulates junctional mechanocoupling during angiogenic collective cell migration. Elife 8: e45853.
7. Wood, M. N., N. Ishiyama, I. Singaram, C. M. Chung, A. S. Flozak *et al*., 2017 α-Catenin homodimers are recruited to phosphoinositide-activated membranes to promote adhesion. J Cell Biol 216: 3767–3783.

8. Schmid, M.-T., F. Weinandy, M. Wilsch-Bräuninger, W. B. Huttner, S. Cappello *et al*., 2014 The role of α-E-catenin in cerebral cortex development: radial glia specific effect on neuronal migration. Frontiers in Cellular Neuroscience 8: 215.
9. Cui, Y., and S. Yamada, 2013 N-Cadherin Dependent Collective Cell Invasion of Prostate Cancer Cells Is Regulated by the N-Terminus of α-Catenin. PLOS ONE 8: e55069.
10. Weber, G. F., M. A. Bjerke, and D. W. DeSimone, 2012 A Mechanoresponsive Cadherin-Keratin Complex Directs Polarized Protrusive Behavior and Collective Cell Migration. Developmental Cell 22: 104–115.
11. Jurado, J., J. de Navascués, and N. Gorfinkiel, 2016 α-Catenin stabilises Cadherin–Catenin complexes and modulates actomyosin dynamics to allow pulsatile apical contraction. Journal of Cell Science 129: 4496–4508.
12. Wang, Y.-C., Z. Khan, and E. F. Wieschaus, 2013 Distinct Rap1 Activity States Control the Extent of Epithelial Invagination via α-Catenin. Developmental Cell 25: 299–309.
13. Ji, H., J. Wang, B. Fang, X. Fang, and Z. Lu, 2011 α-Catenin inhibits glioma cell migration, invasion, and proliferation by suppression of β-catenin transactivation. J Neurooncol 103: 445–451.
14. Shinoura, N., N. E. Paradies, R. E. Warnick, H. Chen, J. J. Larson *et al*., 1995 Expression of N-cadherin and alpha-catenin in astrocytomas and glioblastomas. Br J Cancer 72: 627–633.
15. Dondi, C., B. Bertin, J.-P. Da Ponte, I. Wojtowicz, K. Jagla *et al*., 2021 A polarized nucleus-cytoskeleton-ECM connection in migrating cardioblasts controls heart tube formation in *Drosophila*. Development 148: dev192146.
16. Jammrath, J., I. Reim, and H. Saumweber, 2020 Cbl-Associated Protein CAP contributes to correct formation and robust function of the *Drosophila* heart tube. PLoS One 15: e0233719.

17. Ichikawa, T., M. Kita, T. S. Matsui, A. I. Nagasato, T. Araki *et al*., 2017 Vinexin family (SORBS) proteins play different roles in stiffness-sensing and contractile force generation. J Cell Sci 130: 3517–3531.
18. Arata, M., K. Sugimura, and T. Uemura, 2017 Difference in Dachsous Levels between Migrating Cells Coordinates the Direction of Collective Cell Migration. Dev Cell 42: 479-497.e10.
19. Dearborn, R., and S. Kunes, 2004 An axon scaffold induced by retinal axons directs glia to destinations in the *Drosophila* optic lobe. Development 131: 2291–2303.
20. Zakaria, S., Y. Mao, A. Kuta, C. F. de Sousa, G. O. Gaufo *et al*., 2014 Regulation of neuronal migration by Dchs1-Fat4 planar cell polarity. Curr Biol 24: 1620–1627.
21. Mangione, F., and E. Martín-Blanco, 2018 The Dachsous/Fat/Four-Jointed Pathway Directs the Uniform Axial Orientation of Epithelial Cells in the *Drosophila* Abdomen. Cell Rep 25: 2836-2850.e4.
22. Fulford, A. D., and H. McNeill, 2020 Fat/Dachsous family cadherins in cell and tissue organisation. Curr Opin Cell Biol 62: 96–103.
23. Berg, C. A., 2005 The *Drosophila* shell game: patterning genes and morphological change. Trends Genet 21: 346–355.
24. Su, Y. C., C. Maurel-Zaffran, J. E. Treisman, and E. Y. Skolnik, 2000 The Ste20 kinase misshapen regulates both photoreceptor axon targeting and dorsal closure, acting downstream of distinct signals. Mol Cell Biol 20: 4736–4744.
25. Chaki, S. P., R. Barhoumi, and G. M. Rivera, 2019 Nck adapter proteins promote podosome biogenesis facilitating extracellular matrix degradation and cancer invasion. Cancer Med 8: 7385–7398.

26. Dubrac, A., G. Genet, R. Ola, F. Zhang, L. Pibouin-Fragner *et al*., 2016 Targeting NCK-Mediated Endothelial Cell Front-Rear Polarity Inhibits Neovascularization. Circulation 133: 409–421.

27. Ruusala, A., T. Pawson, C.-H. Heldin, and P. Aspenström, 2008 Nck adapters are involved in the formation of dorsal ruffles, cell migration, and Rho signaling downstream of the platelet-derived growth factor beta receptor. J Biol Chem 283: 30034–30044.

28. Klaus, J., S. Kanton, C. Kyrousi, A. C. Ayo-Martin, R. Di Giaimo *et al*., 2019 Altered neuronal migratory trajectories in human cerebral organoids derived from individuals with neuronal heterotopia. Nat Med 25: 561–568.

29. Deshpande, R. P., M. Panigrahi, C. S. Y B V K, and P. P. Babu, 2019 Expression and clinicopathological significance of Nck1 in human astrocytoma progression. Int J Neurosci 129: 171–178.

30. Boyle, M. J., R. L. French, K. A. Cosand, J. B. Dorman, D. P. Kiehart *et al*., 2010 Division of labor: subsets of dorsal-appendage-forming cells control the shape of the entire tube. Dev Biol 346: 68–79.

31. Ghosh, P., A. O. Beas, S. J. Bornheimer, M. Garcia-Marcos, E. P. Forry *et al*., 2010 A G{alpha}i-GIV molecular complex binds epidermal growth factor receptor and determines whether cells migrate or proliferate. Mol Biol Cell 21: 2338–2354.

32. Li, J., S. Zhu, D. Kozono, K. Ng, D. Futalan *et al*., 2014 Genome-wide shRNA screen revealed integrated mitogenic signaling between dopamine receptor D2 (DRD2) and epidermal growth factor receptor (EGFR) in glioblastoma. Oncotarget 5: 882–893.

33. Solis, G. P., O. Bilousov, A. Koval, A.-M. Lüchtenborg, C. Lin *et al*., 2017 Golgi-Resident Gαo Promotes Protrusive Membrane Dynamics. Cell 170: 939-955.e24.

34. Wang, X., J. Bo, T. Bridges, K. D. Dugan, T. Pan *et al*., 2006 Analysis of cell migration using whole-genome expression profiling of migratory cells in the *Drosophila* ovary. Dev Cell 10: 483–495.

35. Samarasekera, G. D. N. G., and V. J. Auld, 2018 C-terminal Src kinase (Csk) regulates the tricellular junction protein Gliotactin independent of Src. MBoC 29: 123–136.

36. Padash-Barmchi, M., K. Browne, K. Sturgeon, B. Jusiak, and V. J. Auld, 2010 Control of Gliotactin localization and levels by tyrosine phosphorylation and endocytosis is necessary for survival of polarized epithelia. J Cell Sci 123: 4052–4062.

37. Chandran, R. R., E. Iordanou, C. Ajja, M. Wille, and L. Jiang, 2014 Gene expression profiling of *Drosophila* tracheal fusion cells. Gene Expr Patterns 15: 112–123.

38. Llimargas, M., M. Strigini, M. Katidou, D. Karagogeos, and J. Casanova, 2004 Lachesin is a component of a septate junction-based mechanism that controls tube size and epithelial integrity in the *Drosophila* tracheal system. Development 131: 181–190.

39. Ariss, M. M., A. R. Terry, A. B. M. M. K. Islam, N. Hay, and M. V. Frolov, 2020 Amalgam regulates the receptor tyrosine kinase pathway through Sprouty in glial cell development in the *Drosophila* larval brain. J Cell Sci 133: jcs250837.

40. Bobyn, A., M. Zarrei, Y. Zhu, M. Hoffman, D. Brenner *et al*., 2020 Ancestry and frequency of genetic variants in the general population are confounders in the characterization of germline variants linked to cancer. BMC Med Genet 21: 92.

41. Even, İ., İ. Akiva, and N. B. İyison, 2019 An *in vivo* RNAi mini-screen in *Drosophila* cancer models reveals novel potential Wnt targets in liver cancer. Turk J Gastroenterol 30: 198–207.

42. Chiaretti, S., and I. de Curtis, 2016 Role of Liprins in the Regulation of Tumor Cell Motility and Invasion. Curr Cancer Drug Targets 16: 238–248.

43. Sakamoto, S., S. Narumiya, and T. Ishizaki, 2012 A new role of multi scaffold protein Liprin-α: Liprin-α suppresses Rho-mDia mediated stress fiber formation. Bioarchitecture 2: 43–49.

44. Chiaretti, S., and I. de Curtis, 2016 Role of Liprins in the Regulation of Tumor Cell Motility and Invasion. Curr Cancer Drug Targets 16: 238–248.

45. Jakobsen, K. R., E. Sørensen, K. K. Brøndum, T. F. Daugaard, R. Thomsen *et al*., 2013 Direct RNA sequencing mediated identification of mRNA localized in protrusions of human MDA-MB-231 metastatic breast cancer cells. J Mol Signal 8: 9.

46. Li, F., W. Zhang, M. Wang, and P. Jia, 2020 IL1RAP regulated by PRPRD promotes gliomas progression via inducing neuronal synapse development and neuron differentiation *in vitro*. Pathol Res Pract 216: 153141.

47. Zou, J., X. Zhu, D. Xiang, Y. Zhang, J. Li *et al*., 2021 LIX1-like protein promotes liver cancer progression via miR-21-3p-mediated inhibition of fructose-1,6-bisphosphatase. Acta Pharm Sin B 11: 1578–1591.

48. Xu, Y., C. Miao, C. Jin, C. Qiu, Y. Li *et al*., 2018 SUSD2 promotes cancer metastasis and confers cisplatin resistance in high grade serous ovarian cancer. Exp Cell Res 363: 160–170.

49. Sang, J., X. Li, L. Lv, C. Zhang, X. Zhang *et al*., 2021 Circ-TOP2A acts as a ceRNA for miR-346 and contributes to glioma progression via the modulation of sushi domain-containing 2. Mol Med Rep 23: 255.

50. Bravou, V., A. Antonacopoulou, S. Papanikolaou, S. Nikou, I. Lilis *et al*., 2015 Focal Adhesion Proteins α- and β-Parvin are Overexpressed in Human Colorectal Cancer and Correlate with Tumor Progression. Cancer Invest 33: 387–397.

51. Johnstone, C. N., P. S. Mongroo, A. S. Rich, M. Schupp, M. J. Bowser *et al*., 2008 Parvin-beta inhibits breast cancer tumorigenicity and promotes CDK9-mediated peroxisome proliferator-activated receptor gamma 1 phosphorylation. Mol Cell Biol 28: 687–704.

52. Tamir-Livne, Y., R. Mubariki, and E. Bengal, 2017 Adhesion molecule Kirrel3/Neph2 is required for the elongated shape of myocytes during skeletal muscle differentiation. Int J Dev Biol 61: 337–345.

53. Johnson, R. I., A. Sedgwick, C. D'Souza-Schorey, and R. L. Cagan, 2011 Role for a Cindr-Arf6 axis in patterning emerging epithelia. Mol Biol Cell 22: 4513–4526.

54. Hildebrand, J. D., A. D. Leventry, O. P. Aideyman, J. C. Majewski, J. A. Haddad *et al*., 2021 A modifier screen identifies regulators of cytoskeletal architecture as mediators of Shroom-dependent changes in tissue morphology. Biol Open 10: bio055640.

55. Siang, L. C., R. Fernandez-Gonzalez, and J. J. Feng, 2018 Modeling cell intercalation during *Drosophila* germband extension. Phys Biol 15: 066008.

56. Haigo, S. L., J. D. Hildebrand, R. M. Harland, and J. B. Wallingford, 2003 Shroom induces apical constriction and is required for hingepoint formation during neural tube closure. Curr Biol 13: 2125–2137.

57. Razzell, W., M. E. Bustillo, and J. A. Zallen, 2018 The force-sensitive protein Ajuba regulates cell adhesion during epithelial morphogenesis. J Cell Biol 217: 3715–3730.

58. Buchert, M., M. Papin, C. Bonnans, C. Darido, W. S. Raye *et al*., 2010 Symplekin promotes tumorigenicity by up-regulating claudin-2 expression. Proc Natl Acad Sci U S A 107: 2628–2633.

59. Bayer, C. A., S. R. Halsell, J. W. Fristrom, D. P. Kiehart, and L. von Kalm, 2003 Genetic interactions between the RhoA and Stubble-stubbloid loci suggest a role for a type II

transmembrane serine protease in intracellular signaling during *Drosophila* imaginal disc morphogenesis. Genetics 165: 1417–1432.

60. Miao, W., N. Li, B. Gu, G. Yi, Z. Su *et al*., 2020 LncRNA DLGAP1-AS2 modulates glioma development by up-regulating YAP1 expression. J Biochem 167: 411–418.
61. Liu, L., X. Li, Y. Shi, and H. Chen, 2021 Long noncoding RNA DLGAP1-AS1 promotes the progression of glioma by regulating the miR-1297/EZH2 axis. Aging (Albany NY) 13: 12129–12142.
62. Harris, K. E., and S. K. Beckendorf, 2007 Different Wnt signals act through the Frizzled and RYK receptors during *Drosophila* salivary gland migration. Development 134: 2017–2025.
63. Ewen-Campen, B., T. Comyn, E. Vogt, and N. Perrimon, 2020 No Evidence that Wnt Ligands Are Required for Planar Cell Polarity in *Drosophila*. Cell Rep 32: 108121.
64. Cohen, E. D., M.-C. Mariol, R. M. H. Wallace, J. Weyers, Y. G. Kamberov *et al*., 2002 DWnt4 regulates cell movement and focal adhesion kinase during *Drosophila* ovarian morphogenesis. Dev Cell 2: 437–448.
65. Moura, R. S., E. Carvalho-Correia, P. daMota, and J. Correia-Pinto, 2014 Canonical Wnt signaling activity in early stages of chick lung development. PLoS One 9: e112388.
66. Sun, J., F. Macabenta, Z. Akos, and A. Stathopoulos, 2020 Collective Migrations of *Drosophila* Embryonic Trunk and Caudal Mesoderm-Derived Muscle Precursor Cells. Genetics 215: 297–322.
67. Doren, M. V., and R. Lehmann, 1997 Cell migration: Don’t tread on me. Current Biology 7: R148–R150.

68. Haack, T., M. Schneider, B. Schwendele, and A. D. Renault, 2014 *Drosophila* heart cell movement to the midline occurs through both cell autonomous migration and dorsal closure. Dev Biol 396: 169–182.

Supplementary File 2.2. List of references for Supplementary Table 2.1.

1. Mummery-Widmer, J. L., M. Yamazaki, T. Stoeger, M. Novatchkova, S. Bhalerao *et al*., 2009 Genome-wide analysis of Notch signalling in *Drosophila* by transgenic RNAi. Nature 458: 987–992.
2. Syrzycka, M., G. Hallson, K. A. Fitzpatrick, I. Kim, S. Cotsworth *et al*., 2019 Genetic and Molecular Analysis of Essential Genes in Centromeric Heterochromatin of the Left Arm of Chromosome 3 in *Drosophila* melanogaster. G3 (Bethesda) 9: 1581–1595.
3. Berns, N., I. Woichansky, S. Friedrichsen, N. Kraft, and V. Riechmann, 2014 A genome-scale *in vivo* RNAi analysis of epithelial development in *Drosophila* identifies new proliferation domains outside of the stem cell niche. Journal of Cell Science 127: 2736–2748.
4. Petzoldt, A. G., J.-B. Coutelis, C. Géminard, P. Spéder, M. Suzanne *et al*., 2012 DE-Cadherin regulates unconventional Myosin ID and Myosin IC in *Drosophila* left-right asymmetry establishment. Development 139: 1874–1884.
5. González-Morales, N., C. Géminard, G. Lebreton, D. Cerezo, J.-B. Coutelis *et al*., 2015 The Atypical Cadherin Dachsous Controls Left-Right Asymmetry in *Drosophila*. Dev Cell 33: 675–689.
6. Rauskolb, C., G. Pan, B. V. V. G. Reddy, H. Oh, and K. D. Irvine, 2011 Zyxin links fat signaling to the hippo pathway. PLoS Biol 9: e1000624.
7. Sarpal, R., M. Pellikka, R. R. Patel, F. Y. W. Hui, D. Godt *et al*., 2012 Mutational analysis supports a core role for *Drosophila* α-catenin in adherens junction function. J Cell Sci 125: 233–245.
8. Yue, T., A. Tian, and J. Jiang, 2012 The cell adhesion molecule echinoid functions as a tumor suppressor and upstream regulator of the Hippo signaling pathway. Dev Cell 22: 255–267.

9. Mao, Y., B. Kucuk, and K. D. Irvine, 2009 *Drosophila* lowfat, a novel modulator of Fat signaling. Development 136: 3223–3233.
10. Destalminil-Letourneau, M., I. Morin-Poulard, Y. Tian, N. Vanzo, and M. Crozatier, 2021 The vascular niche controls *Drosophila* hematopoiesis via fibroblast growth factor signaling. Elife 10: e64672.
11. Hogan, J., M. Valentine, C. Cox, K. Doyle, and S. Collier, 2011 Two frizzled planar cell polarity signals in the *Drosophila* wing are differentially organized by the Fat/Dachsous pathway. PLoS Genet 7: e1001305.
12. Misra, J. R., and K. D. Irvine, 2016 Vamana Couples Fat Signaling to the Hippo Pathway. Dev Cell 39: 254–266.
13. Revilla-Yates, E., L. Varas, J. Sierra, and I. Rodriguez, 2015 Transcriptional analysis of the dachsous gene uncovers novel isoforms expressed during development in *Drosophila*. FEBS Lett 589: 3595–3603.
14. Ambegaonkar, A. A., G. Pan, M. Mani, Y. Feng, and K. D. Irvine, 2012 Propagation of Dachsous-Fat planar cell polarity. Curr Biol 22: 1302–1308.
15. Harrison, N. J., E. Connolly, A. Gascón Gubieda, Z. Yang, B. Altenhein *et al*., 2021 Regenerative neurogenic response from glia requires insulin-driven neuron-glia communication. Elife 10: e58756.
16. Cho B, Song S, Axelrod JD. 2020. Prickle isoforms determine handedness of helical morphogenesis. Elife. 9:e51456. doi:10.7554/eLife.51456.
17. Zeng, X., L. Han, S. R. Singh, H. Liu, R. A. Neumüller *et al*., 2015 Genome-wide RNAi Screen Identifies Networks Involved in Intestinal Stem Cell Regulation in *Drosophila*. Cell Reports 10: 1226–1238.

18. Wang, Y., V. F. Naturale, and P. N. Adler, 2017 Planar Cell Polarity Effector Fritz Interacts with Dishevelled and Has Multiple Functions in Regulating PCP. G3 (Bethesda) 7: 1323–1337.
19. Tutor, A. S., S. Prieto-Sánchez, and M. Ruiz-Gómez, 2014 Src64B phosphorylates Dumbfounded and regulates slit diaphragm dynamics: *Drosophila* as a model to study nephropathies. Development 141: 367–376.
20. Gao, Y., Y. Mao, R.-G. Xu, R. Zhu, M. Zhang *et al*., 2019 Defining gene networks controlling the maintenance and function of the differentiation niche by an *in vivo* systematic RNAi screen. J Genet Genomics 46: 19–30.
21. Kamiyama, D., R. McGorty, R. Kamiyama, M. D. Kim, A. Chiba *et al*., 2015 Specification of Dendritogenesis Site in *Drosophila* aCC Motoneuron by Membrane Enrichment of Pak1 through Dscam1. Dev Cell 35: 93–106.
22. Gao, Y., Y. Mao, R.-G. Xu, R. Zhu, M. Zhang *et al*., 2019 Defining gene networks controlling the maintenance and function of the differentiation niche by an *in vivo* systematic RNAi screen. J Genet Genomics 46: 19–30.
23. Poon, C. L. C., J. I. Lin, X. Zhang, and K. F. Harvey, 2011 The sterile 20-like kinase Tao-1 controls tissue growth by regulating the Salvador-Warts-Hippo pathway. Dev Cell 21: 896–906.
24. Swaminathan, A., V. L. Barnes, S. Fox, S. Gammouh, and L. A. Pile, 2012 Identification of genetic suppressors of the Sin3A knockdown wing phenotype. PLoS One 7: e49563.
25. Dye, N. A., M. Popović, K. V. Iyer, J. F. Fuhrmann, R. Piscitello-Gómez *et al*., 2021 Self-organized patterning of cell morphology via mechanosensitive feedback. Elife 10: e57964.
26. Misra, J. R., and K. D. Irvine, 2019 Early girl is a novel component of the Fat signaling pathway. PLoS Genet 15: e1007955.

27. Pan, G., Y. Feng, A. A. Ambegaonkar, G. Sun, M. Huff *et al*., 2013 Signal transduction by the Fat cytoplasmic domain. Development 140: 831–842.

28. Huang, H.-L., S. Wang, M.-X. Yin, L. Dong, C. Wang *et al*., 2013 Par-1 regulates tissue growth by influencing hippo phosphorylation status and hippo-salvador association. PLoS Biol 11: e1001620.

29. Nagai, H., H. Tatara, K. Tanaka-Furuhashi, S. Kurata, and T. Yano, 2021 Homeostatic Regulation of ROS-Triggered Hippo-Yki Pathway via Autophagic Clearance of Ref(2)P/p62 in the *Drosophila* Intestine. Dev Cell 56: 81-94.e10.

30. Ke, H., Z. Feng, M. Liu, T. Sun, J. Dai *et al*., 2018 Collagen secretion screening in *Drosophila* supports a common secretory machinery and multiple Rab requirements. J Genet Genomics S1673-8527(18)30097–3.

31. Oh, H., and K. D. Irvine, 2008 *In vivo* regulation of Yorkie phosphorylation and localization. Development 135: 1081–1088.

32. Koon, A. C., and V. Budnik, 2012 Inhibitory control of synaptic and behavioral plasticity by octopaminergic signaling. J Neurosci 32: 6312–6322.

33. Ignatious Raja, J. S., N. Katanayeva, V. L. Katanaev, and C. G. Galizia, 2014 Role of Go/i subgroup of G proteins in olfactory signaling of *Drosophila* melanogaster. Eur J Neurosci 39: 1245–1255.

34. Bredendiek, N., J. Hütte, A. Steingräber, H. Hatt, G. Gisselmann *et al*., 2011 Go α is involved in sugar perception in *Drosophila*. Chem Senses 36: 69–81.

35. Agrawal, T., and G. Hasan, 2015 Maturation of a central brain flight circuit in *Drosophila* requires Fz2/Ca^{2+} signaling. Elife 4.

36. Qin, B., T.-H. Humberg, A. Kim, H. S. Kim, J. Short *et al*., 2019 Muscarinic acetylcholine receptor signaling generates OFF selectivity in a simple visual circuit. Nat Commun 10: 4093.

37. Yan, D., R. A. Neumüller, M. Buckner, K. Ayers, H. Li *et al*., 2014 A regulatory network of *Drosophila* germline stem cell self-renewal. Dev Cell 28: 459–473.

38. Neely, G. G., A. Hess, M. Costigan, A. C. Keene, S. Goulas *et al*., 2010 A genome-wide *Drosophila* screen for heat nociception identifies α2δ3 as an evolutionarily conserved pain gene. Cell 143: 628–638.

39. Czech, B., J. B. Preall, J. McGinn, and G. J. Hannon, 2013 A transcriptome-wide RNAi screen in the *Drosophila* ovary reveals factors of the germline piRNA pathway. Mol Cell 50: 749–761.

40. Zhou, M., N. Chen, J. Tian, J. Zeng, Y. Zhang *et al*., 2019 Suppression of GABAergic neurons through D2-like receptor secures efficient conditioning in *Drosophila* aversive olfactory learning. Proc Natl Acad Sci U S A 116: 5118–5125.

41. Solis, G. P., O. Bilousov, A. Koval, A.-M. Lüchtenborg, C. Lin *et al*., 2017 Golgi-Resident Gαo Promotes Protrusive Membrane Dynamics. Cell 170: 939-955.e24.

42. Lin, C., and V. L. Katanaev, 2013 Kermit interacts with Gαo, Vang, and motor proteins in *Drosophila* planar cell polarity. PLoS One 8: e76885.

43. Hoxha, V., C. Lama, P. L. Chang, S. Saurabh, N. Patel *et al*., 2013 Sex-specific signaling in the blood-brain barrier is required for male courtship in *Drosophila*. PLoS Genet 9: e1003217.

44. Cho, S., A. K. Muthukumar, T. Stork, J. C. Coutinho-Budd, and M. R. Freeman, 2018 Focal adhesion molecules regulate astrocyte morphology and glutamate transporters to suppress seizure-like behavior. Proc Natl Acad Sci U S A 115: 11316–11321.

45. Even, İ., İ. Akiva, and N. B. İyison, 2019 An *in vivo* RNAi mini-screen in *Drosophila* cancer models reveals novel potential Wnt targets in liver cancer. Turk J Gastroenterol 30: 198–207.

46. Urwyler, O., A. Izadifar, D. Dascenco, M. Petrovic, H. He *et al*., 2015 Investigating CNS synaptogenesis at single-synapse resolution by combining reverse genetics with correlative light and electron microscopy. Development 142: 394–405.

47. Valakh, V., S. A. Naylor, D. S. Berns, and A. DiAntonio, 2012 A large-scale RNAi screen identifies functional classes of genes shaping synaptic development and maintenance. Dev Biol 366: 163–171.

48. Vakaloglou, K. M., M. Chountala, and C. G. Zervas, 2012 Functional analysis of parvin and different modes of IPP-complex assembly at integrin sites during *Drosophila* development. J Cell Sci 125: 3221–3232.

49. Takemura, M., and T. Adachi-Yamada, 2011 Cell death and selective adhesion reorganize the dorsoventral boundary for zigzag patterning of *Drosophila* wing margin hairs. Dev Biol 357: 336–346.

50. Sugie, A., D. Umetsu, T. Yasugi, K.-F. Fischbach, and T. Tabata, 2010 Recognition of pre- and postsynaptic neurons via nephrin/NEPH1 homologs is a basis for the formation of the *Drosophila* retinotopic map. Development 137: 3303–3313.

51. Langer, C. C. H., R. K. Ejsmont, C. Schönbauer, F. Schnorrer, and P. Tomancak, 2010 *In vivo* RNAi rescue in *Drosophila* melanogaster with genomic transgenes from *Drosophila* pseudoobscura. PLoS One 5: e8928.

52. Kuckwa, J., K. Fritzen, D. Buttgereit, S. Rothenbusch-Fender, and R. Renkawitz-Pohl, 2016 A new level of plasticity: *Drosophila* smooth-like testes muscles compensate failure of myoblast fusion. Development 143: 329–338.

53. Johnson, R. I., A. Sedgwick, C. D'Souza-Schorey, and R. L. Cagan, 2011 Role for a Cindr-Arf6 axis in patterning emerging epithelia. Mol Biol Cell 22: 4513–4526.

54. Schnorrer, F., C. Schönbauer, C. C. H. Langer, G. Dietzl, M. Novatchkova *et al*., 2010 Systematic genetic analysis of muscle morphogenesis and function in *Drosophila*. Nature 464: 287–291.

55. Ansar, M., H.-L. Chung, A. Al-Otaibi, M. N. Elagabani, T. A. Ravenscroft *et al*., 2019 Bi-allelic Variants in IQSEC1 Cause Intellectual Disability, Developmental Delay, and Short Stature. Am J Hum Genet 105: 907–920.

56. Hildebrand, J. D., A. D. Leventry, O. P. Aideyman, J. C. Majewski, J. A. Haddad *et al*., 2021 A modifier screen identifies regulators of cytoskeletal architecture as mediators of Shroom-dependent changes in tissue morphology. Biol Open 10: bio055640.

57. Shan, L., C. Wu, D. Chen, L. Hou, X. Li *et al*., 2017 Regulators of alternative polyadenylation operate at the transition from mitosis to meiosis. J Genet Genomics 44: 95–106.

58. Marcogliese, P. C., S. Abuaish, G. Kabbach, E. Abdel-Messih, S. Seang *et al*., 2017 LRRK2(I2020T) functional genetic interactors that modify eye degeneration and dopaminergic cell loss in *Drosophila*. Hum Mol Genet 26: 1247–1257.

59. Chen, Z., J.-Y. Zhu, Y. Fu, A. Richman, and Z. Han, 2016 Wnt4 is required for ostia development in the *Drosophila* heart. Dev Biol 413: 188–198.

60. Ewen-Campen, B., T. Comyn, E. Vogt, and N. Perrimon, 2020 No Evidence that Wnt Ligands Are Required for Planar Cell Polarity in *Drosophila*. Cell Rep 32: 108121.

61. Mottier-Pavie, V. I., V. Palacios, S. Eliazer, S. Scoggin, and M. Buszczak, 2016 The Wnt pathway limits BMP signaling outside of the germline stem cell niche in *Drosophila* ovaries. Dev Biol 417: 50–62.

62. Stepanik, V., L. Dunipace, Y.-K. Bae, F. Macabenta, J. Sun *et al*., 2016 The migrations of *Drosophila* muscle founders and primordial germ cells are interdependent. Development 143: 3206–3215.

63. Kumar, S., I.-H. Jang, C. W. Kim, D.-W. Kang, W. J. Lee *et al*., 2016 Functional screening of mammalian mechanosensitive genes using *Drosophila* RNAi library- Smarcd3/Bap60 is a mechanosensitive pro-inflammatory gene. Sci Rep 6: 36461.

64. Pantoja, M., K. A. Fischer, N. Ieronimakis, M. Reyes, and H. Ruohola-Baker, 2013 Genetic elevation of sphingosine 1-phosphate suppresses dystrophic muscle phenotypes in *Drosophila*. Development 140: 136–146.

65. Chabu, C., D.-M. Li, and T. Xu, 2017 EGFR/ARF6 regulation of Hh signalling stimulates oncogenic Ras tumour overgrowth. Nat Commun 8: 14688.

66. Ben-Zvi, D. S., and T. Volk, 2019 Escort cell encapsulation of *Drosophila* germline cells is maintained by irre cell recognition module proteins. Biol Open 8.

67. Sauerwald, J., W. Backer, T. Matzat, F. Schnorrer, and S. Luschnig, 2019 Matrix metalloproteinase 1 modulates invasive behavior of tracheal branches during entry into *Drosophila* flight muscles. Elife 8: e48857.

Supplementary Table 2.2. Statistics for gene expression in Ivy GAP analyses. Graphed data are shown in Figure 2.4 and Supplementary Figure 2.1.

SYPMK

	MP	HBV	PAN	PNZ	CT	IT
LE	0.999	>0.999	0.962	0.954	0.959	0.940
IT	0.735	0.940	>0.999	>0.999	0.999	-
CT	0.678	0.957	>0.999	>0.999	-	
PNZ	0.766	0.954	>0.999	-		
PAN	0.756	0.962	-			
HBV	0.999	-				

NCK1

	MP	HBV	PAN	PNZ	CT	IT
LE	***	**	***	*	0.484	0.980
IT	***	*	***	0.124	0.965	-
CT	***	0.050	***	0.189	-	
PNZ	0.309	0.997	**	-		
PAN	0.850	0.073	-			
HBV	0.737	-				

CTNNA1

	MP	HBV	PAN	PNZ	CT	IT
LE	***	***	***	***	***	***
IT	***	**	***	***	***	-
CT	0.814	0.998	***	0.534	-	
PNZ	0.999	0.959	0.589	-		
PAN	0.293	0.099	-			
HBV	0.996	-				

CTNNA2

	MP	HBV	PAN	PNZ	CT	IT
LE	***	***	***	***	***	0.232
IT	***	***	***	***	0.398	-
CT	***	***	***	**	-	
PNZ	*	0.368	>0.999	-		
PAN	*	0.388	-			
HBV	0.939	-				

CTNNA3

	MP	HBV	PAN	PNZ	CT	IT
LE	0.198	**	***	**	0.140	0.828
IT	0.931	0.157	*	0.103	0.955	-
CT	0.999	0.285	*	0.171	-	
PNZ	0.621	>0.999	>0.999	-		
PAN	0.368	>0.999	-			
HBV	0.716	-				

NEGR1

	MP	HBV	PAN	PNZ	CT	IT
LE	***	***	***	***	***	***
IT	***	***	***	***	***	-
CT	0.120	0.295	**	0.401	-	
PNZ	0.999	>0.999	0.950	-		
PAN	0.997	0.993	-			
HBV	>0.999	-				

DCHS1

	MP	HBV	PAN	PNZ	CT	IT
LE	**	**	**	***	***	0.063
IT	0.979	0.967	0.956	0.836	0.934	-
CT	>0.999	>0.999	>0.999	0.996	-	
PNZ	0.998	0.999	0.999	-		
PAN	>0.999	>0.999	-			
HBV	>0.999	-				

FAT4

	MP	HBV	PAN	PNZ	CT	IT
LE	***	**	0.976	0.988	>0.999	>0.999
IT	***	**	0.962	0.982	0.999	-
CT	***	***	0.973	0.993	-	
PNZ	***	***	>0.999	-		
PAN	***	***	-			
HBV	0.999	-				

KIRREL1

	MP	HBV	PAN	PNZ	CT	IT
LE	***	***	***	***	*	0.759
IT	***	***	***	***	0.670	-
CT	***	***	***	***	-	
PNZ	**	0.062	0.697	-		
PAN	***	***	-			
HBV	0.975	-				

KIRREL2

	MP	HBV	PAN	PNZ	CT	IT
LE	0.992	>0.999	0.844	*	0.465	>0.999
IT	0.972	>0.999	0.869	*	0.456	-
CT	*	0.292	0.996	0.360	-	
PNZ	***	*	0.271	-		
PAN	0.232	0.728	-			
HBV	0.996	-				

KIRREL3

	MP	HBV	PAN	PNZ	CT	IT
LE	***	***	***	***	***	***
IT	***	***	***	***	***	-
CT	***	**	0.371	0.085	-	
PNZ	0.921	0.988	0.975	-		
PAN	0.333	0.638	-			
HBV	>0.999	-				

Appendix A.1 Quantitative RT-PCR analysis to determine the effectiveness of glioblastoma-associated gene RNAi knockdown

Aim: To test the efficiency of RNAi knockdown of cell adhesion positive hits used in Chapter 2, we used Quantitative PCR (qPCR) to validate gene knockdown of targeted genes. One of the limitations of using *in vivo* RNAi constructs for gene silencing is low gene knockdown efficiency. Quantifying the RNAi mediated gene knockdown of GBM-associated adhesion genes will corroborate that the migration defect phenotypes in the RNAi expressing border cells in Chapter 2 was caused by efficient downregulation of genes and not by an off-target effect or a partial knockdown.

Material and methods: The ubiquitously expressed *daughterless*-GAL4 (a gift from Erika Geisbrecht's lab) was used to express UAS-RNAi in the F1 progeny. One RNAi line each for positive hit from the glioblastoma screen was used to test the efficiency of knockdown except α-catenin which was tested in Chen et al. 2020 by antibody staining (Chapter 3). Stocks were obtained from VDRC (33470, 37524, 108863, 36219, 27223, 35524, 38010) and BDSC (*w1118).*A positive control *NUAK* RNAi was borrowed from Erika Geisbrecht's lab. Males targeting knockdown of *Sym* (33470), *Dock* (37524), *Fat* (108863), *Ds* (36219), *Rst* (27223), *Lac* (35524), *Wnt4* (38010), *NUAK* (positive control-Erika Giesbrecht's lab) and *w118* (control) were crossed to da-GAL4 virgins at 25℃ for 48 hours and then moved to 30℃ for optimum gene GAL4 expression. Total RNA was extracted from three wandering L3 instar larvae in singles or triplicates using the RNeasy Mini Kit (Qiagen, Hilden, Germany) with on-column DNA digestion using Qiagen's RNase free DNase set. qRTPCR was performed using the *Power* SYBR™ Green RNA-to-C_T™ *1-Step* Kit (ThermoFisher, Waltham, MA). The following primers were ordered from

Integrated DNA Technologies (IDT, Stokie, IL): *rp49* forward-GCCCAAGGGTATCGACAACA, reverse GCGCTTGTTCGATCCGTAAC; *sym* forward-AGAGCTAAGGTGGTCGATTGG, reverse-GAACCTCCATGTTTGAGTCGT; *ds* forward - GTCGCCAGCGAAACGATGAAC, reverse - CTGCGAAGATCCCAGGAGAA; *Wnt4* forward - CGGGAACATGAACAGCACGAT,

reverse-TCACCGAGGGTACACTCGATG; *dock* forward-ATGAAGCACGGCAAATCTCAG, reverse- GAGCCCTTTTTCACCTTCTTCT; *Fat* forward- GGTAACGGGTGAGGTGAAGAC, reverse-ACATCCAGAACCTTAATCCGCA; *rst* forward- CAATGAGACGGCTGGAAGGT, reverse – CCGATTCCGAGCTGATCTCC, *lac* forward- GCACAGTGGAGTTCGATTGC, reverse- GCAGCTTGTAGGTGGACGAG and *NUAK* forward 5-CAGTTCCAACACAACCACGC, reverse 5'-GGATGATAAACTCCCGCGGA. All primers were synthesized at Integrated DNA Technologies (IDT, Stokie, IL). RNAi knockdown was calculated from raw Ct values using the 2-ΔΔCt method and graphed as overall fold change or raw Ct values were directly plotted (see Challenges in experiments section) using GraphPad Prism 9.0.

Experimental challenges: Crosses were first set up with da-GAL4 at 25℃ throughout the experiment and wandering L3 larvae were then used for RNA extraction. *NUAK* RNAi was used as a positive control to test the efficiency of *daughterless*-GAL (da-GAL4). On analyzing the gene expression data, I noticed there was no apparent knockdown of RNA levels in any of the da-GAL>UAS-RNAi samples including positive control *NUAK* RNAi. NUAK RNAi was previously tested in Brooks *et al.*, 2020 and showed 50-60% knockdown. To achieve better knockdown, I set up all da-GAL4 and RNAi crosses at 25℃ for 48 hours and let the females lay eggs within that time. I then flipped the parents to a fresh vial and moved the original vial with larvae to 30℃. This

higher temperature ensured efficient GAL4-UAS expression, and this condition was then used for the rest of the experiments. For crosses with Sym and Ds RNAi, I could obtain RNA samples in triplicates and calculated the overall fold change (Figure A.1 A). However, very few larvae survived at this high temperature especially with the expression of RNAi under the ubiquitous driver *da*-GAL4. Therefore, with Lac, Rst, Dock Wnt4 and NUAK RNAi, total RNA was extracted from a single sample of three L3 larvae. Most of the Fat RNAi larvae died and Fat RNAi knockdown could not be analyzed. In these cases, raw Ct values were therefore used to plot the graph of RNAi samples with single samples and show overall trend in RNAi knockdown (Figure A.1 B).

Results and conclusion: We performed qRT-PCR to validate *in vivo* gene knockdown for 7 RNAi lines targeting cell adhesion genes. Knockdown of Sym under da-GAL4 was moderate (50%) (Figure A.1A). Whereas knockdown of Ds was mild (20%) using Ds RNAi when normalized to control (Figure A.1A). Comparing the mild migration defects of Ds RNAi from Chapter 2 in border cells, these results suggest that the mild border cell migration defects were due to inefficient knockdown. However, the GAL4 systems used in both these experiments were different, which could also account for knockdown efficiency. Nevertheless, these experiments still provide a reliable system to validate gene knockdown using qRT-PCR. Further, we used raw Ct values to analyze knockdown of all other RNAi lines with the single sample of extracted total RNA. Ct values are the number of cycles required for the signal to cross threshold and is inversely proportional to gene expression. Lower Ct values indicate higher nucleic acid content and thus higher gene expression and vice-versa. We observed that for larvae expressing RNAi line of Lac, Wnt, Rst, Dock and NUAK under da-GAL4, the Ct values were higher for each gene as compared

to their expression in control samples (Fig. A.1 B). Overall, from these experiments we can confirm knockdown of cell adhesion genes using RNAi lines that were used in Chapter 2. This further validates the migration defect phenotypes seen in the border cell cluster upon expression of RNAi lines under c306-GAL4. Future experiments will involve repeating the four RNAi lines for Lac, Wnt4, Rst and Dock to extract RNA samples in triplicates and confirm gene knockdown. We will also analyze additional RNAi lines for each gene to cross compare the gene knockdown efficiency for GBM-related adhesion genes and border cell migration defect phenotypes.

References

Brooks, D., F. Naeem, M. Stetsiv, S. C. Goetting, S. Bawa *et al.*, 2020 *Drosophila* NUAK functions with Starvin/BAG3 in autophagic protein turnover. PLOS Genetics 16: e1008700.

Figures

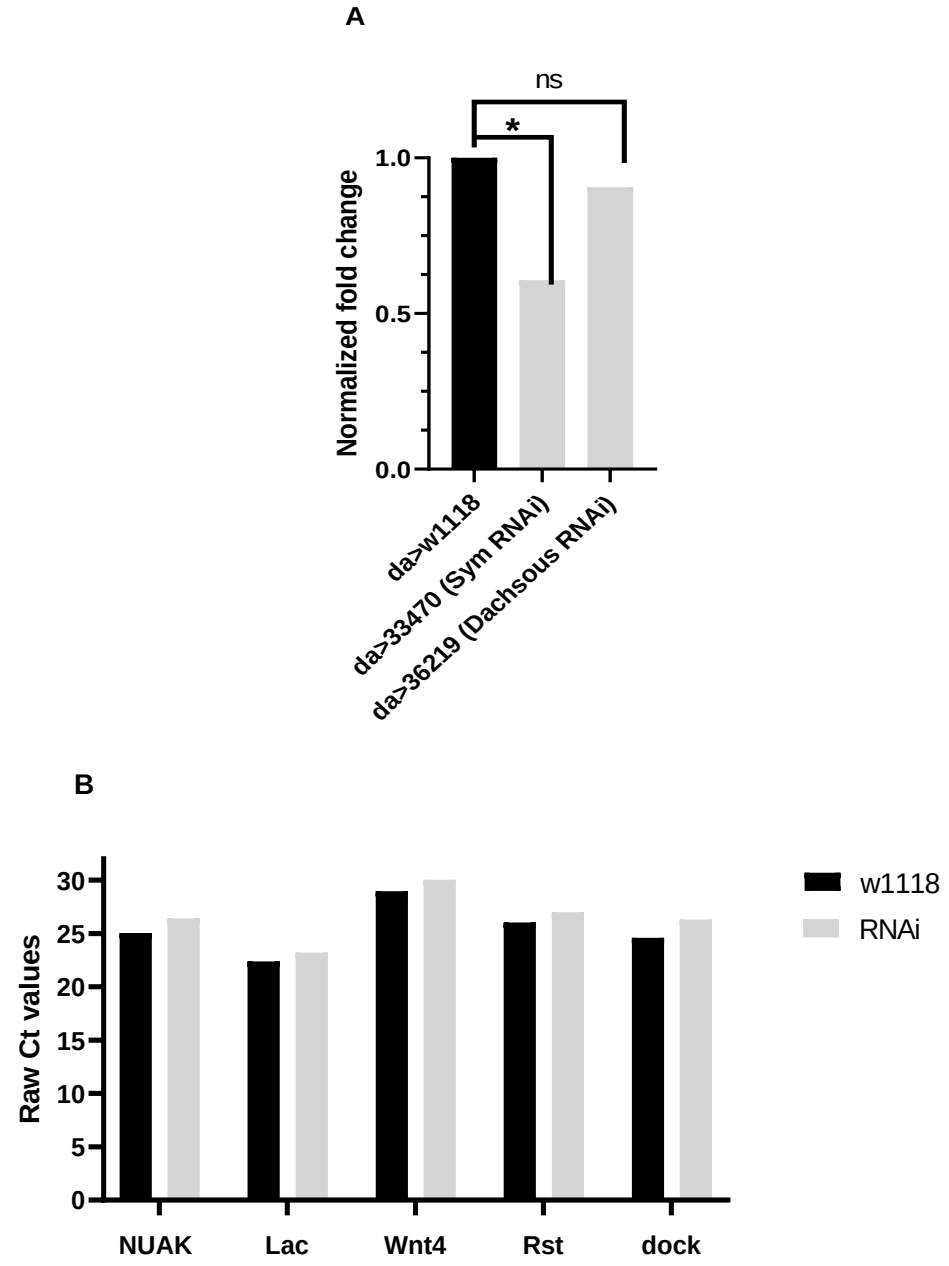

Figure A.1- Validation of GBM RNAi lines by qRT-PCR. A) Overall fold change of gene expression levels of Sym (33470) and Ds (36219) driven by the ubiquitous *da*-GAL4. Unpaired two tailed t-test was used to calculate the p-values for each RNAi sample, * $p<0.05$. B) Raw Ct values graphed from single replicate of each gene mentioned on the Y-axis for RNAi line compared to control (w118).

Appendix B- Chapter 3 supplemental materials

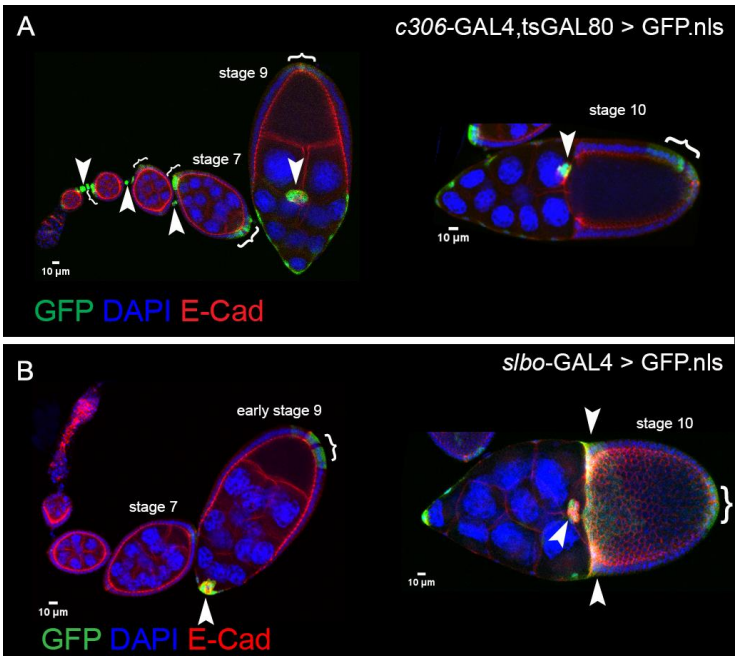

Figure 3.1 – figure supplement 1

Patterns of GAL4s expressed in border cells. Expression patterns of *c306*-GAL4 (**A**) and *slbo*-GAL4 (**B**) during oogenesis, indicated by *UAS*-GFP.nls (green; arrowheads, brackets). All egg chambers were co-stained with DAPI (blue) to label nuclei and E-cadherin (red) to mark cell membranes. (**A**) *c306*-GAL4 drives expression in anterior follicle cells prior to border cell formation (left panel) and continues throughout the whole migration process (left and right panels). *c306*-GAL4 is also expressed in stalk cells early (left panel) and anterior and posterior follicle cells at most stages. (**B**) *slbo*-GAL4 drives expression at early stage 9 in early border cells, just before migration starts (left panel). *slbo*-GAL4 continues in border cells through stage 10, at which point it turns on centripetal cells and posterior follicle cells (right panel).

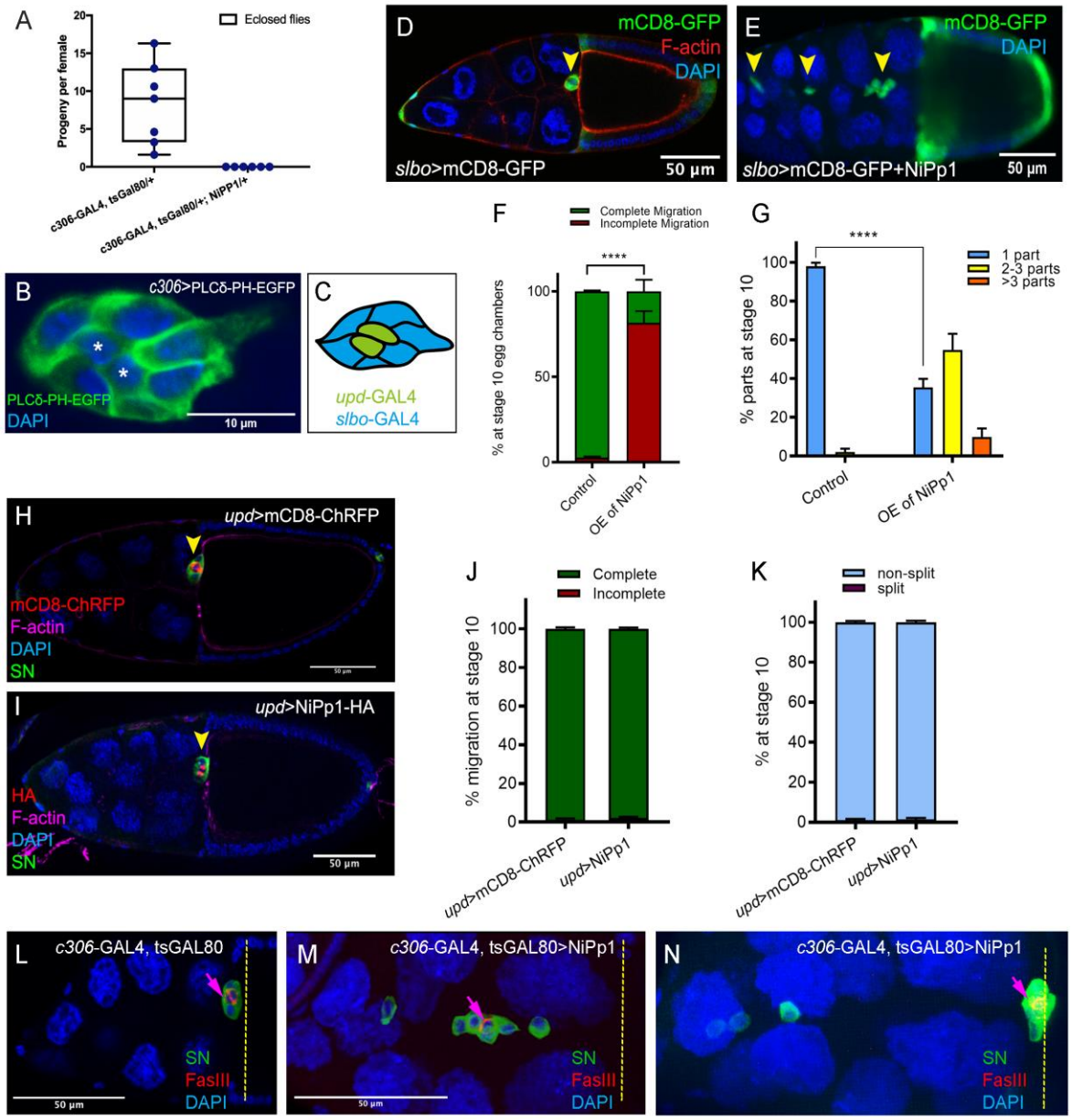

Figure 3.1 – figure supplement 2

Cell-specific phenotypes induced by NiPp1. (**A**) Fertility of control versus NiPp1-expressing females. The average progeny per female in each vial (individual plot points) is shown as a box-and-whiskers plot (see Figure 3.1 legend for details of plot). (**B**) Expression pattern of *c306*-GAL4 in the border cell cluster, as visualized by driving the expression of the membrane marker UAS-PLCδ-PH-EGFP (green). Nuclei are labeled by DAPI (blue). The central polar cells (asterisk)

express GFP. (**C**) Schematic drawing of the border cell cluster showing the patterns of GAL4 drivers. *upd*-GAL4 (green) is used to drive expression in polar cells; *slbo*-GAL4 (blue) is used to drive expression in outer border cells but not polar cells. (**D-G**) Overexpression of NiPp1 in border cells, driven by *slbo*-GAL4, disrupts border cell cluster migration and cohesion. (**D, E**) Stage 10 *slbo*-GAL4 egg chambers expressing mCD8-GFP (green), which is detected in border cells (arrowheads), and stained for DAPI to label nuclei (blue) and phalloidin to label F-actin (red, D). Control border cells (D) reach the oocyte as a single unit, but NiPp1 overexpressing border cells (E) dissociate from the cluster and fail to reach the oocyte. (**F**) Quantification of border cell migration for matched control and NiPp1 overexpression, shown as the percentage that did not complete (red), or completed (green) their migration to the oocyte (see Figure 3.1I for egg chamber schematic). (**G**) Quantification of cluster cohesion, shown as the percentage of border cells found as a single unit (1 part) or split into multiple parts (2-3 parts or >3 parts) in control versus NiPp1-expressing egg chambers. (**F, G**) ****$p < 0.0001$; unpaired two-tailed *t* test. Error bars represent SEM in 3 experiments, each trial assayed $n \geq 62$ egg chambers (total $n \geq 201$ for each genotype). (**H-K**) NiPp1 overexpression in polar cells, driven by *upd*-GAL4, does not impair border cell cluster migration or cohesion. (**H, I**) Stage 10 *upd*-GAL4 egg chambers expressing mCD8-ChRFP (red in H) or NiPp1-HA (red in I), which are detected in the polar cells (arrowheads), and co-stained for phalloidin to detect F-actin (magenta), SN to detect border cells (green), and DAPI to label nuclei (blue). (**J, K**) Quantification of border cell migration (J) and border cell cluster cohesion (K) for matched control and NiPp1overexpression. Error bars represent SEM in 3 experiments, each trial assayed $n \geq 80$ egg chambers (total $n \geq 313$ for each genotype). ****$p < 0.0001$, unpaired two-tailed t test. (**L-N**) Border cells expressing NiPp1 driven by *c306*-GAL4 (M, N), can separate from the polar cells, whereas control border cells (L) stay attached to polar cells.

Stage 10 egg chambers stained for SN (green) to detect border cells, FasIII (red) to detect polar cells (arrows), and DAPI to label nuclei (blue). Yellow dashed line indicates anterior border of the oocyte. Example of a control (L) and two representative NiPp1 overexpressing border cell clusters (M, N). All genotypes are listed in Table 3.2.

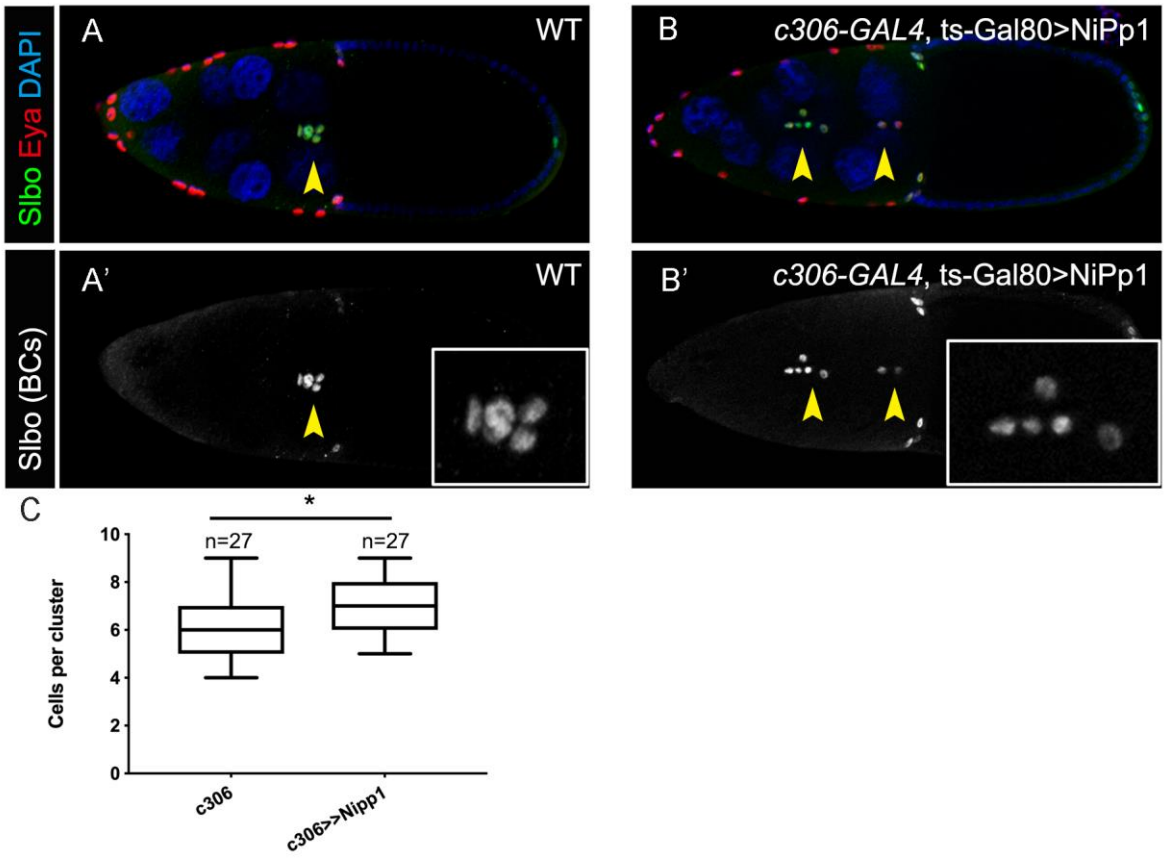

Figure 3.1 – figure supplement 3

NiPp1 does not greatly alter border cell specification or cell number per cluster. (**A-B'**) Stage 10 wild-type (A, A') and NiPp1-expressing (B, B') egg chambers stained with anti-Slbo (green in A, B; white in A', B'), anti-Eya (red in A, B), and DAPI to detect nuclei (blue in A, B). Eya primarily marks the anterior follicle cells with lower levels in border cells but is absent from polar cells. Slbo marks border cells and polar cells (arrowheads). Insets, zoomed-in images of Slbo-expressing cells. (**C**) Quantification of cell number per cluster in control and NiPp1-expressing border cell clusters. The total number of egg chambers scored for cell number in each genotype is shown and was assayed in 3 independent trials. Error bars represent SEM, *p < 0.05, unpaired two-tailed *t* test. All genotypes are listed in Table 3.2.

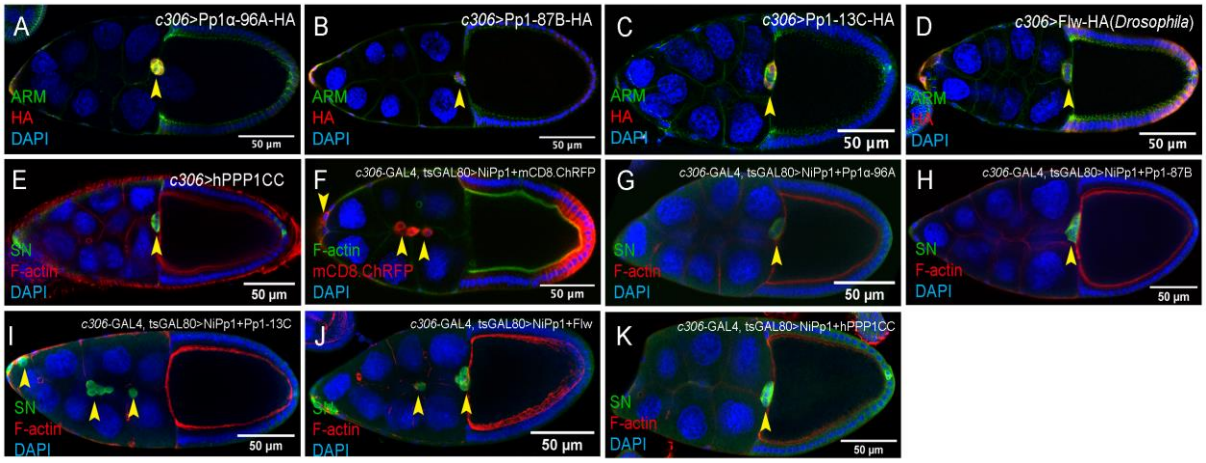

Figure 3.2 – figure supplement 1

Rescue of NiPp1 phenotypes by Pp1c genes. (**A-E**) Overexpression of Pp1c subunits on their own does not impair border cell migration to the oocyte. Stage 10 egg chambers of the indicated genotypes stained for Armadillo (Arm; β-Catenin) to detect cell membranes (green in A-D) or SN to detect border cells (green in E), HA to detect Pp1c overexpression (red in A-D) and DAPI to label nuclei (blue). (**F-K**) Overexpression of Pp1c subunits can rescue NiPp1-induced border cell migration defects and cohesion. Stage 10 egg chambers of the indicated genotypes stained for SN to detect border cells (green in G-K) or phalloidin to detect F-actin (green in F, red in G-K), mCD8-ChRFP (red in F), and DAPI to label nuclei (blue). Border cells in all panels are indicated by arrowheads. All genotypes are listed in Table 3.2.

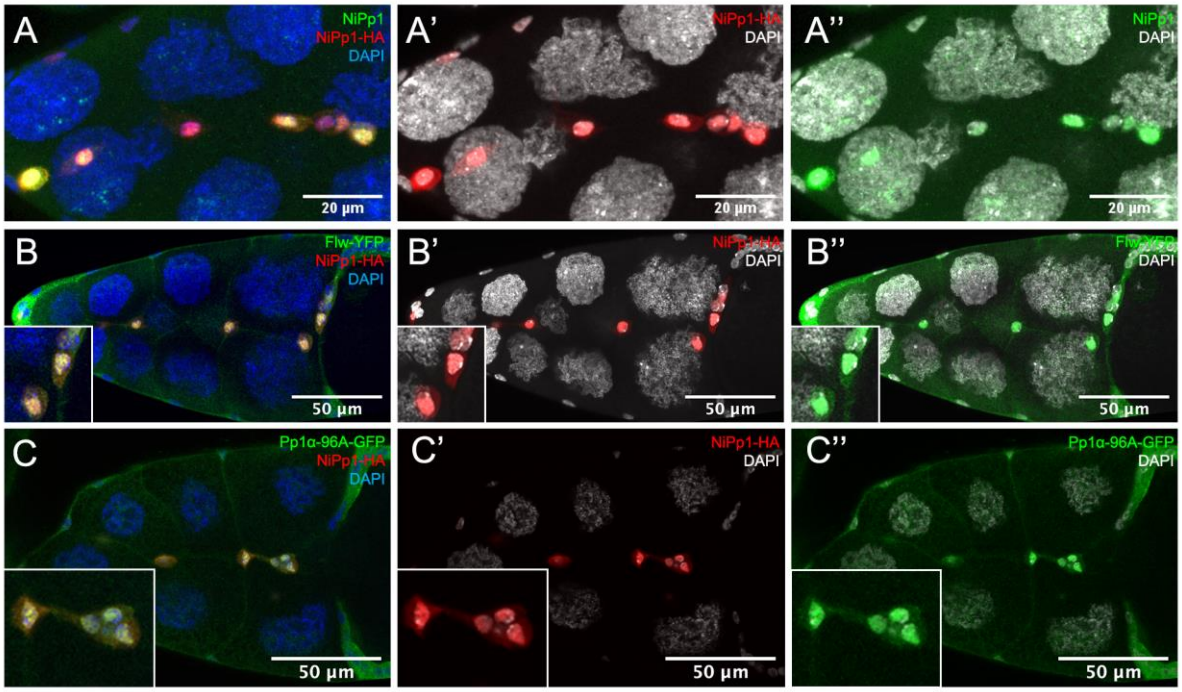

Figure 3.2 – figure supplement 2

NiPp1 promotes nuclear localization of Pp1c subunits. (**A-A**") NiPp1-HA overexpression alone localizes mainly in the nuclei, revealed by HA antibody (red in A, A') and human NiPp1 antibody (PPP1R8; green in A, A''). (**B-C"**) NiPp1-HA overexpression promotes the nuclear localization of two Pp1c subunits, of Flw and Pp1α-96A. Stage 10 egg chambers co-expressing Flw-YFP (green in B, B") or Pp1α-96A-GFP (green in C, C") with UAS-NiPp1 were stained for anti-HA to detect NiPp1 expression (red in B, B', C, C') and DAPI to detect nuclei (blue in B, C; white in B', B", C', C"). Insets, zoomed-in images of border cells.

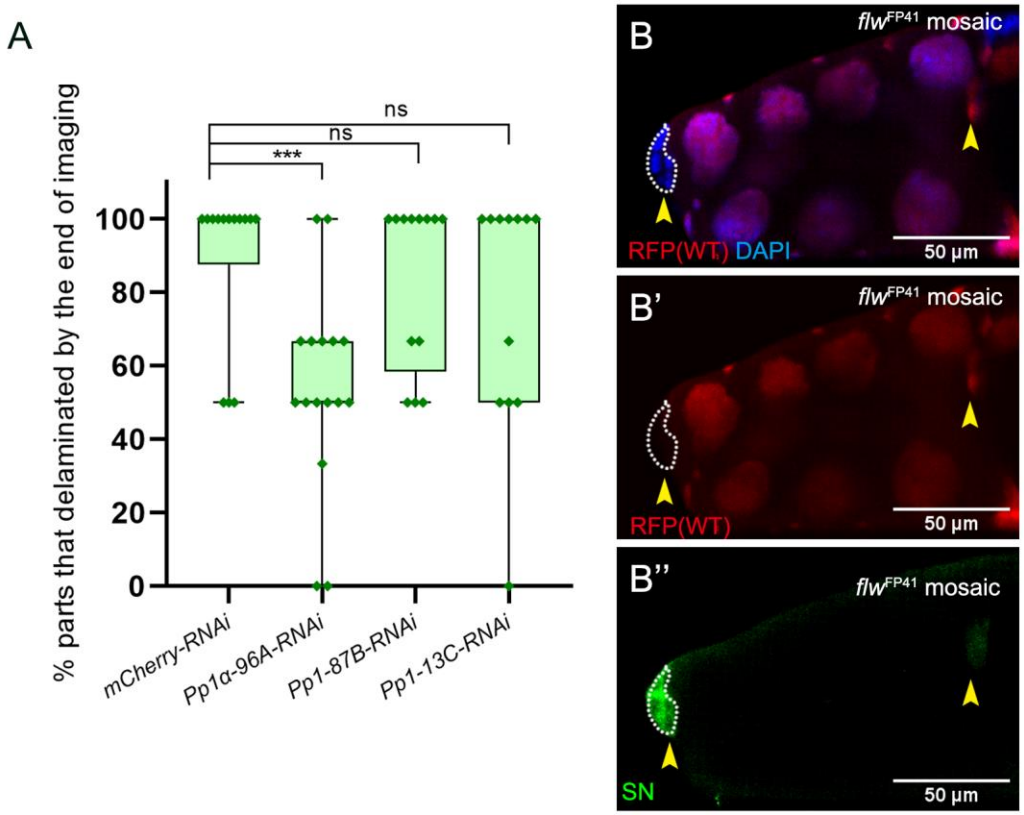

Figure 3.3 – figure supplement 1

Delamination and migration defects caused by loss of *Pp1c*. (**A**) Quantification of live split border cell cluster parts that completed migration during the movie, for matched control and RNAi knockdown of the indicated *Pp1c* genes. N = 14 videos for control, n = 13 videos for *Pp1-87B-RNAi*, n = 12 videos for *Pp1-13C-RNAi*, n = 16 videos for *Pp1alpha-96A-RNAi*, box-and-whiskers plot, ***p < 0.001, unpaired two-tailed *t* test. (**B-B"**) Example of a stage 10 egg chamber with a *flw*^{FP41} mutant clone, marked by the loss of nuclear mRFP (red in B, B'; dotted outline) and stained for SN (green in B") to mark border cells (arrowheads) and DAPI (blue in B) to mark nuclei. All genotypes are listed in Table 3.2.

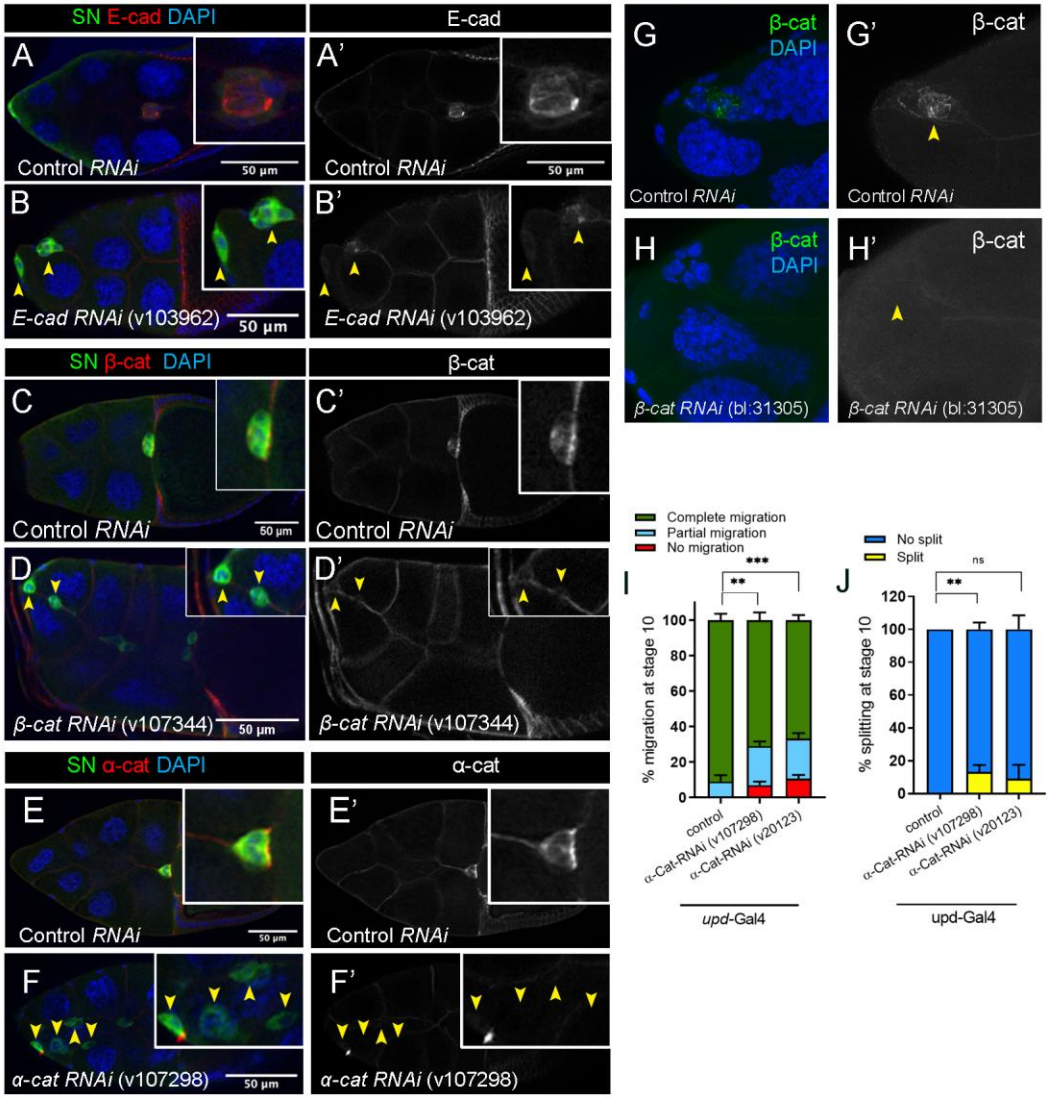

Figure 3.4 – figure supplement 1

RNAi for cadherin-catenin reduces endogenous levels of the specifically targeted gene. (**A-H'**) Efficiency of cadherin-catenin *RNAi* in border cells as detected by antibody staining to the respective proteins. Stage 10 control (A, A', C, C', E, E'), *E-Cad-RNAi* (B, B'), *β-Cat-RNAi* (line v107344; D, D'), and *α-Cat-RNAi* (F, F') egg chambers stained for SN (green), the respective proteins in red (E-Cad in A-B', β-Cat in C-D', and α-Cat in E-F'), and DAPI to label nuclei (blue in A, B, C, D, E, F). Border cells are indicated by arrowheads. Insets, zoomed-in views of border cell clusters. (**G-H'**) Efficiency of matched control (G, G') and *β-Cat-RNAi* (line BL-31305; H,

H') in border cells as detected by β-Cat antibody (green) and DAPI (blue). (**I, J**) Border cell migration (I) and cluster cohesion (J) in control versus *α-Cat-RNAi* driven by *upd*-GAL4 in the polar cells. Quantification at stage 10, $n \geq 44$ (total $n \geq 192$ for each genotype); ns, not significant, $^{**}p < 0.01$, $^{***}p < 0.001$, unpaired two-tailed *t* test. (**I**) Quantification of migration shown as the percentage of egg chambers with complete (green), partial (blue), or no (red), border cell migration. (**J**) Quantification of cluster cohesion, shown as the percentage of border cells found as a single unit (no split, blue) or split into two or more parts (split, yellow). All genotypes are listed in Table 3.2.

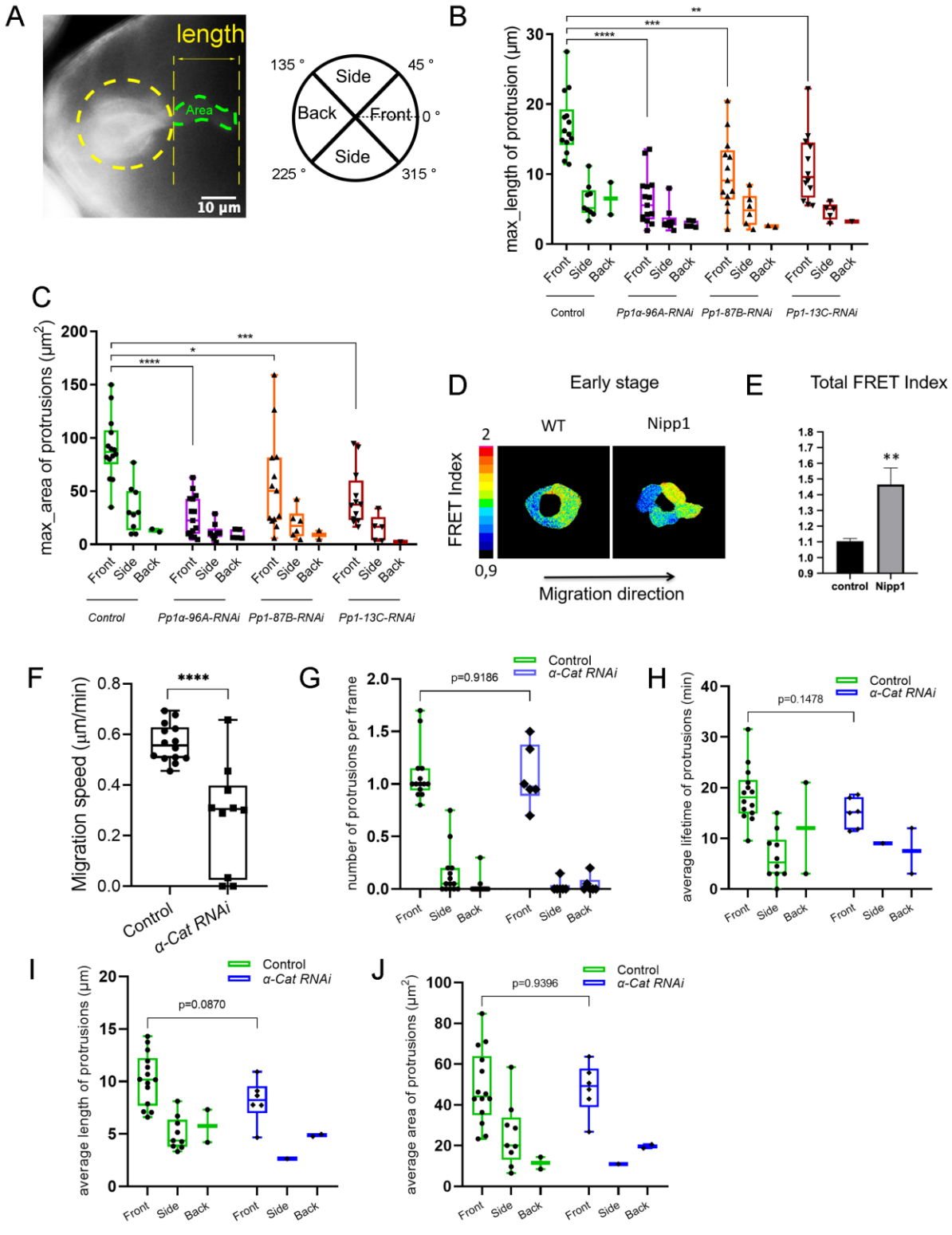
A
length
Area
10 µm
135 °
45 °
Side
Back
Front
0 °
Side
225 °
315 °
B
max_length of protrusion (µm)
Front
Side
Back
Control
Pp1α-96A-RNAi
Pp1-87B-RNAi
Pp1-13C-RNAi
C
max_area of protrusions (µm²)
D
Early stage
WT
Nipp1
FRET Index
Migration direction
E
Total FRET Index
control
Nipp1
F
Migration speed (µm/min)
Control
α-Cat RNAi
G
number of protrusions per frame
p=0.9186
H
average lifetime of protrusions (min)
p=0.1478
I
average length of protrusions (µm)
p=0.0870
J
average area of protrusions (µm²)
p=0.9396

Figure 3.5 – figure supplement 1

Additional quantification of protrusion dynamics and Rac activity in Pp1-inhibited and α-Cat-RNAi border cells. (**A**) Close-up view of a live border cell cluster depicting how protrusions are measured. The main body of the border cell cluster is outlined (yellow circle). The protrusion length and area (green outline) were defined and measured as a cellular projection extending away from the main cluster or border cell. The schematic indicates how protrusion direction is defined. (**B, C**) Quantification of protrusion max_length (B) and max_area (C) in control versus *Pp1c-RNAi* border cells. Data are presented as a box-and-whiskers plot (see Figure 3.1 legend for details of plot and Figure 3.5 legend for protrusion numbers for each genotype). *p < 0.05; **p < 0.01; ***p < 0.001; ****p < 0.0001; unpaired two-tailed *t* test. (**D, E**) Rac-FRET in wild-type versus NiPp1 border cells (n = 22 for control, n = 18 for *slbo*>NiPp1). (D) Representative FRET images of control and NiPp1-expressing border cells, color-coded according to the heat map and FRET index. (E) Quantification of the total FRET index measured in control and NiPp1 border cells. Error bars represent SEM; p = 0.0033 (**), unpaired *t* test with Welch's correction. (**F-J**) Quantification of the migration speed (F), number of protrusions per frame (G), average protrusion lifetime (H), average protrusion length (I), and average protrusion area (J) from videos of *α-Cat*-RNAi versus control border cells. For control, protrusions were measured in 14 videos (n = 51 front-directed protrusions, n = 15 side-directed protrusions, n = 2 back-directed protrusions); for *α-Cat*-RNAi, protrusions were measured in 6 videos (n = 29 front protrusions, n = 1 side protrusion, n = 9 back protrusions). Data are presented as box-and-whiskers plots (see Figure 3.1 legend for details of plot). ****p < 0.0001, unpaired two-tailed *t* test. All genotypes are listed in Table 3.2.

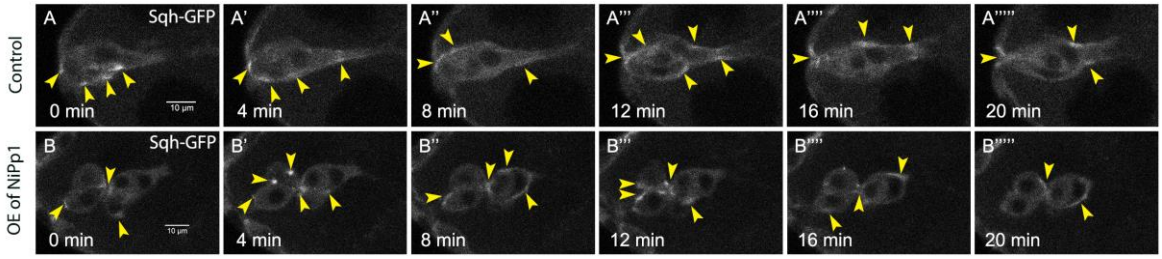

Figure 3.6 – figure supplement 1

Pp1 restricts the distribution of Myo-II to the cluster periphery during early migration. (**A-B’’’’’**) Stills from representative confocal videos of dynamic Sqh-GFP in early-migration borders cells over the course of 20 minutes. Image gain and other acquisition parameters were the same, except that the range of *z*-stacks may vary slightly. (A-A’’’’’) Control border cells (Video 14) have dynamic Sqh-GFP, which is mainly restricted to the cluster perimeter. Some signal is found in the central polar cells. (B-B’’’’’) NiPp1 overexpressing border cells (Video 15) alters the localization of Sqh-GFP, with more Sqh-GFP enriched around individual border cells. All genotypes are listed in Table 3.2.

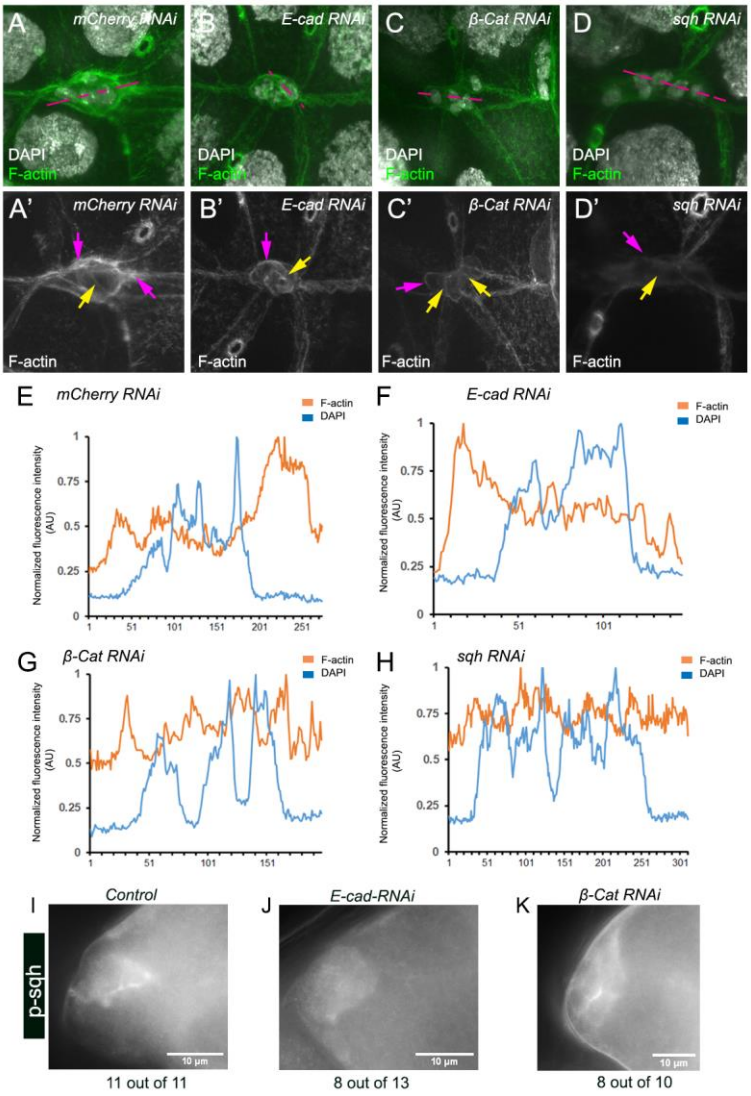

Figure 3.6 – figure supplement 2

RNAi for cadherin-catenin alters the actomyosin pattern of the border cell cluster. (**A, A'**) Control *mCherry-RNAi* border cell cluster has higher F-actin (magenta arrows) at the periphery of the cluster, but lower levels inside (yellow arrow) the group. (**B-D'**) Knocking down *E-Cad (B, B'), β-Cat* (C, C'), or *sqh* (D, D') reduces the relatively high F-actin on the outer surfaces of border cells. (**E-H**) Plot profiles of normalized F-actin (orange) and DAPI (blue) fluorescence pixel intensity (AU, arbitrary units) measured along the lines shown in (A-D); similar results were obtained from additional border cell clusters (n =11 for control, n = 11 for *E-cad RNAi*, n = 9 for

β-Cat RNAi, n = 10 for *sqh RNAi*. (**I-K**) Greyscale images of clusters stained with an anti-phosphorylated Sqh (p-Sqh) antibody in control (I), *E-cad RNAi* (J), and *β-Cat RNAi* (K) clusters, p-Sqh is enriched at the periphery and the protrusion of the control cluster (n = 11 out of 11), while knocking down cadherin-catenin complex abolishes this enrichment (*E-Cad*-RNAi, 8 out of 13 no longer enriched at periphery; *β-Cat*-RNAi, 8 out of 10 no longer enriched at periphery).

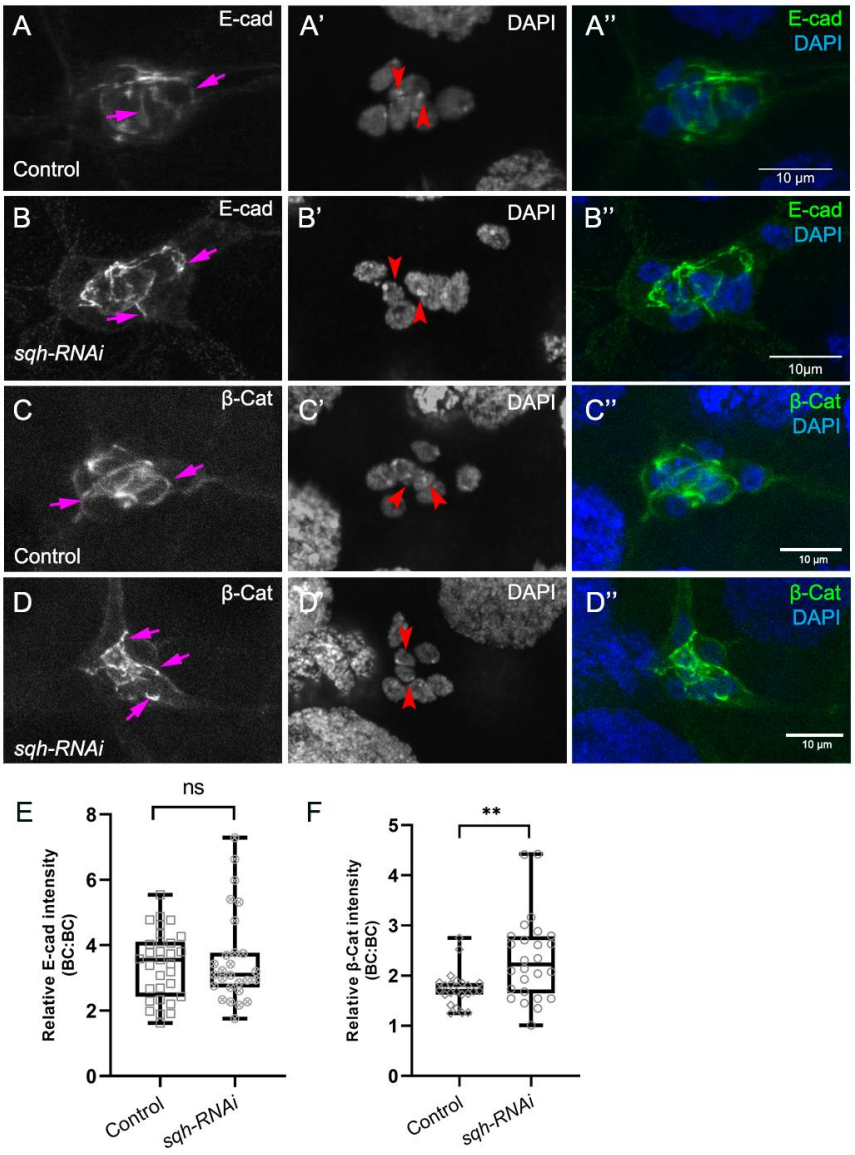

Figure 3.6 – figure supplement 3

Myo-II is not required for cadherin-catenin enrichment at border cell-border cell contacts. (**A-D**) Representative images showing the E-Cad (white in A, B; green in A", B") and β-cat (white in C, D; green in C", D") protein expression patterns in control (A-A'', C-C'') and *sqh-RNAi* (B-B'', D-D'') border cells. Border cells were co-stained for DAPI to mark nuclei (white in A', B', C', D'; blue in A", B", C", D"). Images were generated from merged *z*-sections. The enriched levels of E-Cad (A, B) and β-cat (C, D) between border cells (border cell-border cell contacts) are marked

by magenta arrows. The central polar cells are indicated by red arrowheads (A', B', C', D'). (**E, F**) Quantification of relative E-Cad (E) and β-Cat (F) protein intensity levels in control and *sqh-RNAi* border cell clusters shown as box-and-whiskers plots (see Figure 3.1 legend for details of plot). For E-Cad, 37 border cell-border cell contacts from 9 matched control clusters and 27 border cell-border cell contacts from 9 *sqh-RNAi* clusters were measured. For β-Cat, 23 border cell-border cell contacts from 8 matched control clusters and 26 border cell-border cell contacts from 9 *sqh-RNAi* clusters were measured. **$p < 0.05$, unpaired two-tailed *t* test. All genotypes are listed in Table 3.2.

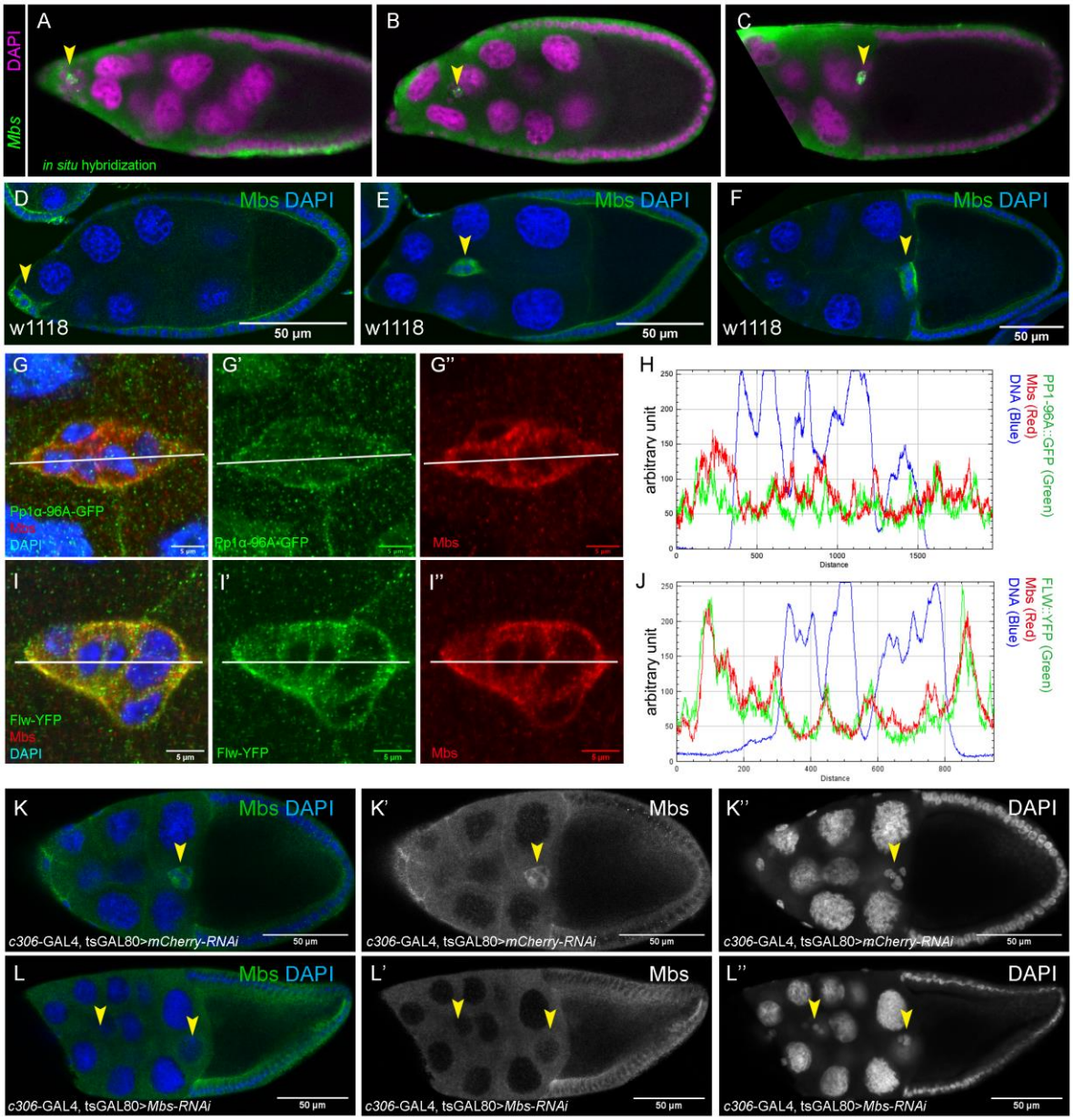

Figure 3.7 – figure supplement 1

Expression of Mbs during border cell migration and specificity of *Mbs*-RNAi knockdown. (**A-J)** Mbs transcript (A-C) and protein (D-I") are found in border cells throughout migration (arrowheads, A-F). (**A-C**) *Mbs* mRNA pattern as detected by *in situ* hybridization (green) in stage 9 to 10 egg chambers. Nuclear DNA, stained for DAPI, is shown in magenta. Images are from the Dresden Ovary Table http://tomancak-srv1.mpi-cbg.de/DOT/main[101]. (**D-F**) Wild-type (w^{1118}) egg

chambers stained for Mbs protein (green) and DAPI to label nuclei (blue). (**G-J**) Colocalization of Mbs with Pp1c subunits in border cells. The border cells are co-stained for Mbs (red in G, G", I, I") and Pp1α-96A-GFP (green in G, G') or Flw-YFP (green in I, I'). DAPI labels the nuclei (blue). (H, J) Plot profiles of the fluorescent image intensities of Pp1α-96A-GFP (H), Flw-YFP (J), Mbs, and DAPI across the lines shown (G-G", I-I"). (**K-L''**) Mbs RNAi results in significant reduction of Mbs protein levels in border cells (L-L") compared to control (K-K"). Stage 10 egg chambers stained for Mbs (green in K, L; white in K', L') and DAPI to label nuclei (blue in K, L; white in K", L"). All genotypes are listed in Table 3.2.

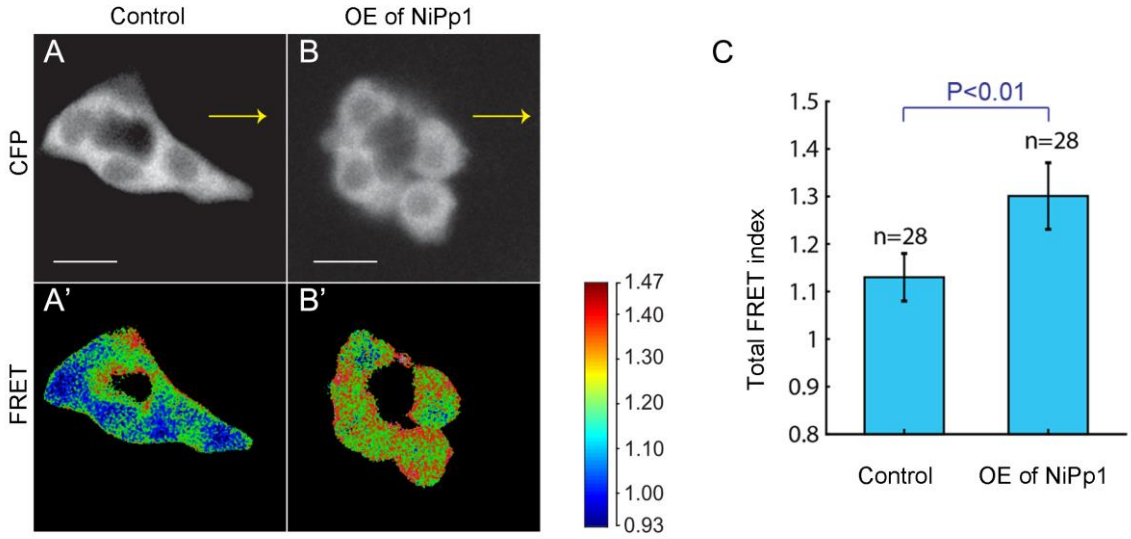

Figure 3.7 – figure supplement 2

Pp1 promotes moderate levels of RhoA activity in border cells. (**A-B'**) Representative processed Rho-FRET images in control (A, A') and NiPp1 overexpressing (B, B') border cells. The CFP channel (A, B) is shown. The FRET images (A', B') are color-coded as indicated in the heat map. (**C**) Measurement of the total FRET index in matched control and NiPp1 overexpressing border cells. The total number of border cell clusters assayed is indicated. All genotypes are listed in Table 3.2.

Appendix C- Chapter 4 Supplemental materials

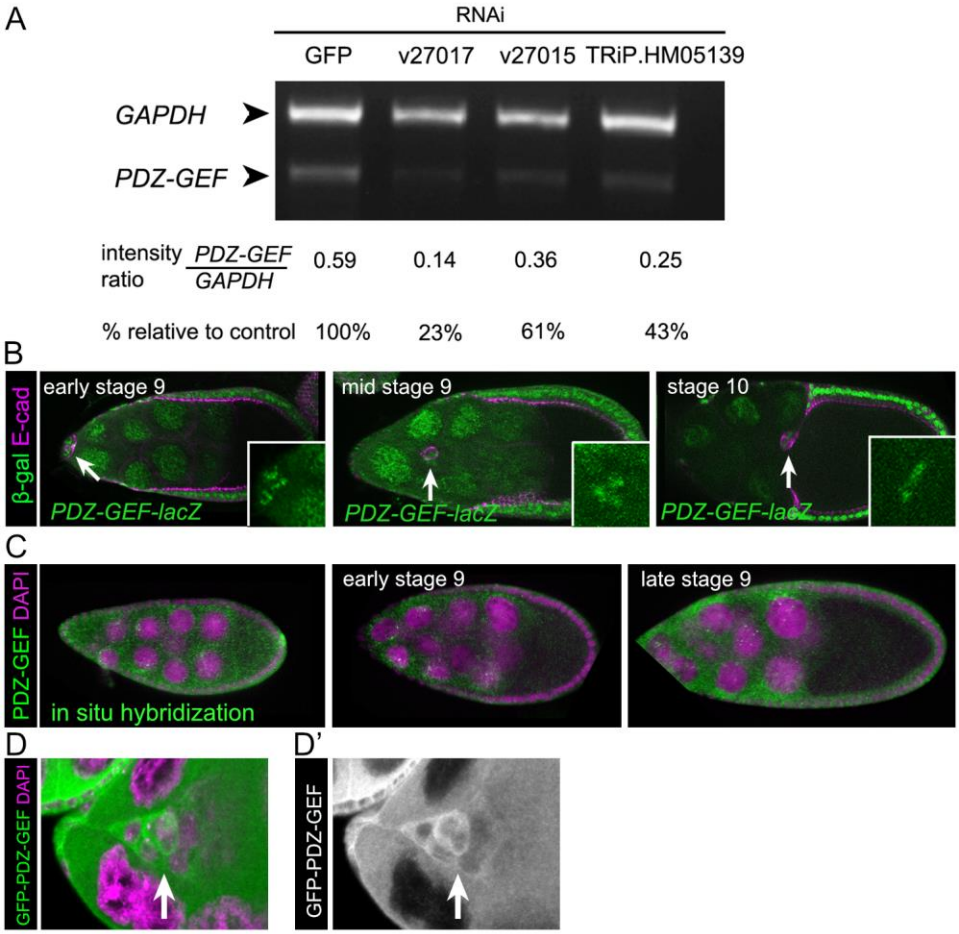

Supplemental Figure 4.1. Expression of *PDZ-GEF* and efficiency of *PDZ-GEF* knockdown by RNAi. (A) Effectiveness of RNAi was confirmed by performing RT-PCR on target mRNA from whole flies expressing GFP RNAi (control) or three different PDZ-GEF RNAi lines (v27017, v27015 and TRiP.HM05139). PCR products that amplified *PDZ-GEF* mRNA and *GAPDH* mRNA (loading control) were run on an agarose gel. Relative band intensities were measured and the ratios of *PDZ-GEF* to *GAPDH* were calculated. Percentage relative knockdown of *PDZ-GEF* was quantified compared to control (GFP RNAi). (B) Expression pattern of *PDZ-GEF-lacZ* during stages 9 and 10. Egg chambers expressing a *lacZ* enhancer trap in *PDZ-GEF* (*PDZ-GEF*^{1}/+) were stained for ß-galactosidase (ß-gal; green) and E-cadherin (E-cad; magenta) to mark cell

membranes. *PDZ-GEF-lacZ* is expressed in all cells including the border cells (arrows). (C) In situ hybridization pattern of *PDZ-GEF* (CG9491) RNA in green at stages 8 and 9. Nuclear DNA stained for DAPI is shown in magenta. Open sourced images and data are from http://tomancak-srv1.mpi-cbg.de/DOT/main (Dresden Ovary Table: insitu56784, insitu56787, insitu56788; probe from RH54455 cDNA) (Jambor *et al.*, 2015). (D and D') Ubiquitous expression pattern of GFP-PDZ-GEF. Close-up view of an early stage 9 border cell cluster (arrow) expressing the GFP-PDZ-GEF genomic rescue construct (anti-GFP antibody; green in D; white in D') (Boettner and Van Aelst, 2007). DAPI (magenta) labels nuclear DNA in all cells.

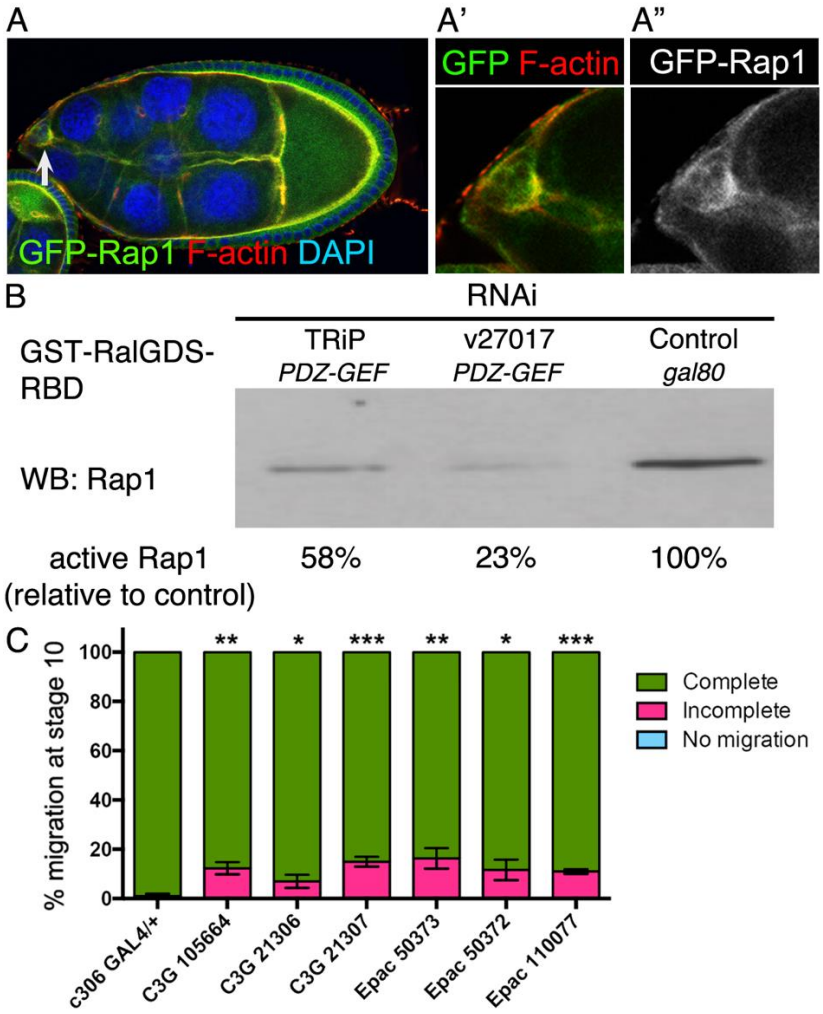

Supplemental Figure 4.2. Rap1 expression in early border cells and regulation by GEFs. (A-A") Stage 9 egg chamber during detachment stage expressing GFP-Rap1 (green in A and A'; white in A"), co-stained for DAPI (blue in A) to label nuclear DNA and phalloidin to label F-actin (red; A and A'). (A' and A'') Magnified view of the border cell cluster in A. Arrow (A) points to border cells. (B) Independent repeat of Rap1 activity pull-down assay on cell extracts from S2 cells treated with double-stranded RNA (RNAi) for PDZ-GEF (v27107 and TRiP.HM05139 RNAi) and *gal80* (control RNAi); see Figure 4.2C and Materials and Methods for further details. Relative band intensities were measured as a percentage of the control, which represents the maximum active Rap1 in this assay. (C) Quantification of complete (green), incomplete (pink), and no (blue) migration in stage 10 control (*c306*-GAL4/+) and UAS-C3G RNAi or UAS-Epac RNAi (*c306*-

GAL4/+; +/UAS-RNAi). The numbers refer to the UAS-RNAi line number (see Materials and Methods for details). Values consist of four trials, with each trial assaying n ≥ 50 egg chambers (total n ≥ 153 egg chambers per genotype); *, $p < 0.05$; **, $p < 0.01$; ***, $p < 0.001$; unpaired two-tailed *t* test, comparing "complete" migration between control and RNAi lines. Error bars: ± SEM.

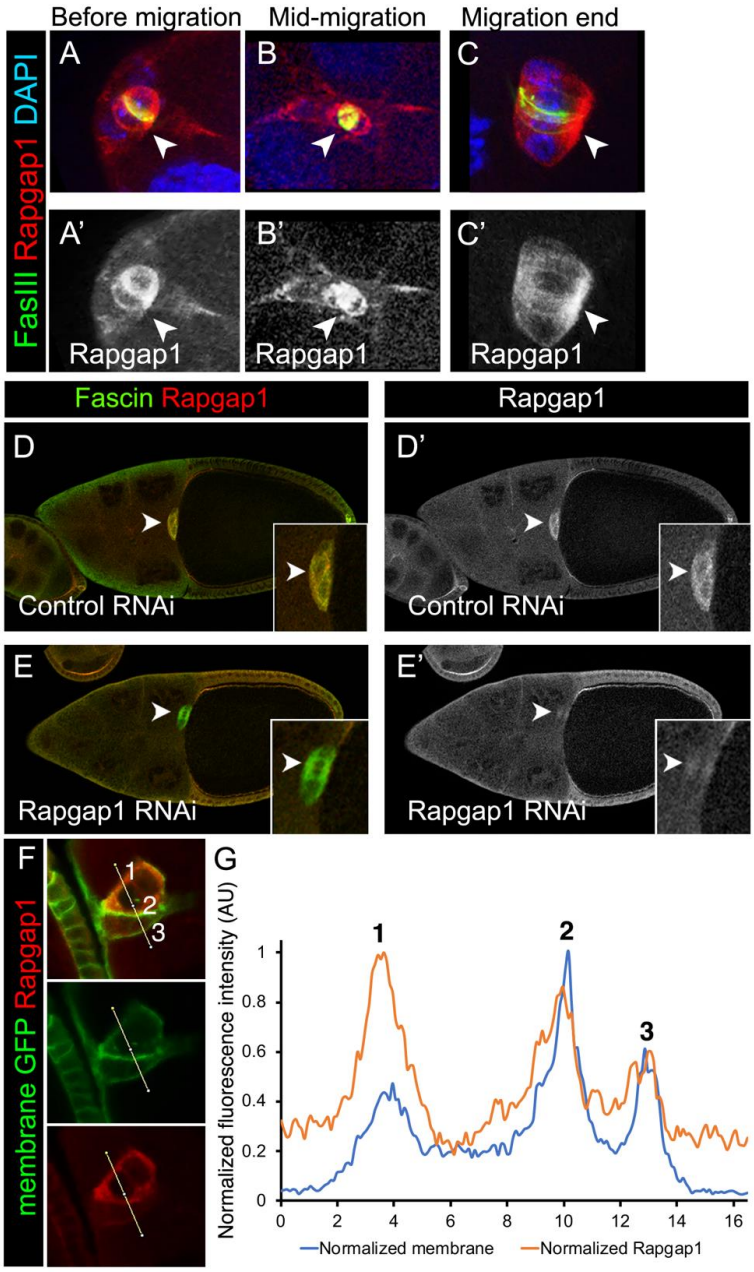

Supplemental Figure 4. 3. Efficiency of Rapgap1 RNAi and Rapgap1 protein expression in polar cells within the border cell cluster. (A-C') Rapgap1 is expressed at high levels in the central polar cells (arrowheads). Stage 9 and 10 egg chambers co-stained for Rapgap1 (red in A-C; white in A'-C') and the polar cell marker Fasciclin III (FasIII; green; colocalization appears as yellow in A-C). FasIII accumulates at the membrane interface between polar cells (Ruohola *et al.*, 1991). (A-B') During the start of migration and during mid-migration, polar cells express high levels of both

Rapgap1 and FasIII; border cells express relatively lower levels of Rapgap1. (C and C') By the end of migration, equally high levels of Rapgap1 are detected in polar cells and border cells. (D-E') Stage 10 control (*slbo*-GAL4/UAS-mCherry RNAi) and Rapgap1 RNAi (*slbo*-GAL4/+; +/UAS-Rapgap1 RNAi) egg chambers were stained for Fascin (green) to label border cells and polar cells and for Rapgap1 (red). Insets, magnified views of the same border cell clusters. (D and D') control border cells and polar cells (arrowheads) have high levels of Rapgap1. (E and E') Rapgap1 RNAi border cells have severely reduced Rapgap1 protein levels; the polar cells (arrowheads) still express Rapgap1 because *slbo*-GAL4 is expressed in border cells but not polar cells (Geisbrecht and Montell, 2002). In the example shown, Rapgap1 RNAi border cells completed their migration; in ~15% of egg chambers, the border cells stopped along the migration pathway (see Figure 4.4I). (F and G) A subset of Rapgap1 protein is membrane-associated. (F) Single slice of a *z*-confocal stack of a border cell cluster that expresses membrane GFP (green; *c306*-GAL4/+; UAS-PLCΔPH-GFP/+) and is co-stained for anti-Rapgap1 (red). A "plot profile" (yellow line) was drawn in FIJI and used to measure relative fluorescence intensity of membrane GFP and Rapgap1 across polar cells (1 and 2) and border cells (3). (G) Plot of normalized membrane GFP (blue) and Rapgap1 (orange line) fluorescence pixel intensity (AU, arbitrary units) across the line shown in F, with numbers referring to the positions along the line. Plot regions to the left of (1) and right of (3) represent fluorescence intensity of adjacent nurse cells. Similar results were obtained from additional border cell clusters (n = 7).

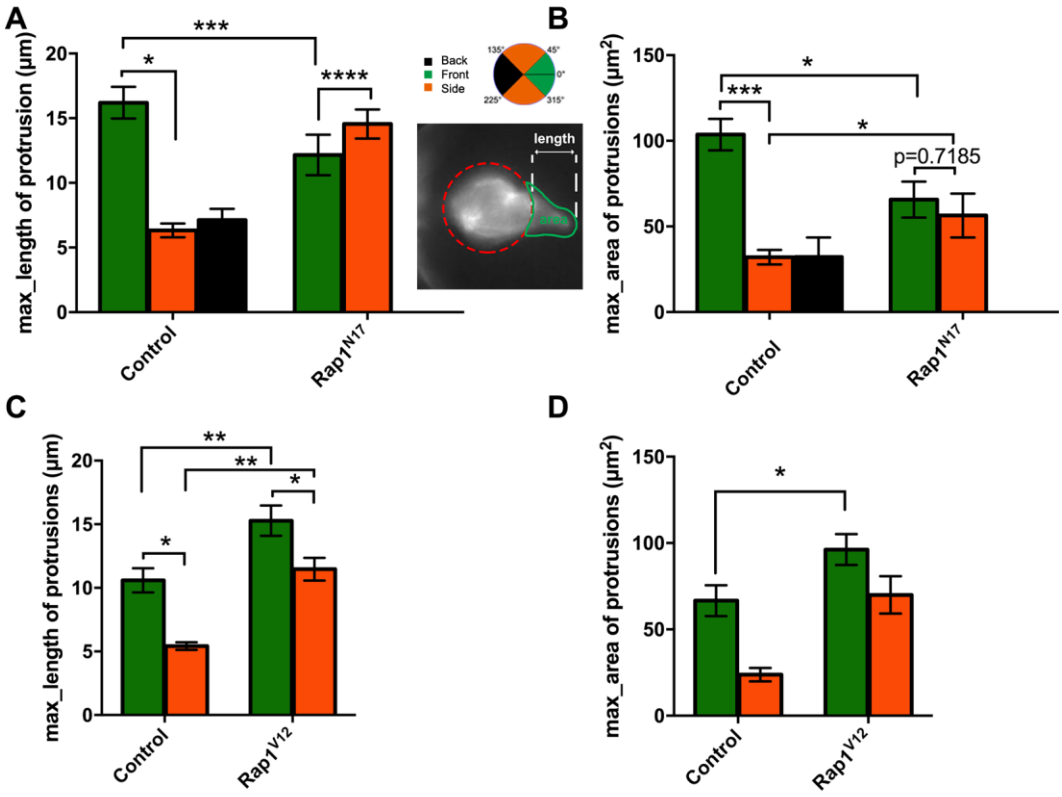

Supplemental Figure 4. 4. Rap1 regulates the maximal protrusion length and area. Quantification of the maximum length (A and C) and maximum area (B and D) of protrusions from time-lapse movies of the indicated genotypes. Protrusions at the front (green), side (orange) and back (black) of control and Rap1 mutant border cell clusters were measured. (Inset, A) Close-up view of a live border cell cluster showing how the main body of the border cell cluster (orange line), protrusion length (white line) and protrusion area (green outlined area) were defined and measured. In this example the protrusion is at the "front" (green) and not at the "side" (orange). (A) Rap1N17 border cells have shorter front protrusions and longer side protrusions compared to control. (B) The maximum area of Rap1N17 front border cell protrusions is reduced, but is increased for side protrusions, compared to control. (C) Rap1V12 border cells have longer front and side protrusions compared to control. (D) The maximum area of Rap1V12 border cell protrusions, especially at the front, is increased compare to control. Genotypes in A and B: c306-GAL4, tsGAL80/+; +/slbo-

LifeAct-GFP (control) and c306-GAL4, tsGAL80/+; UASRap1N17/slbo-LifeAct-GFP (Rap1N17); genotypes in C and D: slbo-GAL4/slbo-LifeAct-GFP (control) and slbo-GAL4/slbo-LifeAct-GFP; UAS-Rap1V12/+ (Rap1V12). Values consist of protrusions measured from $n \geq 7$ movies for each genotype (see Figure 4.5 for details); *, $p < 0.05$; **, $p < 0.01$; ***, $p < 0.001$; all other values were not significant ($p \geq 0.05$) and not shown (except in B); unpaired two-tailed t test. Error bars: SEM.

Supplemental References

Boettner, B., and Van Aelst, L. (2007). The Rap GTPase activator *Drosophila* PDZ-GEF regulates cell shape in epithelial migration and morphogenesis. Mol Cell Biol 27, 7966–7980.

Geisbrecht, E. R., and Montell, D. J. (2002). Myosin VI is required for E-cadherin-mediated border cell migration. Nat Cell Biol 4, 616–620.

Jambor, H., Surendranath, V., Kalinka, A. T., Mejstrik, P., Saalfeld, S., and Tomancak, P. (2015). Systematic imaging reveals features and changing localization of mRNAs in *Drosophila* development. eLife 4, R106.

Ruohola, H., Bremer, K. A., Baker, D., Swedlow, J. R., Jan, L. Y., and Jan, Y. N. (1991). Role of neurogenic genes in establishment of follicle cell fate and oocyte polarity during oogenesis in *Drosophila*. Cell 66, 433–449.

Appendix D- The role of nuclear membrane proteins in migrating border cells

Introduction

During collective cell migration, collectives often need to migrate through densely packed tissues to reach their destination. Navigation through these three-dimensional extracellular environments while coordinating the movement of the cluster is complex. How collectives adapt to the surrounding tissues all while maintaining the supracellularity of the cluster is still unknown. We are now using the *in vivo* collective border cell system to understand how collectives adapt to their surrounding tissues during migration. The border cell cluster moves through a tightly confined path squeezed in the substrate of nurse cells instead of an extracellular matrix. The border cell cluster maintains its polarity, cell shape and cohesion during this process. Collectives either migrate by degrading their ECM to generate a path or undergo cell shape changes to fit into those tight spaces (Friedl *et al.* 2011). Coordinating cluster shape in tissue environments can be challenging due to the stiffness of cell organelles like the nucleus (Jan Lammerding, 2011; Friedl *et al.* 2011). During single cell migration, cells deform their nuclei to accommodate nuclear shape changes and positioning due to physical forces generated during movement (Friedl *et al.* 2011). Whether cell collectives undergo nuclear deformation is unclear. A recent study showed that nuclear positioning is required for collective movement during morphogenesis to achieve left-right (LR) asymmetry (Shin *et al.* 2021). Using the collective border cell model, we are asking if border cells undergo nuclear deformation during migration to adapt their movement in a tightly confined environment. Specifically, we are asking which nuclear membrane proteins are expressed in migrating border cell cluster and essential to regulate collective border cell migration.

The *Drosophila* nuclear envelope comprises of inner and outer nuclear membrane, a lamina underneath nuclear membrane and nuclear pores (Fig. D.1; Wolfner2013; Chang *et al.* 2015). The nuclear lamina is composed of lamins which form an intermediate filament protein meshwork. This nuclear scaffold helps maintain nuclear shape and stiffness (Friedl *et al.* 2011; Jan Lammerding 2011). There are two types of lamins in mammalian cells- A-type (Lamin A/Cs) and B-type (Lamins B1 and B2). Both A- and B-type lamins have distinct roles during development. While B-type lamins are expressed in all cells and are essential for cell viability, A-type Lamins are developmentally regulated and expressed only later during embryogenesis (Lammerding 2011; Maurer and Lammerding 2019; Schulze *et al*. 2009). Lamin A/Cs are required for maintaining nuclear stiffness and Lamin B are essential to anchor nucleus to the cytoskeleton (Lammerding *et al.* 2004 and 2006; Lammerding 2011). Reduced levels of Lamin A/C leads to nuclear deformation during migration (Friedl *et al.* 2011; Harada *et al.* 2014). Next, the LINC (Linker of the Nucleus and Cytoskeleton) complex spans the nuclear envelope and connects the nuclear skeleton with cytoskeletal filaments and allows force transmission between the cytoskeleton and nucleus (Fig. D.1; Maurer and Lammerding 2019). KASH and SUN proteins are the structural proteins of LINC complex (Fig. D.1). To determine how nuclear shape changes can affect collective border cell migration, we performed an RNAi screen targeting members of the LINC complex in the border cell cluster. In flies, there are two lamins, one A-type Lamin-A/C (LamC) and one B-type Lamin-B ($LamD_{m0}$); two KASH proteins; Klar and Msp-300 and one SUN protein (koi) (Fig. D.1; Schulze *et al.* 2009; Chang *et al.* 2015). We determined that knocking down Msp-300 in the border cell cluster caused a significant migration defect. We also demonstrated the expression patterns of LamC and $LamD_{m0}$ using immunostaining approaches in the border cell nuclei. Overall, our

findings suggest a nuclear mechanism through which collectives adapt to surrounding environment during migration.

Material and methods

Drosophila RNAi screen and genetics

All genetic crosses were set up at 25℃. c306-GAL4, tsGal80; Sco/CyO was used to drive UAS-RNAi line expression in border cells. UAS-mCherry RNAi crossed to c306-GAL4 tsGal80; Sco/CyO was used as a control. Multiple RNAi lines for Msp-300, Koi and Klar genes were obtained from the Vienna *Drosophila* RNAi Center (VDRC) or the Harvard Transgenic RNAi Project (TRiP) collection from the Bloomington *Drosophila* Stock Center (BDSC) (Table D.1). Males from each UAS-RNAi line were crossed to virgin c306-GAL4, tsGal80 females. Three-to-five-day old F1 progeny females (c306-GAL4, tsGAL80/+; +/UAS-RNAi) from these crosses were fattened on wet yeast paste for 16 hours at 29C prior to dissection for optimum GAL4-UAS expression.

Immunostaining and Imaging

Ovaries were dissected in Schneider's *Drosophila* Medium (Thermo Fisher Scientific, Waltham, MA, USA). After dissection, whole ovaries were fixed in 4% formaldehyde (Polysciences, Inc., Warrington, PA, USA) in 0.1 M potassium phosphate buffer, pH 7.4 for 10 min. NP40 block (50mM Tris-HCl, pH 7.4, 150mM NaCl, 0.5% NP40, 5 mg/ml bovine serum albumin) was used for intermediate washes and antibody dilutions. For LamC antibody, whole ovaries were further dissected to individual egg chambers and fixed for 20 minutes in 4% formaldehyde (Polysciences, Inc., Warrington, PA, USA) in 0.1 M potassium phosphate buffer, pH 7.4. Primary antibodies were obtained from Developmental Studies Hybridoma Bank (DSHB, University of Iowa, Iowa City, IA, USA) and used at the following dilutions: rat monoclonal anti-

E-Cadherin 1:10 (DCAD2), mouse monoclonal IgG1 anti-Singed 1:25 (Sn7C), mouse monoclonal IgG1 anti-LaminDm0 (ADL67.10) 1:20, mouse monoclonal IgG1 anti-LamC (28.26) 1:10, mouse monoclonal IgG1 anti-Klar (Klar-M 4B5) and mouse monoclonal IgG1 anti-Klar (Klar-N 9E1B). Anti-rat or isotype-specific anti-mouse secondary antibodies conjugated to Alexa Fluor-488 or -568 (Thermo Fisher Scientific) were used at 1:400 dilution. 4',6-Diamidino-2-phenylindole (DAPI, Millipore Sigma) was used at 2.5 mg/ml to label nuclei. Aqua-Poly/Mount (Polysciences, Inc.) was used to mount egg chambers on slides, a coverslip was added, and the mounting media allowed to harden for 2-3 days prior to microscope imaging. The stained egg chambers were imaged either using an upright Zeiss AxioImager Z1 microscope with Apotome.2 optical sectioning or on a Zeiss LSM 880 confocal microscope (KSU College of Veterinary Medicine Confocal Core), using a 20x 0.75 numerical aperture (NA) objective. Images were processed in Zeiss ZEN 2 or FIJI software. Figures were prepared in Affinity Design software.

Results and Conclusion

We drove expression of each RNAi line shown in Table D.1 using border cell specific c306-GAL4 tsGAL80. Each RNAi line was crossed to c306-GAL4 tsGAL80 two times. Msp-300 RNAi line 50192 (bolded in Table D.1) was crossed three times to confirm the migration defects observed in the first two replicates. To determine real "hits" from the screen, RNAi lines with >10% migration defects were identified as positive hits. The migration defects were moderate for this line, with consistent defects between 15-20% (Table D.1). For other RNAi lines targeting Klar, koi and *Msp-300*, the migration defects were very mild and did not affect border cell migration.

Next, I used immunostaining approaches to analyze the localization of nuclear proteins LamC, $LamD_{m0}$ and LINC complex protein, Klar. Both A/C- and B- type Lamins were enriched in the nuclear membrane of border cell nuclei (Figure D.2, A-L) in stages 9 and 10 egg chambers

during pre-, mid- and end- migration. $LamD_{m0}$ (ADL67.10) also localized to nuclei of nurse cells, oocyte and follicular epithelium (A-F). Next, LamC localized to the nuclei of border cells and follicular epithelium but was not present in the nurse cells stages 9 and 10 egg chambers (Fig. D.2 G-L). LamC was also enriched in the polar cell nuclei in early stage 9 and stage 8 but not in the border cell nuclei (Fig. D.2 M and N, yellow arrowheads). Looking at early-stage egg chambers however showed that LamC was indeed localized to the nurse cell nuclei until stage 8 and lost in the nurse cells between stage 9-10 (Fig. D.2 N). Preliminary staining experiments showed that Klar M4B5 localized to border cell and nurse cell membranes instead of the nucleus (data not shown). Another Klar epitope N9E1B, showed a high cytoplasmic staining in the egg chamber (data not shown). Klar antibodies targeting epitopes M4B5 and N91EB were thus not optimized further due to non-specific staining patterns in the egg chamber.

Future experiments will focus on analyzing nuclear shape dynamics in Msp-300 RNAi 50192 and loss-of-function alleles and determining the spatial restriction of LamC in polar cell nuclei in early stages by using fixed and live imaging experiments are required to validate the phenotype observed in RNAi. To summarize, these experiments will help reveal the imperative functional role of structural nuclear membrane proteins and nuclear mechanotransduction during collective border cell migration.

Figures and tables

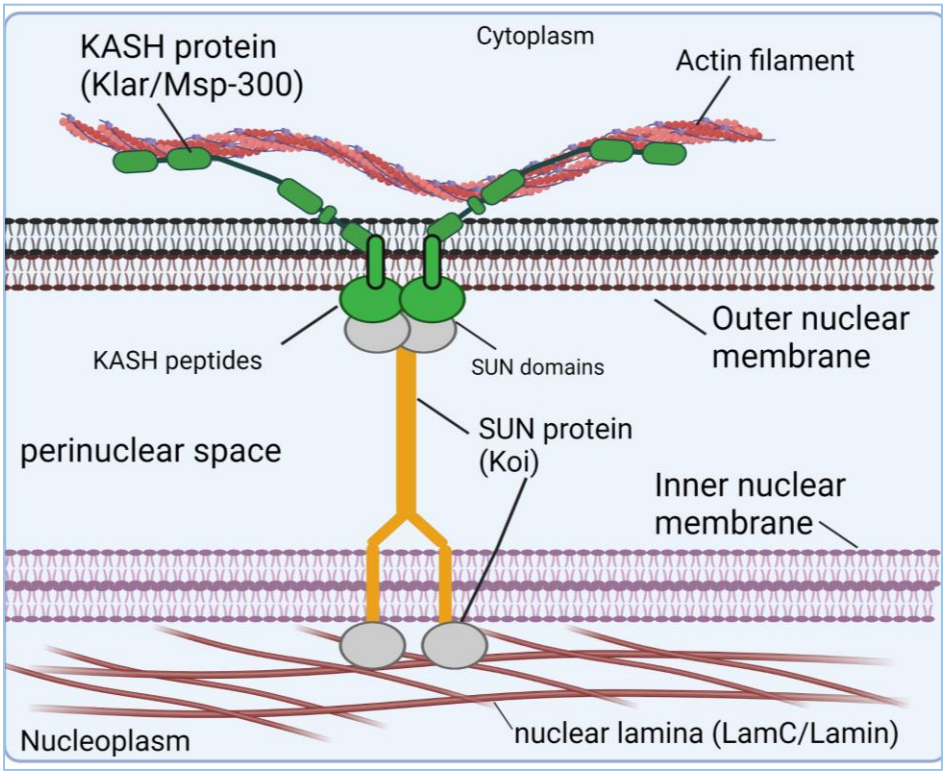

Appendix figure D.1. Schematic of nuclear membrane with associated structural proteins. The LINC complex connects the cytoskeleton to the nucleus through KASH proteins (green) in the outer nuclear membrane and SUN proteins (grey and orange) in the inner membrane. KASH protein interacts with cytoskeletal actin filament and links the nuclear membrane to the cytoplasm. SUN proteins anchor the LINC complex to the nuclear lamina in the nucleoplasm (created with Biorender.com and adapted from Chang *et al.* 2015).

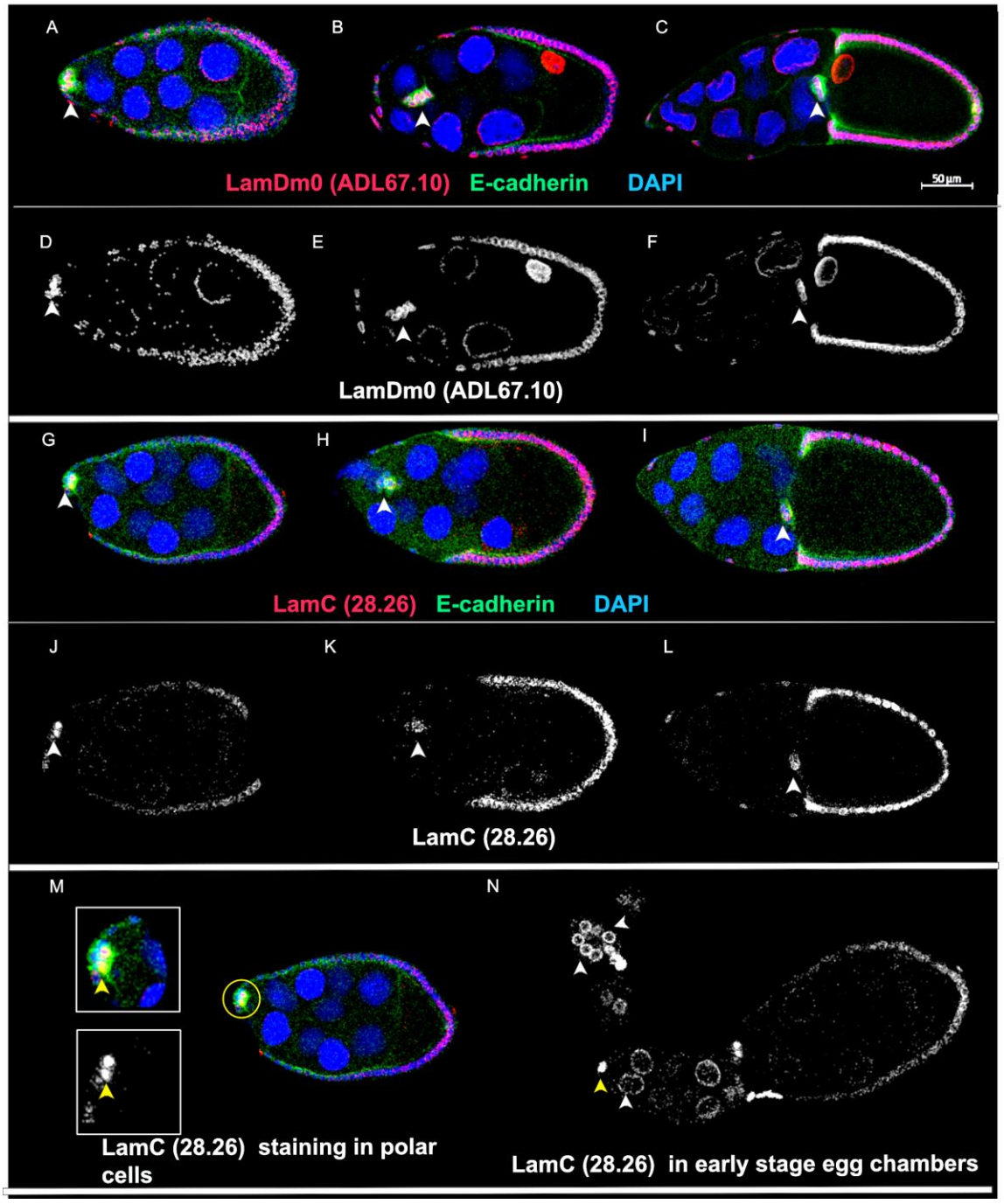

Appendix figure D.2. Expression of nuclear membrane proteins LamC and $LamD_{m0}$ in w1118 egg chambers. Representative examples of stage 9 and stage 10 egg chambers stained for $LamD_{m0}$ (ADL67.10) in red costained with E-cadherin (green) and DAPI (blue). Same egg chambers showing specific $LamD_{m0}$ staining in black and white (D-F). G-I) Representative

examples of stage 9 and stage 10 egg chambers stained for LamC (28.26s) in red costained with E-cadherin (green) and DAPI (blue). Same egg chambers showing specific $LamD_{m0}$ staining in black and white (J-L). Arrowheads in A-L represent the position of border cell cluster in the egg chamber. M) Focused inset of a stage 9 egg chamber pre migration shows LamC enriched in the polar cells. N)Early-stage egg chambers stained with LamC (28.26s) to show nurse cell nuclei localization of LAmC. White arrowheads indicate egg chambers with nurse cell nuclei membrane showing LamC expression and yellow arrowhead shows staining in polar cells in stage 8 egg chamber.

Table D.1. Results of the border cell screen of LINC complex genes. Migration defects are calculated by examining stage 10 egg chambers for each genotype.

Gene name	**RNAi line**	**Migration defects**
Msp-300	V107183	7%
	V50192	**15-20%**
	BL32377	2-3%
	V25906	1%
	BL32848	2-5%
Koi	V3990	5%
Klar	BL36721	8%
	BL28313	0%
	V32836	2%
Control (mCherry RNAi)	BL35785	3-5%

References

Chang, W., H. J. Worman, and G. G. Gundersen, 2015 Accessorizing and anchoring the LINC complex for multifunctionality. Journal of Cell Biology 208: 11–22.

Friedl, P., K. Wolf, and J. Lammerding, 2011 Nuclear mechanics during cell migration. Curr Opin Cell Biol 23: 55–64.

Lammerding, J., P. C. Schulze, T. Takahashi, S. Kozlov, T. Sullivan *et al.*, 2004 Lamin A/C deficiency causes defective nuclear mechanics and mechanotransduction. J Clin Invest 113: 370–378.

Lammerding, J., L. G. Fong, J. Y. Ji, K. Reue, C. L. Stewart *et al.*, 2006 Lamins A and C but not lamin B1 regulate nuclear mechanics. J Biol Chem 281: 25768–25780.

Lammerding, J., 2011 Mechanics of the nucleus. Compr Physiol 1: 783–807.

Maurer, M., and J. Lammerding, 2019 The Driving Force: Nuclear Mechanotransduction in Cellular Function, Fate, and Disease. Annual Review of Biomedical Engineering 21: 443–468.

Schulze, S. R., B. Curio-Penny, S. Speese, G. Dialynas, D. E. Cryderman *et al.*, 2009 A Comparative Study of *Drosophila* and Human A-Type Lamins. PLOS ONE 4: e7564.

Shin, D., M. Nakamura, Y. Morishita, M. Eiraku, T. Yamakawa *et al.*, 2021 Collective nuclear behavior shapes bilateral nuclear symmetry for subsequent left-right asymmetric morphogenesis in *Drosophila*. Development 148: dev198507.

Appendix E- Copyright permissions

This appendix chapter includes the copyright permissions for the chapters compiled in this thesis.

Chapter 2- Kotian *et al.* 2022

This G3 article is distributed under the terms of the Creative Commons Attribution License which permits unrestricted reuse, distribution, and reproduction in any medium, provided the original work is properly cited.

Chapter 3– Chen *et al.* 2020

This eLife article is distributed under the terms of the Creative Commons Attribution License, which permits unrestricted use and redistribution provided that the original author and source are credited.

Chapter 4– Sawant, Chen, Kotian *et al.* 2018

This Molecular Biology of the Cell (MBoC) article is distributed under Attribution–Noncommercial–Share Alike 3.0 Unported Creative Commons License.

Figure 1.5 was used with permission from Springer Nature and **Figure 1.6** was used with permission from Cell (see images below).

Licensee:	Ms. Nirupama Kotian
Order Date:	Apr 12, 2022
Order Number:	5286720486639
Publication:	Nature Reviews Cancer
Title:	Tumour-cell invasion and migration: diversity and escape mechanisms
Type of Use:	Thesis/Dissertation

Licensee:	Ms. Nirupama Kotian
Order Date:	Apr 14, 2022
Order Number:	5287790736622
Publication:	Cell
Title:	Cancer Invasion and the Microenvironment: Plasticity and Reciprocity
Type of Use:	reuse in a thesis/dissertation